

DOT/FAA/TC-22/20

Federal Aviation Administration
William J. Hughes Technical Center
Aviation Research Division
Atlantic City International Airport
New Jersey 08405

Post Small-Flame Forensic Analysis of Aerospace Composites

January 2024

Final report



U.S. Department of Transportation
Federal Aviation Administration

NOTICE

This document is disseminated under the sponsorship of the US Department of Transportation in the interest of information exchange. The US Government assumes no liability for the contents or use thereof. The US Government does not endorse products or manufacturers. Trade or manufacturers' names appear herein solely because they are considered essential to the objective of this report. The findings and conclusions in this report are those of the author(s) and do not necessarily represent the views of the funding agency. This document does not constitute FAA policy. Consult the FAA sponsoring organization listed on the Technical Documentation page as to its use.

This report is available at the Federal Aviation Administration William J. Hughes Technical Center's Full-Text Technical Reports page: actlibrary.tc.faa.gov in Adobe Acrobat portable document format (PDF).

Form DOT F 1700.7 (8-72)

Reproduction of completed page authorized

1. Report No. DOT/FAA/TC-22/20		2. Government Accession No.		3. Recipient's Catalog No.	
4. Title and Subtitle Post-Small Flame Forensic Analysis of Aerospace Composites				5. Report Date January 2024	
				6. Performing Organization Code	
7. Author(s) Abhijith Madabhushi, Dounia Boushab, Hasnaa Ouidadi, Hajar Righi, Thomas Lacy, Santanu Kundu, Charles Pittman, and Matthew W. Priddy				8. Performing Organization Report No.	
9. Performing Organization Name and Address Mississippi State University 479-1 Hardy Road Mississippi State, MS 39762				10. Work Unit No. (TRAIS)	
				11. Contract or Grant No.	
12. Sponsoring Agency Name and Address U.S. Department of Transportation Federal Aviation Administration Washington, DC 20591				13. Type of Report and Period Covered Final Report	
				14. Sponsoring Agency Code AIR-600	
15. Supplementary Notes The FAA Technical Monitor for this research was Dave Stanley at the FAA William J. Hughes Technical Center in Atlantic City, NJ.					
16. Abstract Fire can dramatically alter the exposed surfaces of composite aircraft structures in ways that inhibit forensic analysis. The char, soot, and several other fire by-products often mask relevant aspects of the structural damage morphology, impeding identification of the underlying failure mechanisms of composite materials. In this report, the effects of small-flame direct fire exposure and efficacy of char removal techniques on mechanically failed Cytec T40-800/Cycom® 5215 graphite/epoxy and pristine Hexcel® SGP370-8H/8552 carbon/epoxy specimens were examined. Small-flame vertical and horizontal Bunsen burner fire tests were performed on mechanically failed unnotched compression, short beam strength, and in-plane shear graphite/epoxy specimens. Vertical burn tests were conducted on pristine carbon/epoxy specimens for initial char removal assessment. Both visual inspection and scanning electron microscopy (SEM) were used to characterize the fracture surface morphology of the mechanically failed specimens, investigate the induced thermal damage due to fire exposure, and assess the effectiveness of the char removal techniques. The fire damage consisted of matrix decomposition, melt dripping, char and soot deposition, matrix cracking, delamination, and residual thickness increases due to explosive outgassing. The composite thermal degradation due to heat conduction, combustion, and/or thermal deformation was significantly affected by the specimen layup, ply orientation relative to the heat source, and the fracture surface morphology. Char removal approaches, including ultrasonication, chemical solvent soaking, liquid nitrogen dipping, and a combination of thermal cycling and ultrasonication, were explored, resulting in partial char removal. This research is intended to be related work to the <i>Composite Failure Analysis Handbook</i> , DOT/FAA/AR-91/23 WL-TI-91-4032 published through a joint research effort by the U.S. Air Force at Wright-Patterson AFB and the FAA. It should be noted these tests were conducted using a small methane flame, rather than a large pool fire, and therefore conclusions pertaining to aircraft accidents involving fire may not be directly applicable. The next phase for this project will address the fuel type and flame intensity to more accurately represent realistic accident conditions.					
17. Key Words Fire, thermal damage, small flame, char removal, composite materials, carbon fibers			18. Distribution Statement This document is available to the US public through the National Technical Information Service (NTIS), Springfield, Virginia 22161. This document is also available from the Federal Aviation Administration William J. Hughes Technical Center at actlibrary.tc.faa.gov .		
19. Security Classif. (of this report) Unclassified		20. Security Classif. (of this page) Unclassified		21. No. of Pages 174	22. Price

Contents

1	Introduction.....	1
1.1	Background	1
1.2	Overview of fire effects on composite materials.....	2
1.3	Motivation	7
1.4	Overview of surface cleaning and char removal techniques.....	10
1.4.1	Chemical cleaning processes	12
1.4.2	Thermal-based techniques for char removal from aerospace composites	14
2	Pre-fire fractographic analysis of mechanically failed graphite/epoxy composite specimens.....	15
2.1	Fractographic imaging of ASTM D3039 UNT0 graphite/epoxy specimen failure surfaces.....	19
2.2	Fractographic imaging of ASTM D6641 unnotched compression (UNC0) graphite/epoxy specimen failure surfaces	24
2.3	Fractographic imaging of ASTM D2344 SBS specimen failure surfaces	30
2.4	Fractographic imaging of ASTM D3518 IPS specimen failure surfaces.....	39
3	Effects of fire exposure on mechanically failed graphite/epoxy composite specimens..	49
3.1	Fire application methods	49
3.1.1	Direct fire application methods	49
3.1.2	Indirect fire application method.....	53
3.2	Analysis of mechanically failed graphite/epoxy composites subjected to fire	54
3.2.1	Enclosed vertical fire testing of Cytec T40-800/Cycom® 5215 graphite/epoxy specimens.....	55
3.2.2	Enclosed horizontal fire testing of Cytec T40-800/Cycom® 5215 graphite/epoxy specimens.....	85
3.2.3	Cone calorimeter testing of Cytec 5215 T40-800 graphite/epoxy compression-after-impact (CAI) specimen.....	94
3.3	Effect of specimen geometry, fracture surface morphology, and fire exposure time on fire damage and char formation	98

4	Char removal and forensic analysis of burned continuous fiber-reinforced aerospace composites.....	101
4.1	Fundamental principles of surface cleaning and char removal	101
4.1.1	The nature of char	101
4.1.2	Selection of chemical solvents for surface cleaning experiments	102
4.2	Surface cleaning of pristine burned aerospace composite specimens	105
4.2.1	Sonication experiments on pristine burned Hexcel carbon/epoxy composites	105
4.2.2	Initial sonication experiments for solvent selection	105
4.2.3	Surface characterization of pristine burned Hexcel specimens after ultrasonic cleaning in acetone	109
4.3	Surface cleaning of mechanically failed Cytec T40-800/Cycom® 5215 graphite/epoxy composite specimens.....	114
4.3.1	Ultrasonic cleaning of mechanically failed Cytec T40-800/Cycom® 5215 graphite/epoxy specimens.....	114
4.3.2	Surface characterization of mechanically failed Cytec T40-800/Cycom® 5215 graphite/epoxy specimens after ultrasonic cleaning in acetone	115
4.4	Effect of sonication parameters, pretreatment, and char morphology on char removal	123
5	Conclusions.....	127
6	Future work.....	128
7	References.....	130
A	SEM micrographs of Cytec T40-800/Cycom® 5215 specimens that failed under mechanical loading conditions.....	A-1
B	Effect of fire exposure on pristine Hexcel® SGP370-8H/8552 woven-fabric carbon/epoxy composites	B-1

Figures

Figure 1. Reaction process of a hot, decomposing polymer composite during fire exposure.....	3
Figure 2. Woven E-glass/polyester composite cross-section after heat flux exposure.....	5
Figure 3. Comparison of (a) fire-damaged region (b) char layer (c) area between char layer and unburned composite (d) delamination cracks (e) unburned composite resin-rich area.	7
Figure 4. Comparison of 21-ply cross-ply Cytec specimen failed in compression after vertical burning	10
Figure 5. Schematic of cavitation action during ultrasonication	13
Figure 6. Typical high-vacuum sputter-coater setup	18
Figure 7. Low magnification SEM micrograph of graphite/epoxy UNT0 specimen fracture surface	20
Figure 8. SEM micrograph of a graphite/epoxy UNT0 specimen showing tensile failure features	21
Figure 9. SEM micrographs of a graphite/epoxy UNT0 specimen tensile failure with (a) fibers pull-outs and (b) radial marks.....	22
Figure 10. SEM micrograph of shear-hackles in 90°-plies of a UNT0 specimen	24
Figure 11. Micrograph of representative graphite/epoxy UNC0 specimen fracture surface	25
Figure 12. SEM micrograph of a typical compressive fracture surface in a graphite/epoxy UNC0 specimen	26
Figure 13. SEM micrographs of graphite/epoxy UNC0 showing (a) chop marks (b) individual fractured filament end	27
Figure 14. SEM micrographs of 90°-plies in graphite/epoxy UNC0 specimen with (a) shear-hackles and (b) compressive failure matrix debris	29
Figure 15. Low magnification (70×) SEM micrograph of representative graphite/epoxy SBS specimen fracture surface	31
Figure 16. SEM micrograph of outermost ply surface of graphite/epoxy SBS specimen showing kink bands.....	32
Figure 17. SEM micrographs of graphite/epoxy SBS specimen fracture surface with (a) kink bands (b) terrace of micro-buckled fibers	34
Figure 18. SEM micrographs of graphite/epoxy SBS specimen with (a) chop marks (b) micro-buckled fibers.....	35
Figure 19. SEM micrographs of SBS specimen micro-buckled fibers (a) above laminate neutral axis (b) below laminate neutral axis	37
Figure 20. SEM micrograph near lower surface of graphite/epoxy SBS specimen showing radial lines on fractured fiber ends	38

Figure 21. SEM micrograph of graphite/epoxy SBS specimen fracture surface covered with matrix debris	39
Figure 22. SEM micrograph of representative failed graphite/epoxy IPS specimen.....	41
Figure 23. SEM micrographs of IPS specimen in-plane fracture surface.....	42
Figure 24. SEM micrographs of IPS specimen with (a) shear fracture surface (b) cusps	44
Figure 25. SEM micrographs of IPS specimen fracture surface with (a) gouges (b) triangular cusps.....	45
Figure 26. SEM micrograph of longitudinally split fiber tows in mechanically failed IPS specimen.....	47
Figure 27. SEM micrographs of fractured graphite fibers in IPS specimen (a) under tension (b) under combined tension and transverse shear	48
Figure 28. Draft-free cabinets that meet the FAA fire testing requirements.....	49
Figure 29. Burner plumbing and burner flame height indicator.....	50
Figure 30. Specimen positioning with flame (a) for vertical fire tests and (b) horizontal fire tests	51
Figure 31. 21-ply cross-ply Cytec UNCO specimen during vertical burning test using Bunsen burner	52
Figure 32. 21-ply cross-ply Cytec UNCO specimen during horizontal burning test with Bunsen burner	53
Figure 33. A schematic view of a cone calorimeter.....	54
Figure 34. Fire sparkles during 12 s vertical burn test on 21-ply cross-ply Cytec UNCO specimen	56
Figure 35. Comparison of 21-ply cross-ply Cytec UNCO specimen (a) before (b) after and (c) after vertical burning for 60 s	57
Figure 36. Char and soot on fracture surface of 21-ply cross-ply Cytec UNCO specimens burned vertically for (a) 12 s (b) 36 s and (c) 60 s	59
Figure 37. Fuzzy char on single fibers in 21-ply cross-ply Cytec UNCO specimen burned vertically for (a) 12 s (b) 36 s (c) 60 s.....	60
Figure 38. Fracture characteristics on (a) 21-ply cross-ply Cytec UNCO specimen showing recessed fibers after vertical burning	62
Figure 39. Micro-buckling terraces on compression failed CFRP specimen (x700).....	63
Figure 40. SEM image of micro-buckled fibers in a 21-ply cross-ply Cytec UNCO specimen burned vertically for 60 s.....	63
Figure 41. (a) Melt dripping on fracture fiber ends of 21-ply cross-ply Cytec UNCO specimen burned vertically for 36 s (b) filaments with melt dripping	64
Figure 42. Delamination in 21-ply cross-ply Cytec UNCO specimen burned vertically for 60 s .	65

Figure 43. Matrix cracking in 21-ply cross-ply Cytec UNC0 specimen burned vertically for 60 s	66
Figure 44. Picture of 45-ply unidirectional Cytec SBS specimen (a) before and (b) after vertical burning for 60 s.....	67
Figure 45. Char and soot on fracture surface of 45-ply unidirectional Cytec SBS specimens after vertical burning for (a) 12 s (b) 36 s and (c) 60 s	69
Figure 46. Fuzzy char around single fibers in 45-ply unidirectional Cytec SBS specimens burned vertically for (a) 36 s and (b) 60 s.....	70
Figure 47. Fracture characteristics on (a) 45-ply unidirectional SBS Cytec specimen showing recessed fibers after (b) 12s, (c) 36s, and (d) 60 s vertical burning	72
Figure 48. Micro-buckled fibers in Cytec SBS specimens	73
Figure 49. Micro-buckled fibers in Cytec SBS specimens completely covered in melt dripping.	74
Figure 50. Positioning of IPS specimen during vertical burn tests.....	76
Figure 51. 16-ply Cytec IPS specimen (a) before (b) after and (c) after vertical fire exposure for 6 s.....	77
Figure 52. (a) longest lateral edge (b) center and (c) shortest lateral edge of 16-ply Cytec IPS specimens	78
Figure 53. Char formation on (a) longest and (b) shortest lateral edges of 16-ply Cytec IPS specimens burned vertically for 12 s.....	80
Figure 54. Char formation on (a) longest and (b) shortest lateral edges of 16-ply Cytec IPS specimens burned vertically for 36 s.....	81
Figure 55. Char formation on (a) longest and (b) shortest lateral edges of 16-ply Cytec IPS specimens burned vertically for 60 s.....	82
Figure 56. Fiber-end thinning of filaments at mid-plane of 16-ply Cytec IPS specimens burned vertically for (a) 12 (b) 36 and (c) 60 s	84
Figure 57. Void and cavities on fiber of 16-ply Cytec IPS specimen burned vertically for 60 s..	85
Figure 58. 21-ply cross-ply Cytec UNC0 specimen before and after horizontal burning for 75 s	86
Figure 59. Char and soot at fracture surface of 21-ply cross-ply Cytec UNC0 specimen used on 15 s horizontal fire test.....	87
Figure 60. Comparison of 45-ply unidirectional Cytec SBS specimen before and after horizontal burning for 75 s.....	88
Figure 61. Fracture surface of 45-ply unidirectional Cytec SBS specimens used for (a) 15 s (b) 45 s and (c) 75 s horizontal burning.....	90
Figure 62. 16-ply Cytec IPS specimen after horizontally burning for 75 s with approximate location of flame axis.....	92

Figure 63. Fiber tows from centerline of 16-ply Cytec IPS specimens after horizontal burning for (a) 15 s (b) 45 s and (c) 75 s	93
Figure 64. Cone calorimetry testing of 4 x 4 in ² 2 32-ply Cytec CAI specimen.....	95
Figure 65. (a) 4 x 4 in ² 32-ply CAI specimen after cone calorimeter fire testing with heat flux of 50 kW/ m ² (b) loose fibers (c) edge delamination	96
Figure 66. Melt dripping from 4 x 4 in ² 32-ply Cytec CAI specimen	97
Figure 67. Sonication action along surface of in-plane fibers of burned pristine 4-ply cross-ply Hexcel specimens.....	107
Figure 68. Color change of acetone before and after 60 min of ultrasonication of representative pristine burned Hexcel specimen	108
Figure 69. Sonication results (60min, acetone) of 4-ply cross-ply Hexcel woven fabric.....	112
Figure 70. Sonication (60min, acetone) results of 4-ply cross-ply [0/90/90/0] Hexcel woven fabric	113
Figure 71. Sonication (60min, acetone) results of Cytec UNCO	116
Figure 72. Sonication (60min, acetone) results of 21-ply cross-ply Cytec UNCO	118
Figure 73. Thermal cycling and sonication results of 21-ply cross-ply Cytec UNCO	120
Figure 74. Thermal cycling and sonication results of 21-ply cross-ply Cytec UNCO	122

Tables

Table 1. Typical Fracture Characteristics for Different Failure Modes.....	8
Table 2. Summary of the properties of mechanically failed Cytec specimens.....	16
Table 3. List of commercially available cleaning products for carbon residue removal	103
Table 4. Chemical solvents used in char removal experiments.....	104

Acronyms

Acronym	Definition
ASTM	American Society for Testing and Materials
CAI	compression after impact
CFRP	carbon fiber reinforced polymer
CNT	carbon nanotubes
FAA	Federal Aviation Administration
FE-SEM	field emission - scanning electron microscope
GA	General Aviation
IPS	in-plane shear
NIAR	National Institute for Aviation Research
NCAMP	National Center for Advanced Material Performance
PAN	polyacrylonitrile
SBS	short beam strength
SEM	scanning electron microscopy
UNC0	unnotched compression
UNT0	unnotched tension

Executive summary

The use of composite materials in aircraft structures has increased dramatically over the last decade. While continuous carbon fiber-reinforced composite materials have outstanding mechanical properties, they are vulnerable to fire damage. The formation of char and other thermal by-products due to small-flame fires involving mechanically failed composite materials can mask relevant aspects of the structural damage morphology and other evidence necessary to identify the underlying failure mechanisms.

The primary goal of this work was to investigate, document, and confirm characteristic failure features of mechanically failed specimens and compare the surface fracture morphology of each specimen type before fire exposure, after fire exposure, and after char removal.

This report focuses on investigating the thermal damage development in mechanically-failed Cytec T40-800/Cycom® 5215 graphite/epoxy (Cytec) specimens, as well as the establishment of strategies for char removal from burned composite surfaces. The mechanically failed specimens included [90/0/90]7 unnotched compression (UNC0), [0]45 short beam strength (SBS), [45/-45]4S in-plane shear (IPS), and [45/0/-45/90]4S compression after impact (CAI) specimens. Initially, extensive fractographic imaging of the fracture surfaces of Cytec graphite/epoxy specimens were performed to identify and document the surface failure features. In general, composite laminate failure involves local fiber microbuckling, fiber fracture, matrix cracking, matrix crushing, fiber splitting, chop marks, radial lines, cusps, matrix microflow, riverlines, and delamination. These key fractographic features can be used to determine the loading conditions during the mechanical failure of an aerospace composite structure.

Vertical and horizontal fire tests were performed on the mechanically failed graphite/epoxy composite specimens. In addition, a series of burn tests performed on pristine Hexcel® SGP370-8H/8552 carbon/epoxy (Hexcel) specimens were used for preliminary assessment of char removal techniques. The fire damage was characterized by visual inspection and scanning electron microscopy (SEM). The specimen layup, its relative ply orientation to the heat source, and fracture surface morphology significantly influenced fire damage formation (i.e., melt dripping, matrix decomposition, char, soot, matrix cracking, delamination, and residual thickness increase). The thermal damage development was also influenced by the specimen layup and the total available free surface area due to increased airflow and oxygen availability. In some cases, it was observed that the fracture surfaces of recessed fibers sometimes remain relatively unaffected by fire exposure, which may permit limited post-fire forensic analysis.

In this report, various surface treatment/cleaning techniques (e.g., chemical soaking, ultrasonication, and thermal cycling-ultrasonication) were considered for char removal purposes. Ultrasonication experiments were performed on pristine Hexcel carbon/epoxy and mechanically failed graphite/epoxy specimens in acetone. Under the influence of ultrasonic frequencies, surface char is separated from the underlying composite surface. In some cases, thermal cycling was performed by dipping the specimens in liquid N₂ or dipping them in boiling water before ultrasonication to create thermal instabilities that could weaken the interfacial bonding between char and the composite surface. While the sonication experiments showed more promise in removing char from the circumferential surfaces of the in-plane (90°) fibers, char removal from the exposed fiber ends of the out-of-plane (0°) fibers was more challenging. Thermal cycling in boiling water before ultrasonication significantly improved char removal from the fiber ends of the out-of-plane fibers. In many cases, the surrounding resin matrix, and its associated failure surface features, are completely decomposed following fire application. However, further experiments are required to quantify the effectiveness of char removal techniques on principal aerospace composite structural elements.

It should be noted that the small-flame type used in this research is more typical of a small-flame ignition, like those that would be seen due to spilled chemicals during maintenance, or short-circuit ignitions. It is not what you would expect in a post-crash aircraft fire. In an actual post-crash fire event, it is likely that the intensity of a pooled fuel fire will have much higher intensity and heat flux, with carbon fibers completely decomposed. There is unlikely to be any residual char on fractured fiber ends, and remaining structure some distance away from the fracture surface may also be decomposed.

The next phase for this project will address similar experimental char removal techniques and burning of thicker primary structural elements using an oil-fed burner to more accurately represent realistic accident conditions.

1 Introduction

1.1 Background

Typical continuous fiber aerospace composite materials have many advantageous mechanical and thermal properties over metals. They are lightweight, corrosion-resistant, take complex shapes, and can have low maintenance and manufacturing costs (Kabche, 2006). Also, fiber-reinforced composite materials can offer better fatigue resistance than metals. The high stiffness and strength of continuous fibers facilitate fiber-crack bridging that mitigates the nucleation and growth of matrix cracks and improves fatigue properties (Botelho, Silva, Pardini, & Rezende, 2006). As a result, the use of composite materials in primary structural applications has increased dramatically over the past decades. They are now used in aerospace, automotive, and many other high-tech and low-tech applications that require high stiffness/weight or strength/weight ratios. Despite their high specific properties, composite materials often suffer from relatively high moisture absorption and low fracture toughness (Botelho, Silva, Pardini, & Rezende, 2006). Moreover, their structural performance and damage tolerance generally degrade at elevated temperatures (Mouritz & Gibson, 2007; Mouritz A. P., 2003).

Although continuous-fiber carbon/epoxy composite materials for aerospace applications provide high specific mechanical and thermal properties, their use should not affect the post-fire safety already assured by aluminum aircraft (E7-20031, 2007). The aluminum lower wing panels used on commercial passenger aircraft wings have been certified as fire-resistant over a wide range of typical skin thicknesses.

Compared to metallic aircraft structures, carbon/epoxy composite structures can have low thermal conductivities, affecting heat transfer and the spread of a flame in the event of fire (Mouritz & Gibson, 2007). However, due to their organic matrix (and sometimes fibers), they are prone to react with fire (Mouritz & Gibson, 2007; Zhang, 2010). When a thermoset composite material is exposed to elevated temperatures below the resin curing temperature, the polymer matrix softens, increasing the likelihood of instability or matrix-dominated failures and loss of aircraft structural integrity. Once the resin curing temperature is exceeded, thermosetting matrices will further cure, decompose, and start to combust. At extremely high temperatures encountered during aircraft fires, the organic matrices and fibers of the composite structures start decomposing, leading to the generation of toxic smoke and gases. Also, the decomposition of these organic parts leads to the formation and deposition of char and other fire by-products on the burned composite surfaces (Mouritz & Gibson, 2007; Mouritz A. P., 2003). Moreover, thermally-induced large-scale matrix decomposition, fiber ablation/sublimation, and

delamination due to fire exposure can result in significant decreases in composite moduli and strengths (Mouritz & Gibson, 2007; Zhang, 2010; Chen, 2018; Mouritz & Mathys, 2001; Mouritz, Gardiner, Mathys, & Townsend, 2001; Mouritz, et al., 2009).

Composite aircraft structures undergo complex multi-mode mechanical failure in critical structural elements during accidents (Kumar, Raghavendra, Venkataswamy, & Ramachandra, 2012; Camanho, Bowron, & Matthews, 1998; Xiao & Ishikawa, 2005; Greenhalgh, 2009).

A crash scenario often leads to post-crash fire, causing fire damage to principal structural elements. The resulting changes to the failure surfaces make it difficult to identify the root cause of the structural failure. Therefore, there is a need to develop an effective fire-damage assessment methodology to perform fire forensics on the burned aircraft structural elements and assess the effect of fire damage on the fracture surfaces developed during mechanical failure.

1.2 Overview of fire effects on composite materials

Fire damage in continuous-fiber-reinforced composite materials involves the concurrent and sequential interaction between complex physical, chemical, thermal, and failure processes (Mouritz, et al., 2009). The physical processes include constituent material expansion and contraction, ply-delamination, matrix cracking, and the formation of high-pressure regions due to matrix outgassing. The chemical processes involve the phase changes that occur inside the composite material, including the softening, melting, and decomposition of the matrix and char formation and growth. The thermal processes involve the evolving temperature distributions, heat transfer through the material due to conduction, convection of the gases formed during the decomposition, and pyrolysis of the polymeric matrix and organic fibers. Lastly, the failure processes involve the permanent degradation of the mechanical properties of the composites and failure of the load-carrying capability of the composite structures due to fire (Mouritz & Gibson, 2007; Mouritz, et al., 2009). Figure 1 (Mouritz, et al., 2009) shows a schematic of the reaction processes in the through-thickness direction of a hot, decomposing polymer composite during fire exposure.

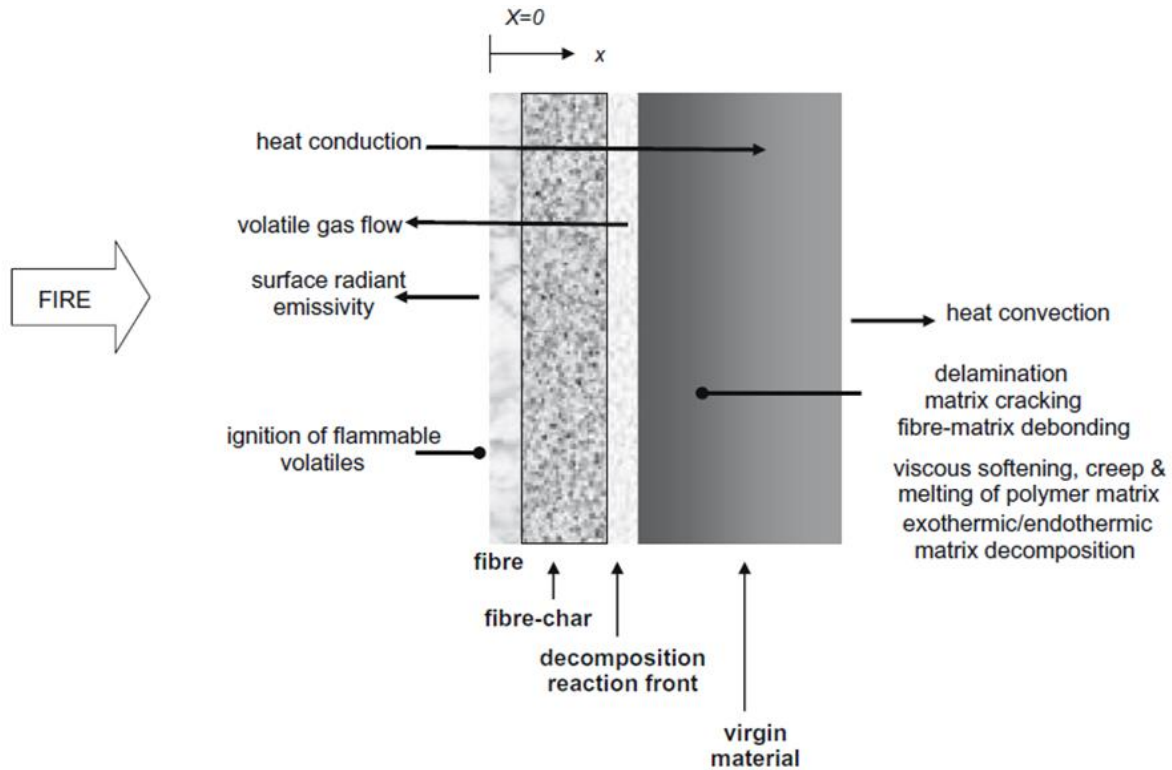


Figure 1. Reaction process of a hot, decomposing polymer composite during fire exposure

When a mechanically failed composite material specimen is subsequently exposed to a fire or a heat flux, the elevated temperature at the exposed fractured surface leads to significant localized heat conduction within the specimen. As the local temperature initially increases, the resulting matrix softening can contribute to various matrix-dominated instability failures that can jeopardize aircraft structural integrity. Once the increasing temperature exceeds the thermoset resin curing temperature, the matrix will further cure and decompose, leading to char formation and the generation of smoke, toxic gases, and vaporized moisture (Mouritz & Gibson, 2007; Zhang, 2010). Due to the initial low permeability and porosity of typical aerospace composites, combustion-induced gases trapped inside vacancies (voids) created during the burning result in matrix regions with very high internal local pressures. These voids can eventually rupture, leading to extreme ply-delamination and a significant increase in residual laminate thickness after fire exposure (Mouritz & Gibson, 2007; Zhang, 2010; Mouritz, et al., 2009). In addition, expanding hot gasses from matrix outgassing dramatically increase convective heat transfer through the specimen and spread decomposed matrix residues over fire/heat-exposed composite surfaces. Such residues contribute to the deposition of solid carbonaceous soot and char on the fractured surface, which can obscure salient aspects of failure surface morphology necessary to identify operative mechanical failure mechanisms. One key aspect of this research is to

characterize how varying levels of fire exposure alter aerospace composite failure surfaces, and document those outcomes to facilitate post-fire forensic analysis.

The degree and amount of char formation depend on both the original polymer matrix and organic fibers (Mouritz & Gibson, 2007). Char structures consist of 85-98% carbon and particles of aromatic-aliphatic compounds, often with heteroatoms (O, N, P, and S). Depending on the fire environment, temperature, and chemical composition of the polymer matrix and organic fibers, char can contain crystalline or amorphous regions (Mouritz & Gibson, 2007). Char can vary in composition from the melted and partly oxidized matrix (resin) to a highly carbonized material.

Due to its low thermal conductivity, char formed at the exposed surface of the burned composite material may serve as a protective layer that impedes further burning (Mouritz & Gibson, 2007). Mouritz and Mathys (2001) used cone calorimetry to investigate the effect of through-thickness heat flux and fire exposure duration on the char formation in an 11.5 mm thick E-glass woven roving fabric isophthalic polyester composite laminate. Figure 2 (Mouritz & Mathys, 2001) shows the cross-section of the woven composite after being exposed to an upper surface heat flux of 50 kW/m^2 for four different durations in seconds: (a) 0 s, (b) 85 s, (c) 325 s, and (d) 1800 s. As shown in the figure, the char layer thickness increased with the increase in heat flux exposure- duration. Moreover, the char developed through the entire 11.5 mm specimen thickness due to the total thermal decomposition and combustion of the polyester matrix.

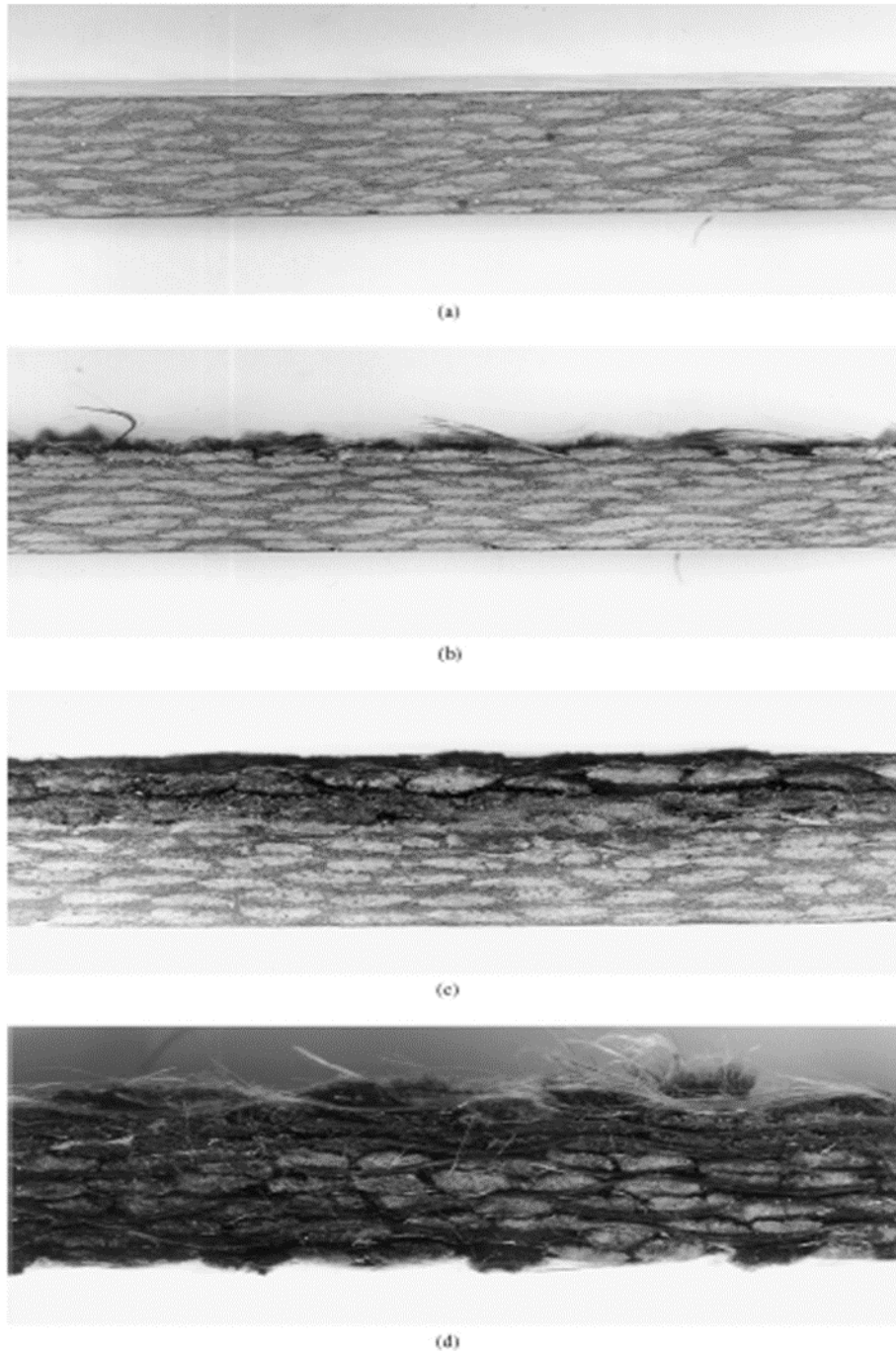


Figure 2. Woven E-glass/polyester composite cross-section after heat flux exposure

Mouritz and Mathys (2001) also showed that the rate of char formation was independent of the heat flux. Exothermic decomposition of the polyester matrix enhanced the combustion process upon the ignition of the composite. However, the char growth rate depended on the post-ignition heat exposure time and the rate of oxygen transfer to the combustion front. The combustion front is defined as the interface between the burned and unburned layers of the composite. The oxygen

transport rate dropped as the char thickness increased (Mouritz & Mathys, 2001), leading to decreased char formation rate.

In general, composite fire damage involves extensive matrix thermal decomposition, soot deposition, char formation, severe fire-induced delamination, matrix cracking, residual thickness increases, and fiber-matrix debonding (Mouritz, et al., 2009). Scanning electron microscopy (SEM) images of the fire damage induced in an E-glass woven roving fabric and an isophthalic polyester composite are presented in Figure 3 (Mouritz & Mathys, 2001). Figure 3(a) shows a through-thickness schematic of the fire damage in the specimen. Figure 3(a) through 3(e) show representative SEM images of the char layer, an interfacial region (combustion front) between the char layer and unburned composite, delamination cracks, and a matrix-rich region in the unburned part of the composite, respectively. The char region primarily comprised burned fibers since the matrix was mostly decomposed. In the combustion front shown in Figure 3(c), many fibers displayed longitudinal cracking and were generally detached from the matrix.

Delamination occurred between the underlying unburned layers. The delamination was assumed to be due to the significant difference in thermal conductivities (and coefficients of thermal expansion) between the char and underlying composite layers. Finally, the unburned region of the composite was thermally degraded and contained some matrix-rich pockets (Mouritz & Mathys, 2001). This research sought to identify appropriate char removal procedures that enhance the analysis of the specimen damage assessment.

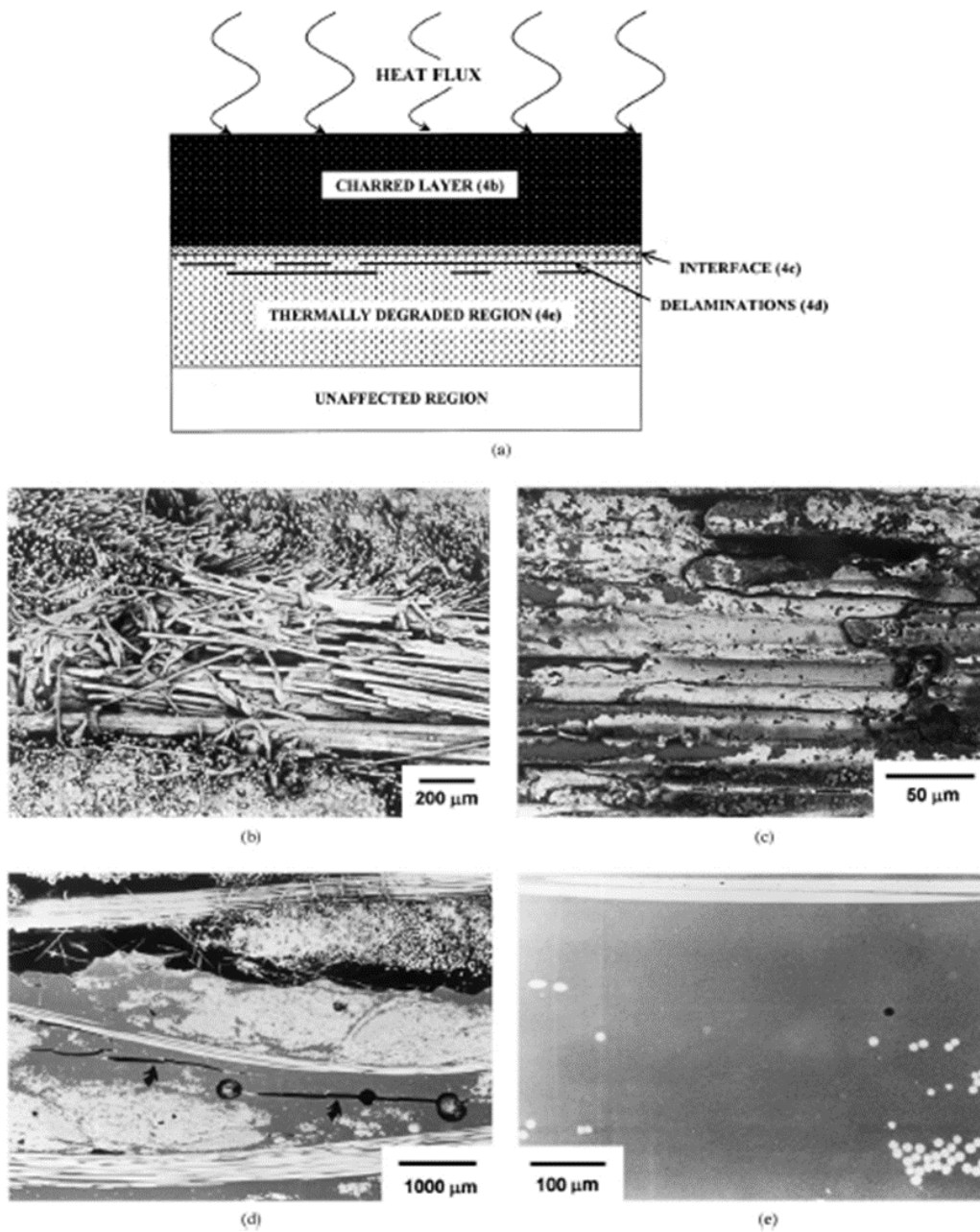


Figure 3. Comparison of (a) fire-damaged region (b) char layer (c) area between char layer and unburned composite (d) delamination cracks (e) unburned composite resin-rich area.

1.3 Motivation

The causes of in-flight fires are well understood, and the Federal Aviation Administration (FAA) and other aviation authorities have set strict fire safety standards. Consequently, in-flight fires on commercial and General Aviation (GA) aircraft are very uncommon (Mouritz & Gibson, 2007).

Non-fire-related aircraft crashes, however, can result in major post-crash fires on the ground. For example, after an aircraft crash, fuel tank ruptures may allow direct contact between fuel and ignition sources (electrical circuits, engines, etc.) (Wood & Sweginnis, 1995).

Post-crash fires involving composite aircraft structures are very undesirable for two main reasons. First, burning composites can generate thick toxic gases and smoke that can delay and jeopardize aircraft evacuation, as well as pose a serious health risk to passengers and emergency personnel (Mouritz & Gibson, 2007). Second, post-crash fires can dramatically alter the exposed surfaces of mechanically failed structures in ways that inhibit post-crash forensic analysis and impede accident reconstruction analyses. The latter issue is the primary focus of this research. In essence, the formation of char and other thermal by-products due to post-crash fires can mask relevant aspects of the structural damage morphology and other evidence necessary to identify the underlying failure mechanisms that caused the crash (Wood & Sweginnis, 1995; O'Donnell, 2009).

Similar to metals, composite failure surface fractography can be used to identify operative failure mechanisms crucial for post-crash forensic analyses and aircraft accident reconstruction (Rakow & Pettinger, 2007). Each relevant failure mode (interlaminar tension, interlaminar shear, translaminar tension, translaminar compression, translaminar flexure, etc.) has specific macroscopic and microscopic fractographic features. Table 1 (Kar, 1992) summarizes typical fracture characteristics for different laminated composite material failure modes.

Table 1. Typical Fracture Characteristics for Different Failure Modes

Failure Mode	Macroscopic Features	Microscopic Features
Interlaminar ¹ tension	Smooth, glassy fracture surface.	Smooth surface, river marks, resin microflow.
Interlaminar shear	Flat surface with milky appearance under oblique lighting.	Rough surface, straight lines of parallel hackles.
Translaminar ² tension	Rough, jagged fracture surface with individual fibers protruding from the surface.	Fiber end fracture, fiber pullout, radial marks at the fiber ends.
Translaminar compression	Extreme surface damage, very few fibers protruding from the surface.	Fiber micro-buckling for thin laminate, fiber ends show radial topology (tension) and smooth/ratcheted topology (compression) separated with a neutral axis, fiber ends with slanted shear type failure for thick laminate.

Failure Mode	Macroscopic Features	Microscopic Features
Translaminar Flexure	Two distinct regions, exhibiting translaminar tension and compression separated by a neutral axis.	Both translaminar tension and compression features.
¹ Interlaminar is used to connote failures between plies.		
² Translaminar refers to axial failures in the local fiber direction (fracture, micro-buckling, etc.).		

When fractured composite specimens are exposed to extremely high temperatures due to fire or elevated heat fluxes, the char, and other carbonaceous residues deposited on the fracture surface and broken fiber ends can mask key features necessary to characterize the nature of the original mechanical failure, as described in Table 1. For instance, Figure 4 compares SEM images before and after burning a 21-ply cross-ply Cytec specimen failed in compression. Before fire exposure, shown in Figure 4(a), the characteristic compressive fracture surface features are visible. These include “chop” marks on broken fiber surfaces that demarcate the transition between tensile and compressive failure in individual fibers (i.e., neutral axis), and matrix debris at the fractured surface. These critical features can be obscured or destroyed after fire exposure; large-scale char formation on the broken fiber ends and extensive matrix decomposition, as shown in Figure 4(b) impede traditional fractographic assessments of mechanical failure. The goal of research is to investigate techniques for char removal that will enable the identification of relevant mechanical failure mechanisms and facilitate forensic analysis of composites exposed to post-crash fires. This research aims to clarify the mechanisms responsible for thermal damage and char formation in mechanically failed aerospace composite specimens. The nature and formation of char and damage due to direct contact with open flames needs to be investigated by performing a series of fire-exposure experiments in various orientations/exposure times. Finally, an effective surface cleaning strategy must be devised to remove the generated char for subsequent failure surface characterization and failure identification. In the following section, a concise review of various surface treatment strategies will be presented. Since research on removing burned residue from plastic/composite substrates is limited, the section will focus on a generalized discussion of commonly used surface cleaning protocols, with a specialized focus on ultrasonic cleaning.

It should be noted that the small-flame type used in this research is more typical of a small-flame ignition, like those that would be seen due to spilled chemicals during maintenance or short-circuit ignitions. It is not what you would expect in a post-crash aircraft fire. In an actual post-crash fire event, it is likely that the intensity of a pooled fuel fire will have much higher intensity, with carbon fibers completely decomposed. There is unlikely to be any residual char on fractured

fiber ends, and remaining structure some distance away from the fracture surface may also be decomposed.

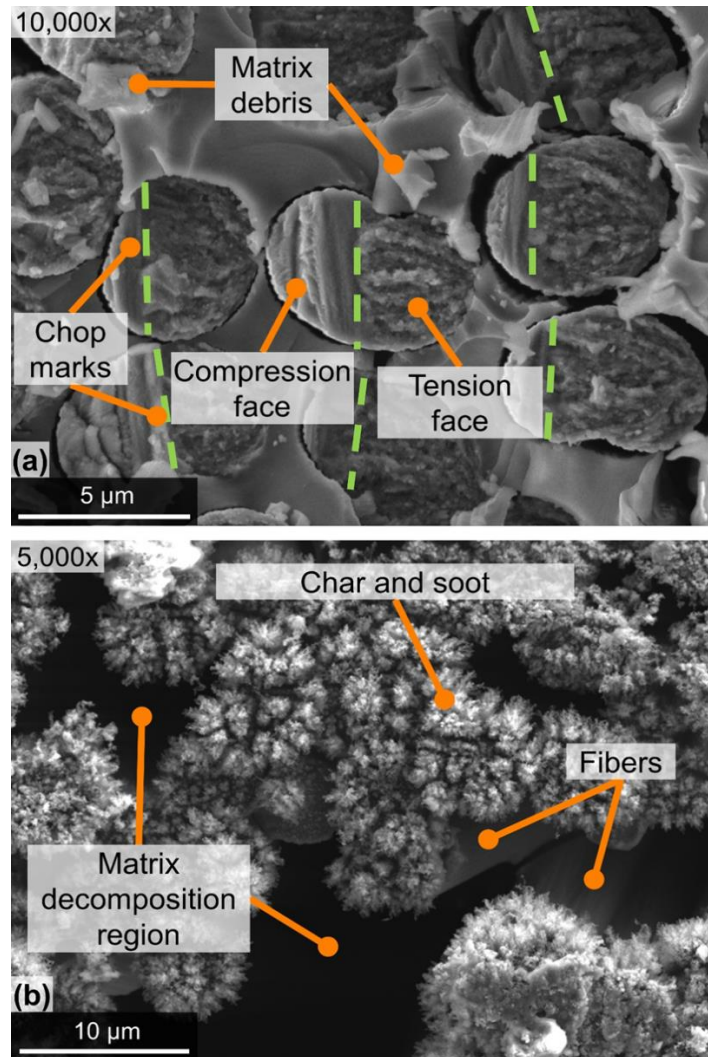


Figure 4. Comparison of 21-ply cross-ply Cytec specimen failed in compression after vertical burning

1.4 Overview of surface cleaning and char removal techniques

The development of effective char removal techniques for the surface treatment of a fire-exposed composite structure is essential in fire forensic analysis. Research on the removal of burned residue from plastic/composite substrates is limited; however, a few authors published cleaning procedures for carbon-based materials. Tagawa et al. (2010) used ultrasonication to remove carbon-black coatings from three polymer film substrates—polyethylene, nylon-6, and cellulose acetate. A quartz crystal microbalance (QCM) sensor was used to measure the carbon amount deposited on the polymer films. A water/ethanol mixture was used as the detergent for the

ultrasonic cleaning. They found that penetration into the interface between particle and substrate played an important role in the cleaning process (Tagawa & Gotoh, 2010).

Rinaldi et al. (2011) used sonication to remove amorphous carbon from carbon nanotubes (CNTs). As received and mildly washed, carbon nanotubes were subjected to sonication in a 10% aqueous ethanol solution with a probe-tip sonicator. The mildly washed CNTs were washed with 3M nitric acid (HNO₃). After sonication, the obtained solid was washed with 1M sodium hydroxide (NaOH) to dissolve the oxidized amorphous carbon and other debris. It was found that the acid wash does not affect the structural integrity of the CNTs. The overall process was easy-to-handle, non-corrosive, eco-friendly, and fast (Rinaldi, Frank, Su, Hamid, & Robert, 2011). The following paragraphs will briefly review the nature of contaminants, commonly used chemical and physical surface cleaning processes used for metallic/polymer surfaces, and the applicability of these techniques for char removal.

The cleansing of surface contaminants using solvents and other chemical cleaners is essential for many industrial applications (Kohli & Mittal, 2015). Surface contaminants are a cause for concern because their presence often results in the degradation of the substrate properties and can even lead to the failure of critical components. This property degradation is mainly due to the generation of contaminants through induced chemical, mechanical, or physical phenomena or deposited as foreign matter from adjacent surroundings. They often adhere to the part surface under the action of high mechanical forces (Kohli & Mittal, 2009). Contaminants can be broadly categorized into two kinds: films and particulates (Calle, et al., 2008). Film contaminants are usually deposited in layers along the substrate. They are a form of molecular contamination such as organic (hydrocarbon) or inorganic (acid, base, and ionic (Na⁺, K⁺, Cl⁻, F⁻)) (Kohli & Mittal, 2018). Particulate contaminants usually range from various particles like film fragments, biological residue (dead skin, hair), soot, dust, glass, and plastics. In either case, contaminants of the size range 1 nm – 100 μm are usually the subject of specialized cleaning procedures—since contaminants bigger than 100 μm can be removed using filters. Contaminants smaller than 1 nm are too small to cause impurity related failures (Kohli & Mittal, 2018). Fire by-products like char and soot are generated through complex thermochemical reactions and are strongly bonded to the fire-exposed surface. The polymer char-morphology can be considered a layered film of carbonaceous residue, whereas soot particles are particulate contaminants (Ray & Kuruma, 2019; Levchik & Wilkie, 2000). Surface characterization of substrates contaminated from particulate soot due to the burning of thermoset and thermoplastic polymers reveals that the burned residue (size ranging between 1 nm and 100 μm) is a cause for concern due to contamination-related failures (Shemwell & Levendis, 2000). Moreover, a persistent layer of char on the composite surface would effectively mask the salient fracture surface features (Greenhalgh, 2009).

A variety of contaminant removal techniques will be reviewed in this section to obtain a robust understanding of the advantages, disadvantages, and challenges in using these techniques for char removal from burned aerospace composites.

1.4.1 Chemical cleaning processes

1.4.1.1 Overview of chemical cleaning processes

Surface cleaning processes involve removing surface contaminants with an organic solvent without physically or chemically changing the underlying substrate (Ebnesajjad & Landrock, 2014). Solvent soaking is defined as immersing the contaminated part in the organic solvent for specific immersion times. Additional surface cleaning processes include vapor degreasing and ultrasonic cleaning (Snogren, 1969). Vapor degreasing involves scrubbing the part with hot solvent vapors to remove oils, greases, waxes, and other particulate matter contaminants from metallic or non-metallic surfaces. The vapors are initially made to condense on the part surface. Eventually, the depositing vapors condense into liquid at a high rate resulting in the dissolution and washing away of the contaminants. The condensed liquid containing the contaminants is then drained off by gravity. However, the effectiveness of vapor degreasing is limited by heavy contamination on the candidate surface (Ebnesajjad & Landrock, 2014). In such cases, ultrasonic cleaning or degreasing can be adopted as an alternative cleaning method.

1.4.1.2 Ultrasonic cleaning processes

Sonication technology has been predominantly used as an effective precision cleaning process to remove metallic, organic, film-based, and other particulate contaminants in multiple industrial applications (Ranade, 1987; Cooper, 1986; Menon, 2018). Sonication uses acoustic waves to promote acoustic cavitation—a phenomenon in which vacuum bubbles are initially created in locations where negative pressures are induced due to the rarefaction of the liquid. The formation of vacuum bubbles is due to the extension of liquid molecules outward within the medium against their natural attraction forces. With the passing of the acoustic wavefront, these vacuum bubbles grow until they become unstable and eventually collapse violently. The resulting implosions cause shock waves to be radiated across the solvent from the cavitation sites. Sonication irradiation releases a tremendous amount of energy into the medium, with highly localized pressures and temperatures of 10,000 psi and 10,000°F, respectively. However, these extreme conditions are sustained for extremely small-time scales since acoustic cavitation is generated in the order of microseconds (Awad S. B., 1996; Kanegsberg & Kanegsberg, 2011). A schematic of the cavitation process is shown in Figure 5. Cavitation is classified into two types, stable and transient, and is dependent on the operating frequencies during sonication. Stable cavitation occurs at higher operating frequencies (60-80 kHz) with smaller bubbles and lower

oscillations (about the size of a bubble radius). In comparison, transient cavitation occurs at lower frequencies (20-40 kHz) with larger bubble sizes and is usually a violent phenomenon (Atchley & Crum, 1985; Tuziuti, 2016).

Ultrasonic cleaning is achieved through two mechanisms; acoustic cavitation and acoustic streaming, as illustrated in Figure 5. When the cavitation bubbles implode, the resulting shock waves lead to microscopic jets of liquid impinging on the stained surface. The high-velocity jets clean the surface, chipping away at the contamination, and transporting additional solvent to the contaminated surface (Awad & Nagarajan, 2010). Acoustic streaming is the bulk movement of liquid due to the transfer of acoustic waves within the solvent. During this process, the sonication residues are also transported away from the clean surfaces to prevent particle redeposition.

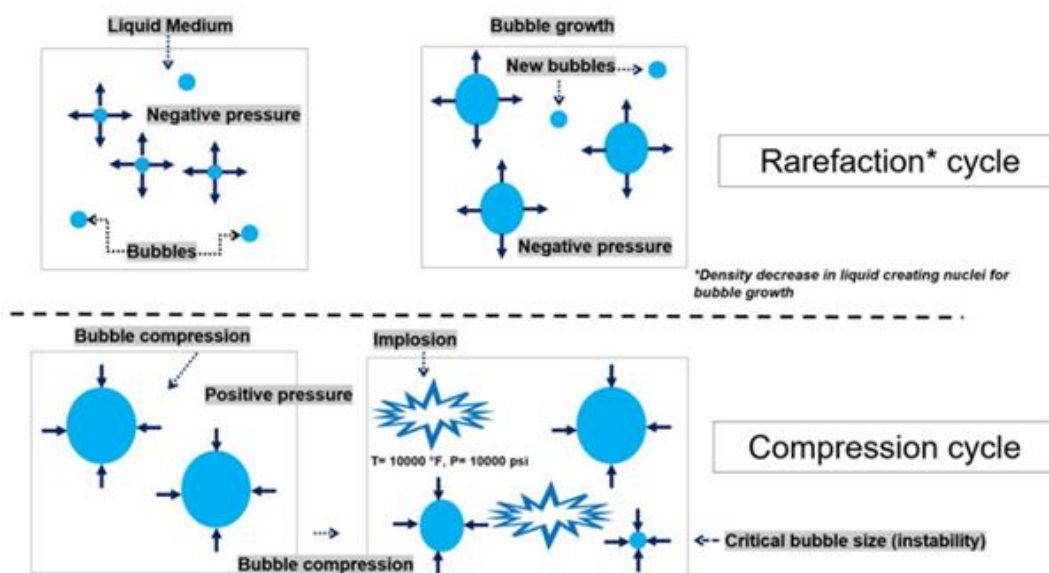


Figure 5. Schematic of cavitation action during ultrasonication

1.4.1.3 The role of solvent selection in ultrasonic cleaning and char removal

Solvent selection plays an important role in ultrasonic cleaning. Cleaning agents are generally divided into aqueous solutions and non-aqueous (organic) solvents (Kanegsberg & Kanegsberg, 2011). Organic solvents with higher viscosities and surface tension have higher cohesive energies, leading to difficulties in cavitation initiation (Mason, 1998; Santos, Lodeiro, & Capelo-Martinez, 2009). Most organic contaminants (long, medium, and short-chain) can be removed using organic solvents by two mechanisms. The first mechanism is the dissolution of the organic contaminant in the solvent. The molecular structure of the solvent influences the degree of solubilization of the contaminant. The second mechanism involves the displacement of the contaminant particles from the substrate by a surfactant. This process is known as detergency. The surfactants can also form aggregates known as micelles, which encapsulate the sonication

residue to avoid redeposition (Awad S. B., 1996). Moreover, the strong hydro-mechanical forces within the solvent during cavitation may aid in the chemical breakdown of the contaminant due to the generation of free radicals ($\text{H}_3\text{C}\cdot$, $\text{OH}\cdot$, $\text{HO}_2\cdot$) (Riesz, Berdahl, & Christman, 1985), that are highly reactive (Prasad, Vithanage, & Kapley, 2019) and could provide pathways for controlled reduction/oxidation required to initiate the chemical breakdown of char and soot deposits from the burned composite surface. Secondary sonication events such as shock waves, micro-jets, and shear forces facilitate particle removal through physical means.

The development of a multistage surface cleaning process for char and soot removal from burned aerospace composites can help in the fractographical assessment of the underlying damaged surfaces. Adopting a pretreatment stage like quenching, where the burned specimen is suddenly exposed to a drastic change in temperature results in thermal shocks. These thermal shocks lead to the induction of shear forces between the contaminants and the underlying substrate leading to a more effective particle removal (Wang, Singh, & Lowden, 1997). Therefore, an effective chemical surface treatment process for effective removal of char and other fire by-products from the burned carbon reinforced epoxy composite surface will involve a pretreatment stage where the sample is prepared for cleaning, the cleaning stage where the char and soot deposits are actively removed, a rinsing stage to avoid particle/solvent redeposition, and a drying stage for preparation of the sample for surface characterization. Alternatively, thermal-based techniques commonly used in the composite recycling industry (Yang, et al., 2012) can also be explored for char and soot removal from the polymer composite surfaces.

1.4.2 Thermal-based techniques for char removal from aerospace composites

Several thermal-based techniques exist for removing cured thermosetting matrices from the surrounding fiber preforms. For carbon/epoxy composites, these include standard “matrix ignition” approaches for fiber volume fraction determination (ASTM-D2584-18, 2018), as well as approaches aimed at recycling carbon fibers from discarded thermoset composites (Fernández, Lopes, González, & López, 2018; Yang, et al., 2012). Such approaches may prove useful in removing char, melt dripping, and other fire by-products from carbon filament-ends in a manner that aids fractographic assessments of broken fibers. In matrix ignition techniques, the thermoset matrix is completely burned off, which allows the visual examination of the fibers and laminate architectures (ASTM-D2584-18, 2018). The American Society for Testing and Materials (ASTM) standard ignition-loss test method for cured reinforced thermoset resins is used to determine the mass fraction of matrix and fiber. Essentially, a crucible is heated to 500-600°C for 10 min or more, cooled at room temperature, and then weighed to the nearest 1.0 mg. A composite specimen is placed in the crucible, and the specimen/crucible combination is weighed.

The crucible is heated in an open flame using a Bunsen burner until complete combustion of the specimen matrix occurs, and only ash and carbon fibers remain. The filled crucible is then reheated in a furnace at 565°C to remove all the carbonaceous residues due to initial burning. The duration of each heating step is highly dependent on the sample geometry. Finally, the sample and crucible are cooled to room temperature inside a desiccator and then weighed to assess mass loss due to matrix ignition.

Similar pyrolysis-based techniques are used to recycle carbon fibers to damage the fiber surfaces (Fernández, Lopes, González, & López, 2018; Yang, et al., 2012). Such processes involve the thermo-chemical decomposition of a composite organic matrix at temperatures of 450-700°C in an inert environment. The temperature levels are dependent on the thermosetting matrix. For polyester matrix and epoxy matrix composites, pyrolysis reactions are performed at 450°C and up to 550°C, respectively (Yang, et al., 2012). Due to the high pyrolysis temperatures, char is deposited on the surface of the recycled fibers.



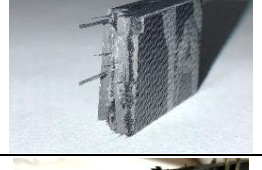

Consequently, pyrolysis is usually combined with an oxidation process to remove char and obtain clean fibers. The coupled pyrolysis/oxidation is performed using specialized thermolysis equipment, consisting of a heating system (for pyrolysis) and a gas condensation device (for oxidation). The oxidation time should be carefully optimized to avoid the degradation of the carbon fibers. While not part of this research, thermal-based approaches appear to be promising techniques for char removal from aerospace composites.

2 Pre-fire fractographic analysis of mechanically failed graphite/epoxy composite specimens

Many mechanically failed Cytec specimens were obtained from the National Institute for Aviation Research (NIAR) to perform post-failure fire forensic analyses. The specimens were fabricated and oven-cured following the National Center for Advanced Material Performance (NCAMP) Process Specification (NPS) 81323 cure cycle 'C' (Kwan, MacCleod, Ng, & Tomblin, 2007). The graphite/epoxy composite specimens were mechanically tested at NIAR per the ASTM standards at ambient conditions (Clarkson, 2012; Man, Ng, Tomblin, & Hooper, 2012). These samples included unnotched tension (UNT0), unnotched compression (UNC0), short beam strength (SBS), and in-plane shear (IPS) specimens. Many of the SBS and IPS specimens were not completely severed during initial mechanical testing at NIAR. For this study, these specimens were subsequently loaded under displacement control conditions to completely rupture the specimens and facilitate the SEM imaging of the fracture surfaces. Table 2 summarizes the mechanical test standard, layup, number of plies, and fiber volume fraction for

each specimen type and shows a typical laboratory-scale picture of a mechanically failed half-sample for each specimen.

Table 2. Summary of the properties of mechanically failed Cytec specimens

Type	Test standard	Layup	Number of plies	Fiber volume fraction	Specimen image
UNT0	ASTM D3039	[0/90]3S	12	57.22%	
UNC0	ASTM D6641	[90/0/90]7	21	57.40%	
SBS	ASTM D2344	[0]45	45	56.33%	
IPS	ASTM D3518	[45/-45]4S	16	56.12%	

Fractography of mechanically failed graphite/epoxy specimens was performed using a TESCAN FERA-3 Model GMH scanning electron microscope. This microscope uses a Schottky field-emission electron source to provide an enhanced image resolution. It has a large chamber that can fit specimens of dimensions up to $5 \times 5 \times 10 \text{ cm}^3$ (W \times L \times H). The FERA-3 microscope can deliver a beam of energy of up to 30 kV at a high vacuum (Hrncir, et al., 2012). Since graphite/epoxy composite materials are less conductive than metals, a low beam voltage of 5 kV was used to reduce electron charge build-up on the specimen surface, hence, improving the resolution of the micrographs. In general, improved composite material SEM image resolution was obtained by using a low beam intensity (i.e., decreasing the number of electrons passing through the probe); a short working distance (WD) between the final pole piece of the lens and the specimen fracture surface; and a slow-scanning speed for image acquisition. For this study, the FERA-3 microscope parameters used included a beam accelerating voltage of 5 kV, a low beam intensity of 8, a scanning speed of 7 with an image acquisition time of 45 s, and a WD of 9 mm. In the case of specimens with large variations in the fracture surface geometry, such as the IPS specimens included in Table 2, the WD was increased to prevent damage to the microscope

lenses. Also, wide field of view micrographs of the fracture surfaces for each specimen type were obtained at a WD greater than 9 mm.

A high-vacuum evaporator was used to sputter coat deposit a thin layer of carbon particles approximately 3 nm thick on the fracture surface of the graphite/epoxy composite specimens to facilitate the flow of electrons and prevent charge build-up during microscopy. The sputter coater setup consisted of a carbon rod mounted between two electrical electrodes, as shown in Figure 6. The coating process is initiated by electrically charging the sputtering cathode, which forms a plasma, causing carbon particles to be ejected from the carbon rod and deposited onto the specimen. The coating layer was thin enough to prevent obscuring the fine details on the specimen fracture surface while providing a conductive path for the impinging electrons. Each specimen was then mounted on a pin stub and electrically grounded using carbon tape to inhibit charging the specimen fracture surface. The following subsections discuss the fractographic failure features of mechanically failed UNT0, UNC0, SBS, and IPS graphite/epoxy specimens before fire testing.

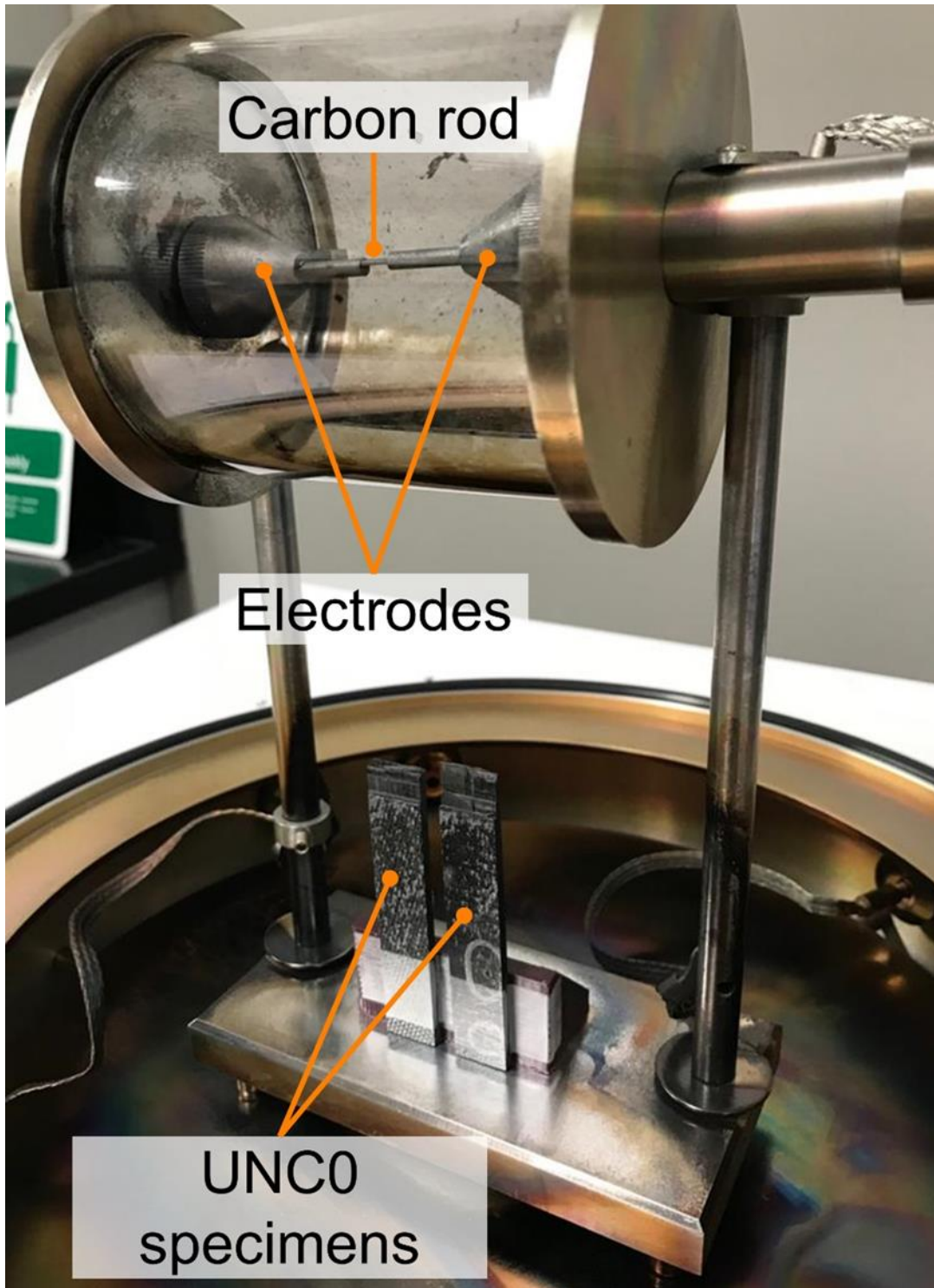


Figure 6. Typical high-vacuum sputter-coater setup

2.1 Fractographic imaging of ASTM D3039 UNT0 graphite/epoxy specimen failure surfaces

ASTM standard D3039 tensile testing was performed at NIAR on cross-ply $[0/90]_{3S}$ T40-800/5215 graphite/epoxy UNT0 specimens under ambient conditions (Clarkson, 2012; Man, Ng, Tomblin, & Hooper, 2012). As part of the current study, UNT0 specimen fracture surfaces were examined using a FERA-3 microscope to document the tensile failure features. As mentioned earlier, the ultimate goal is to assess and validate the efficiency of char removal techniques by comparing the fracture surface morphologies of the mechanically failed specimens before and after fire application and char removal. Figure 7 shows a low magnification ($100\times$) SEM micrograph of a representative UNT0 specimen (half sample) fracture surface before fire testing. Tensile failure of the 0° -plies resulted in an uneven fracture surface with multiple fiber pull-outs and large numbers of individual fibers protruding from the fractured surface. These results are consistent with those reported throughout the literature (Naito, 2018; Kumar, Raghavendra, Venkataswamy, & Ramachandra, 2012; Hernandez, Soufen, & Orlandi, 2017).

In contrast, tensile failure of the 90° -plies tended to result in relatively flat fracture surfaces parallel to the fiber directions. For UNT0 cross-ply specimens, the 90° -plies do not contribute significantly to the load-carrying capability of the composite and become susceptible to transverse cracking before laminate failure. As the axial load is monotonically increased, the 0° -plies carry most of the applied load, whereas the 90° -plies progressively fail due to transverse matrix cracking. This process will typically continue until a saturation density of transverse cracks occurs, followed by the onset of delamination between 0° - and 90° -plies (or ply splitting), subsequent fiber fractures in 0° -plies, and ultimate composite failure. Figure 8 shows a $2500\times$ magnification SEM image of a UNT0 specimen fracture surface. Tensile fractures of 0° -fibers are visible, with evidence of 0° -fiber pull-outs and ply splitting.

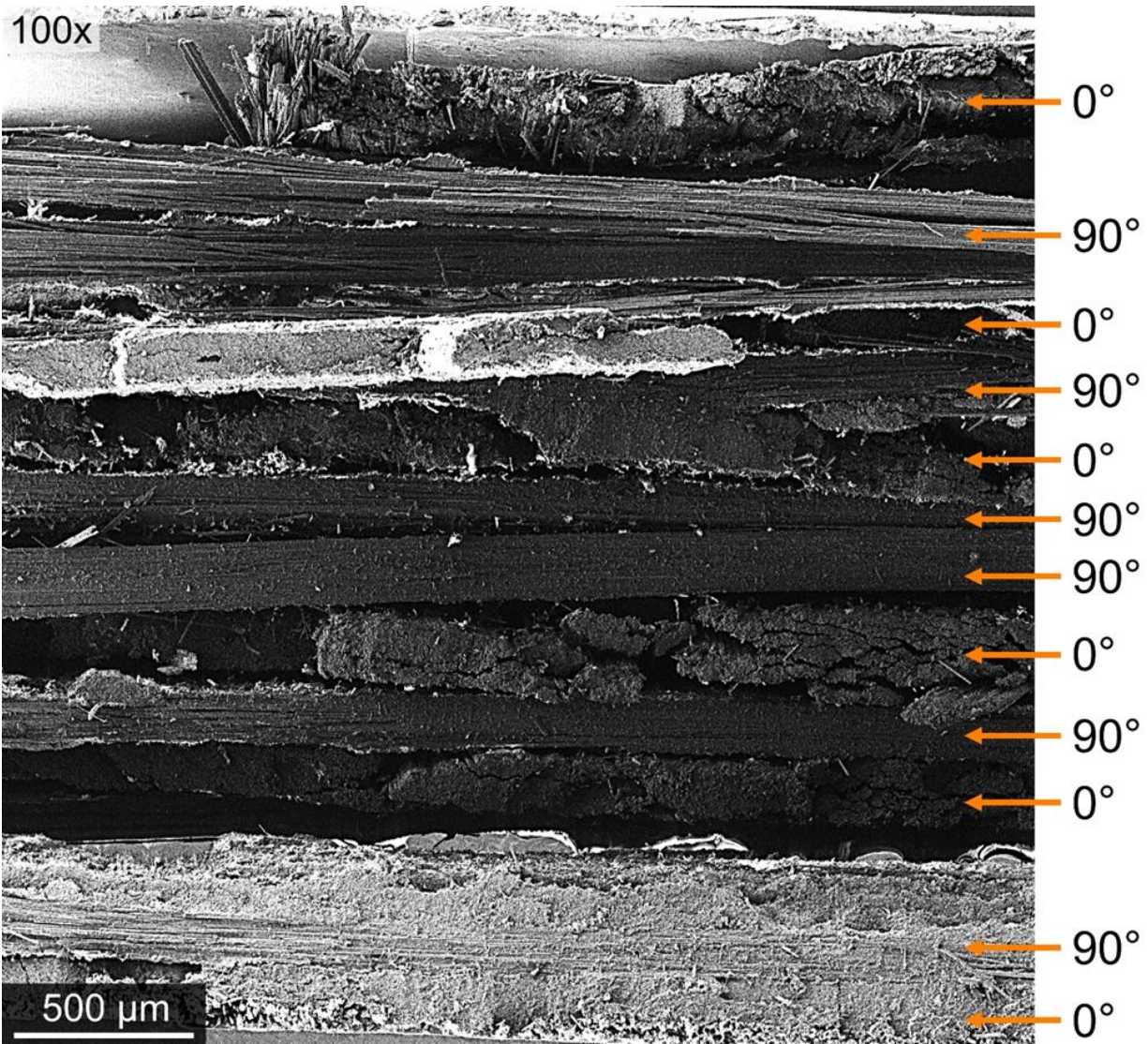


Figure 7. Low magnification SEM micrograph of graphite/epoxy UNT0 specimen fracture surface

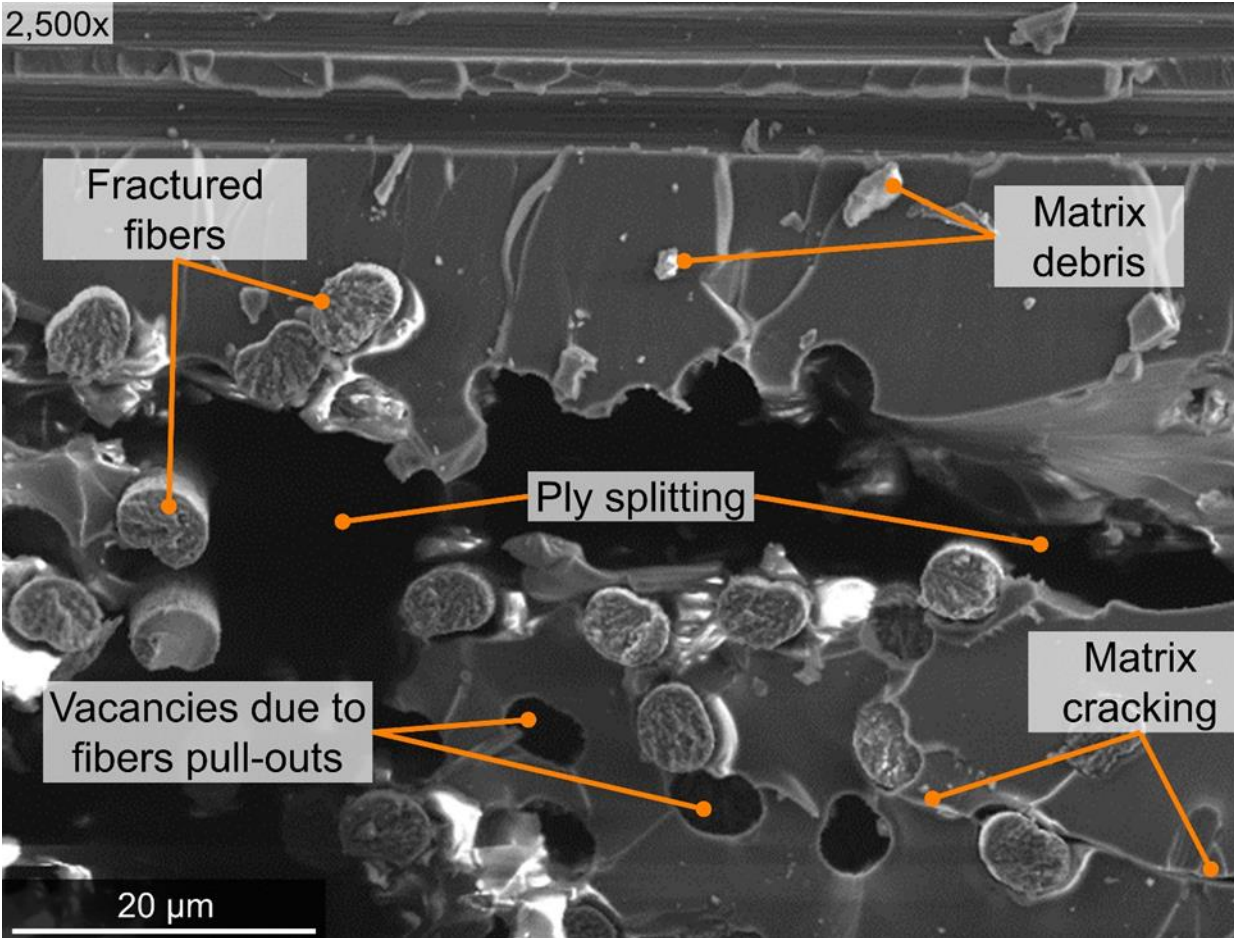


Figure 8. SEM micrograph of a graphite/epoxy UNT0 specimen showing tensile failure features

Tensile cleavage failure of individual 0° -fibers generally involves crack initiation at a local defect along the fiber outer circumferential surface, followed by brittle crack propagation across the fiber's diameter. Such fibers will tend to fail in local clusters about a common fracture plane. For example, Figure 9 shows typical fracture surfaces from a 0° -ply in a UNT0 graphite/epoxy specimen. The white arrows shown in Figure 9a indicate the crack propagation directions for a family of fractured graphite fibers. Figure 9(b) shows a magnified view ($20,000\times$) of an individual broken graphite filament. The tensile fracture surface is characterized by a rough appearance with radial lines emanating from the crack initiation site (o) and oriented along the local crack growth path, as suggested by the white arrows shown in Figure 9(b). Such radial marks are typical of tensile graphite or carbon fiber failures in laminated continuous fiber composites (Kar, 1992).

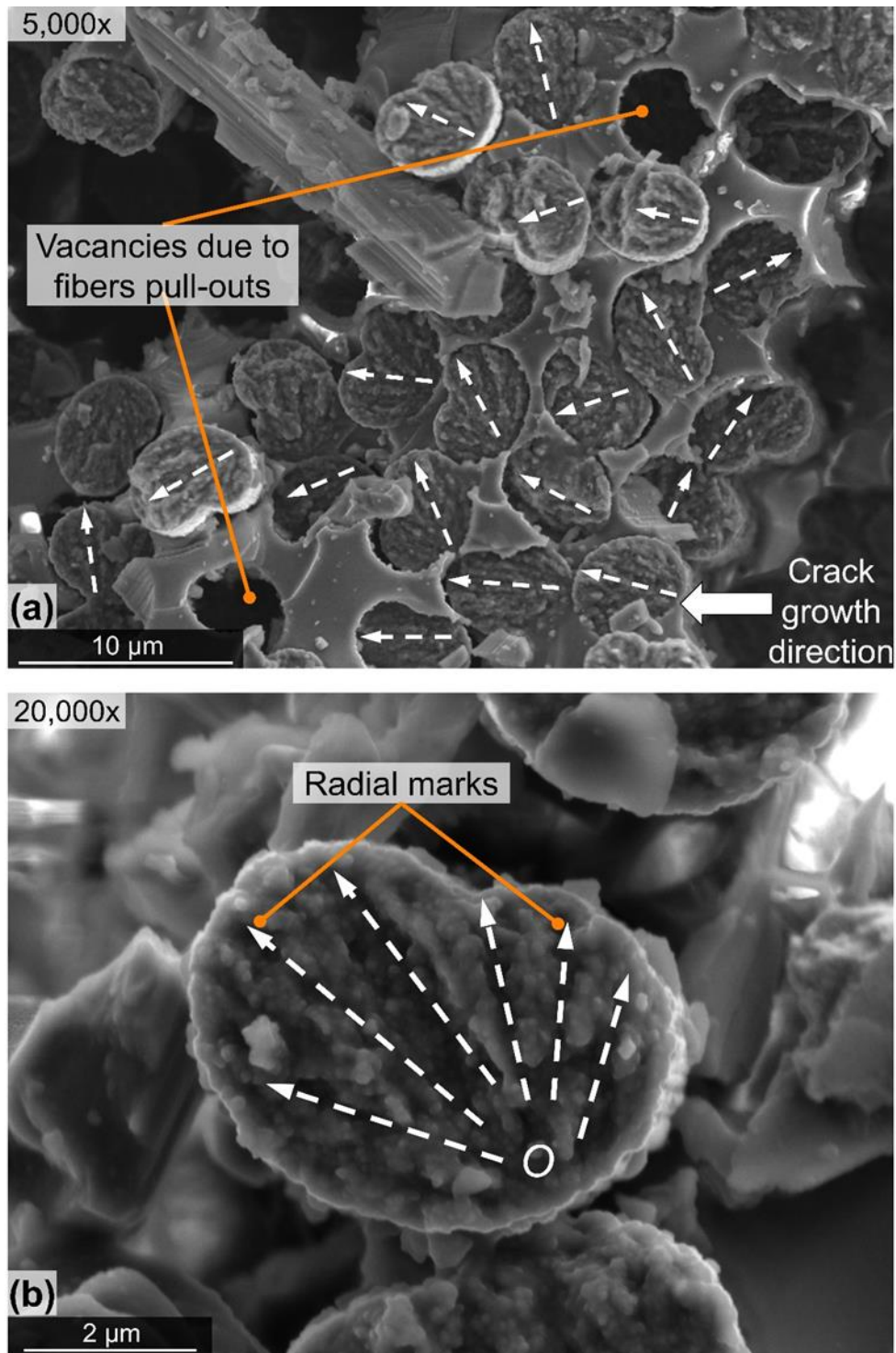


Figure 9. SEM micrographs of a graphite/epoxy UNT0 specimen tensile failure with (a) fibers pull-outs and (b) radial marks

Similarly, Figure 10 shows a micrograph of a failed 90°-ply in a UNT0 specimen. Such failure surfaces typically contain transverse cracking, troughs where individual 90° fibers have been pulled away from the underlying matrix, along with shear-induced ‘hackles’ where the matrix has failed in-between the fibers (Gilchrist & Svensson, 1995). The individual hackles (cusps) have a flake-like appearance. Groups of hackles can overlap in a shingle-like fashion in a direction parallel to the fibers (Liechti, Masters, Ulman, & Lehman, 1982). The direction of overlaps is indicative of the local shearing deformation in the matrix during failure. Hackles form on both fracture surfaces and have a consistent tilt inclination direction on each surface. For example, the yellow half-arrow shown in Figure 10 defines the hackles’ tilt orientation on one fracture surface, which indicates the relative local shearing direction. The local shearing direction on the mating fracture surface would have the opposite sense to the one shown in the figure. The cusps can be used to identify the crack propagation direction in the laminate. The presence of shear-hackles in failed UNT0 specimens is generally less pronounced than for IPS or SBS specimens.

Crenulations can be observed along the 90° fiber circumferential topology in Figure 10. The T40-800 graphite fibers were produced from polyacrylonitrile (PAN) precursors. Such fibers exhibit irregular non-circular bean-like cross-sectional shapes (cf., Figure 9(b)) with narrow parallel grooves (crenulations) along the length of the fibers. These crenulations result from the PAN solution out-diffusion during the wet spinning process of the fibers.

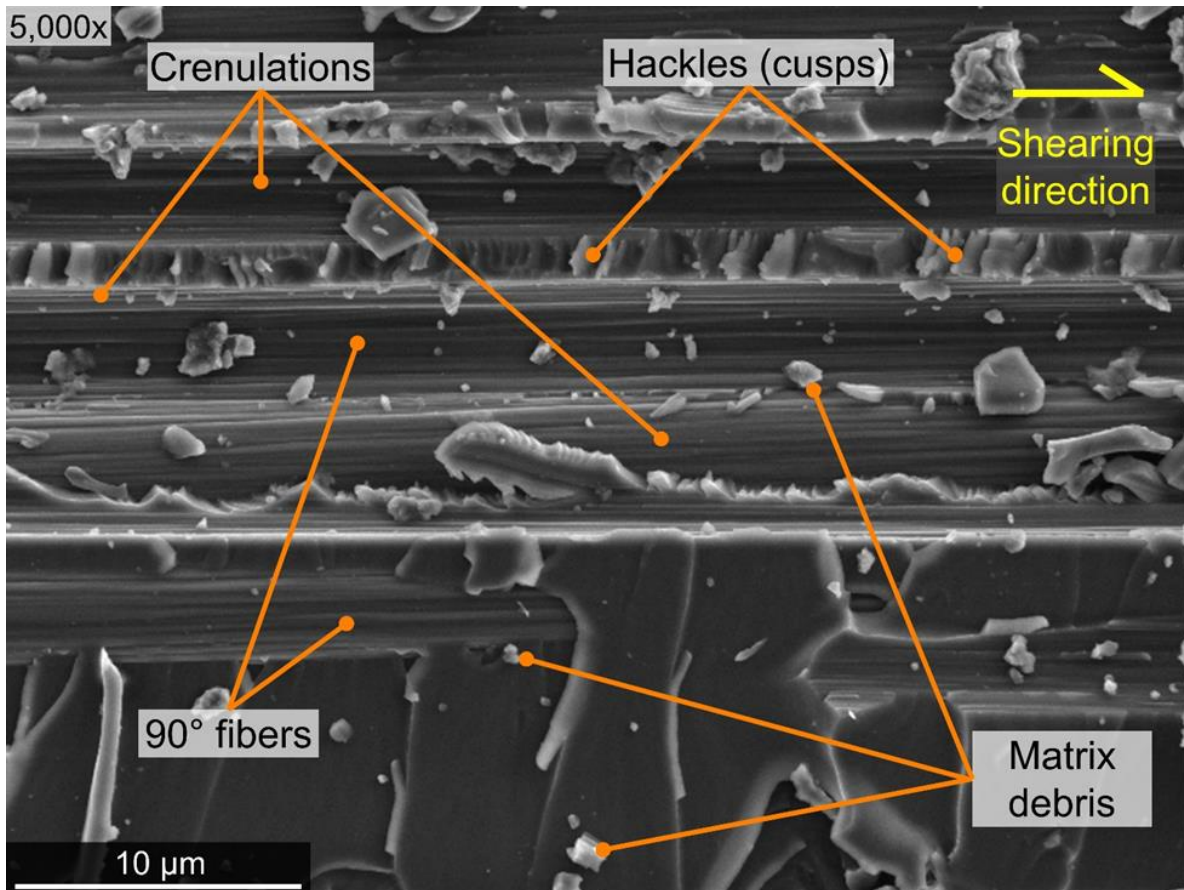


Figure 10. SEM micrograph of shear-hackles in 90°-plies of a UNT0 specimen

2.2 Fractographic imaging of ASTM D6641 unnotched compression (UNC0) graphite/epoxy specimen failure surfaces

ASTM standard D6641 compression testing was carried out at NIAR on cross-ply [90/0/90]₇ T40-800/5215 graphite/epoxy UNC0 specimens at ambient conditions (Clarkson, 2012; Man, Ng, Tomblin, & Hooper, 2012). In this work, scanning electron microscopy was performed on UNC0 half-specimens to identify compressive failure features. The purpose of these fractographic assessments was to compare the fracture surface morphologies of UNC0 specimens before/after fire testing and after char removal to validate the fire forensic analyses. Figure 11 shows a low magnification (9×) wide field of view SEM image of a representative UNC0 specimen fracture surface. As previously discussed, the tensile fracture surface in a UNT0 specimen is characterized by a rough appearance because of protruding broken fibers as shown in Figure 7. In contrast, a compressive fracture surface in a UNC0 specimen is smooth and slightly angled to the loading direction due to the induced in-plane shear, as shown in Figure 12.

Generally, compressive failure is distinct from tensile failure in a cross-ply laminate. It is characterized by several instability-related failures such as fiber-matrix interfacial debonding, followed by micro-buckled/fractured 0° fibers, kink bands, micro-buckling ‘terraces,’ matrix fracture/crushing in 90° -plies, and delamination. As the compressive load increases, the matrix cracks increase in the composite laminate, causing a cumulative weakening and ultimately complete failure. Also, delamination and buckling are more pronounced in compression. As will be discussed in later sections, extensive delamination in a composite laminate allows for more oxygen flow between separated plies, leading to extended burn duration during the fire testing resulting in more thermal damage to the underlying plies.

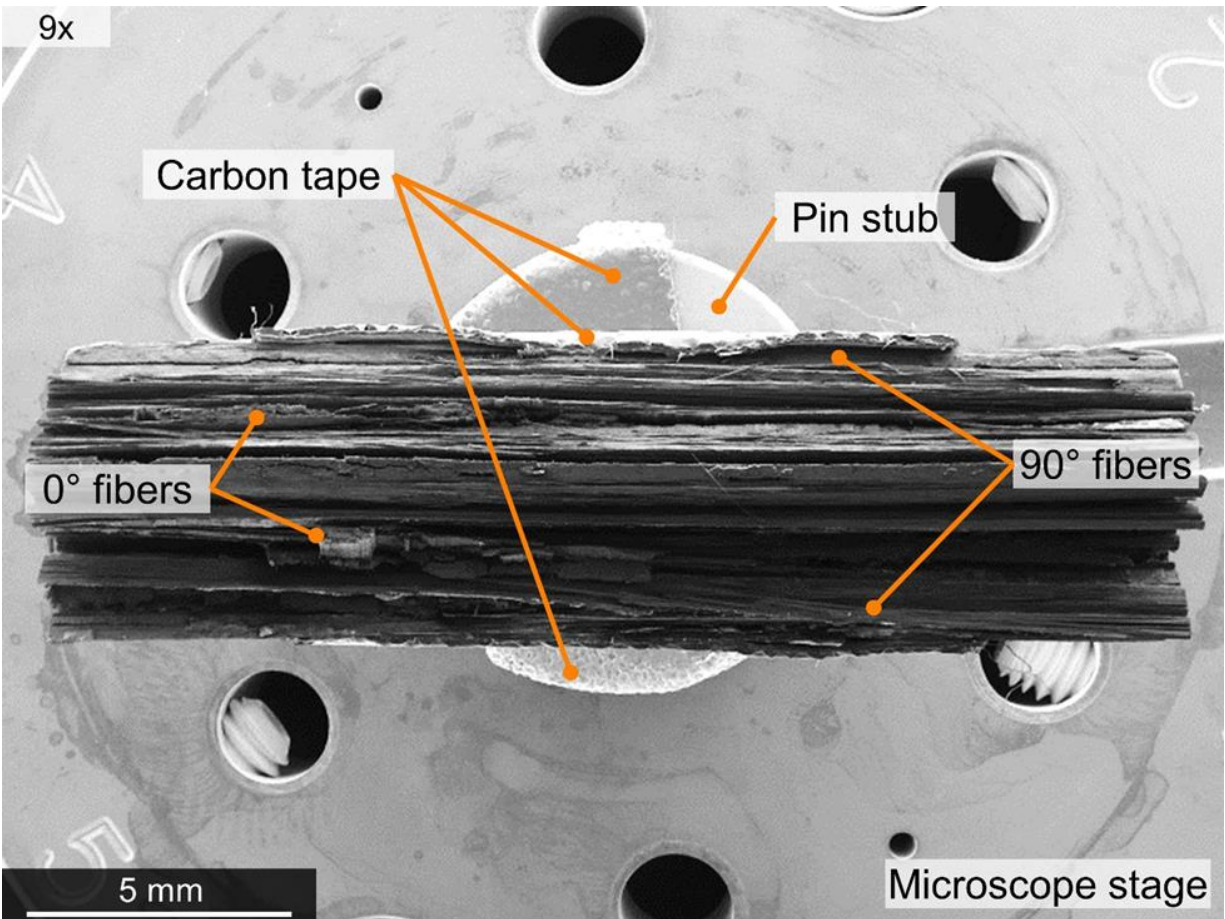


Figure 11. Micrograph of representative graphite/epoxy UNCO specimen fracture surface

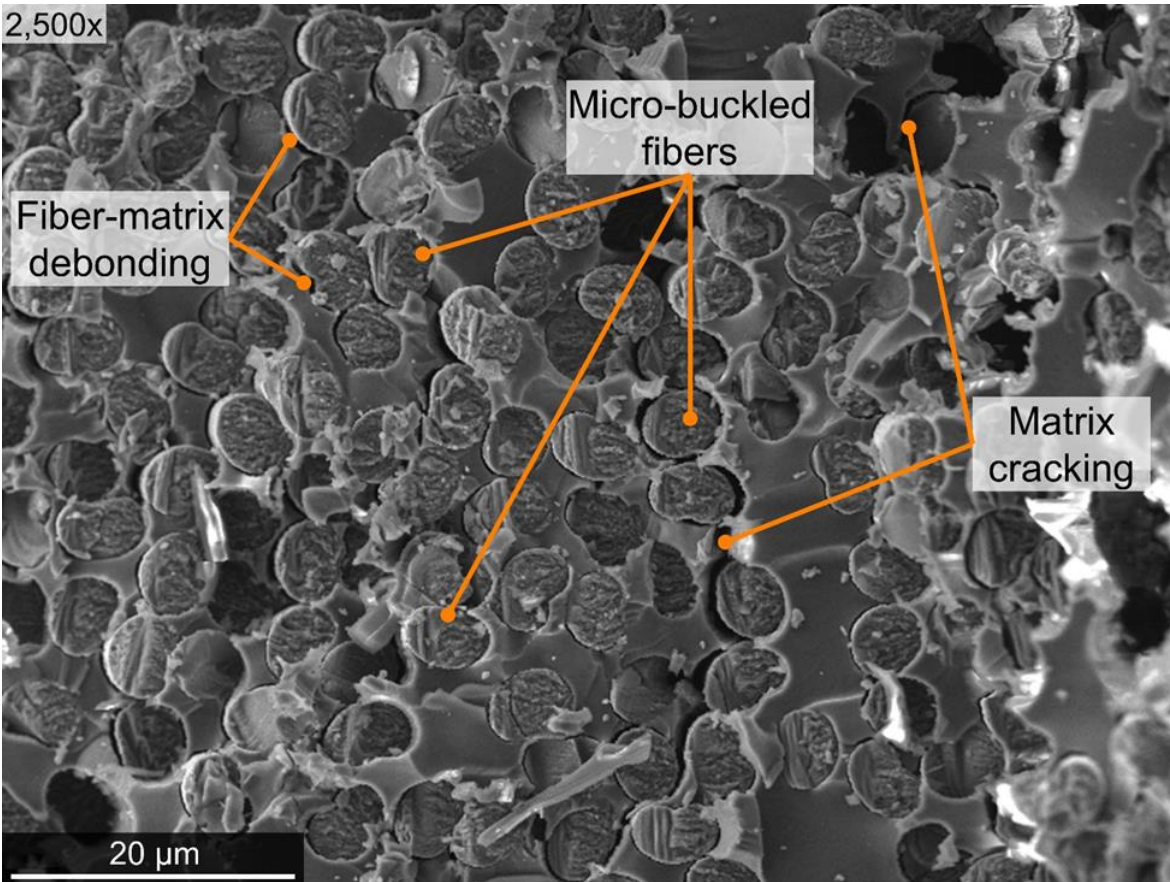


Figure 12. SEM micrograph of a typical compressive fracture surface in a graphite/epoxy UNC0 specimen

For a cross-ply UNC0 specimen subjected to uniaxial compression parallel to the 0° fibers, the damage zone may contain kink bands, or short fiber segments with dimensions on the order of 5 to 10 fiber diameters (Opelt, Cândido, & Rezende, 2018). Such failure features may occur due to local fiber instabilities (micro-buckling), weak fiber-matrix interfaces, and local fiber misalignment relative to the applied compressive load. Kink bands were observed in SEM imaging of an SBS specimen planar surface and reported in the following section.

SEM imaging of a UNC0 specimen fracture surface showed evidence of fiber micro-buckling characterized by chop mark formation on individual filament ends, as indicated by the dashed green lines in Figure 13(a). These chop marks demarcate a transition from the tensile face (rough appearance with radial marks) to compressive face (smooth surface with parallel longitudinal splits) on the fiber fracture surfaces. A high magnification ($20,000\times$) micrograph (Figure 13(b)) of an individual graphite filament suggests that the chop mark coincides with the neutral axis, where individual fibers experience combined tension and compression failures as they undergo local bending/buckling. These chop marks can be used to identify the laminate crack growth direction, as indicated by the white arrow shown in Figure 13(a).

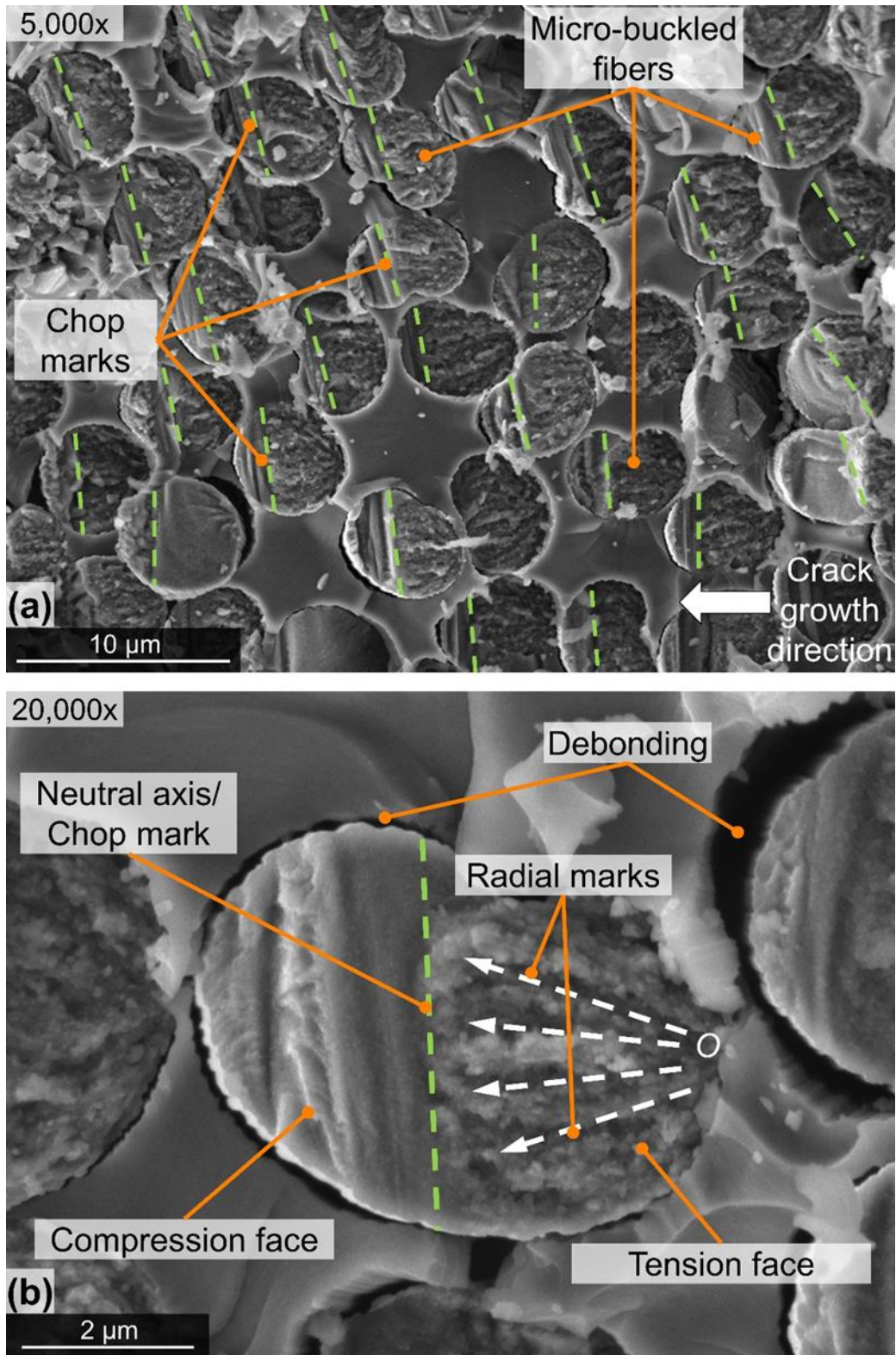


Figure 13. SEM micrographs of graphite/epoxy UNC0 showing (a) chop marks (b) individual fractured filament end

Further examination of fractured 90°-plies in UNC0 specimen shows rows of overlapping hackles that form parallel to the fibers as shown in Figure 14(a); the direction of overlap opposes the local shearing direction. Hackles indicate the existence of locally induced shearing deformation during failure of specimens subjected to macroscale compression. Unlike the tensile fracture of UNT0 specimens, compressive failure of UNC0 specimens generated an extensive amount of matrix debris, as shown in Figure 14(b), resulting from relative sliding of the mating surfaces due to compression-induced shear. Such pulverized matrix fragments can partially obscure chop marks, cusps, microcracking, fiber-matrix debonding, and other compressive damage. As will be discussed in the following sections, this debris can decompose when subjected to fire, forming a thick gooey layer over the entire fracture surface, inhibiting forensic fractography.

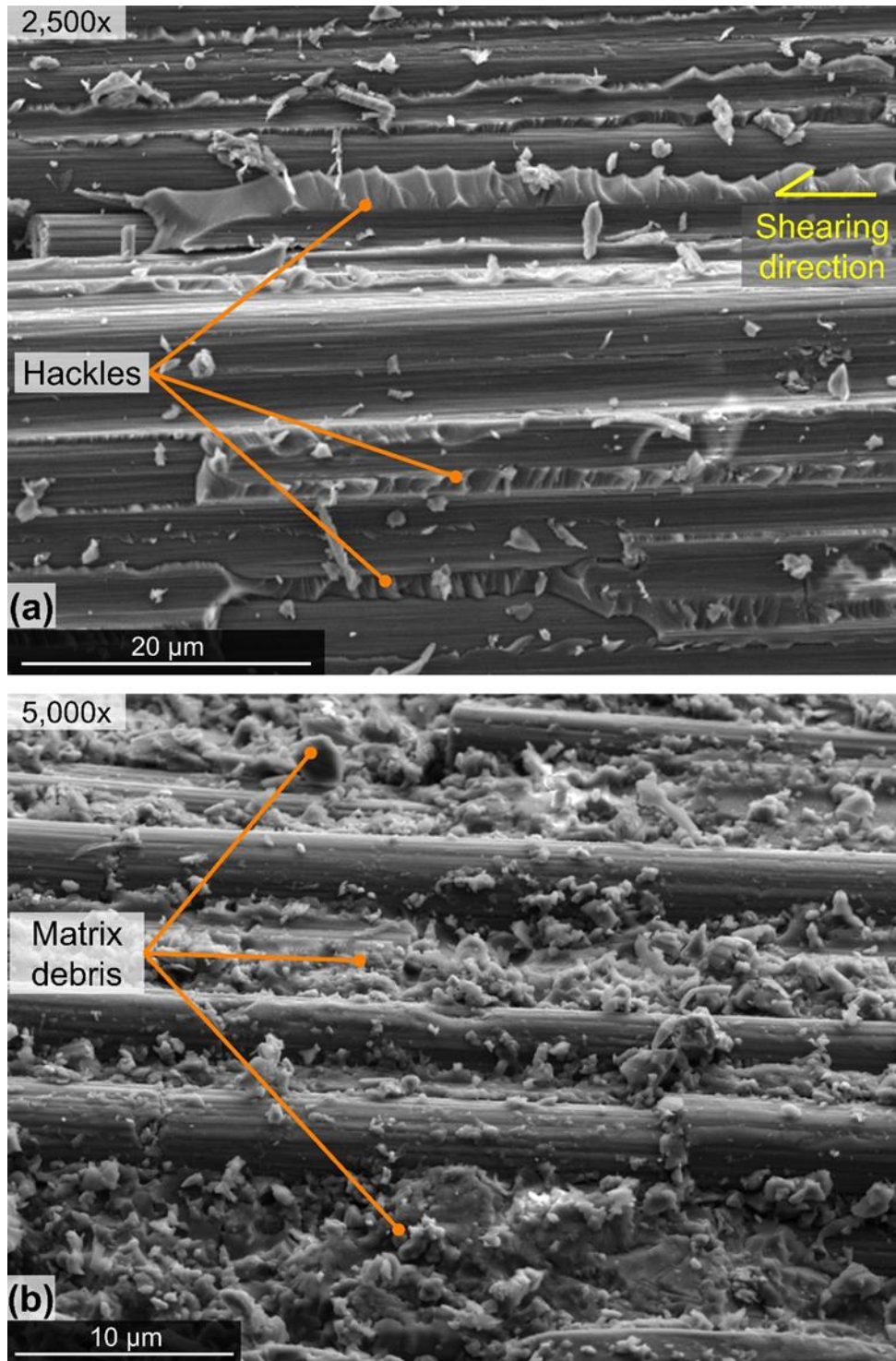


Figure 14. SEM micrographs of 90°-plies in graphite/epoxy UNC0 specimen with (a) shear-hackles and (b) compressive failure matrix debris

2.3 Fractographic imaging of ASTM D2344 SBS specimen failure surfaces

Three-point bending tests were performed at NIAR per ASTM standard D2344 at room temperature dry ($70\pm 5^\circ\text{F}$) (ambient conditions) on unidirectional $[0]_{45}$ short beam strength (SBS) T40-800/5215 graphite/epoxy specimens (Clarkson, 2012; Man, Ng, Tomblin, & Hooper, 2012). As previously mentioned, the SBS specimens were not severed during the mechanical testing at NIAR. For this study, these specimens were placed in a three-point bend fixture and loaded under displacement control conditions in a servo-hydraulic load frame to rupture the specimens into two halves and expose the fracture surfaces. The SBS specimen fracture surfaces were examined using a FERA-3 microscope to characterize the flexural failure features before fire testing. Figure 15 shows a low magnification ($70\times$) wide-field-of-view SEM image of a representative SBS specimen fracture surface. The damage zone in a unidirectional SBS specimen can generally be divided into two distinct failure regions associated with translaminar tension and compression, separated by a neutral axis. Damage can include fiber fractures, fiber pull-outs, matrix cracking, micro-buckled fibers, kink bands, and terraces of micro-buckled fibers. SBS plies failing in translaminar tension typically contained large numbers of individual broken fiber ends that were either extended beyond the fracture surface or recessed within the composite. Such failures are consistent with classical fiber pull-out behavior where there is a spatial distribution of fiber strength values along each filament length.

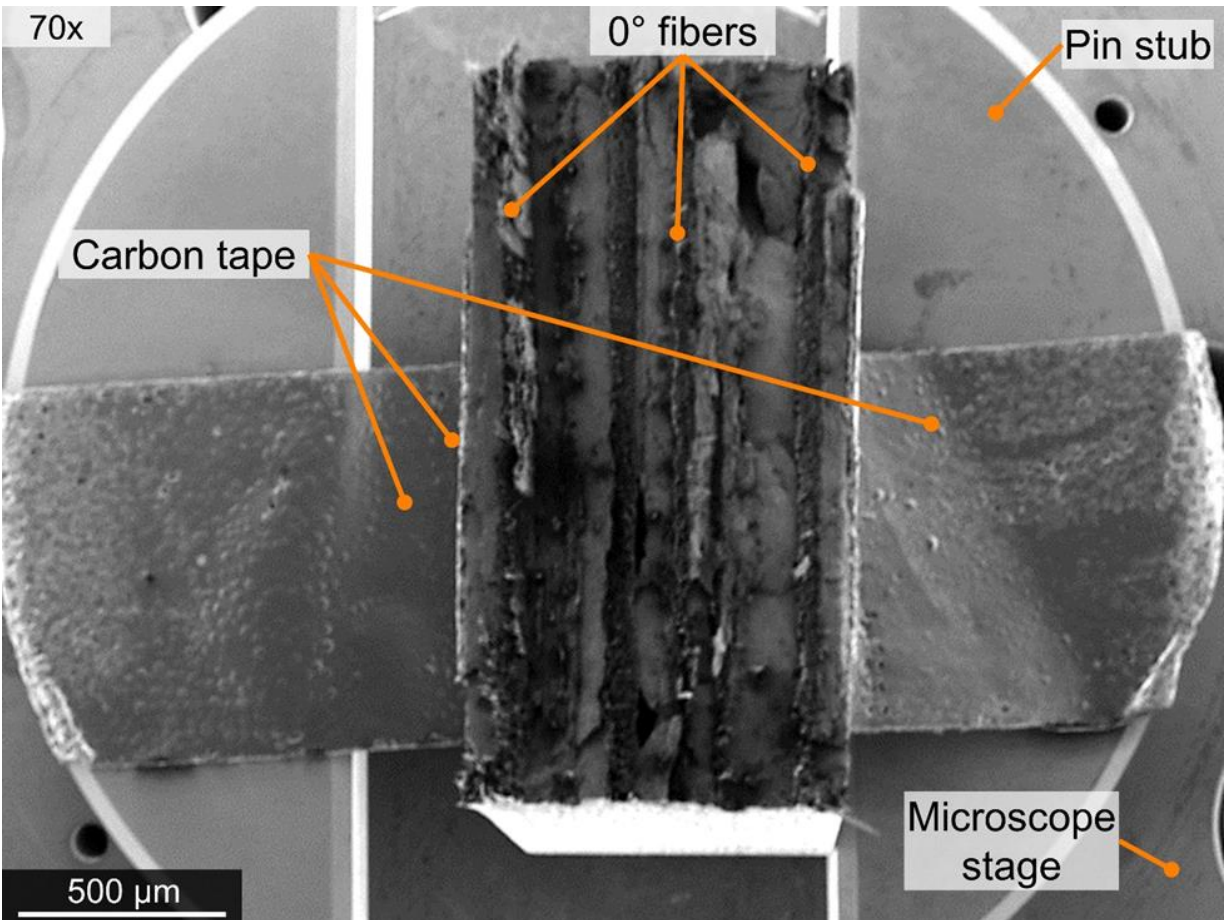


Figure 15. Low magnification (70×) SEM micrograph of representative graphite/epoxy SBS specimen fracture surface

SEM imaging was used to assess damage in SBS specimens along the outer ply (in-plane) surfaces, as well as through-the-thickness along the fracture surface. For example, Figure 16 shows an SEM micrograph of the outermost ply in an SBS specimen that experienced translaminar compression. Compressive kink bands were visible; the dashed white lines demarcate the kink band boundaries. Kink bands form due to local compressive instabilities involving a combination of compressive matrix failure, local fiber micro-buckling, and fiber fracture. Once an individual filament and surrounding matrix fail, local load shedding occurs that can cause adjacent fibers to fail in roughly the same plane, leading to kink band formation (Greenhalgh, 2009). The kink band thickness typically is on the order of the fiber micro-buckling wavelength, roughly 5-10 fiber diameters. Kink bands can form in multiple adjacent parallel planes in the composite laminate, giving rise to a series of step-like terraces of micro-buckled fibers, as shown in Figure 17. In addition to large-scale matrix cracking and fiber ruptures in the kink band planes, matrix cracks can also form parallel to the fibers, resulting in the longitudinal splitting of the terraces as shown in Figure 17(b).

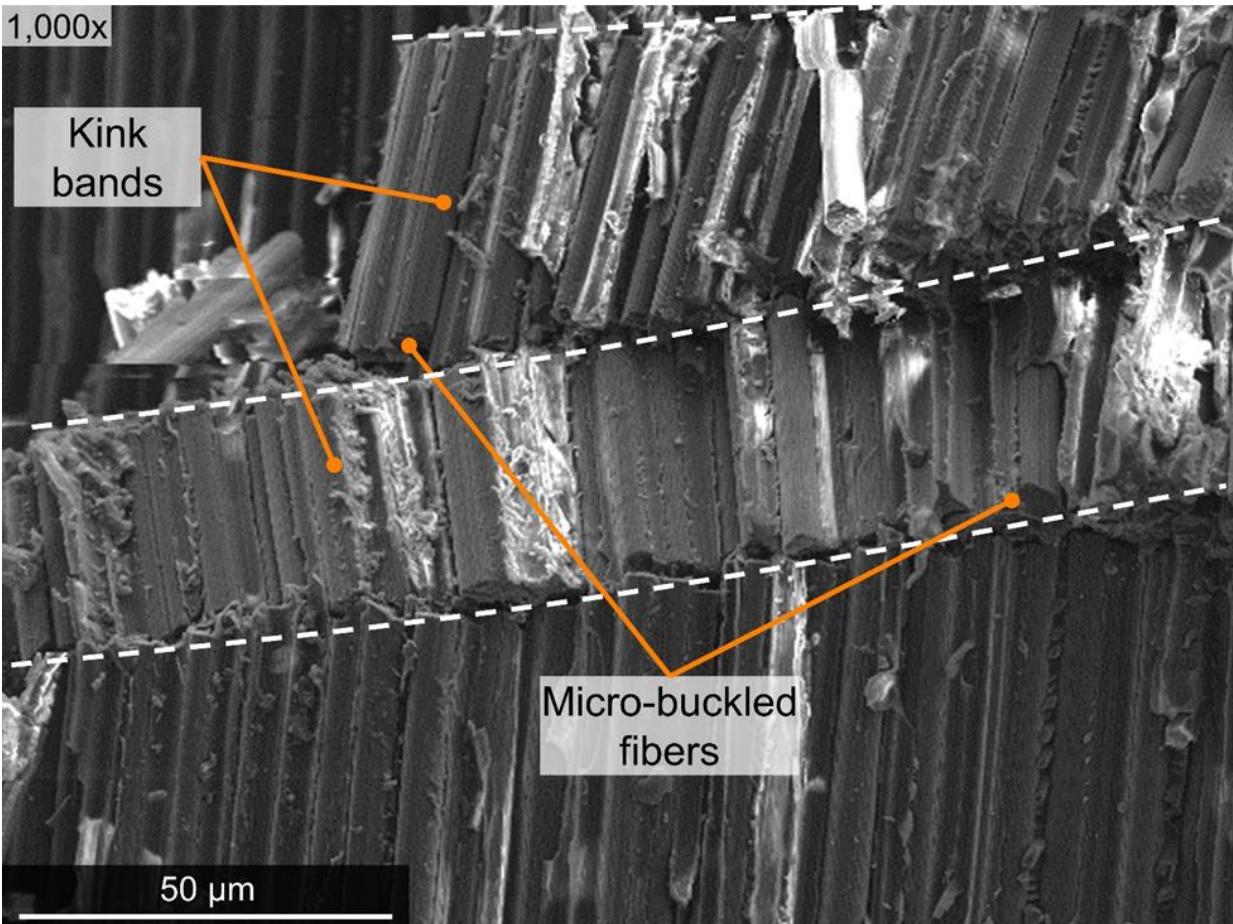


Figure 16. SEM micrograph of outermost ply surface of graphite/epoxy SBS specimen showing kink bands

Fractographic inspection of typical SBS specimen terrace structures revealed clear evidence of local compressive stability-related fiber failures (i.e., micro-buckling/fracture). For example, Figure 18 shows SEM micrographs from an SBS specimen failure surface subjected to translaminal compression. In the figure, each broken filament appeared to fail in local flexure, consistent with micro-buckling. Chop marks were visible at each fiber's neutral axis (NA) that demarcated the transition from tensile to compressive failure, labelled (T) and (C) respectively in some figures. These results are consistent with those observed for fractured 0° fibers in UNCO specimens as shown in Figure 13. Since the neutral axes for this set of fibers were roughly parallel, the local crack propagation in the kink plane occurred perpendicular to these axes in a direction proceeding from local fiber tensile failure to local fiber compressive failure as shown in Figure 18(a). Figure 18(b) contains a similar SEM image of an SBS failure surface associated with a terrace of micro-buckled fibers, along with the exposed failure surface of the underlying (adjacent) terrace. While the chop marks defining the orientations of the fiber-neutral-axes for both surfaces are roughly parallel, the relative positions of the tensile and compressive fiber

regions for each terrace surface are opposite. This suggests that the local crack propagation direction in each kink plane is also opposite from one another, which is consistent with significant transverse shearing deformation. This makes sense given that the three-point bend SBS specimens have a relatively low span-to-thickness ratio and are primarily loaded in shear, and to a lesser degree, flexure.

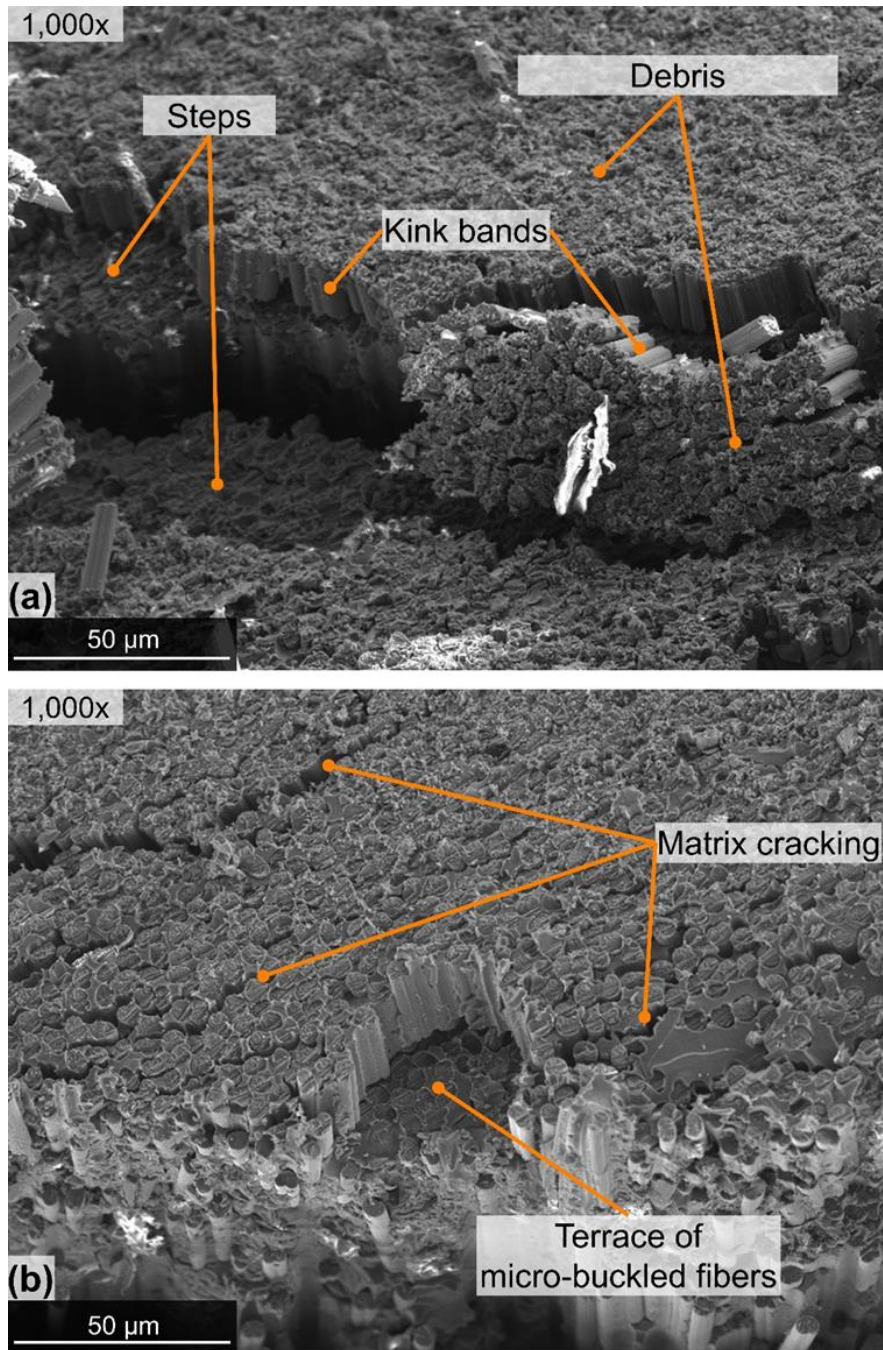


Figure 17. SEM micrographs of graphite/epoxy SBS specimen fracture surface with (a) kink bands (b) terrace of micro-buckled fibers

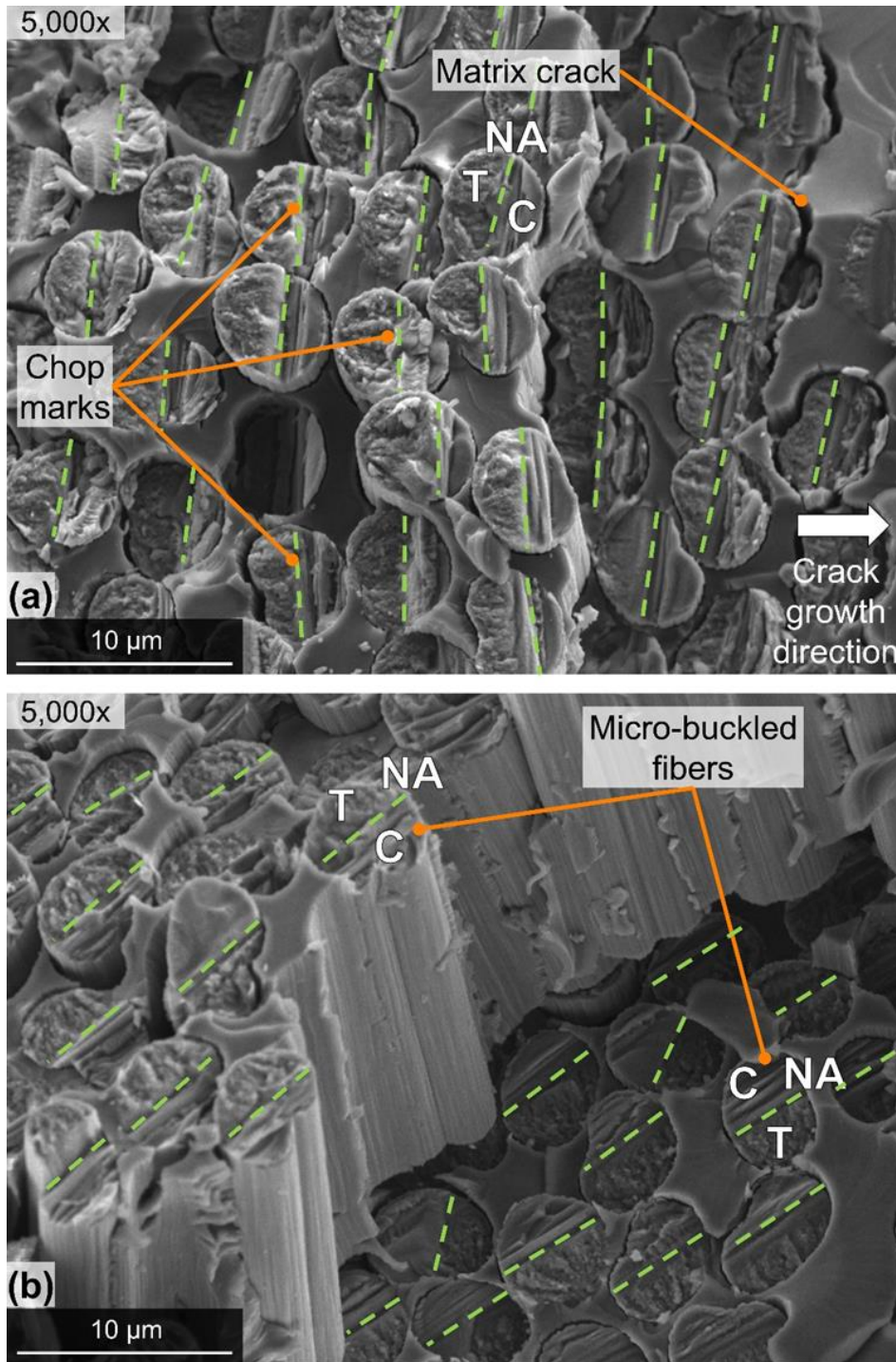


Figure 18. SEM micrographs of graphite/epoxy SBS specimen with (a) chop marks (b) micro-buckled fibers

The unidirectional SBS specimens will generally fail due to combined transverse shear and flexure. The local stress state within a given cross-section can affect local damage initiation and failure. The Cytec specimen plies have significantly lower compressive strength in the fiber

direction than that for tension. In the three-point bending SBS experiments, material points near the laminate upper surface will be loaded in pure compression. Once the compressive strength in the fiber direction is exceeded, a combination of distributed matrix cracking and fiber micro-buckling will occur. As demonstrated previously, fiber micro-buckling failures are readily identifiable by the presence of chop marks that separate the compressive and tensile failure regions on a given filament fracture surface. Figure 19(a) shows a failed graphite fiber located near the upper surface of an SBS specimen where the fiber was subjected to nearly pure compression. The chop mark roughly passes through the fiber centroid, indicating that the fiber failed primarily due to micro-buckling/flexure, as the tensile and compressive faces are approximately the same size. Before the laminate failure, material points located closer to the laminate neutral axis will experience proportionally lower compressive axial stresses and significant transverse shear stresses. This should manifest itself in a smooth appearance of the broken fiber ends. Figure 19(b) shows a failed fiber located near the lower surface of an SBS specimen (i.e., the fiber was subjected to axial tension). The location of the chop mark suggests that the fiber failed primarily in tension.

Similarly, Figure 20 shows an SEM image of a cluster of protruding broken fibers located near the bottom of an SBS specimen. Each fiber failure surface included several radial marks emanating from the site of fracture initiation; such features are consistent with those seen in failed UNT0 specimens such as those shown in Figure 9. The relative sizes of the tensile and compressive failure zones for individual filaments indicate the local state of flexural stress at the time of fracture (Greenhalgh, 2009).

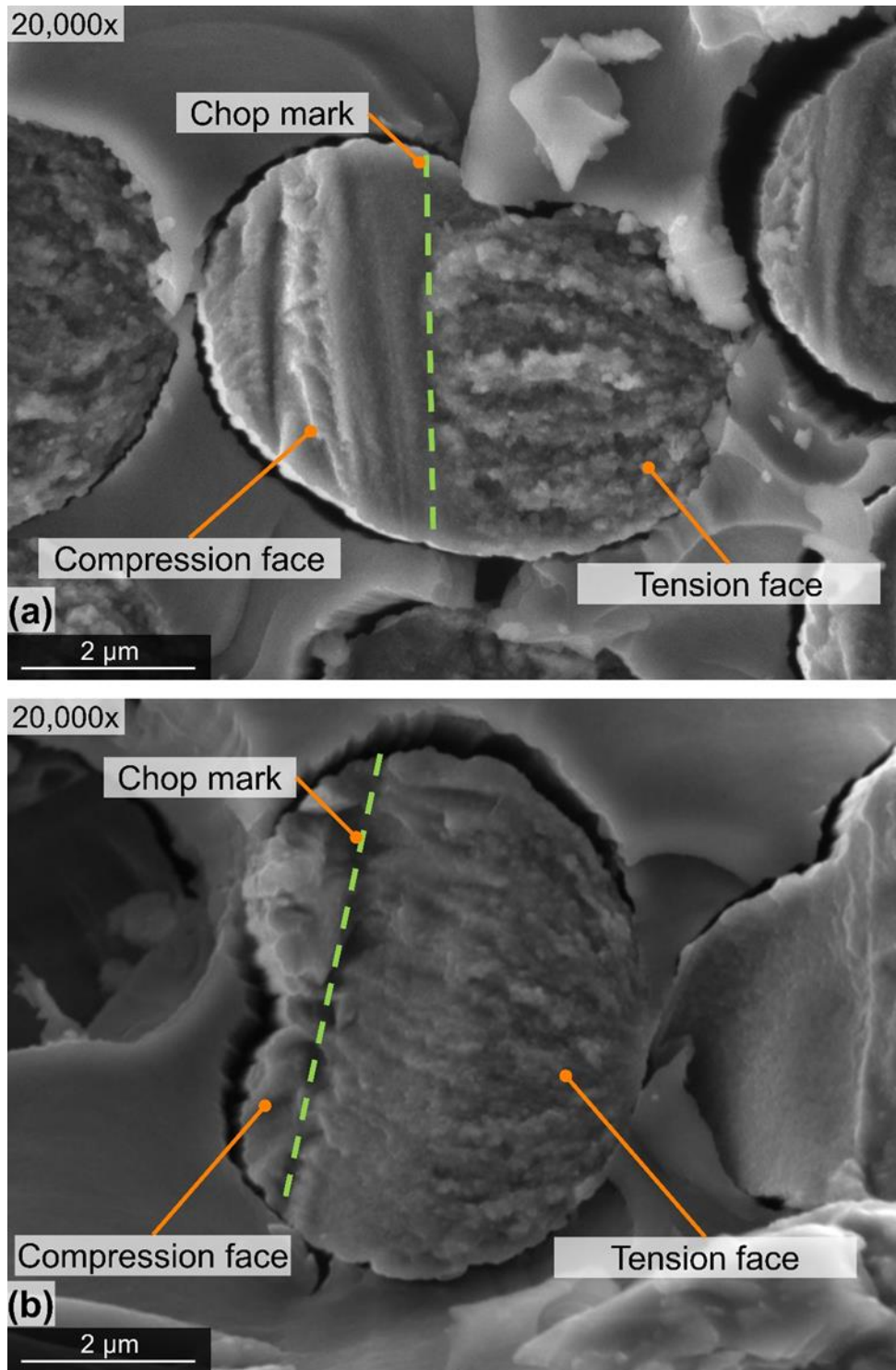


Figure 19. SEM micrographs of SBS specimen micro-buckled fibers (a) above laminate neutral axis (b) below laminate neutral axis

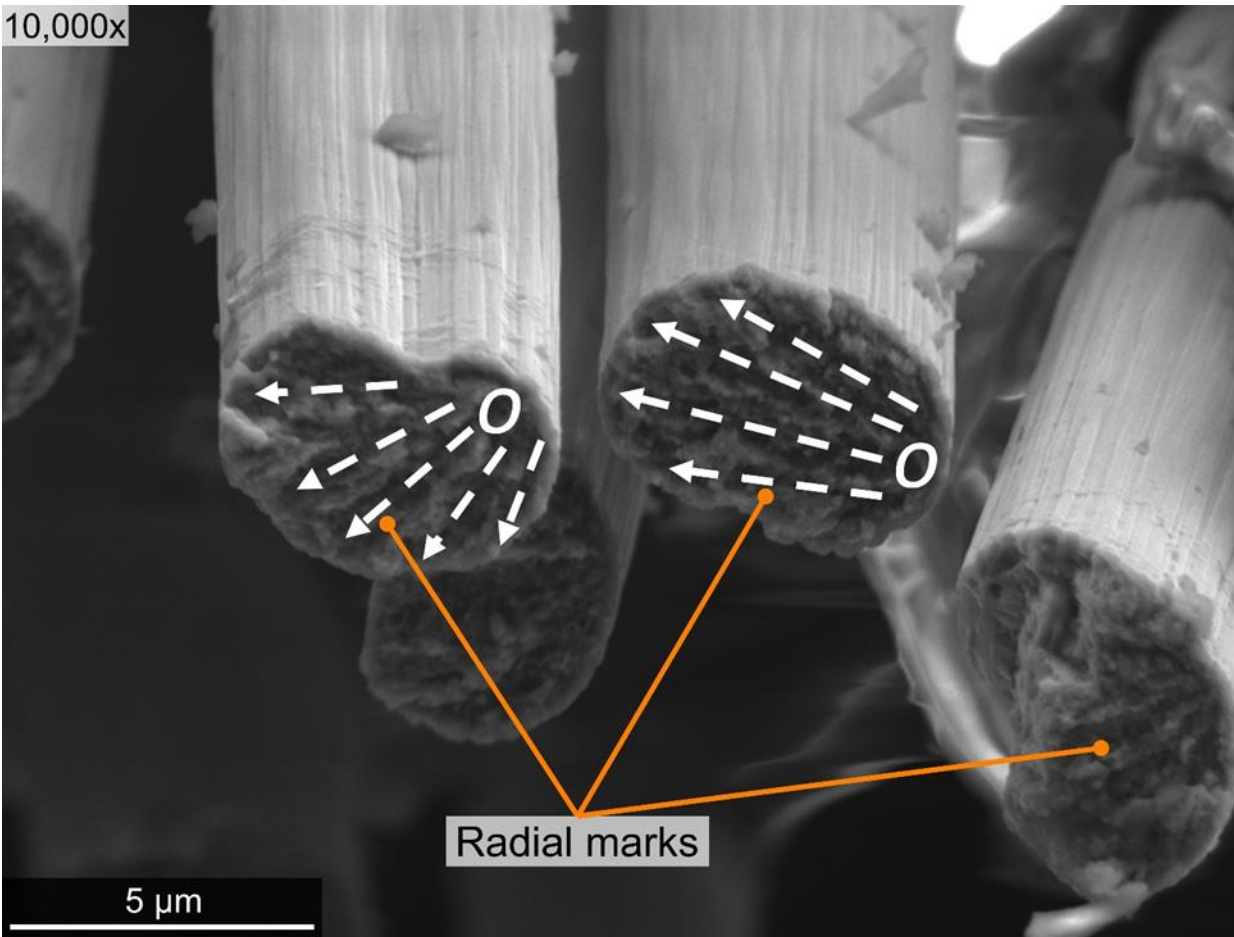


Figure 20. SEM micrograph near lower surface of graphite/epoxy SBS specimen showing radial lines on fractured fiber ends

These preceding results for SBS specimens suggest that SEM imaging can be used to assess differences in the local state of stress at failure in laminated graphite/epoxy composites. However, the specifics of failure surface morphology can be obscured by significant amounts of crushed matrix debris and broken fiber segments generated during matrix cracking, fiber micro-buckling, and kink band formation. For example, Figure 21 contains an SEM image of the massive amounts of debris that can accumulate on the surfaces of micro-buckled terrace structures common in failed SBS specimens; these results are similar to those for UNCO specimens shown in Figure 14(b). When exposed to flame, such debris can decompose, pyrolyze, and/or burn. This can result in melt dripping and char deposits on the failure surface that can dramatically impede forensic fractography to identify specific mechanical failure mechanisms.

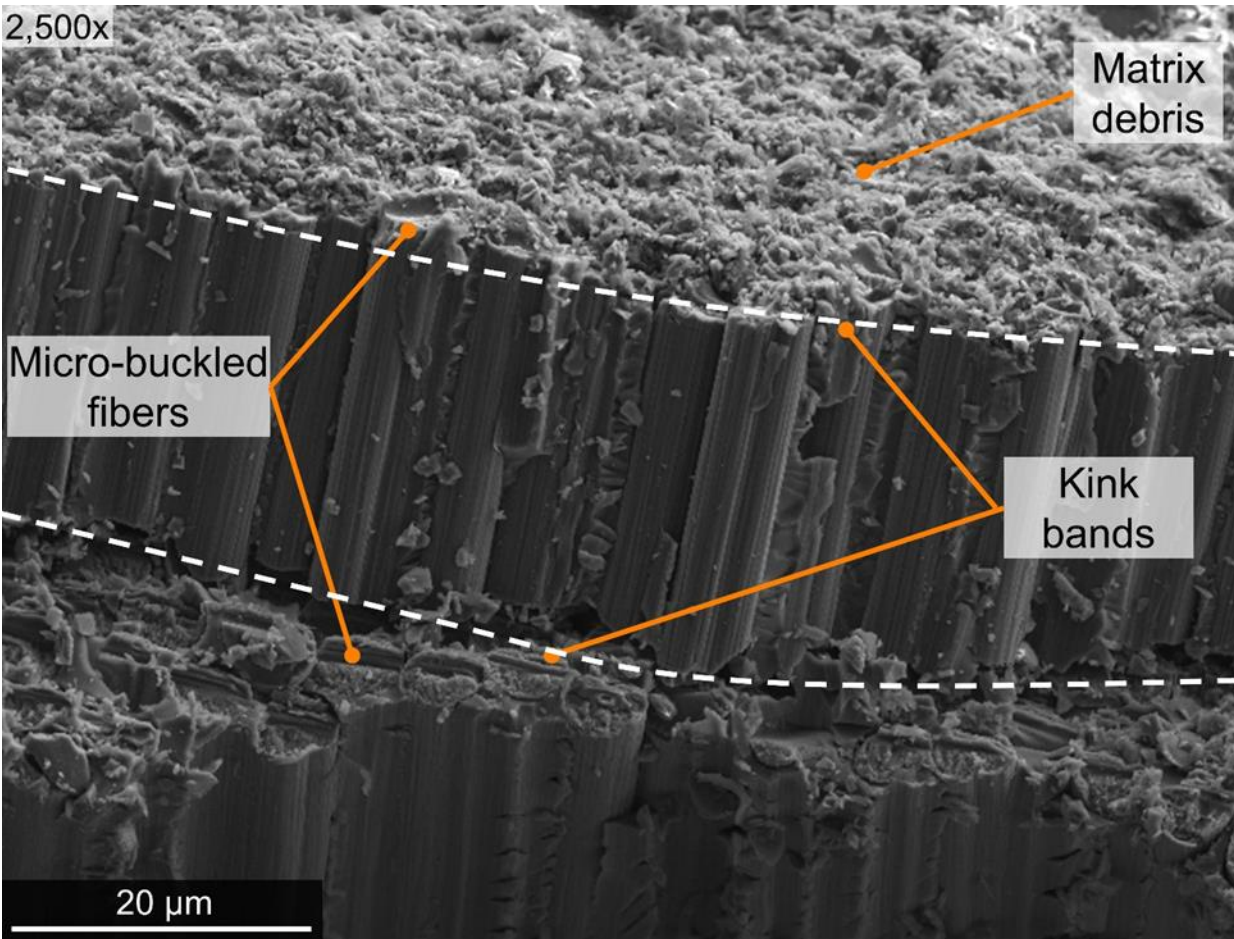


Figure 21. SEM micrograph of graphite/epoxy SBS specimen fracture surface covered with matrix debris

2.4 Fractographic imaging of ASTM D3518 IPS specimen failure surfaces

NIAR performed ASTM standard D3518 tensile testing on angle-ply $[45/-45]_{4S}$ T40-800/5215 graphite/epoxy IPS specimens under ambient conditions (Clarkson, 2012; Man, Ng, Tomblin, & Hooper, 2012). These tests are intended to induce in-plane shear failures within the angle-ply laminates. The 16-ply IPS specimens are somewhat consistent with thinner aerospace composite laminates designed to carry torsional and shear loads, such as wing skins and spar webs. As mentioned previously, any unsevered IPS specimens were subsequently loaded under displacement control conditions until rupture to expose the fracture surfaces fully. Unlike UNCO and SBS specimens that tend to fail within a more planar damage zone, IPS specimen failures consist of multiple translaminar fractures of individual $\pm 45^\circ$ plies with a non-uniform distribution of ply fracture planes along the specimen gage section, longitudinal splitting of fiber tows, and large-scale ply-delamination. Consequently, there is much more free surface area

created during IPS specimen failures than for cross-ply UNT0, UNCO, and unidirectional SBS specimen failures. As will be discussed in later sections, specimens with a greater total free surface area tend to promote better airflow and combustion during fire exposure, which accelerates matrix decomposition, char formation, and severe fiber thermal degradation for a given flame exposure.

The presence of widespread and diffuse failure surfaces made the fractography of IPS specimens extremely challenging. The IPS specimen failure surfaces were examined using a FERA-3 microscope. Figure 22 shows a low magnification (4×) wide-field-of-view SEM image of a representative failed graphite/epoxy IPS half-specimen that illustrates the extensive nature of the damage in the IPS specimens. In order to assess interlaminar shear failures between $\pm 45^\circ$ plies (i.e., delamination), IPS specimens were placed on top of the microscope stage with the laminate mid-plane oriented orthogonal to the microscope lens. Figure 23 shows a typical SEM micrograph of an IPS specimen interlaminar shear failure surface delamination with fiber imprints, cracking, and local residual deformation in the matrix-rich region between the $\pm 45^\circ$ plies. The IPS delamination surface contained clear evidence of fiber-matrix decohesion, longitudinal splitting between fibers, and intense local shearing deformation in the matrix, as indicated by the presence of hackles/cusps, riverlines, scallops, and crenulation imprints. In addition, a significant amount of debris (crushed matrix fragments and small broken fiber segments) was visible on the delamination surfaces. Forensic assessment of the IPS interlaminar failure surfaces depends heavily on information gleaned from the features contained in the epoxy matrix; such information would be irrevocably lost if these surfaces are exposed to direct flame.

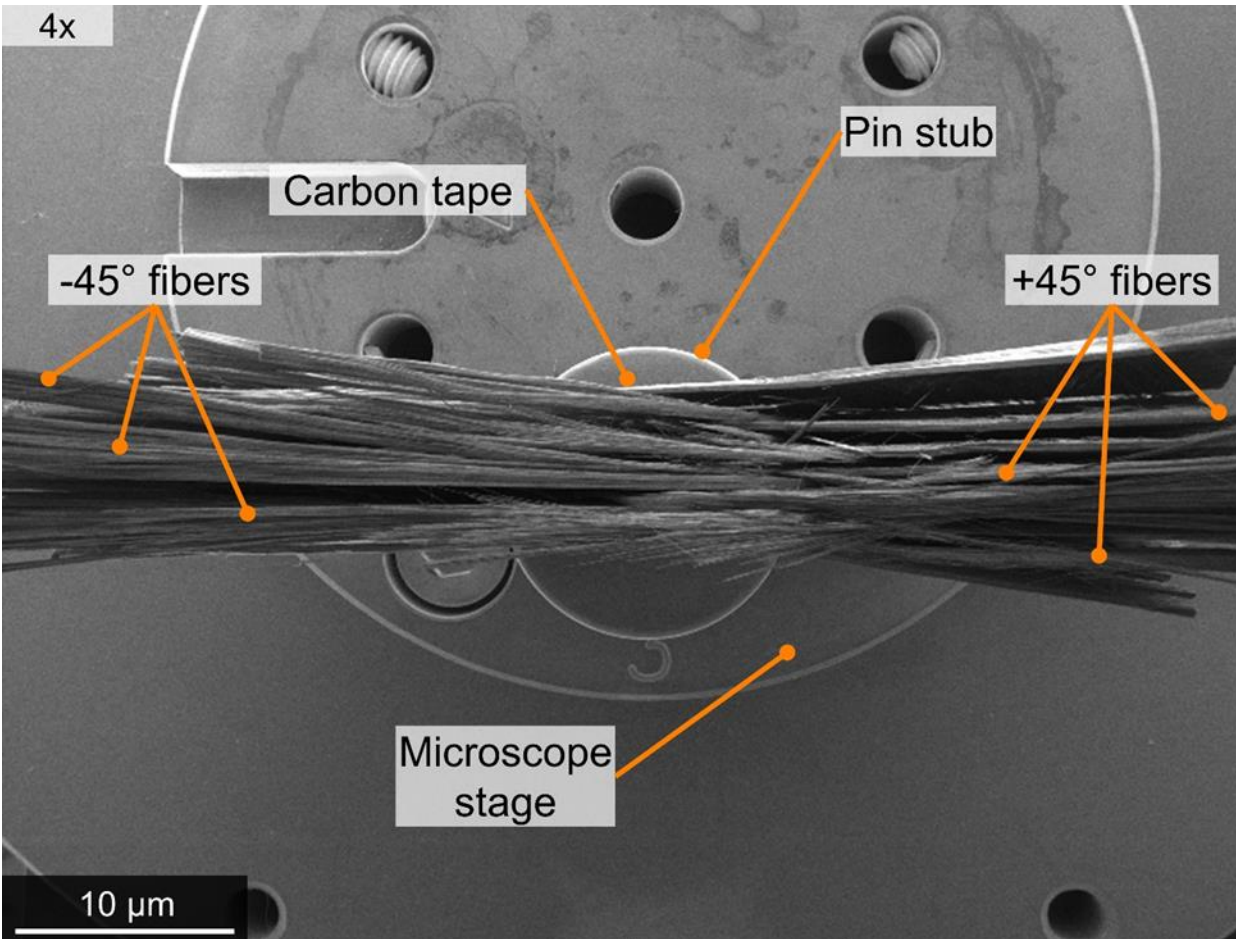


Figure 22. SEM micrograph of representative failed graphite/epoxy IPS specimen

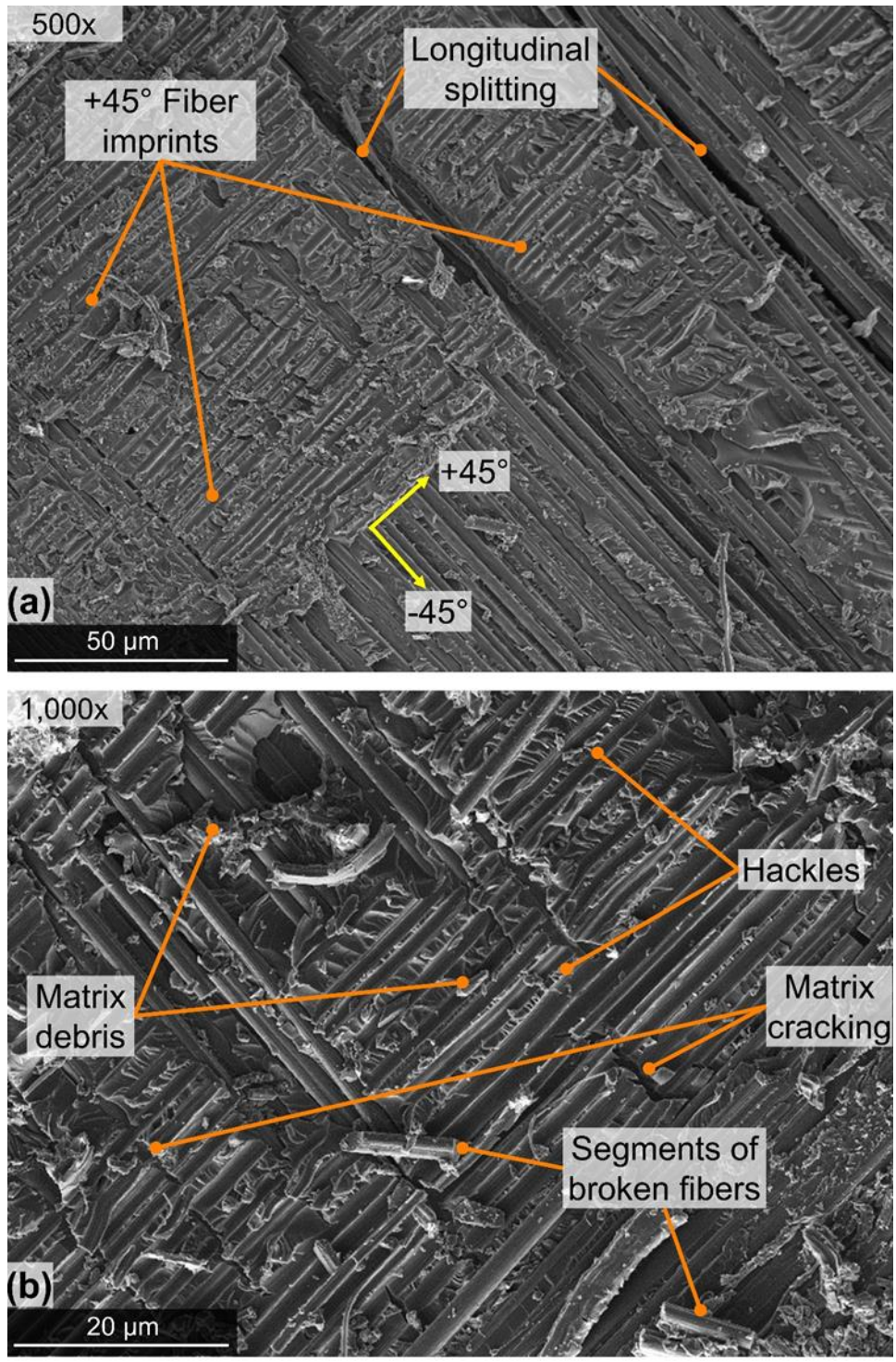


Figure 23. SEM micrographs of IPS specimen in-plane fracture surface

IPS specimen interlaminar shear failures are characterized by the formation of matrix cusps (i.e., inclined platelets), as shown in Figure 24 and Figure 25. Cusps are the most dominant fractographic feature in fiber-reinforced composite matrix shear failures (Greenhalgh, 2009; Purslow, 1986). The IPS interlaminar failure surfaces contained well-defined sharp cusps as

shown in Figure 24(b) and large triangular-shaped cusps as shown in Figure 25(b). While not visible here, more rounded and less distinct cusps can form due to the relative rotations between adjacent angle plies before coalescing into the primary delamination crack (Smith, Grove, & Munns, 1986). In addition, the size and distribution of cusps are influenced by the local fiber spacing and the crack propagation velocity; the greater the crack speed, the smaller the cusp (Smith, Grove, & Munns, 1986). The relative local shearing motion between adjacent $\pm 45^\circ$ plies can be determined by inspecting the tilt orientation of the cusps on the two mating surfaces as shown in Figure 24(b). Such surfaces will have cusps oriented in the opposite direction from one another (Greenhalgh, 2009). Cusps located on one surface will have corresponding “scallops” on the mating surface. Cusps and scallops have associated textured microflows and branched riverlines, as in Figure 24(b) and Figure 25(b) respectively. Such features appear to emanate from regions of fiber-matrix debonding and propagate in the direction of the local crack growth (Purslow, 1986). Lastly, imprints of T40-800 graphite fiber crenulations can be observed along the fiber troughs in Figure 24(b).

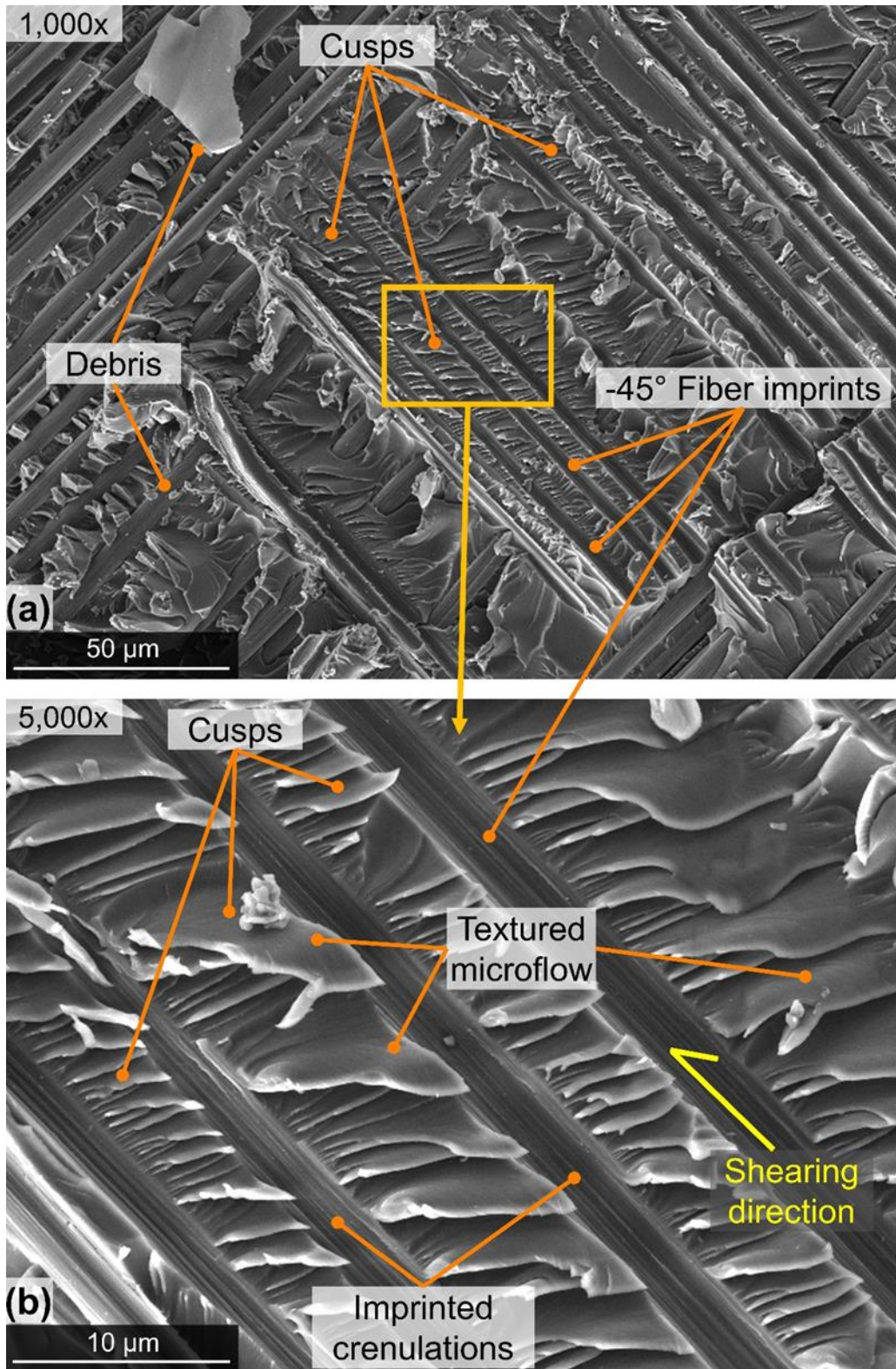


Figure 24. SEM micrographs of IPS specimen with (a) shear fracture surface (b) cusps

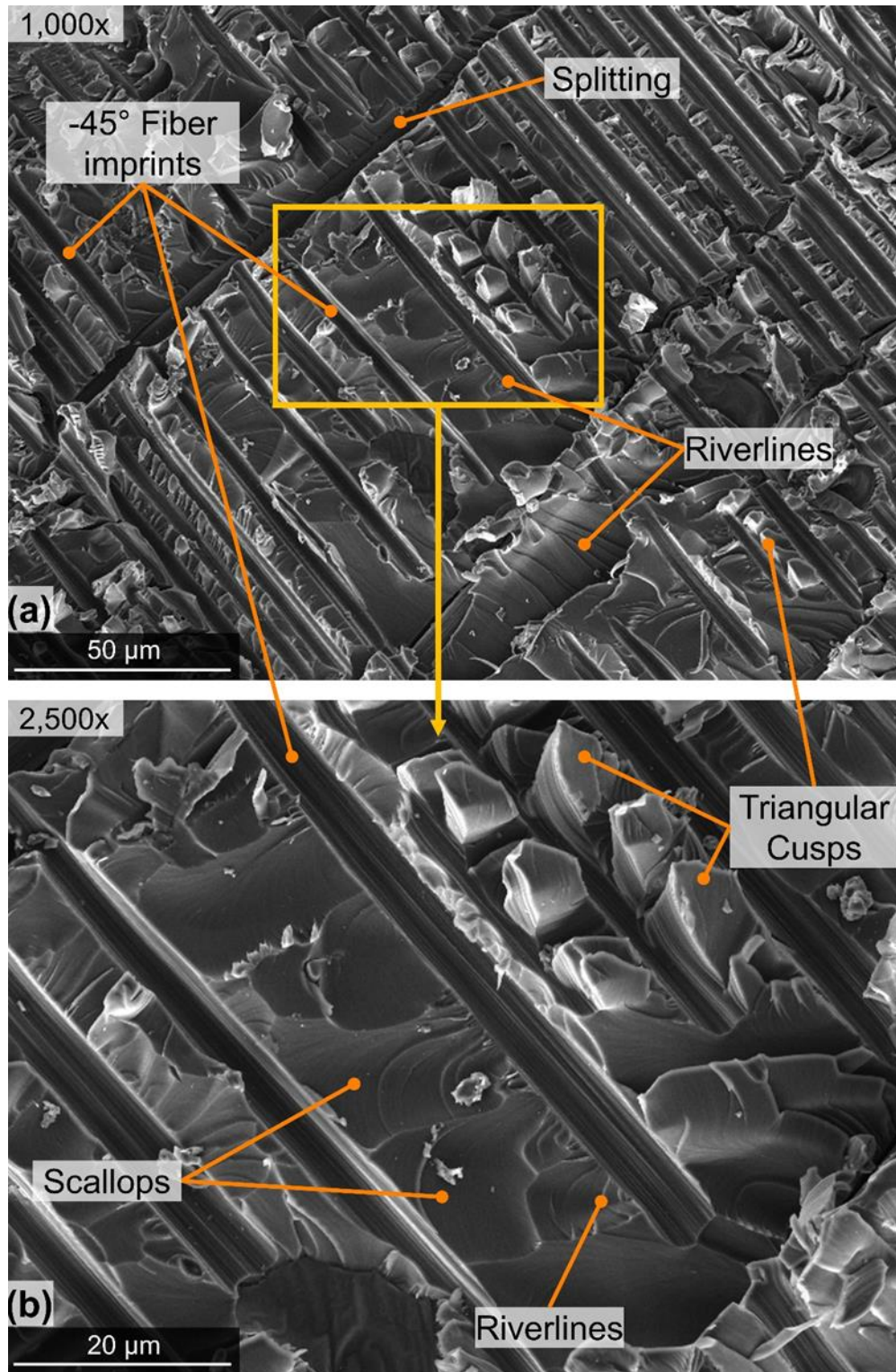


Figure 25. SEM micrographs of IPS specimen fracture surface with (a) gouges (b) triangular cusps

SEM imaging was also used to inspect the ends of broken graphite fiber bundles that were ruptured during translaminar fracture of the $\pm 45^\circ$ plies. As mentioned previously, the individual ply fracture planes were distributed at varying locations along the IPS specimen gage section. In general, there was significant shear-induced delamination between $\pm 45^\circ$ plies accompanied by widespread and non-uniformly distributed longitudinal splitting within plies, leading to a broom-like appearance (Table 2 inset, Figure 22). Such damage is typical for angle-ply laminates subjected to in-plane off-axis loading, resulting from extensive fiber-matrix debonding before fiber fracture (Greenhalgh, 2009). Figure 26 shows an SEM micrograph of a typical bundle of fractured fibers from a failed IPS specimen. The individual filaments failed at different locations surrounding the nominal fracture plane. They were covered with distributed loose matrix debris, and perhaps some globules of the remaining matrix adhered to the fiber surfaces. As will be seen in later sections, any matrix material present at the fiber surfaces will decompose during flame exposure and can contribute to char and soot accumulation on these surfaces.

The sequential ply delamination, fiber-matrix debonding, and longitudinal fiber tow splitting during IPS specimen failure led to a loss in the surrounding matrix constraint. This allowed for some off-axis split fiber tows to rotate and partially align with the applied uniaxial tensile load, leading to tensile fiber fractures during laminate rupture. Figure 27 shows SEM micrographs of broken fiber ends in an IPS specimen fracture surface. In the figure, crenulations are visible. Figure 27(a) shows an individual filament that failed primarily in tension; the fracture surface was relatively flat with a rough topology consistent with that for failed 0° fibers in UNT0 specimens as shown in Figure 9.

In contrast, Figure 27(b) shows a fiber that appeared to fail due to combined tension and transverse shear; the failure surface was not orthogonal to the fiber axis (i.e., slant fracture occurred). In the future, SEM images of failed fibers loaded in transverse shear (e.g., fibers located at the neutral axis in failed SBS specimens) should be examined to assess better the effects of off-axis loading on local fiber failures. These results show that SEM imaging of failed IPS specimens can be used to assess differences in the local state of stress at failure in laminated graphite/epoxy composites.

Fractography of the mechanically-failed T40-800/5215 graphite/epoxy specimens revealed key failure features associated with tension, compression, and shear loading conditions. These features included local fiber microbuckling, fiber fracture, matrix cracking, fiber/matrix crushing, fiber splitting, chop marks, radial lines, cusps, matrix microflow, riverlines, and delamination. The effect of direct flame exposure on graphite/epoxy composite failure surfaces and its impact on forensic analysis will be addressed in the following sections.

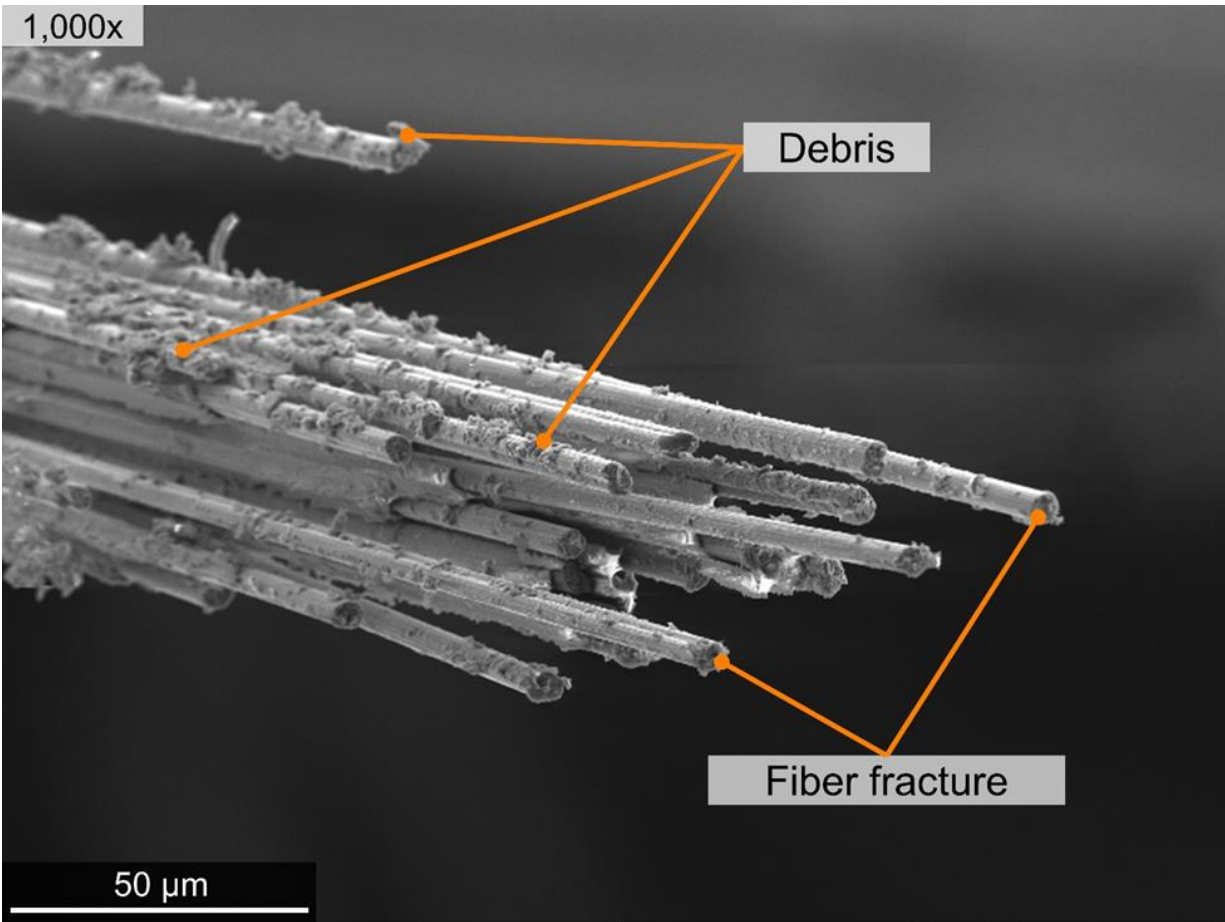


Figure 26. SEM micrograph of longitudinally split fiber tows in mechanically failed IPS specimen

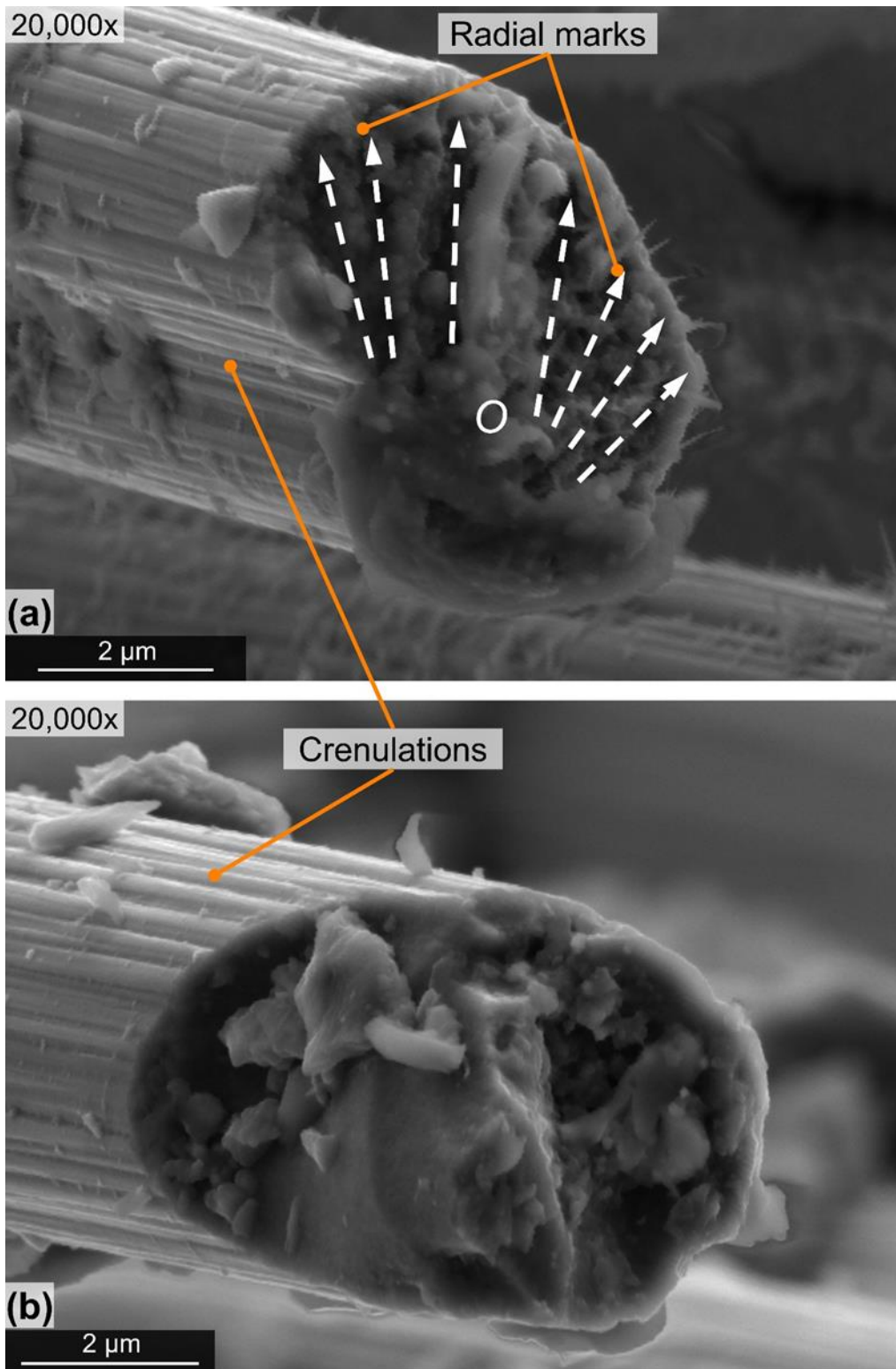


Figure 27. SEM micrographs of fractured graphite fibers in IPS specimen (a) under tension (b) under combined tension and transverse shear

3 Effects of fire exposure on mechanically failed graphite/epoxy composite specimens

3.1 Fire application methods

3.1.1 Direct fire application methods

3.1.1.1 Direct fire application using FAA-approved draft-free cabinets

The FAA has defined vertical and horizontal Bunsen burner test protocols in Policy No. PS-ANM-25.853-01-R2 and summarized in the aggregated *Aircraft Materials Fire Test Handbook*, DOT/FAA/AR-00/12 (Horner, 2000) to address fire tests specified in Title 14, Code of Federal Regulations 14 CFR §25.853 and §25.855. These protocols are commonly used to verify the fire resistance of aircraft cabin and cargo compartment materials. The protocols were used as a guideline in this study in an effort to develop a methodology to deposit some flame byproducts on the fracture surfaces. Note that there were no fire durability or burn-through tests conducted in this research. Using this protocol as a guideline, draft-free cabinets as shown in Figure 28 that meet the FAA fire test requirements were used to conduct vertical and horizontal Bunsen burner tests; however, the specimen size does not meet the outlined 14 CFR §25.853 requirements.

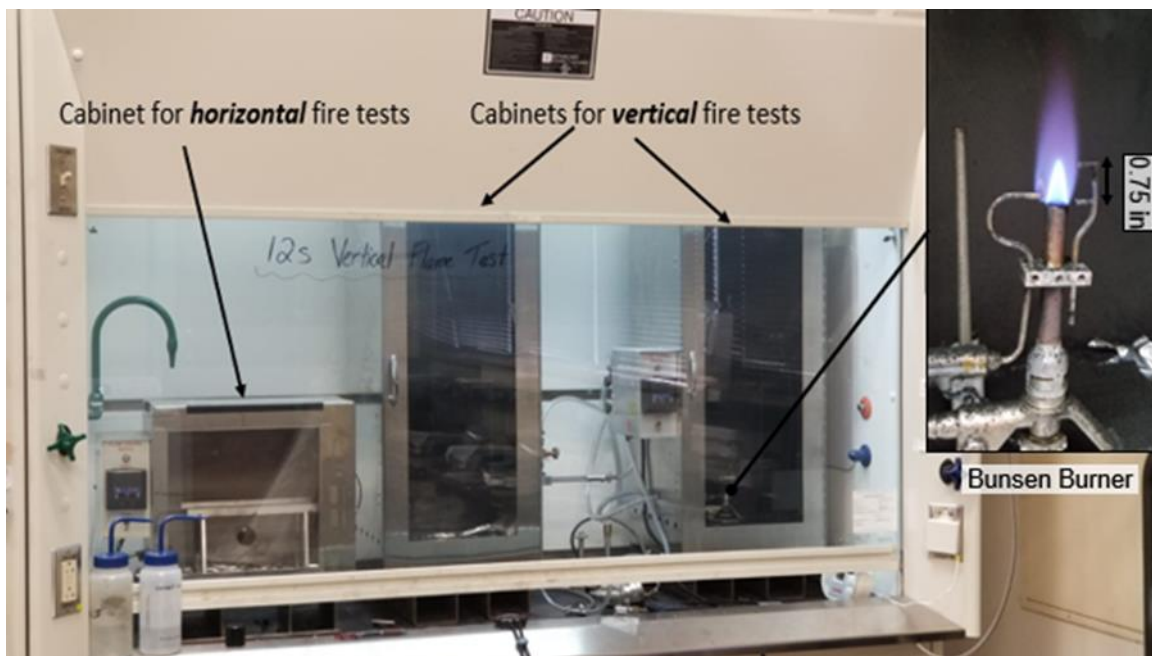


Figure 28. Draft-free cabinets that meet the FAA fire testing requirements

Figure 29 (Horner, 2000) shows a schematic of the burner plumbing and burner flame height indicator used for horizontal and vertical burning test configurations per the FAA *Aircraft Materials Fire Test Handbook* recommendations. All burning tests were performed using

methane fuel and an optimal flame profile consisting of an inner cone height of $7/8$ in and flame tip height of 1.5 in. During the burning tests, the fractured specimen ends were completely immersed in the flame with a standoff distance of $3/4$ in from the edge of the burner. Consistent with the handbook, this standoff distance puts the fractured surface of the specimen at the top of the inner (blue) cone of the flame. Figure 30(a) and Figure 30(b) adapted from Horner (2000) show schematics of specimen positioning with respect to the flame for (a) vertical fire tests and (b) horizontal fire tests.

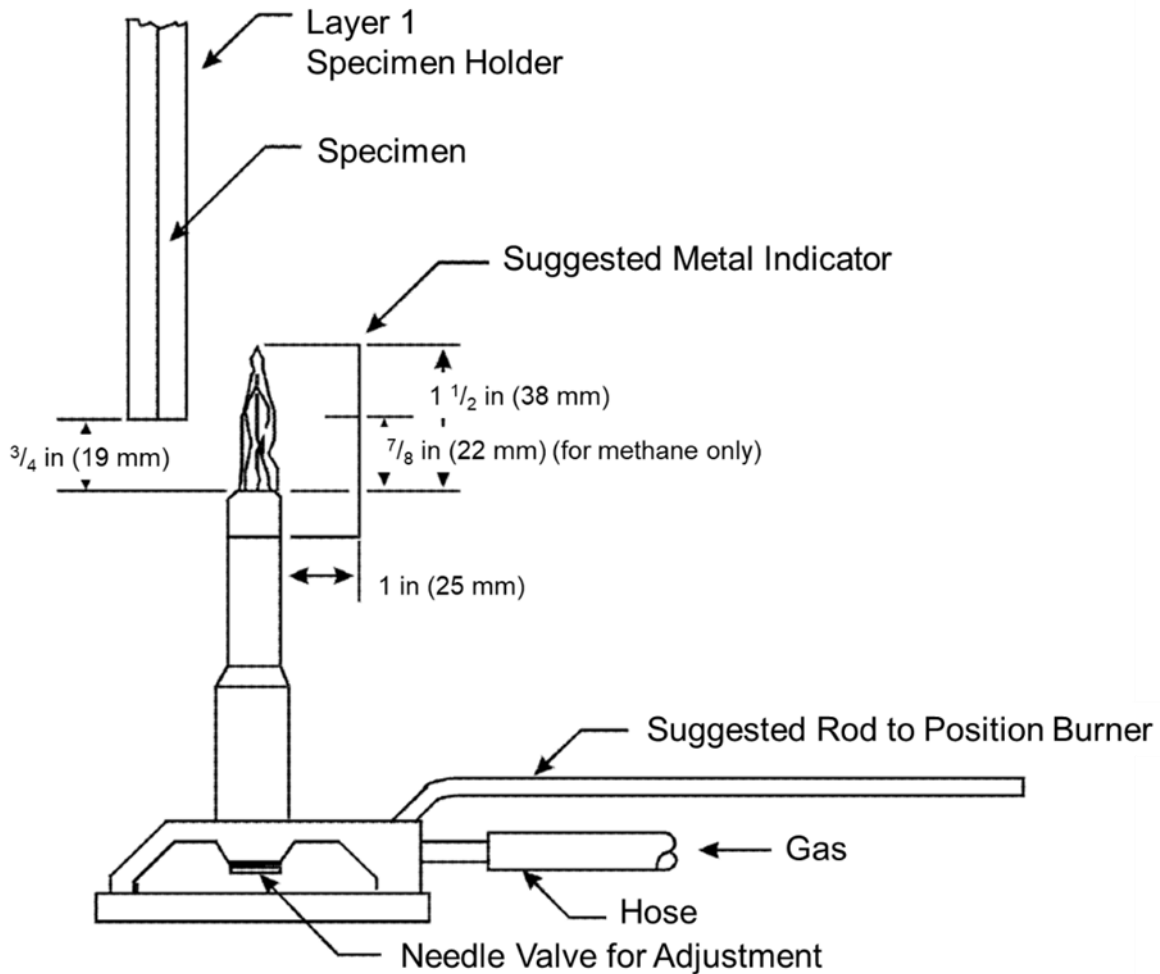


Figure 29. Burner plumbing and burner flame height indicator

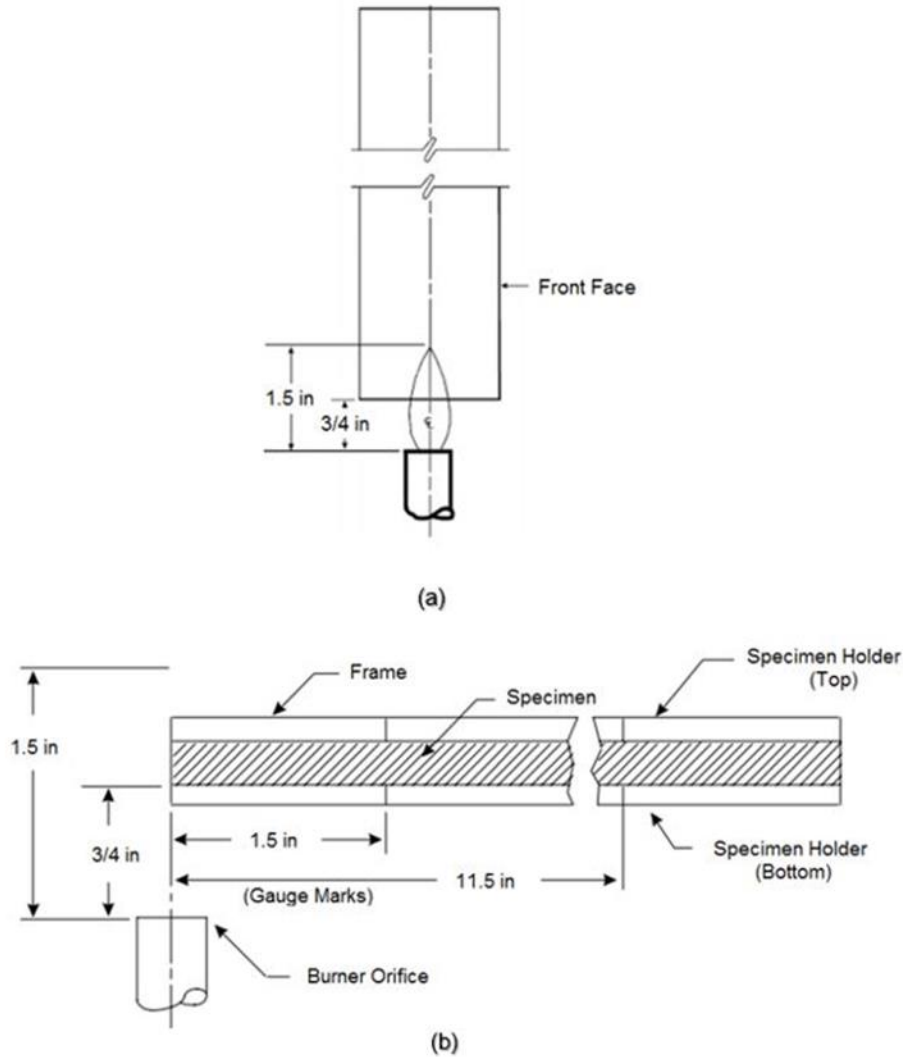


Figure 30. Specimen positioning with flame (a) for vertical fire tests and (b) horizontal fire tests

3.1.1.1.1 Vertical Bunsen burner tests in enclosed (draft-free) cabinet consistent with § 25.853 and §25.855 (methane)

The fire exposure durations adopted for the vertical burning tests on mechanically failed graphite/epoxy UNCO, SBS, and IPS specimens were based on low exposure (12 s) and high exposure (60 s) durations with an intermediate test duration of 36 s added to establish a center point. To ensure the reproducibility of the results, a minimum of three replicates was used for all burning tests. Figure 31 shows a 21-ply cross-ply Cytec UNCO specimen during a vertical test using a Bunsen burner. The thinner 16-ply IPS specimens subjected to 12 s, 36 s, and 60 s vertical fire tests experienced extreme thermal damage to individual graphite fibers, along with nearly complete matrix decomposition. This is likely due to the large free combustible surface

areas that provided the opportunity for increased oxygen supply air flow during the burning of this type of specimen. As a consequence, a fourth set of vertical fire tests was performed on IPS specimens using a shortened fire duration of 6 s.



Figure 31. 21-ply cross-ply Cytec UNCO specimen during vertical burning test using Bunsen burner

3.1.1.1.2 Horizontal Bunsen burner tests (draft-free) cabinet per § 25.853 (methane)

In this work, horizontal fire testing was performed on mechanically failed graphite/epoxy UNCO, SBS, and IPS specimens for durations of 15 s, 45 s, and 75 s. These durations allowed incremental fire exposure times similar to the vertical burning tests. For both vertical and horizontal tests, the intermediate and long exposure times were three and five times longer than the low exposure time defined by the FAA standards. Again, to ensure the reproducibility of the results, a minimum of three replicates was used for all horizontal burning tests. Figure 32 shows a 21-ply cross-ply Cytec UNCO specimen during a horizontal test using a Bunsen burner.



Figure 32. 21-ply cross-ply Cytec UNCO specimen during horizontal burning test with Bunsen burner

3.1.2 Indirect fire application method

3.1.2.1 Cone calorimeter tests

The cone calorimeter shown in Figure 33 is an instrument used for small-scale fire testing (Babrauskas & Peacock, 1992). Cone calorimetry can be used to determine many fire reaction properties for a bench-scale coupon within only a single test. These properties include the peak and average heat release rate, ignition time, time of sustained flaming, mass loss, smoke density, and the yield of soot, CO, CO₂, and other combustion gases formed during the burning process (Mouritz & Gibson, 2007). The cone calorimeter is based on the oxygen-depletion calorimetry technique that allows the measurement of the heat release rate by measuring the amount of oxygen consumed by the fire during the test (Mouritz & Gibson, 2007; Mouritz, Gardiner, Mathys, & Townsend, 2001). The measurement of oxygen consumption is possible because the heat released per unit of oxygen consumed is constant (Beyler, Croce, Dubay, Johnson, & McNamee, 2017).

The cone calorimeter is widely used in flammability tests since it provides similar burning conditions to a real (direct) fire test. Cone calorimetry permits a wide range of heat fluxes (e.g., 0-100 kW/m²) and can be used to predict the fire performance of a material in a large-scale fire test, compare the fire reaction properties of different materials, check whether or not a material

meets the fire requirements necessary for a certain application, and produce data to validate fire models (Mouritz & Gibson, 2007).

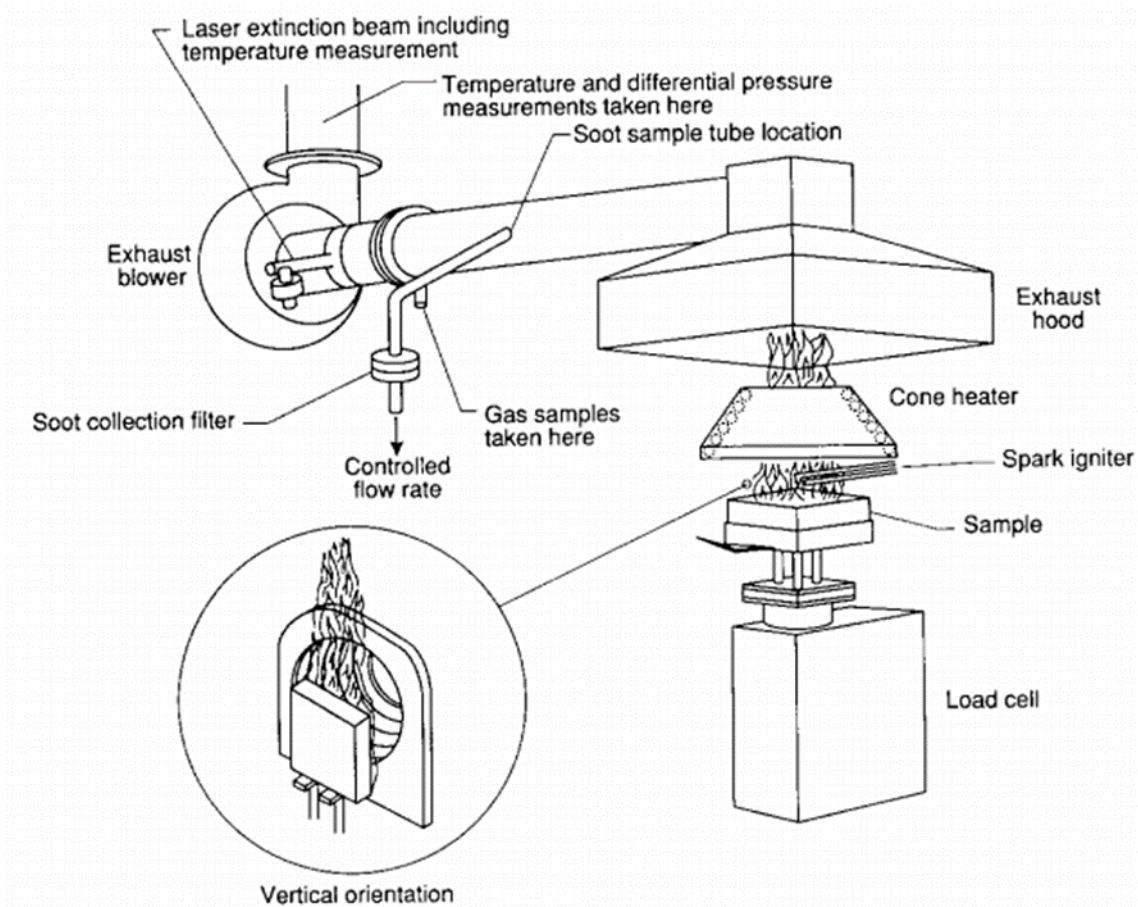


Figure 33. A schematic view of a cone calorimeter

3.2 Analysis of mechanically failed graphite/epoxy composites subjected to fire

The vertical and horizontal fire tests on mechanically failed 21-ply UNCO, 45-ply SBS, and 16-ply IPS Cytec specimens were performed. The fire damage on the fracture surface of the burned specimens was then investigated using a scanning electron microscope. For this purpose, the Tescan FERA-3-FIB-SEM was used to perform microscopy on vertically and horizontally burned UNCO, SBS, and IPS specimens. Due to the conductive nature of the residual char formed on the burned fracture surfaces, as well as the presence of naturally conductive graphite fibers, no sputter-coating was used. A conductive carbon tape was secured on the lateral surfaces of the specimens to reduce specimen charging and improve the quality of SEM images. All the

SEM images presented in this section were taken at a voltage of 5 kV, a beam intensity of 8, and a WD of 9 mm (unless otherwise stated).

3.2.1 Enclosed vertical fire testing of Cytec T40-800/Cycom[®] 5215 graphite/epoxy specimens

3.2.1.1 UNCO specimens (*Exposure times: 12, 36, 60 s*)

Fire tests on vertically-oriented 21-ply cross-ply Cytec UNCO specimens (layup: [90/0/90]₇) were performed for durations of 12, 36, and 60 s. Three repeat vertical fire tests were considered for each fire exposure duration. During the vertical tests on the UNCO specimens, only the through-thickness lateral specimen edges (sides) continued to burn after extinguishing the burner flame. The fracture surface, which was immersed in the source flame, extinguished a few seconds after the flame was stopped. This is likely due to the compact fracture surface area (Table 2), which restricted the oxygen transfer to the interior of the specimen. Also, the char deposited at the fracture surface formed a thermal barrier that mitigated the spread of flame to the interior of the specimens (Mouritz & Mathys, 2001). For all three fire exposure durations, the fire damage on the UNCO specimens involved extensive pockets of matrix decomposition, soot deposits, char formation, and fire-induced delamination. The severity of the damage increased with increasing fire exposure duration.

Melt dripping of the epoxy matrix was observed during the 12 s fire tests. This tar-like melt-dripping substance induced fire “sparkles” during specimen burning and leaked onto the tip of the Bunsen burner after the tests as shown in Figure 34. The melt dripping of a given polymer strongly depends on its glass transition temperature and the original polymer melt viscosity and degradation (Ray & Kuruma, 2019). Unlike matrix decomposition, which involves polymer bond breakage, during melt dripping, a solid-viscous liquid phase change takes place inside the material due to high-temperature exposure. The relative degree and extent of the melt dripping were undoubtedly affected by the vertical specimen orientation during fire testing. In essence, any epoxy-based melt dripping would tend to accumulate on the broken carbon filament ends extending from the fracture surface; this contributed to increased char deposits at and near these surfaces. Recessed broken fibers were somewhat less prone to large-scale char deposition. Based upon both visual inspection and SEM imaging, char and soot were clearly visible on the extended fractured fiber ends and at the fracture surface. In general, fire damage was more severe at and near the fracture surface compared to the lateral edges (sides) and outer planar surfaces of the composites. In addition, the severity of char and soot deposition was more pronounced around the perimeter of the fracture surface, where the airflow and oxygen availability were ostensibly greater. In contrast, the region of the fracture surface in close

proximity to the laminate mid-plane and specimen centerline tended to display relatively little char formation on the broken fiber ends, suggesting that any char formed due to matrix decomposition or melt dripping was burned off during direct flame exposure.

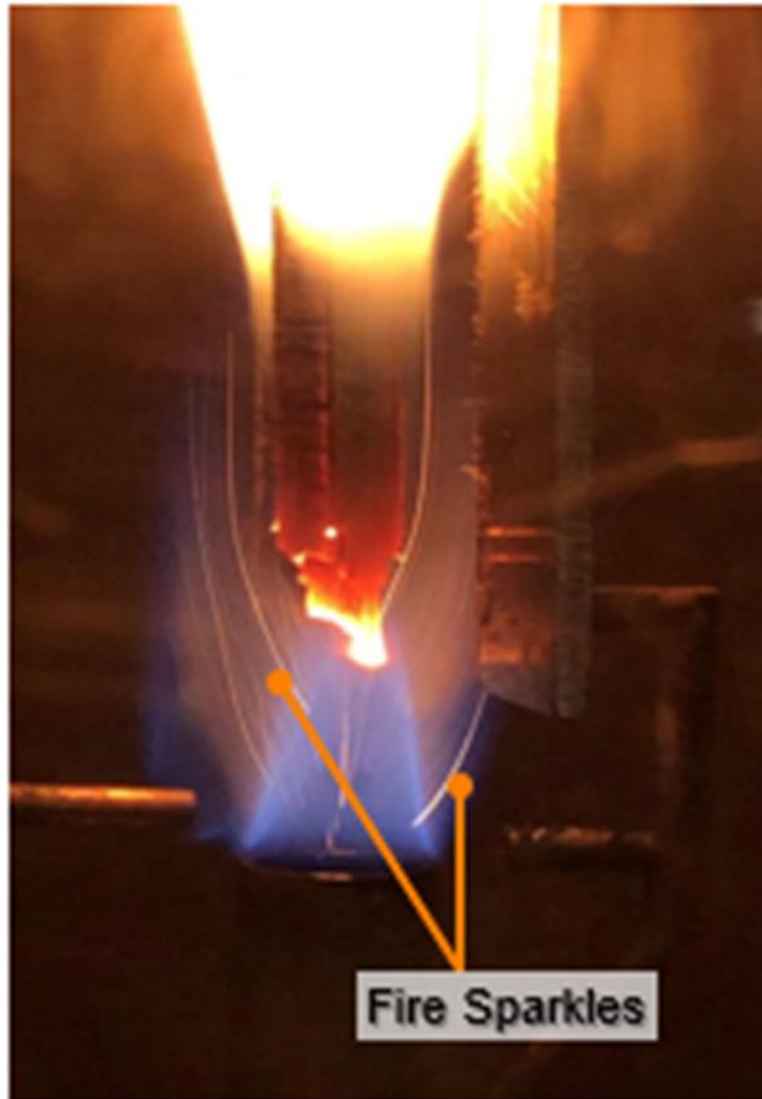


Figure 34. Fire sparkles during 12 s vertical burn test on 21-ply cross-ply Cytec UNCO specimen

The fire damage (i.e., extensive fire matrix decomposition, fire-induced delamination, and residual thickness increase) on specimens exposed to the 36 s and 60 s fire tests was more widespread and severe than that for the 12 s exposure. For specimens burned for the 36 s and 60 s exposure durations, the damage extended throughout the total length of the specimens, and fire-induced delamination occurred. The smoke released during the burning of the specimens was more intense as the fire exposure duration increased. The through-thickness delamination induced by the fire was more severe at the specimen outer plies. In addition, extensive intra-ply

planar cracks formed in the outer 90°-plies of the specimens. Figure 35 shows typical macro-scale pictures of an UNC0 specimen before and after burning for 60 s. The fire damage includes char and soot deposition on the lateral edges and planar surfaces of the specimen and extensive intra-ply cracking and ply-delamination.

In addition, the time for UNC0 specimens to self-extinguish after the burner flame was stopped was highly dependent on the fire exposure duration. UNC0 specimens burned for the 12 s short duration took more time to self-extinguish compared to specimens burned for the longer 36 s and 60 s fire durations. This makes sense since the degree of epoxy matrix decomposition, and consumption for specimens with longer direct fire exposure was greater than that for specimens burned for less time. Moreover, the increased char layers formed in specimens with longer fire exposure likely impeded further burning once the direct flame was discontinued (Mouritz & Gibson, 2007; Mouritz & Mathys, 2001).

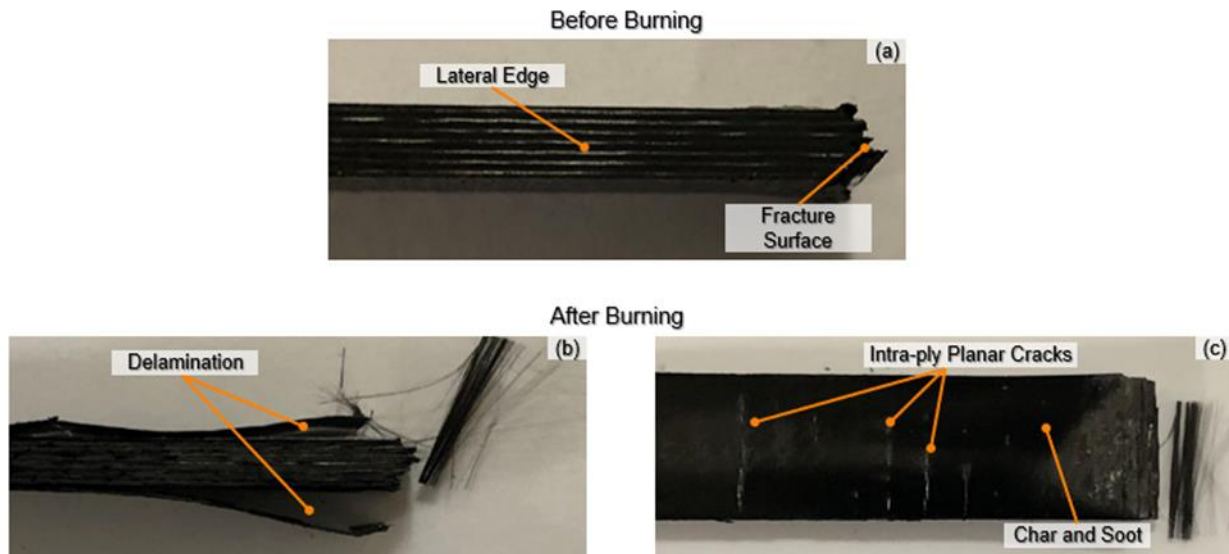


Figure 35. Comparison of 21-ply cross-ply Cytec UNC0 specimen (a) before (b) after and (c) after vertical burning for 60 s

In general, char formation was more pronounced around the perimeter than at the mid-plane of the fractured surfaces. Figure 36 shows typical SEM images of the char and soot that were deposited around the perimeter of the fracture surface of UNC0 specimens burned for 12 s, 36 s, and 60 s, respectively. The figures identify char and soot deposition on the fractured fibers, pockets of matrix decomposition, and recessed fibers. Char was present on the broken fiber ends for all three fire exposure durations and was more pronounced for fibers along the perimeter edges that did not self-extinguish once the applied flame was removed. For all three fire exposure durations, the overall char formed on the fracture surface of the specimens increased slightly with increasing the fire duration. The residual char on the extended broken fibers had a

fuzzy (cotton-candy-like) appearance and formed uniformly around the circumference of each fiber, with noticeably more char accumulation at the fractured filament ends. Figure 37 shows high magnification SEM images of char formation around single fibers located on the perimeter of the fracture surface of UNCO specimens burned for 12 s, 36 s, and 60 s, respectively.

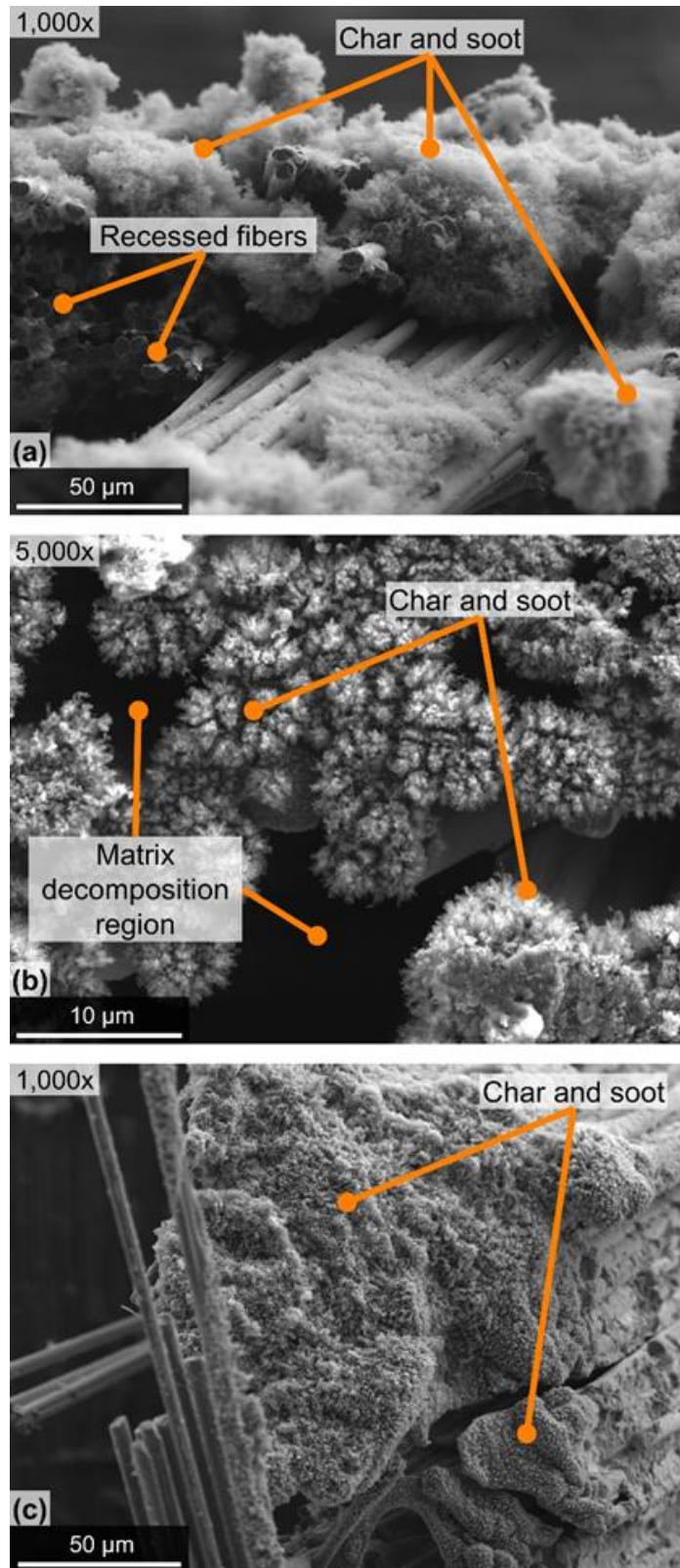


Figure 36. Char and soot on fracture surface of 21-ply cross-ply Cytec UNC0 specimens burned vertically for (a) 12 s (b) 36 s and (c) 60 s

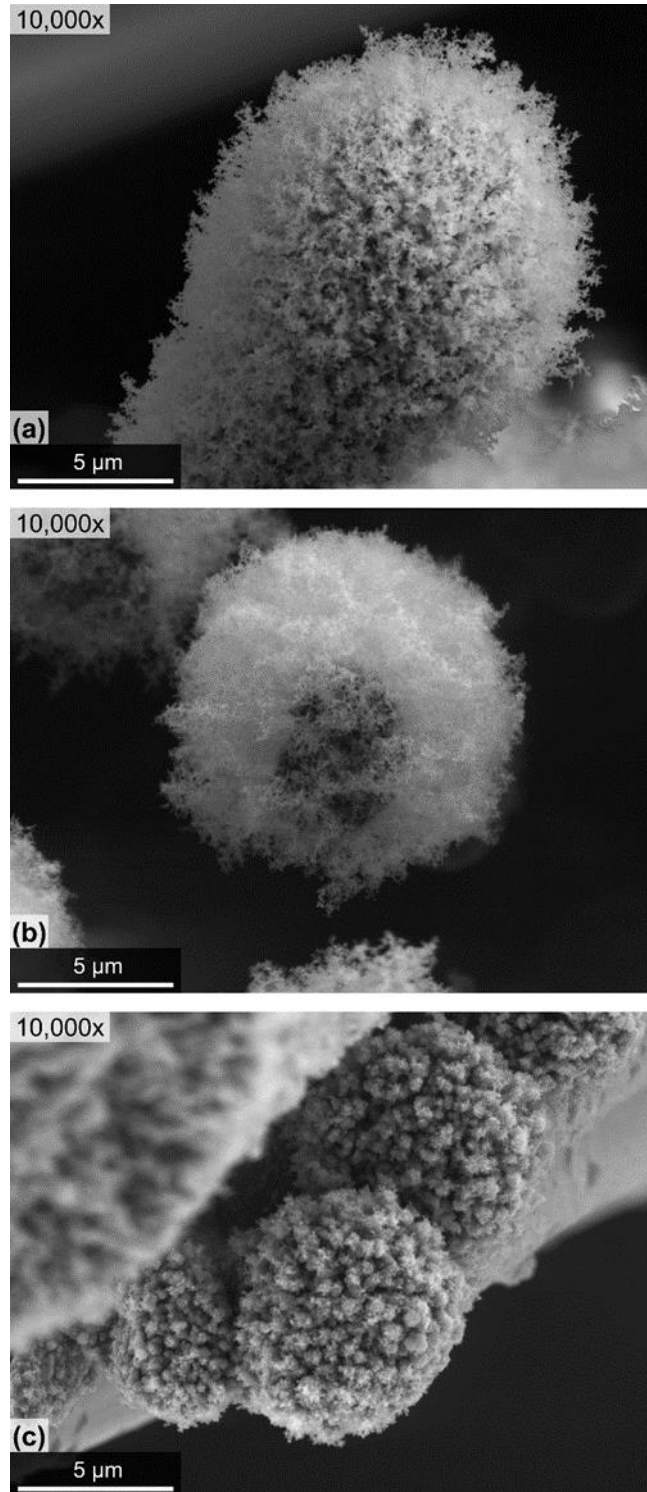


Figure 37. Fuzzy char on single fibers in 21-ply cross-ply Cytec UNC0 specimen burned vertically for (a) 12 s (b) 36 s (c) 60 s

As mentioned previously, the residual char was not uniformly distributed over the composite fracture surface. Little to no char was formed on broken fibers that were visibly recessed inside the specimens, which made it straightforward to identify key fracture characteristics of failed fibers even after fire exposure. This held true for all three fire exposure durations. For cross-ply laminates loaded in compression, fibers in the 0°-plies typically fail due to buckling instabilities (i.e., bending). A portion of a typical failed fiber fracture surface will have a rough appearance consistent with tensile failure. The remainder of the fiber cross-section will display chop marks that demarcate the transition from tensile to compressive failure. The appearance of chop marks can be used to define the location and orientation of the fiber's neutral axis. Such features were still clearly visible for many recessed fibers in the burned UNCO specimens. Figure 38 compares the fiber fracture characteristics of (a) an UNCO specimen before burning with those for slightly recessed fibers in UNCO specimens after burning for 12 s, 36 s, and 60 s. In each burned specimen, indications of recessed fiber flexural failures were completely visible even though such features became more difficult to see on extended broken fibers due to increased char formation.

Fractured translaminar compression specimens may contain multiple thin “terraces” of failed and micro-buckled filaments (Greenhalgh, 2009). Essentially, local material instabilities can give rise to kink bands consisting of terraces of short fractured fibers of approximately the same length. The kink band thickness is inversely proportional to the matrix modulus and is typically on the order of multiple fiber diameters. Figure 39, adapted from Greenhalgh (2009), shows a micrographic image of micro-buckling terraces at the fracture surface of a carbon fiber-reinforced polymer (CFRP) composite specimen failed in compression. Similar terraces of micro-buckled fibers were also observed in SEM images of the fracture surface of UNCO specimens vertically burned for 60 s as shown in Figure 40. Even after extreme fire exposure, kink bands, micro-buckled fibers, and their fracture surfaces were clearly identifiable. Given the loose arrangement of terrace-like structures, it may be possible to dislodge severely burned layers to expose relatively unaffected interior surfaces.

These results suggest that it may be possible to machine away or otherwise dislodge heavily charred regions of burned aerospace composite structures to reveal underlying unburned failure surfaces that can be used in forensic analyses. In addition to cotton-candy-like char deposits on broken fiber ends, as shown in Figure 37, several extended fibers appeared covered with solidified remnants of melt dripping or its by-products that had a cauliflower-like appearance. Figure 41 shows two SEM images of increasing magnification from a UNCO graphite/epoxy specimen burned for 36 s that clearly show the enveloped fiber ends, along with some evidence of char and soot residues. As shown in Figure 41, these cauliflower-like melt drip deposits had a

solid viscous appearance that contrasts with the more fuzz-like char appearing elsewhere in the cross-section as shown in Figure 37. Both types of deposits, however, completely mask the salient aspects of fiber fracture surface-morphology necessary to identify the operative mechanical failure modes. Any chemical or physical attempts at char removal aimed at facilitating forensic analysis in composites subjected to fire would likely have to account for key differences in the chemistry and morphology of the carbonaceous fire by-products deposited on the broken filament ends.

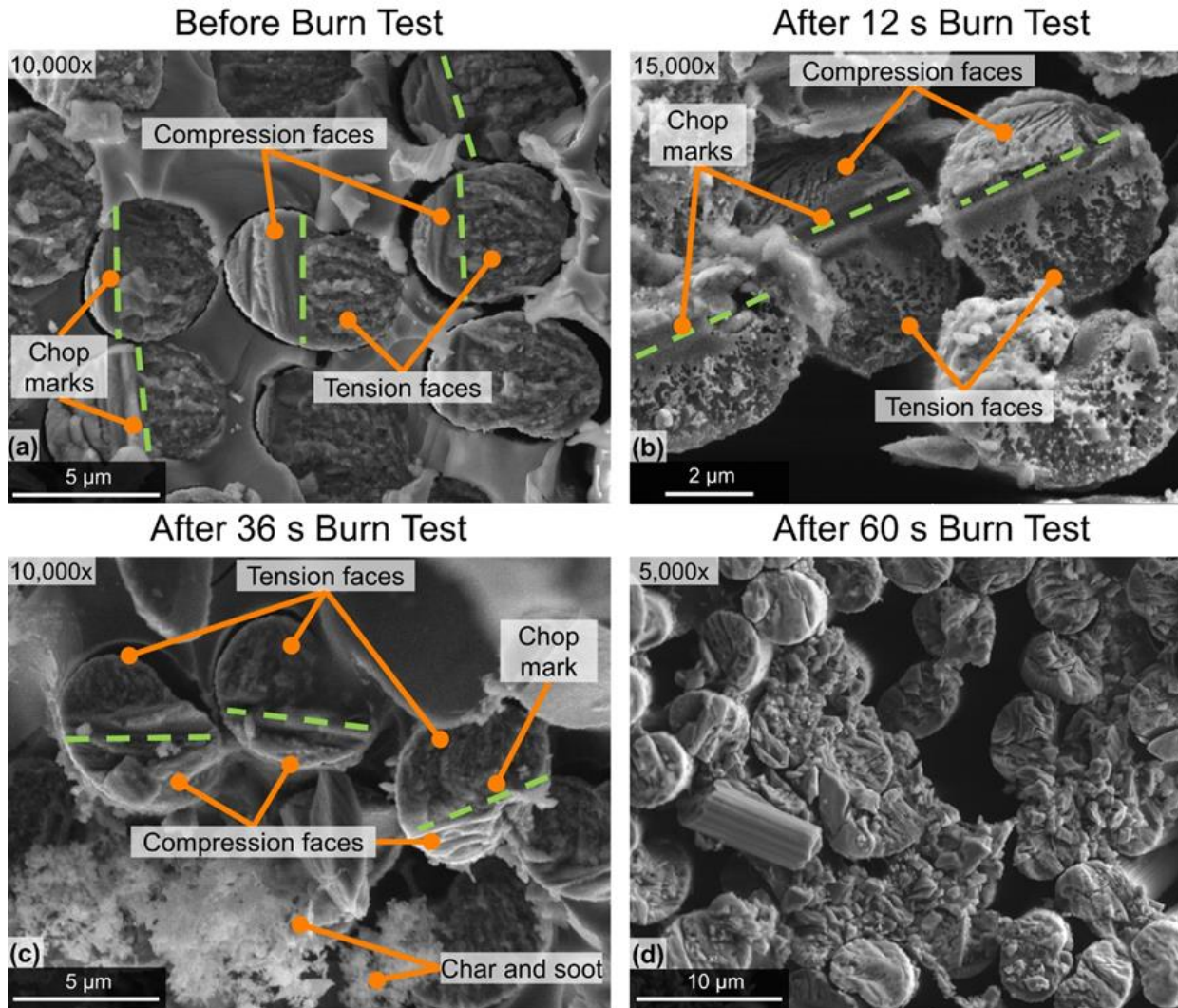


Figure 38. Fracture characteristics on (a) 21-ply cross-ply Cytec UNC0 specimen showing recessed fibers after vertical burning

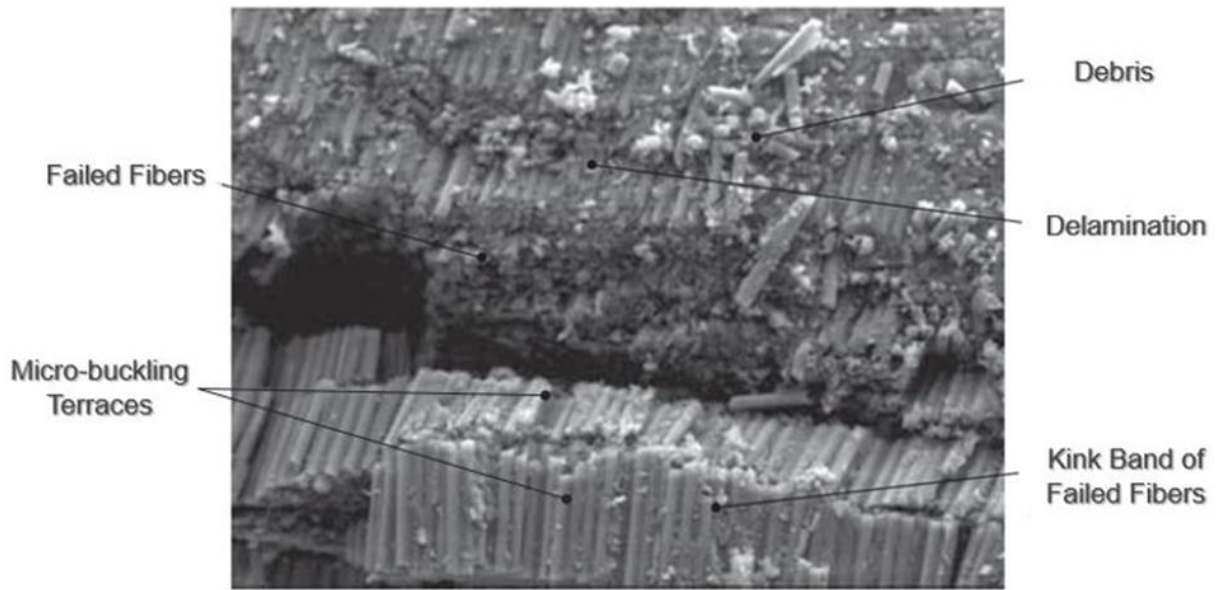


Figure 39. Micro-buckling terraces on compression failed CFRP specimen (x700)

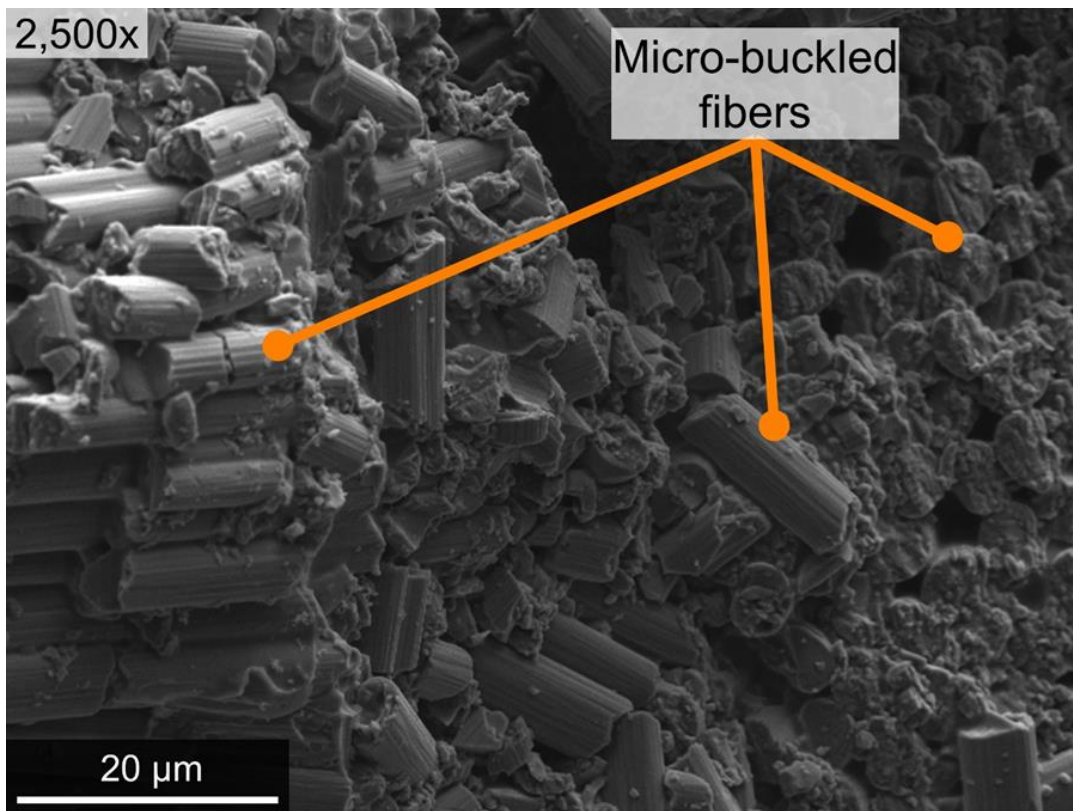


Figure 40. SEM image of micro-buckled fibers in a 21-ply cross-ply Cytec UNCO specimen burned vertically for 60 s

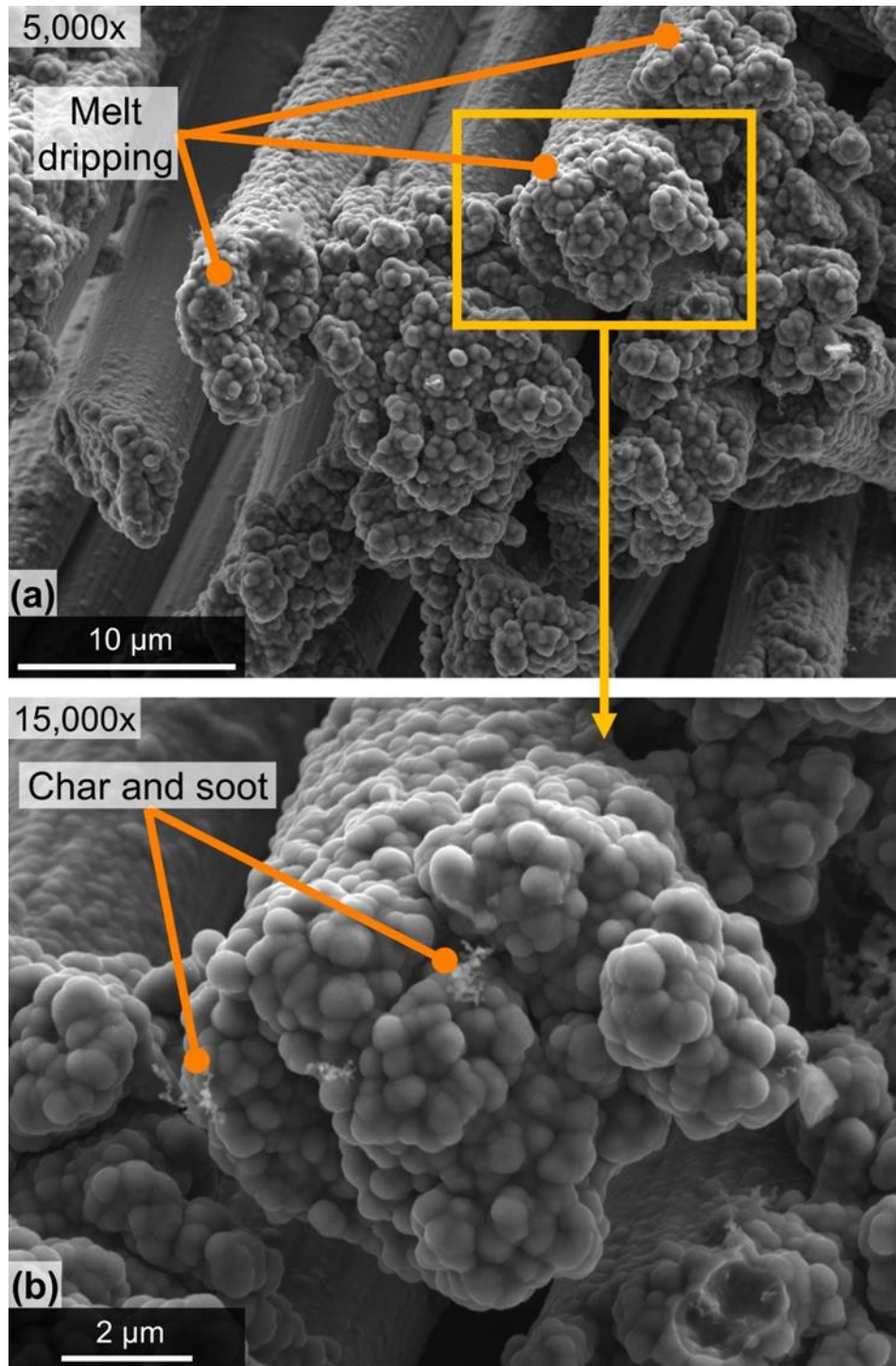


Figure 41. (a) Melt dripping on fracture fiber ends of 21-ply cross-ply Cytec UNC0 specimen burned vertically for 36 s (b) filaments with melt dripping

UNC0 graphite/epoxy specimens burned for extended durations also experienced fire-induced delamination, ply-splitting, and matrix-cracking. Figure 42(a) and Figure 42(b) show

delamination between plies and ply-splitting in an UNCO specimen after a 60 s burn test. Figure 43 shows matrix cracking in the same specimen. Delamination, ply-splitting, and matrix cracking result from large internal local pressures due to the formation of combustion gases, smoke, and vaporized moisture that try to escape to the exterior. Such damage can also arise from thermally induced-strain and temperature gradients in a laminate, which can be exacerbated by large differences in local ply orientations such as those occurring in cross-ply UNCO specimens. In addition, temperature-induced thermal softening of the matrix can result in significant reductions in composite interlaminar fracture toughness and contribute to increased matrix cracking and delamination (Mouritz, et al., 2009).

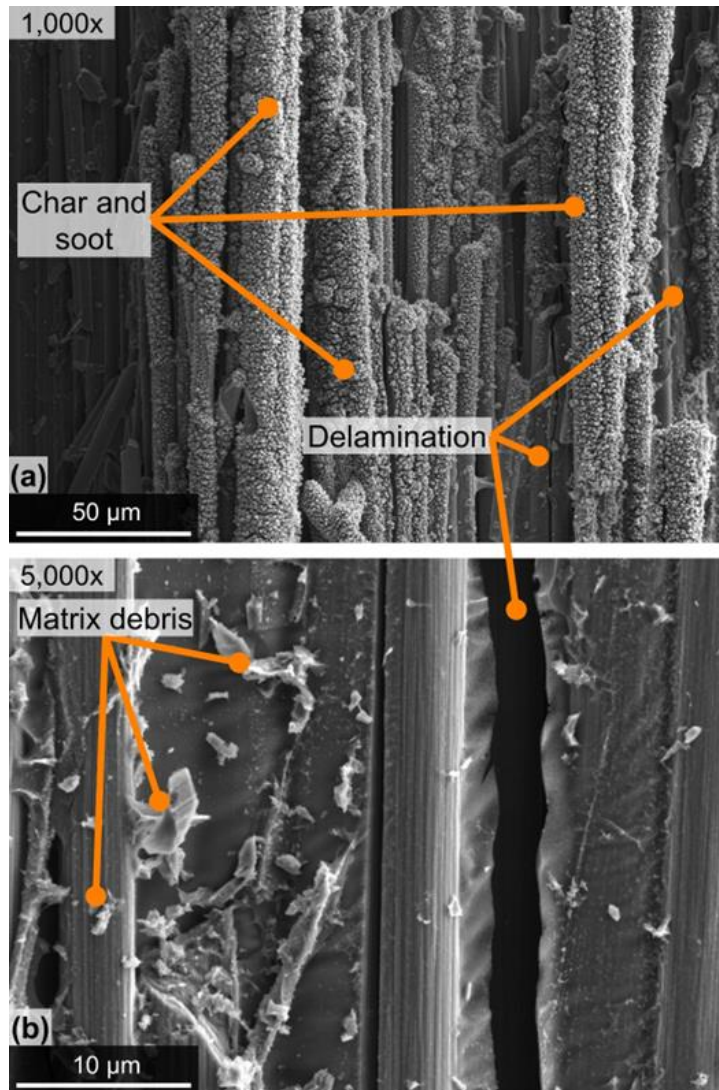


Figure 42. Delamination in 21-ply cross-ply Cyttec UNCO specimen burned vertically for 60 s

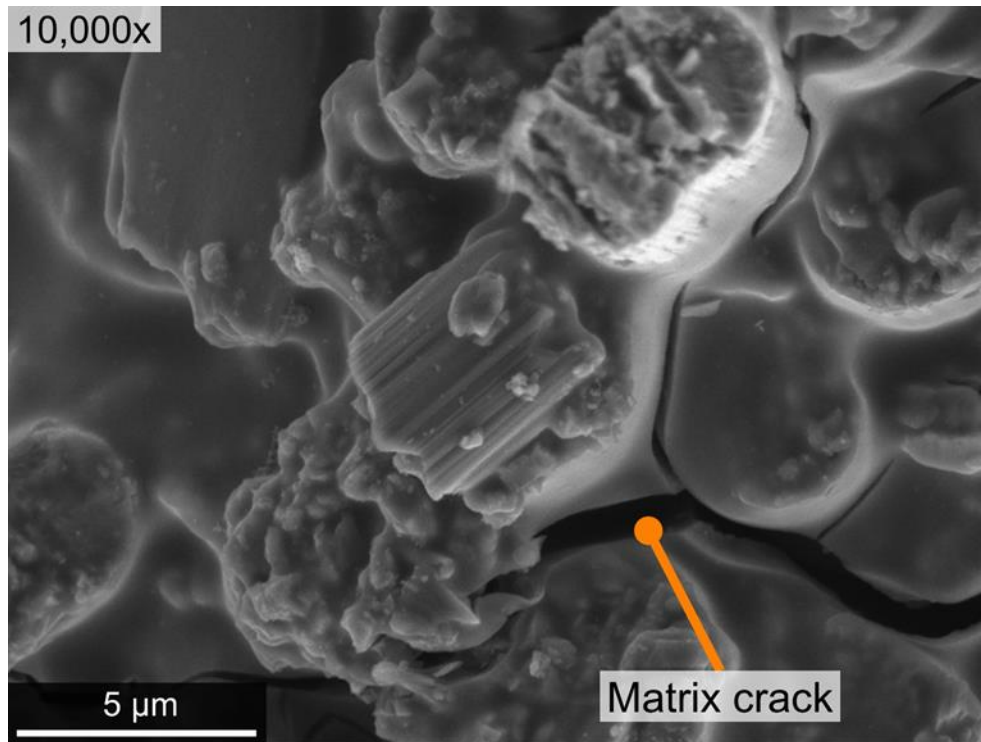


Figure 43. Matrix cracking in 21-ply cross-ply Cytec UNCO specimen burned vertically for 60 s

3.2.1.2 SBS specimens (Exposure times: 12 s, 36 s, 60 s)

Vertical fire tests were performed on 45-ply unidirectional Cytec SBS specimens (layup: $[0]_{45}$) for durations of 12 s, 36 s, and 60 s to assess the effects of flame exposure time on char formation. Three repeats were performed for each fire exposure time. Fire damage (i.e., extensive fire matrix decomposition, soot, char, and residual thickness increase) observed was more severe for specimens subjected to the flame for 36 s and 60 s. The fire damage mechanisms generated in the vertical burning tests on the SBS specimens were similar to those in the UNCO specimens and extended throughout the length of the burned specimens. Again, the relatively thick SBS and UNCO specimens both display a more compact failure surface that inhibits oxygen flow to the interior of the specimens, resulting in more char formation around the perimeter of the cross-section. Char deposition at the SBS fracture surfaces also served as a thermal barrier that reduced fire damage penetration into the composite at the laminate interior; this is consistent with observations from the literature (Mouritz & Gibson, 2007; Mouritz & Mathys, 2001). As with prior tests, for all three fire exposure durations, the lateral specimen edges (sides) continued to burn after the flame was extinguished. Similar to UNCO specimens, SBS specimens exposed for 12 s took longer to self-extinguish than for 36 s and 60 s fire tests. Figure 44 shows typical macro-scale pictures of an SBS specimen before and after fire exposure for 60 s. The fire damage included local delamination near the fracture surface, char formation, and soot

deposition on the lateral edges and outer ply surfaces, and a significant increase in the residual thickness of the burned specimen.

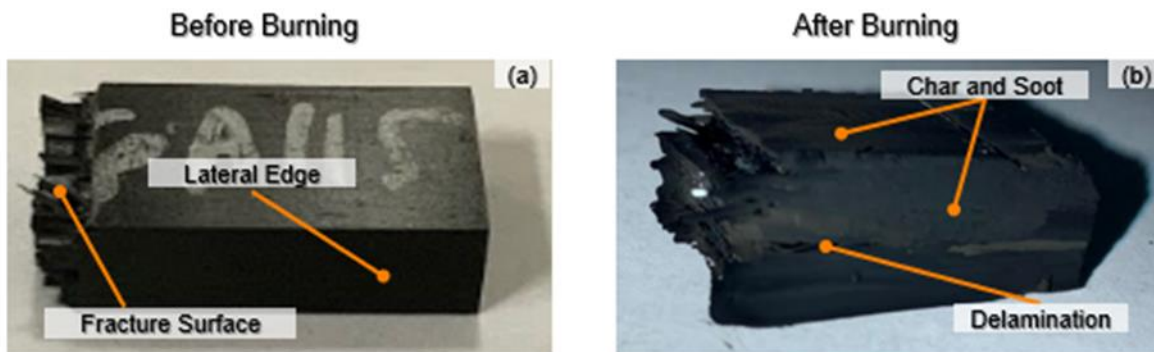


Figure 44. Picture of 45-ply unidirectional Cytec SBS specimen (a) before and (b) after vertical burning for 60 s

Mechanically failed SBS specimens subjected to three-point bending will break into two distinct halves, as suggested by the single half shown in Figure 44(a). Occasionally, an individual half will longitudinally split or completely delaminate into two $\frac{1}{4}$ -specimens due to high inter-laminar stresses. Pairs of mating $\frac{1}{4}$ -specimens were clamped together and subjected to 12 s, 36 s, and 60 s fire exposure tests. After 12 s of fire exposure, the mating pieces remained separated. After 36 s and 60 s of fire exposure, however, the mating pieces adhered together. Clearly, increased fire exposure led to some degree of interfacial bonding between initially separated layers. This is likely due to various aspects of melt dripping, melted resin rehardening, and subsequent matrix decomposition or the presence of tougheners, surfactants, plasticizers, flame retardants, or other additives blended into the commercial Cycom[®] 5215 epoxy prior to resin infusion and curing. The exact composition of most commercially available thermosetting epoxies is proprietary and very difficult to determine. It is unclear whether the use of unmodified epoxy would lead to the same adhesion between separated layers upon reheating; this issue remains to be fully explored. Nonetheless, the local chemistry at these interfaces for Cycom[®] 5215 epoxy may be similar to that for the melt dripping observed throughout these family of tests and may provide insight into char formation and removal on graphite/carbon fiber surfaces. The effect of melt dripping or similar phenomena may become increasingly pronounced for thicker specimens where the total volume of the cured matrix is greater, and incomplete decomposition/combustion of the matrix is increasingly likely.

Figure 45 shows SEM micrographs taken from the perimeter of the fracture surface of vertically burned SBS graphite/epoxy specimens exposed to direct flame for 12 s, 36 s, and 60 s, respectively. Similar to the UNCO specimens shown in Figure 36, proportionally more char accumulated at and near extended broken fibers located around the perimeter of the cross-section

where the airflow was greater; little char formed on extended fibers located near the laminate mid-plane. Specimens burned for only 12 s displayed apparent accumulations from melt dripping at the broken filament ends, as shown in Figure 45(a), with very little soot and char deposits. The presence of melt dripping coupled with low amounts of char suggests relatively incomplete combustion/decomposition of the epoxy matrix occurred for the 12 s flame exposure, which no doubt was influenced by the relatively thick SBS specimen geometry. While not shown here, melt dripping was also observed along the lateral edges (sides) of the SBS specimens. Specimens burned for 36 s and 60 s, shown in Figure 45(b) and (c), exhibited increasing amounts of extensive char formation on extended broken fibers, as well as appreciable soot deposition. Similar to results for UNCO specimens, the char formed at and around the extended fiber ends exhibited a fuzzy (cotton-candy-like) appearance shown in Figure 46.

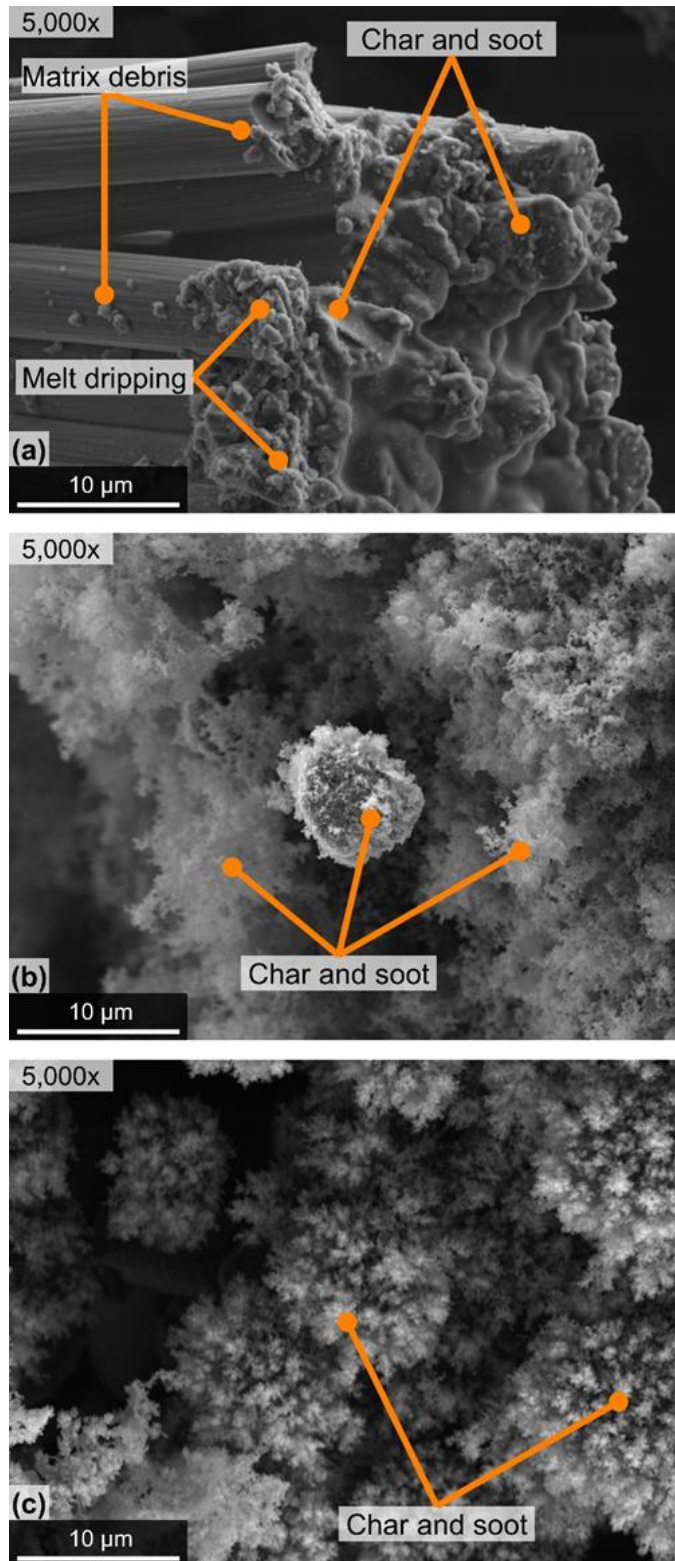


Figure 45. Char and soot on fracture surface of 45-ply unidirectional Cytec SBS specimens after vertical burning for (a) 12 s (b) 36 s and (c) 60 s

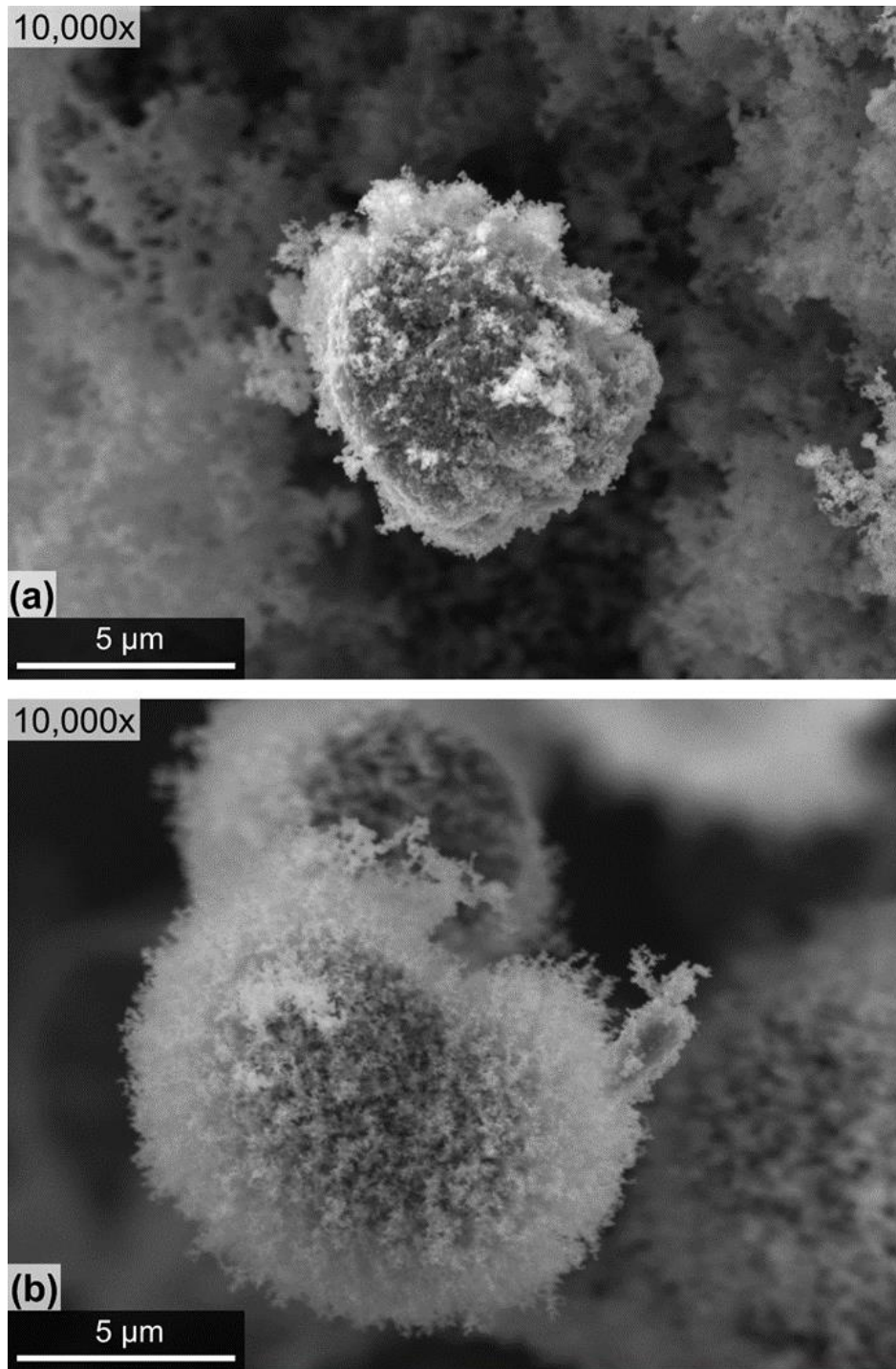


Figure 46. Fuzzy char around single fibers in 45-ply unidirectional Cytac SBS specimens burned vertically for (a) 36 s and (b) 60 s

It is clear that extended fibers emanating from the mean fracture surface of failed UNCO and SBS specimens are prone to accumulation of melt dripping, char, soot, and other deposits that mask key aspects of fracture surface morphology. Hence, physical, chemical, or thermal strategies for char removal must be developed in order to perform forensic analysis of these

original mechanical failure surfaces without damaging or destroying the surfaces. As mentioned previously, an inspection of visible recessed broken fibers may permit the identification of operative mechanical fiber failure mechanisms. For example, Figure 47 contains SEM images of recessed fibers in an unburned SBS specimen, as well as for specimens burned for 12, 36, and 60 s. In each case, rough tensile failure surfaces and compressive chop marks were clearly visible on numerous recessed fibers; such features became increasingly obscured on extended filament ends as the fire duration was increased.

Similar to UNC0 specimens shown in Figure 39, adapted from Greenhalgh (2009), terraces of micro-buckled fibers formed in compressive regions of failed three-point bend SBS specimens. Figure 47(a) and Figure 47(b) show SEM images of micro-buckled fibers in a SBS specimen before fire exposure. Figure 48(c) shows the same specimen after vertical burning for 60 s. After burning, parallel clusters of micro-buckled fibers indicative of compressive failure were still visible, albeit covered in char; some slant-like fiber fracture features also remained. In nearby regions of the specimen, micro-buckled fibers in terrace structures were completely covered with melt dripping, as shown in Figure 49. This suggests that removal of the outer terraces may be desirable to identify operative mechanical failure mechanisms better.

The vertical fire tests performed on UNC0 and SBS specimens suggest that a sequence of thermally activated processes contribute to char formation on broken graphite fibers that strongly depend on the flame duration, specimen geometry, and layup, spatial location within a given cross-section, original fracture surface morphology, local extension/recession of individual filaments, airflow, oxygen availability, and other factors. A potential sequence of these events can be summarized as follows: Upon initial heating of the composite, melt dripping occurs that leads to thick goeey deposits on the extended filament-ends emanating from the fracture surface, shown in Figure 45(a). As the fire exposure is increased, these deposits increasingly decompose and combust, leading to fuzzy or cotton-candy-like char deposits on the fiber ends, shown in Figure 45(b) and Figure 45(c). As the flame duration is further increased, the char is completely decomposed/consumed, leaving bare fibers; this may explain a large number of exposed fibers at the laminate mid-planes after significant fire exposure. This sequence of events is not terribly dissimilar from processes used in ASTM standard matrix ignition tests (ASTM-D2584-18, 2018) and efforts aimed at recycling carbon fibers from thermoset composites (Fernández, Lopes, González, & López, 2018; Yang, et al., 2012). Of course, large-scale fire exposure to bare graphite or carbon fibers has the potential to damage and decompose the fibers severely.

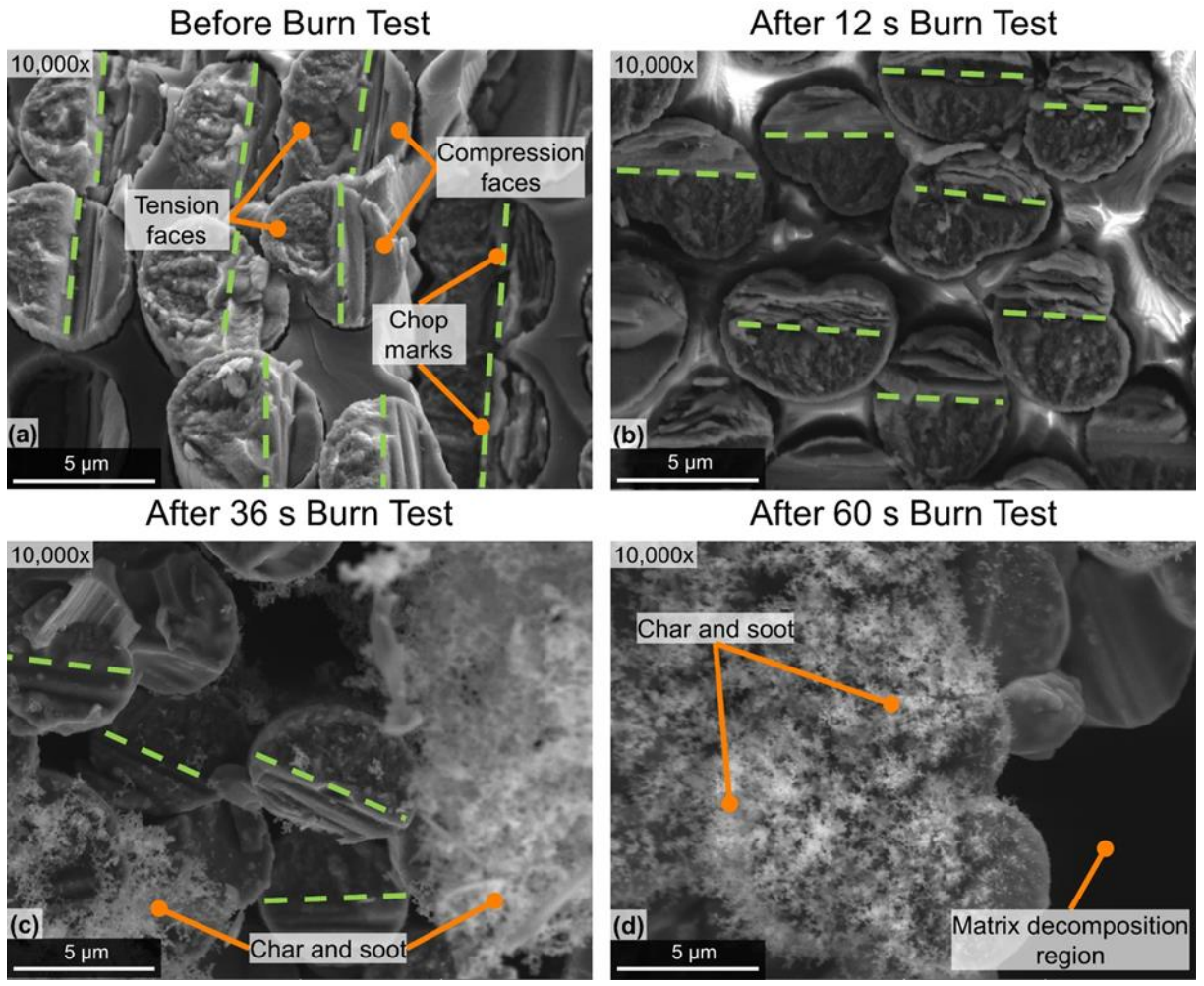


Figure 47. Fracture characteristics on (a) 45-ply unidirectional SBS Cytec specimen showing recessed fibers after (b) 12s, (c) 36s, and (d) 60 s vertical burning

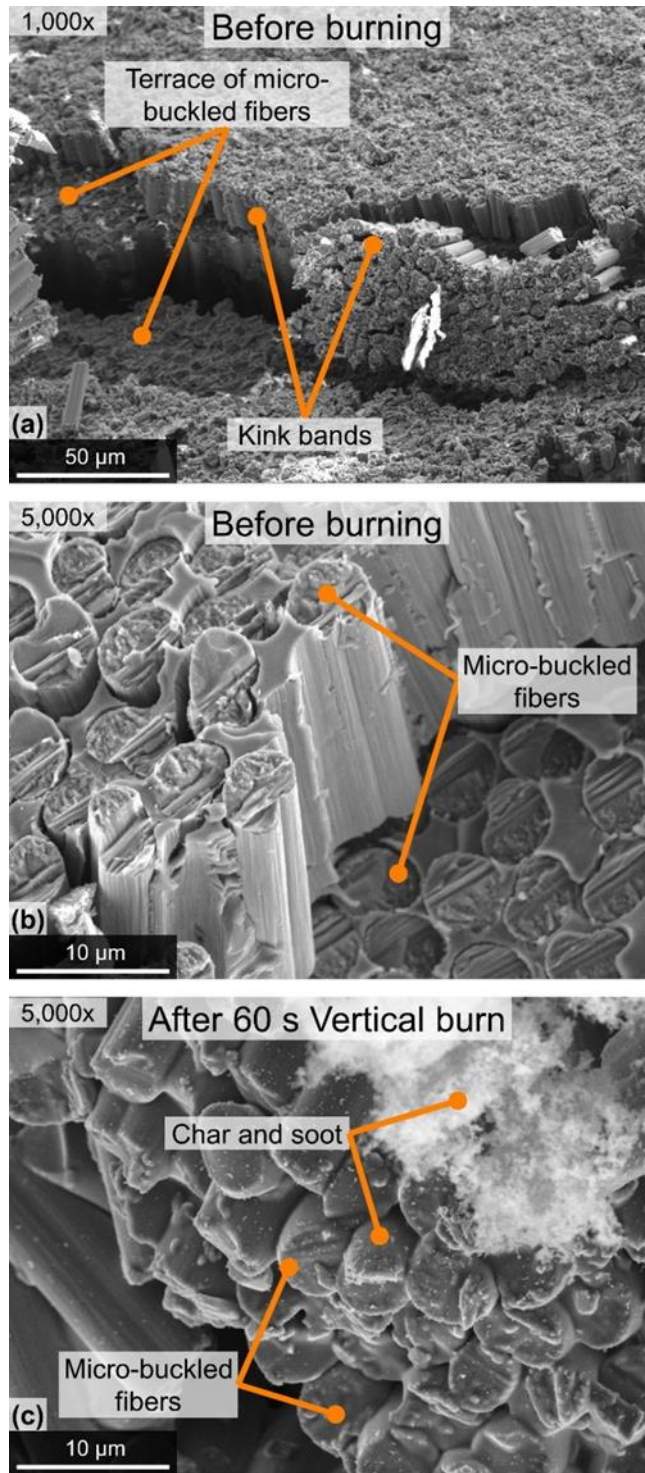


Figure 48. Micro-buckled fibers in Cytec SBS specimens

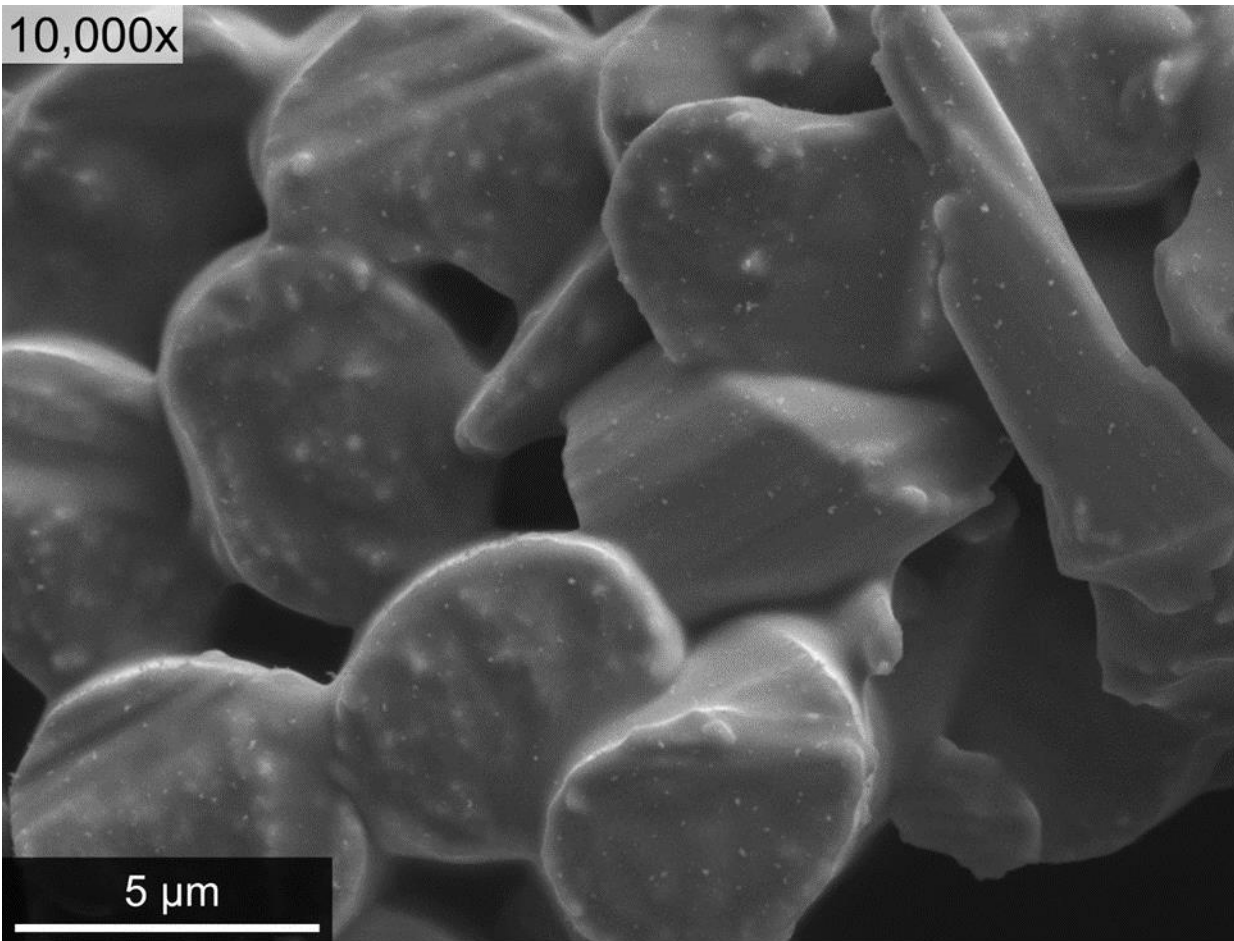


Figure 49. Micro-buckled fibers in Cytec SBS specimens completely covered in melt dripping

3.2.1.3 IPS specimens (Exposure times: 6 s, 12 s, 36 s, 60 s)

Vertical fire tests were performed on 16-ply Cytec IPS specimens (layup: $[45/-45]_{4s}$) for durations of 6 s, 12 s, 36 s, and 60 s to assess the effect of fire exposure on char formation. Three repeats were performed for each exposure time. Unlike UNCO and SBS specimens that tend to fail within a more planar damage zone, individual IPS plies tend to fail along multiple offset planes that are oriented at $\pm 45^\circ$ to the axial loading direction (i.e., perpendicular to the local ply orientation). In addition, failure involves extensive fiber tow splitting and delamination between plies. As a consequence, there is much more free-surface (combustible) area created during failure of the angle-ply IPS specimens than for cross-ply UNCO and unidirectional SBS specimens, and the IPS damage distribution is far-more diffuse (see inset figure included in Table 2).

Due to their highly irregular fracture surface geometries, the IPS specimens were positioned above the Bunsen burner during fire tests such that the blue tip of the flame was at the same level as the fractured fibers at the longest lateral edge of the specimen, as shown in Figure 50 and

location 1 in Figure 51(a). Specimens subjected to fire exposures of 12 s, 36 s, and 60 s each experienced large-scale matrix decomposition and delamination that increased substantially with increasing fire exposure. For longer exposure times, almost complete matrix decomposition occurred over the majority of the specimens, and fire-induced delamination spanned the entire length of the specimens. Virtually no char, soot, or epoxy was visible at the graphite filament ends located at the laminate midplane along the centerline of the composite that was exposed to direct flame, shown in location 2 in Figure 51(a); bundles of bare graphite fibers (with no evidence of cured epoxy matrix or char) remained at this location after burning. IPS specimens burned for 12 s, 36 s, and 60 s were largely destroyed during fire testing. These specimens displayed much higher degrees of matrix decomposition, significantly lower levels of residual char formation, and more fiber thermal damage than the UNCO and SBS specimens tested under similar conditions. The large free surface area present in failed IPS specimens resulted in enhanced oxygen flow throughout the specimens, complete combustion of the organic matrix, and relatively little residual char formation. For these reasons, additional vertical tests of IPS specimens were performed with a reduced fire exposure duration of 6 s. In contrast to the UNCO and SBS specimens, which generated more char on exposed fiber ends with increasing fire exposure times, the maximum char formed on extended fibers in IPS specimens occurred for a 6 s exposure time.



Figure 50. Positioning of IPS specimen during vertical burn tests

Figure 51 shows typical macro-scale pictures of an IPS specimen (a) before and (b, c) after fire exposure for 6 s. Char and soot were observed on the exposed filament ends, lateral specimen edges (sides), and on planar outer ply surfaces. Pre-existing mechanical delamination appeared to grow significantly after fire exposure. The locations 1 (longest lateral edge), 2 (laminar centerline), and 3 (shortest lateral edge), shown in Figure 51(a), define the approximate locations of SEM images taken of the failure surfaces. Figure 52 shows that IPS specimens burned for 6 s developed significant char on extended fibers at both lateral edges, as well as the laminar centerline.

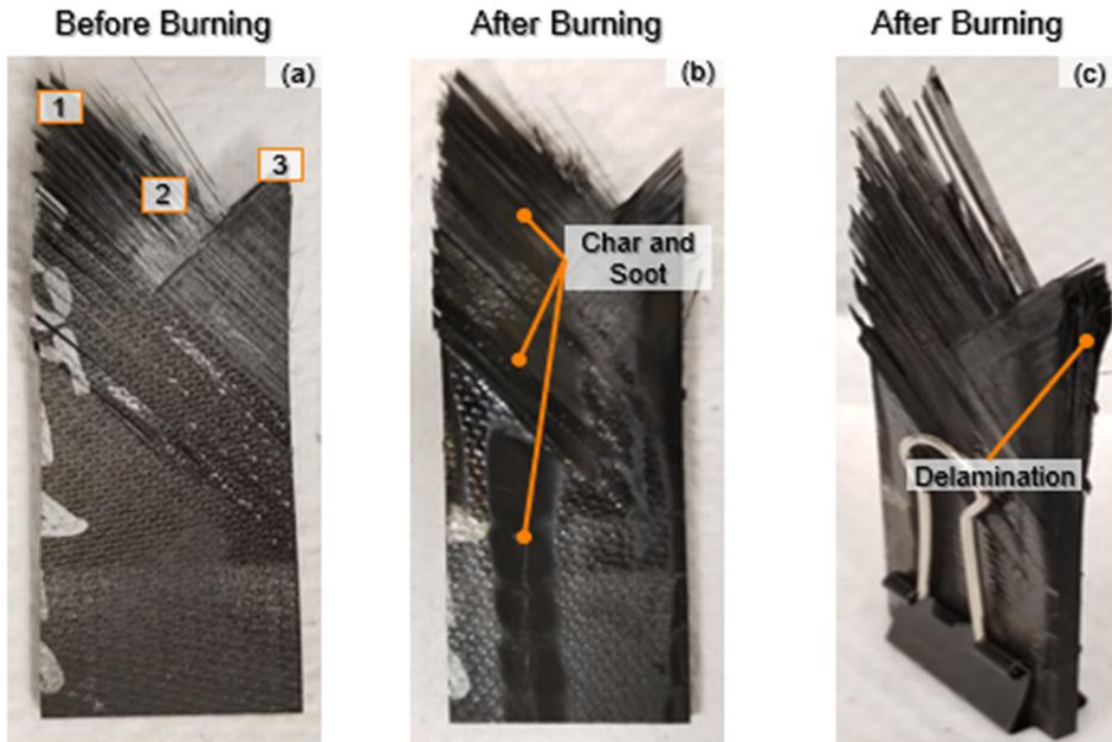


Figure 51. 16-ply Cytec IPS specimen (a) before (b) after and (c) after vertical fire exposure for 6 s

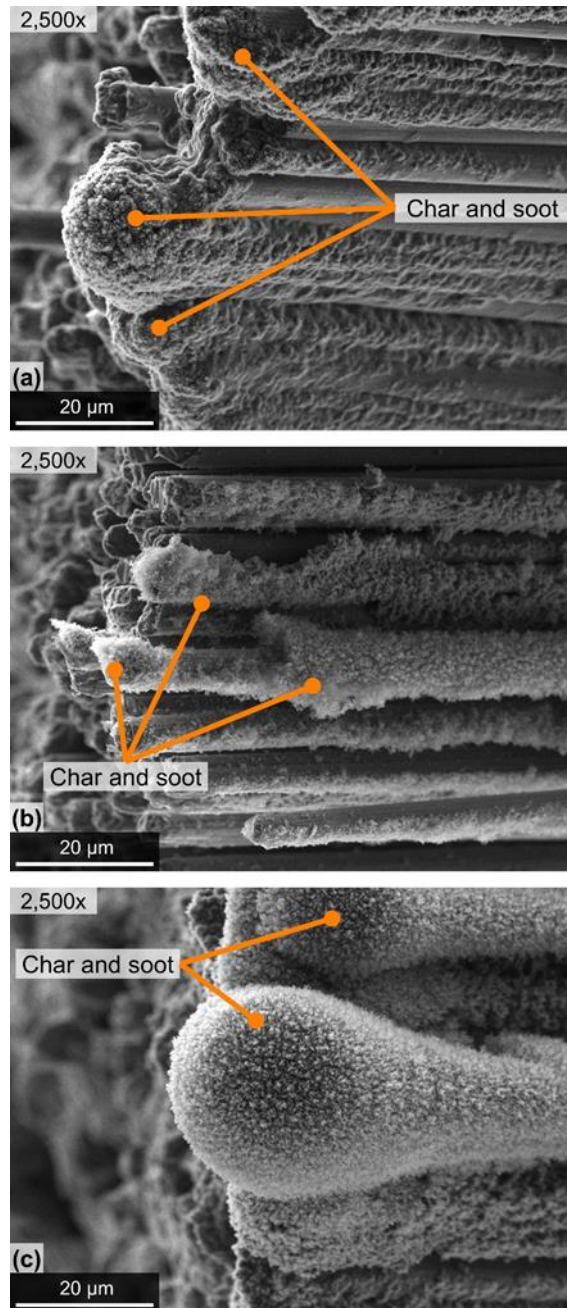


Figure 52. (a) longest lateral edge (b) center and (c) shortest lateral edge of 16-ply Cytec IPS specimens

For IPS specimens subjected to longer fire exposure times (i.e., 12, 36, and 60 s), virtually no residual char formed on fibers located near the longest lateral edge, shown in location 1 in Figure 51(a), or at the specimen centerline, shown in location 2 in Figure 51(a). In contrast, significant char only formed on broken fiber ends located near the shortest lateral edge, shown in location 3 in Figure 51(a); this location was farther removed from the blue flame tip than the other points considered. Figure 53(a) through Figure 55(a) show SEM images of the fracture surface at the

longest lateral edge for specimens burned for 12 s, 36 s, and 60 s, respectively. Similarly, Figure 53(b) through Figure 55(b) show SEM images of the increasing amounts of char and soot deposited on fibers at the shortest lateral edge for specimens burned for 12 s, 36 s, and 60 s, respectively. Since no significant char was present at the longest lateral edge for specimens due to the relative location of the fuel source, epoxy matrix cracks, angled fiber fractures, matrix debris, and micro-buckled fibers are all clearly visible in the images. These features are similar to typical fracture characteristics found in unburned IPS specimens. Any char that did form and then was subsequently burned off did not appear to change the identifiable mechanical failure mechanisms significantly. This trend did not hold true, however, for fibers located along the centerline of the IPS specimens. As an aside, the SEM images presented in Figure 53, Figure 54, and Figure 55 were taken at different WDs to accommodate large variations in specimen geometries, as well as differences in the out-of-plane locations of individual clusters of fibers.

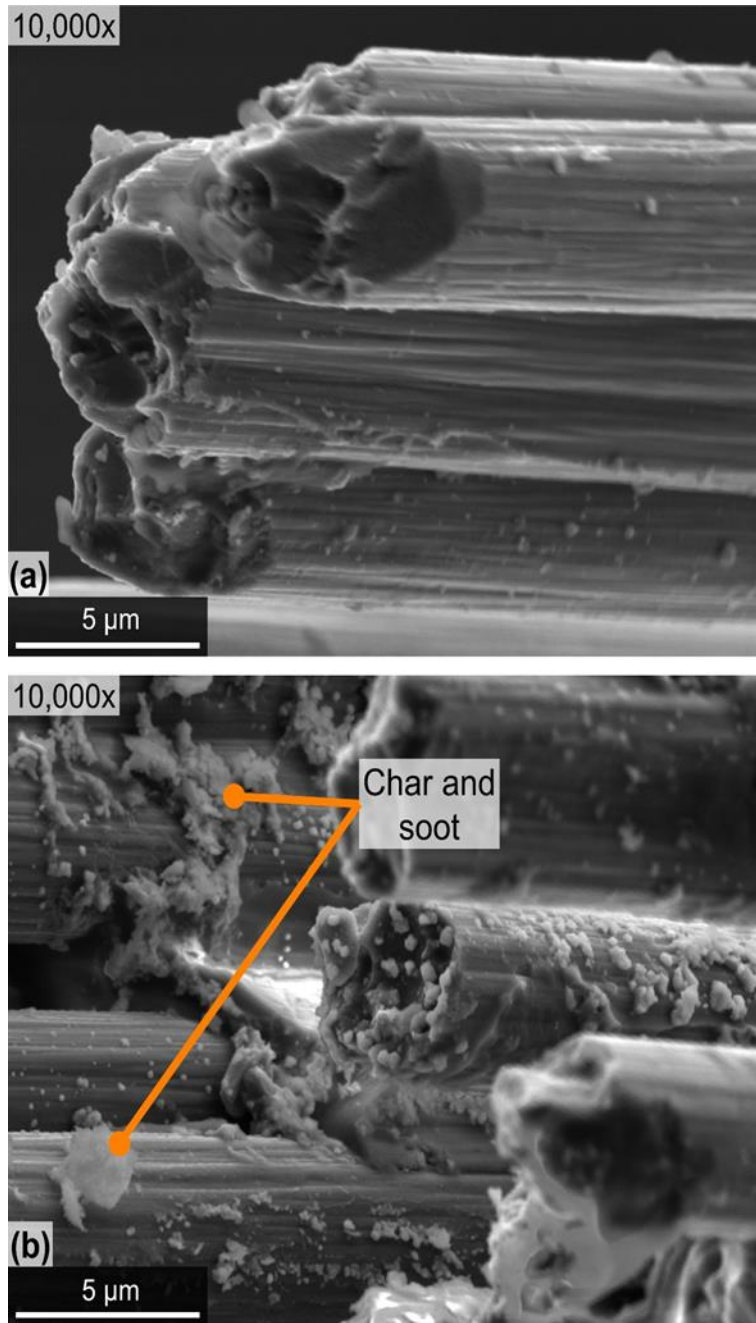


Figure 53. Char formation on (a) longest and (b) shortest lateral edges of 16-ply Cytec IPS specimens burned vertically for 12 s

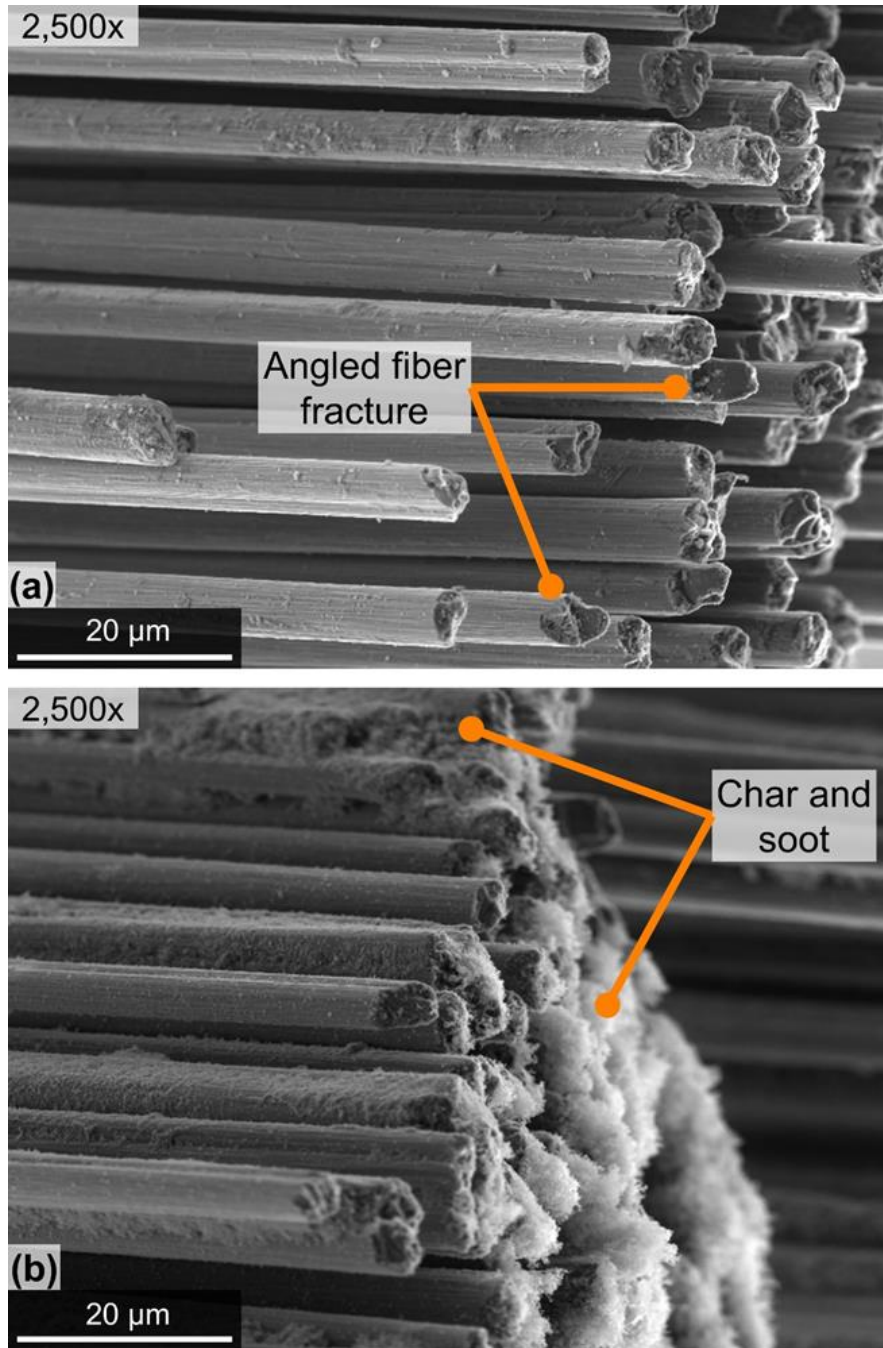


Figure 54. Char formation on (a) longest and (b) shortest lateral edges of 16-ply Cytec IPS specimens burned vertically for 36 s

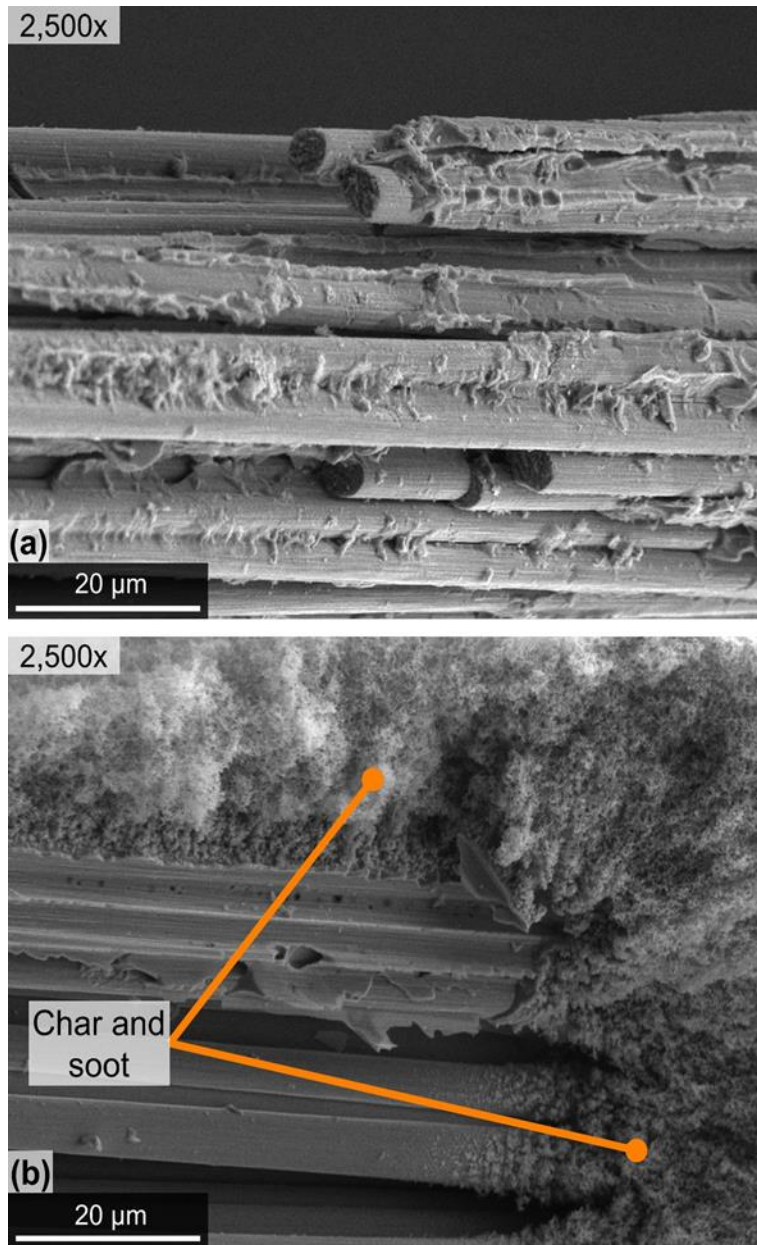


Figure 55. Char formation on (a) longest and (b) shortest lateral edges of 16-ply Cyttec IPS specimens burned vertically for 60 s

Exposed graphite filaments located near the mid-plane of the fracture surface along the IPS specimen centerline, shown in location 3 in Figure 51(a), were severely altered when specimens were burned for 12 s, 36 s, and 60 s. The fibers' thermal degradation was so severe that it eliminated any possibility of identifying fiber mechanical failure mechanisms. Figure 56 shows SEM images of broken fibers located along the centerline of IPS graphite/epoxy specimens burned for (a) 12 s, (b) 36 s, and (c) 60 s. In each case, the family of fibers became longitudinally thinner and developed needle-like shapes. Moreover, voids and cavities formed at the fiber-ends in specimens burned for 60 s (Figure 57). Graphite/carbon fiber ends thinning is mainly caused

by oxidation (Greenhalgh, 2009) occurring about a threshold temperature of 350-450°C (Mouritz & Gibson, 2007). Graphite/carbon fiber oxidation occurs at very low rates when the fibers are initially embedded in an epoxy matrix (Mouritz & Gibson, 2007) since the char formed and deposited on the fiber surfaces during burning acts as a protective layer that effectively stops the oxygen from reaching the surface of the fiber (Mouritz & Mathys, 2001) (Mouritz & Mathys, 2001). In addition, impurities like sodium can accelerate the oxidation process in graphite fibers (Sussholz, 1980). These results suggest that extreme fire conditions leading to oxidation or sublimation of graphite/carbon fibers can render fractographic assessments of composite failure surfaces useless. In addition, any pyrolysis- or thermal-based approach aimed at removing char from burned graphite/epoxy fracture surfaces should be performed at temperatures near the matrix decomposition and well below oxidation threshold and sublimation temperatures to avoid fiber thermal degradation.

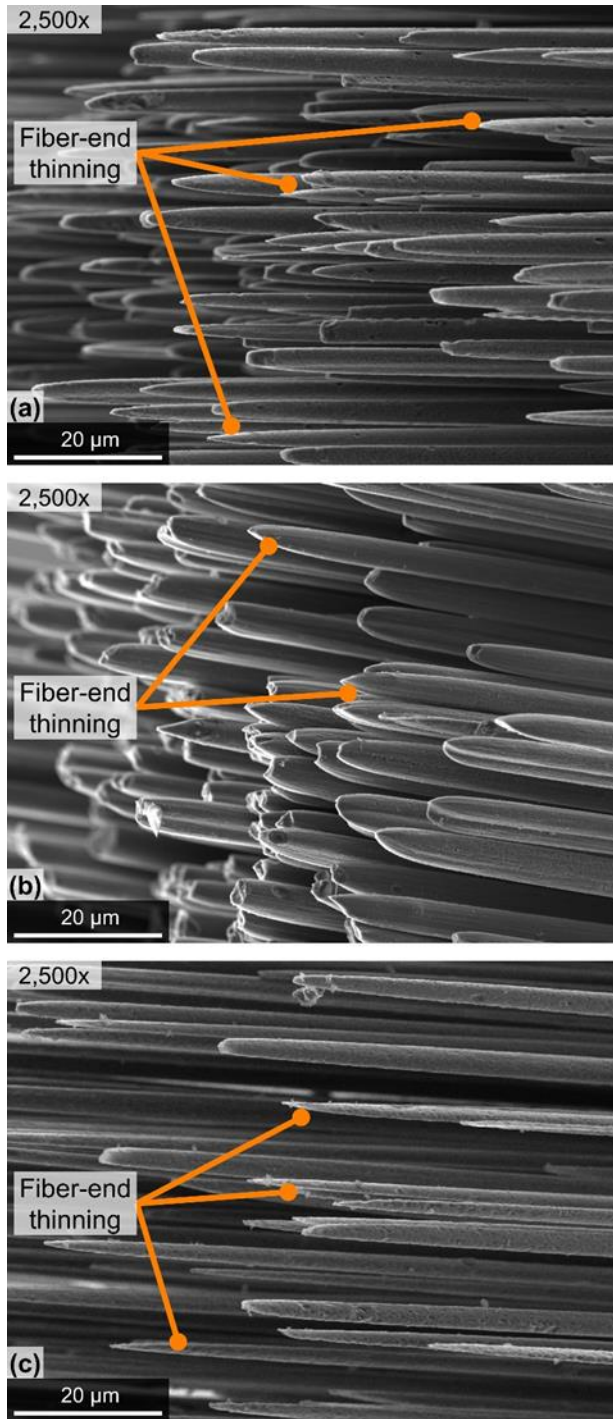


Figure 56. Fiber-end thinning of filaments at mid-plane of 16-ply Cytec IPS specimens burned vertically for (a) 12 (b) 36 and (c) 60 s

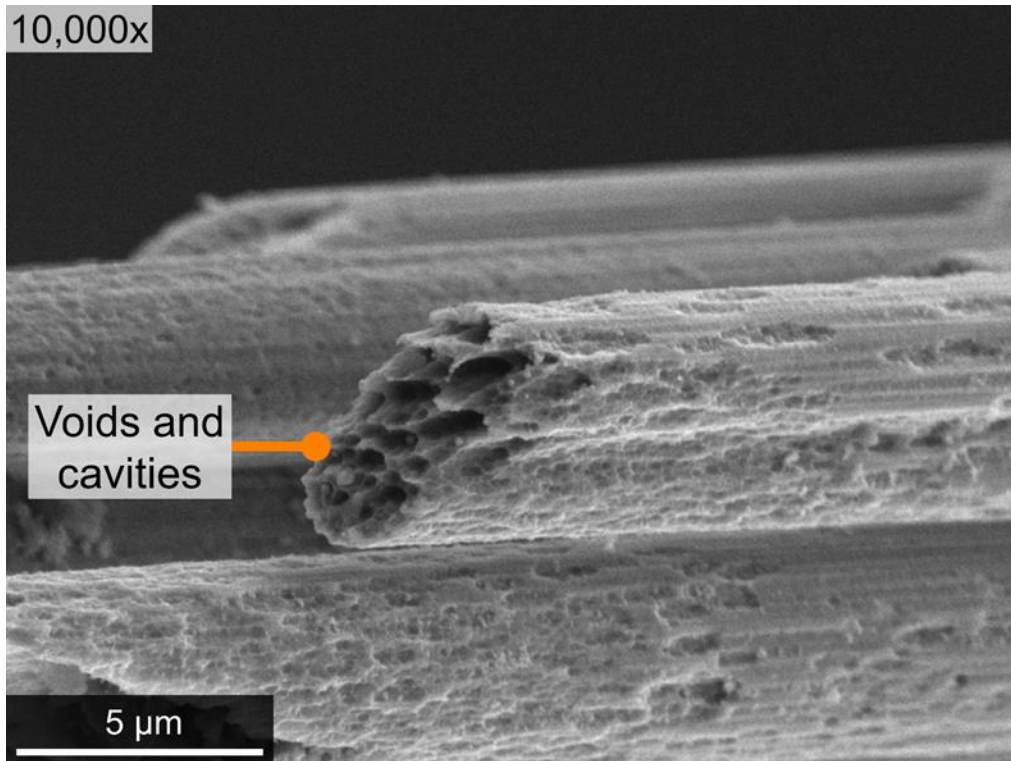


Figure 57. Void and cavities on fiber of 16-ply Cytec IPS specimen burned vertically for 60 s

3.2.2 Enclosed horizontal fire testing of Cytec T40-800/Cycom[®] 5215 graphite/epoxy specimens

3.2.2.1 UNCO specimens (Exposure times: 15 s, 45 s, 75 s)

Fire tests on horizontally-oriented 21-ply cross-ply Cytec specimens (layup: $[90/0/90]_7$) were performed for durations of 15 s, 45 s, and 75 s to assess the effects of specimen orientation and flame exposure time on fire damage formation. Three repeat horizontal fire tests were performed for each exposure time. The horizontally-oriented specimens typically experienced *lower* degrees of thermal damage than vertically-oriented specimens since a much smaller fraction of the total specimen volume is located above the tip of the flame. In each horizontal test, the UNCO specimens self-extinguished as soon as the applied flame was stopped. The local matrix decomposition, surface char, and soot were more severe over the lower outer ply surface exposed to direct flame; such damage was more pronounced for the 45 s and 75 s fire tests. Unlike the case for vertical tests, no delamination or residual thickness increase occurred for all three fire exposure durations (i.e., 15 s, 45 s, and 75 s). Figure 58 shows typical macro-scale images of the lower and upper surfaces of an UNCO specimen before and after horizontal burning for 75 s. The lower surface of the specimen, shown in Figure 58(a) and Figure 58(b) suffered matrix

decomposition over the region exposed to direct flame. In contrast, the upper surface of the specimen, shown in Figure 58(c) and Figure 58(d) was not appreciably affected by the fire.

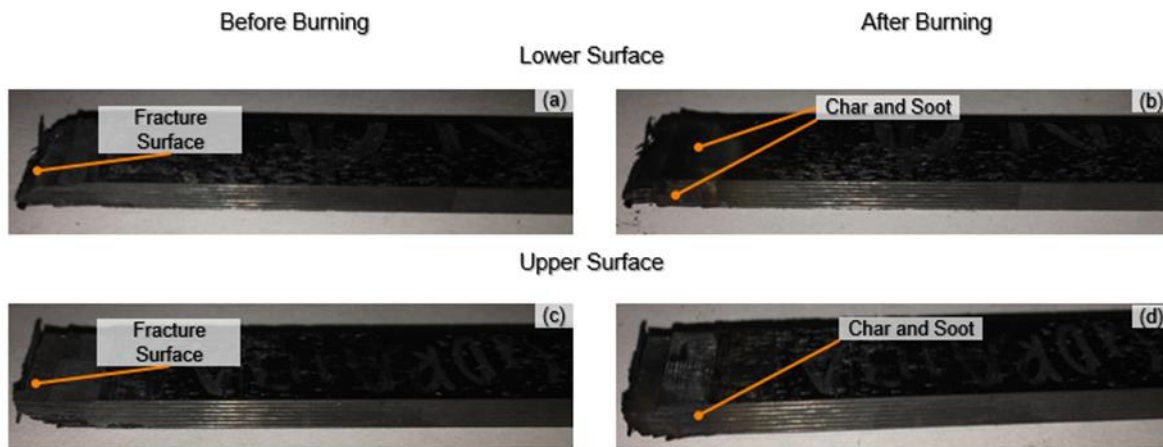


Figure 58. 21-ply cross-ply Cytec UNC0 specimen before and after horizontal burning for 75 s

In the vertical fire test configuration, the specimens were held upside down into the flame, as in Figure 30(a). In the horizontal fire test configuration, only the fractured edge of the bottom planar surface of the specimen was immersed into the flame, see Figure 30(b). The difference in fire damage extent and severity between UNC0 specimens used in vertical tests (Figure 35) and horizontal tests (Figure 58) may be due to differences in specimen in-plane and through-thickness thermal conductivities and other thermal properties. For example, the heat conduction parallel to the fibers will be much greater than through the ply thickness. The thermal conductivities of typical polyacrylonitrile (PAN)-based carbon/graphite fibers in the axial and radial directions are approximately 20 W/mK and 0.32 W/mK, respectively (Mouritz & Gibson, 2007). This compares to a value of 0.23 W/mK for a typical epoxy matrix (Mouritz & Gibson, 2007). This suggests that, for horizontal tests, heat conduction in the outermost ply exposed to the flame will be greatest in the fiber direction. This may explain the greater degree of outer ply matrix decomposition parallel to the plane in comparison to the through-thickness fire damage, as the fire damage was more concentrated in the outermost ply. In contrast, for vertically burned specimens, the 0° fibers provide a more direct heat conduction path to the interior of the specimen, resulting in far more severe internal fire damage (melt dripping, matrix decomposition, delamination, explosive outgassing, etc.).

The amount of char formed at the fracture surface of UNC0 specimens burned horizontally was different from specimens burned vertically. For horizontal tests, char was only deposited at the fire-exposed edge at the perimeter of the fractured surface. Figure 59 shows a typical SEM image of a horizontal UNC0 specimen burned for 15 s. Also, no large-scale cotton-candy-like char was deposited at the fractured fiber ends. Some char formed along the length of the extended fibers.

SEM images of the fracture surface of UNCO specimens used in the 45 s and 75 s horizontal fire tests have not yet been performed due to the closure of the Texas A&M Material Characterization Facility during the COVID 19 period.

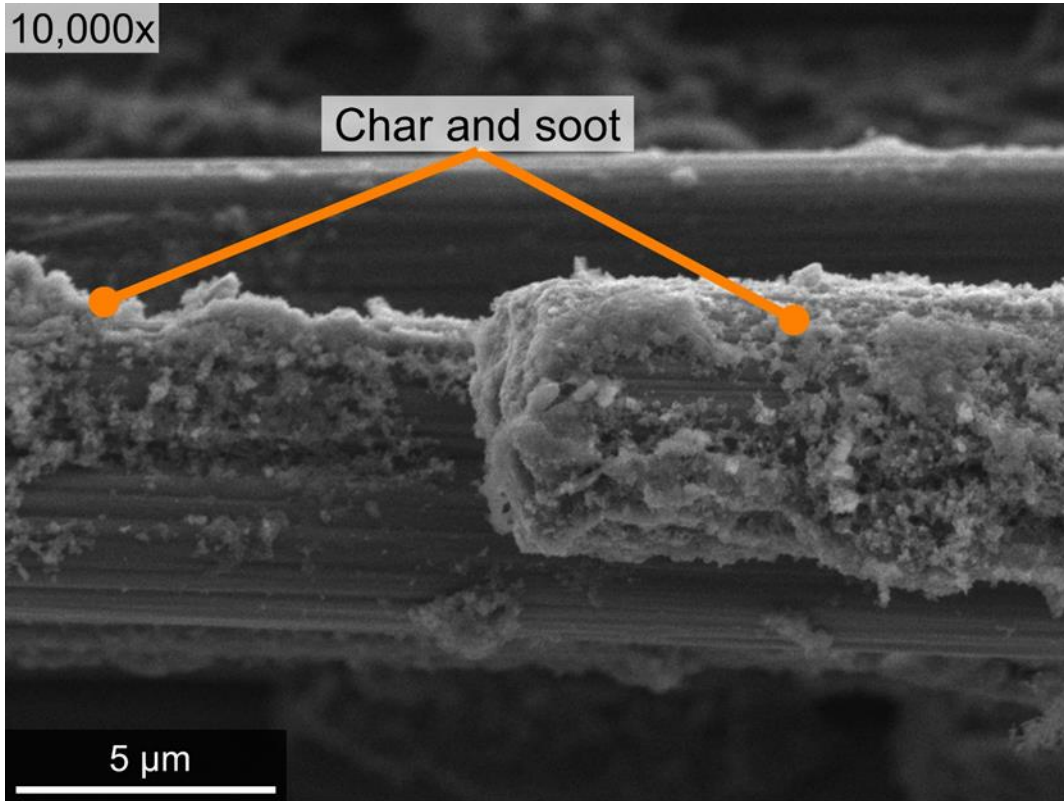


Figure 59. Char and soot at fracture surface of 21-ply cross-ply Cytec UNCO specimen used on 15 s horizontal fire test

3.2.2.2 SBS specimens (Exposure times: 15 s, 45 s, 75 s)

Horizontal fire tests on 45-ply unidirectional Cytec SBS specimens (layup: $[0]_{45}$) were performed for durations of 15 s, 45 s, and 75 s to assess the effects of specimen orientation and flame exposure time on fire damage formation. Three repeat horizontal fire tests were performed for each exposure time. Similar to horizontally-oriented UNCO specimens, horizontally burned SBS specimens typically experienced much lower degrees of thermal damage than vertically-oriented SBS specimens since a much smaller fraction specimen volume is located directly into the flame. In each horizontal test, the SBS specimens self-extinguished the instant the applied flame was stopped. Fire damage to horizontal SBS specimens was largely limited to large scale matrix decomposition concentrated near the fire-exposed surface, with little char/soot deposition and negligible residual thickness increase.

Figure 60 shows typical macro-scale pictures of the lower planar surface of a typical SBS specimen before and after horizontal burning for 75 s. The outermost ply exposed to direct

flame, shown in Figure 60(a) and Figure 60(b), sustained far more fire damage than did the interior plies. The lower edges of the fracture surface and lateral sides of the specimen also displayed proportionally more matrix decomposition than points more removed from the fire-exposed surface; this was particularly true for regions directly immersed in flame. In contrast, the upper outer ply and upper (unexposed) surface, shown in Figure 60(c) and Figure 60(d), showed little fire damage at the proximity of the fracture surface.

As mentioned previously, during mechanical testing, an individual half of a failed SBS specimen would sometimes longitudinally split into two ¼-specimens due to high inter-laminar stresses induced in the three-point bending tests. These mating ¼-specimens were subsequently clamped together during vertical and horizontal fire testing. After a longer duration (36 s and 60 s) vertical fire tests, initially separated ¼-specimens were bonded together after fire exposure. Conversely, in horizontal tests, the ¼-specimens remained separated for all exposure times (15 s, 45 s, and 75 s). Clearly, the relative orientation of any fissures and fracture surfaces relative to the flame can influence fire damage development. In addition, fire exposure has the potential to bond aircraft composite fracture surfaces together in ways that might impede subsequent forensic analyses.

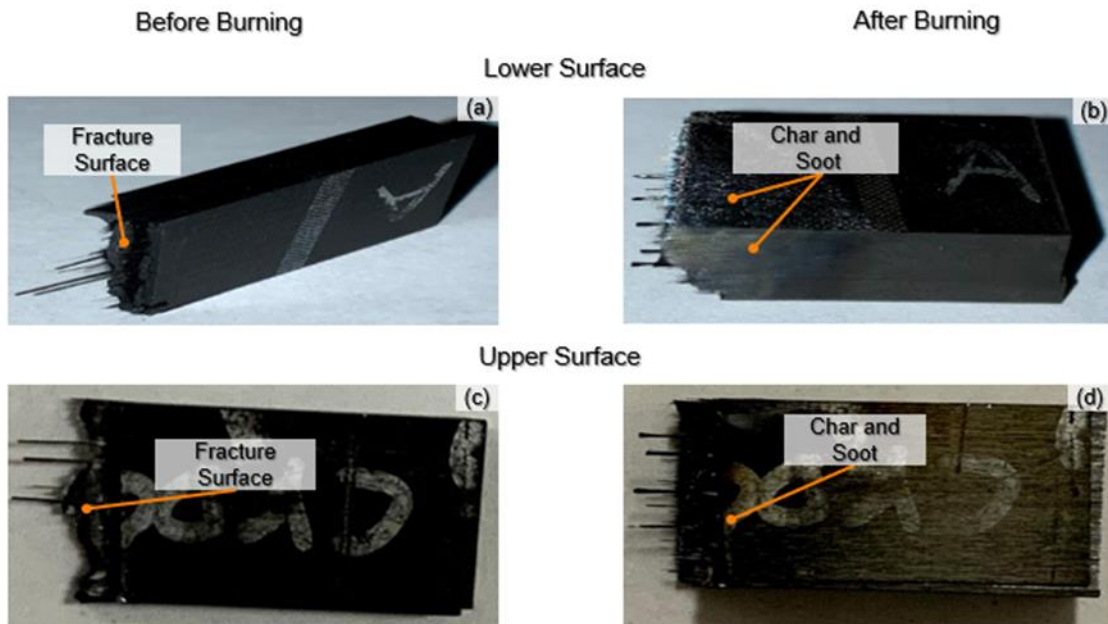


Figure 60. Comparison of 45-ply unidirectional Cytec SBS specimen before and after horizontal burning for 75 s

The degree of char formation and soot deposits on the fracture surfaces of horizontally-burned SBS specimens was much lower than that for similar specimens used in vertical fire tests (Figure 45). Figure 61 shows SEM images of the fracture surface of SBS specimens burned horizontally

for (a) 15 s, (b) 45 s, and (c) 75 s. For specimens burned for 15 s and 45 s, relatively minor amounts of char and soot residues formed on the fiber ends, and tensile failure regions and compressive chop marks were clearly visible, as seen in Figure 61(a) and Figure 61(b). For the 75 s tests, shown in Figure 61(c), many extended and recessed fibers were covered with melt dripping that obscured fracture surface features. In contrast to vertical fire tests where melt dripping by-products flowed parallel to the fibers due to gravity and tended to accumulate at the filament ends, these by-products flowed parallel to the fracture surface in horizontal fire tests. Again, this suggests the relative orientation of both the flame and fracture surfaces affect composite thermal damage development, as well as post-fire forensic assessments.

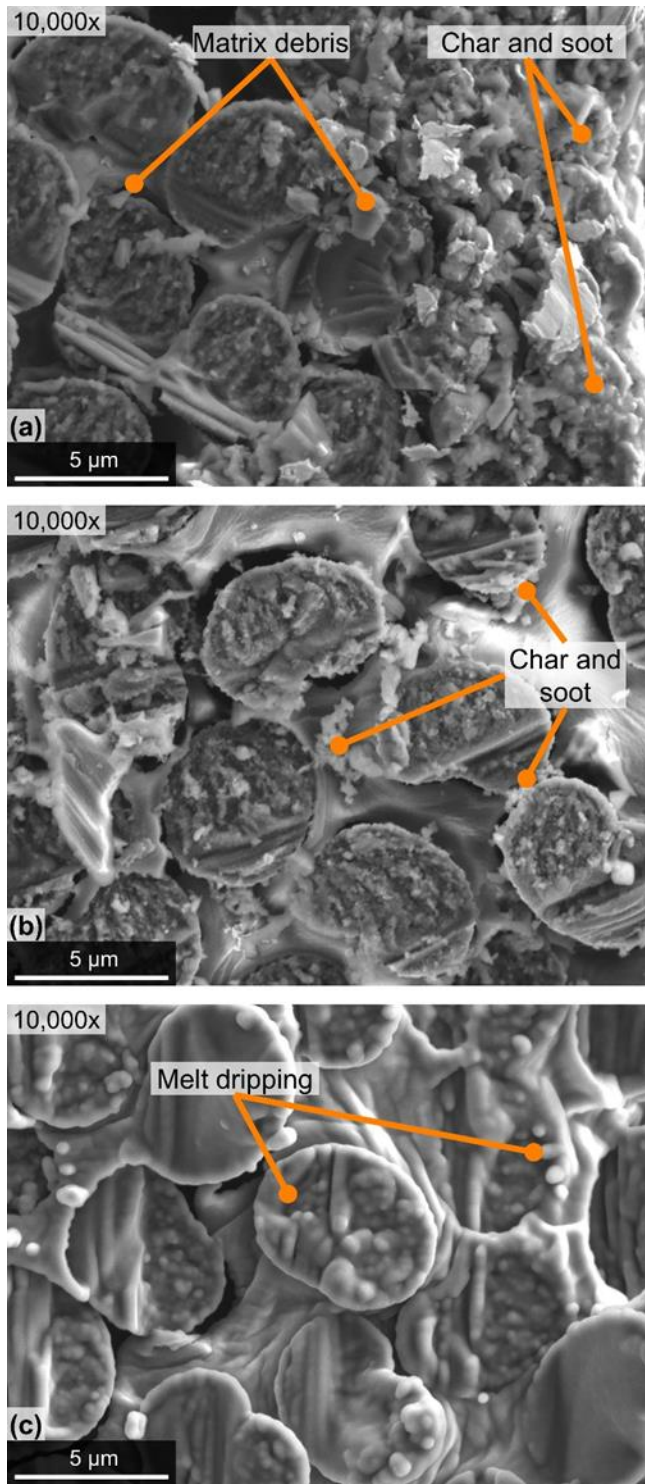


Figure 61. Fracture surface of 45-ply unidirectional Cytec SBS specimens used for (a) 15 s (b) 45 s and (c) 75 s horizontal burning

3.2.2.3 IPS specimens (Exposure times: 15 s, 45 s, 75 s)

Horizontal fire tests on 16-ply Cytec IPS specimens (layup: $[45/-45]_{4S}$) were performed for durations of 15 s, 45 s, and 75 s to assess the effects of specimen orientation and flame exposure time on fire damage formation. Three repeat horizontal fire tests were performed for each exposure time. Similar to horizontal testing of both the UNCO and SBS specimens, the angle-ply IPS specimens self-extinguished when the flame was stopped. The IPS specimens were positioned such that the midplane of the laminate was at the same height as the blue tip of the Bunsen burner flame, shown in Figure 30(b); the flame axis intersected the longitudinal axis of the specimen and lied in a vertical plane at the extreme edge of the fracture surface, the “x” marks located in Figure 62(b) and Figure 62(d). Because of the highly irregular fracture surface, material at the laminate centerline and along the shortest lateral edge was slightly removed from the flame tip. Therefore, heat transfer at these two locations was primarily from convection of the hot air, gases, and smoke.

Figure 62 shows typical macro-scale images of the lower and upper surfaces of an IPS specimen before and after horizontal burning for 75 s. Soot and char were clearly visible on the lower, fire-exposed surface of the specimen, as shown in Figure 62(a) and Figure 62(b). In contrast, no significant soot/char was observed on the upper surface of the IPS specimen (Figure 62(c) and Figure 62(d)). In addition, no large-scale char or other fire damage was visible at the fractured fiber bundles protruding from the specimen fracture surface. The results from 15 s and 45 s horizontal tests were consistent with those shown in Figure 62.

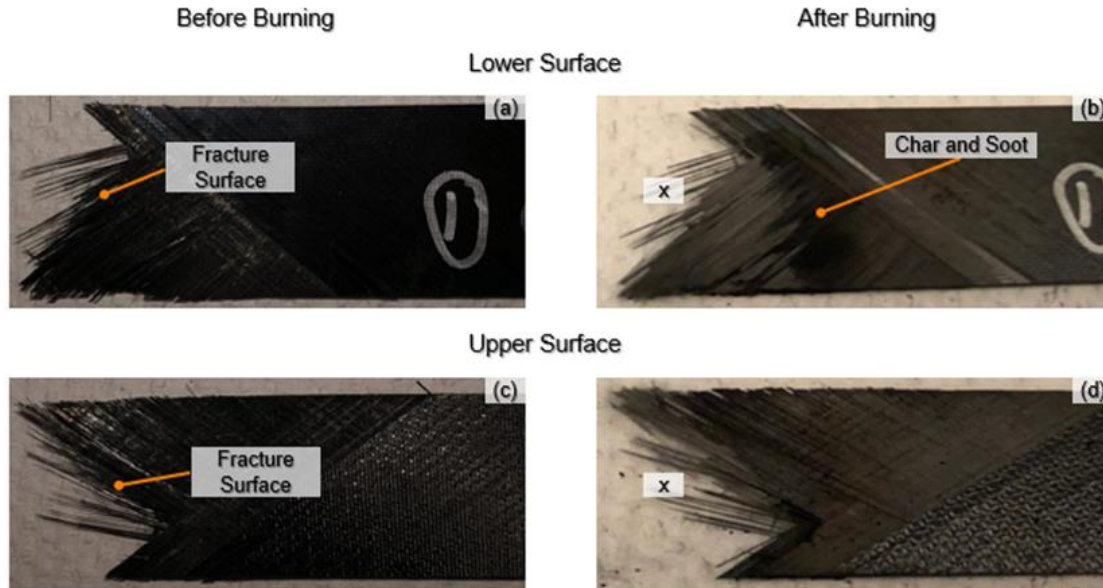


Figure 62. 16-ply Cytec IPS specimen after horizontally burning for 75 s with approximate location of flame axis

For vertical fire tests of IPS specimens, fibers located at the laminate centerline, shown in location 2 in Figure 51(a), suffered severe thermal degradation. In those cases, the matrix surrounding the fiber bundles was completely decomposed, and individual filaments experienced substantial oxidation damage and thinning (Figure 56). For horizontal fire tests, however, fiber bundles located along the laminate centerline were not as adversely affected by fire exposure. Figure 63 shows SEM images of fiber bundles located at the centerline of IPS specimens horizontally burned for (a) 15 s (b) 45 s and (c) 75 s. For the 15 s and 45 s fire exposures, individual fiber bundles remained encased in the epoxy matrix, and there was little evidence of char formation, see Figure 63(a) and Figure 63(b). For the 75 s tests, the epoxy matrix was largely decomposed, but the individual fibers appeared to remain relatively intact. Moreover, angled/slant fracture of individual filaments typical of in-plane shear failure was clearly visible, see Figure 63(c). It is obvious that horizontal testing of IPS specimens resulted in significant heat transfer due to convection that bypassed the specimen, resulting in far less thermal damage than for the case of vertical burning. These results suggest that under certain circumstances, post-crash fires may leave portions of composite aircraft structures relatively unaffected.

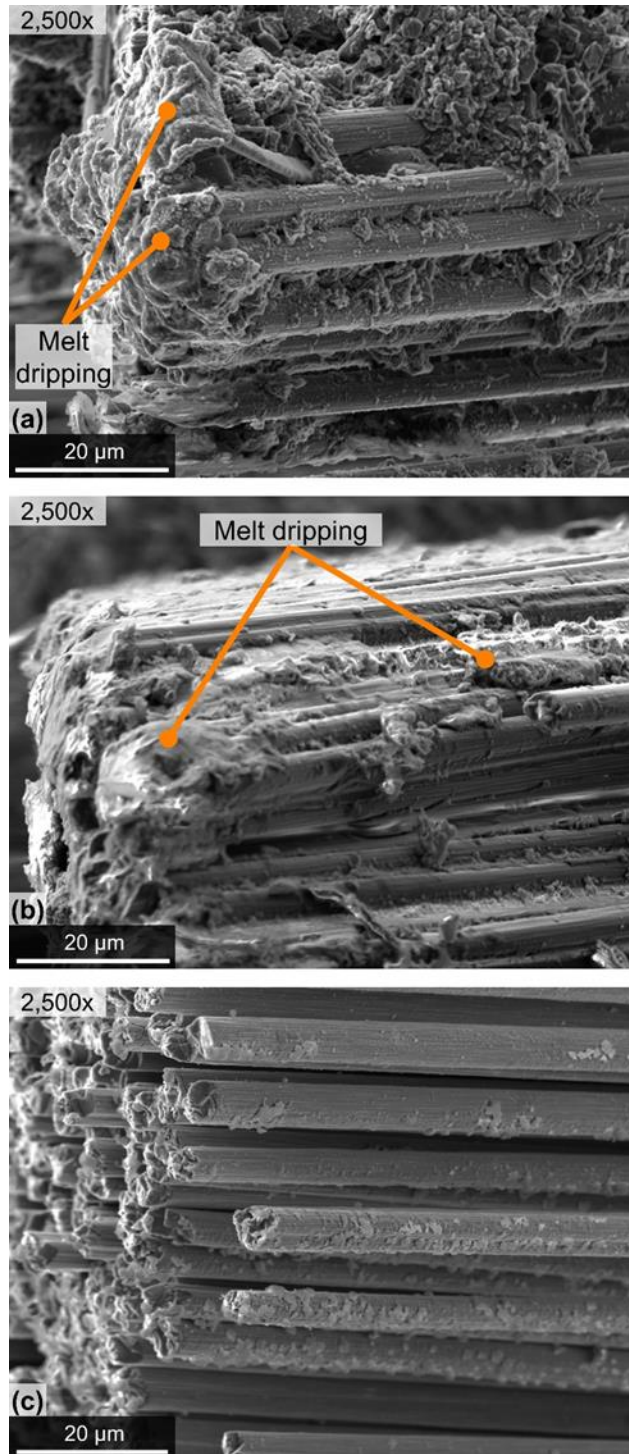


Figure 63. Fiber tows from centerline of 16-ply Cytec IPS specimens after horizontal burning for (a) 15 s (b) 45 s and (c) 75 s

3.2.3 Cone calorimeter testing of Cytec 5215 T40-800 graphite/epoxy compression-after-impact (CAI) specimen

In the preceding fire tests, failed UNCO, SBS, and IPS specimens were exposed to direct flame in draft-free cabinets to assess the effects of specimen geometry, layup, orientation, failure surface morphology, and flame duration on composite thermal degradation. As part of a corollary exercise, a single cone calorimetry test was performed to assess the effect of indirect fire exposure on thermal damage development in a 32-ply quasi-isotropic Cytec plate (layup [45/0/-45/90]_{4S}).

Prior to indirect fire testing, the composite plate was subjected to compression-after-impact (CAI) loading performed at Wichita State University (Man, Ng, Tomblin, & Hooper, 2012). During CAI testing, a 6 x 4 in² plate was first subjected to low velocity drop-weight normal impact with a spherical indenter to induce localized damage (fractured fibers, matrix cracks, ply-delamination, etc.) in and around a centrally-located impact site. The impacted specimen was then subjected to monotonically increasing in-plane compressive loading until failure. Laminate CAI failure, in this case, involved a combination of local fiber micro-buckling, fiber fracture, pure compressive fiber failure, matrix crushing, and other compressive instability related mechanisms that initiated at the impact site and propagated across the panel in a plane perpendicular to the loading direction. Unlike the UNCO, SBS, and IPS specimens, the failed CAI specimen was not separated into two distinct pieces after mechanical testing. Before cone calorimetry testing, a wet tile saw was used to machine a 4 x 4 in² sample from the failed CAI specimen such that the impact site was centrally located, and the composite failure plane bisected two opposing edges of the sample.

During cone calorimetry testing, the 4 x 4 in² CAI sample was positioned horizontally under the cone (i.e., indirect heat source), and a through-thickness heat flux of 50 kW/m² was applied continuously until the specimen self-extinguished. The specimen auto-ignited 81 s after initial heat flux exposure and self-extinguished 373 s after ignition. Figure 64 shows the CAI specimen after auto-ignition during cone calorimetry testing. During the test, large-scale matrix decomposition was initiated at the upper heat-exposed surface of the specimen and eventually penetrated the entire thickness. After testing, no epoxy matrix or char was visible at the heat-exposed upper surface of the sample; nearly complete matrix decomposition occurred (Figure 65(a)). The upper 45° ply of the composite appeared to consist of a blanket of loose bare graphite fibers (Figure 65(b)), which hindered SEM imaging of the upper surface. The unconfined loose arrangement of fibers at the composite outer surface made the broken and micro-buckled fibers at the CAI failure plane virtually indistinguishable from the surrounding fibers, based upon

visual inspection. As an aside, the inability to use visual inspections to precisely identify composite aircraft structural failure locations has the potential to limit the efficiency of fire forensic analysis seriously.

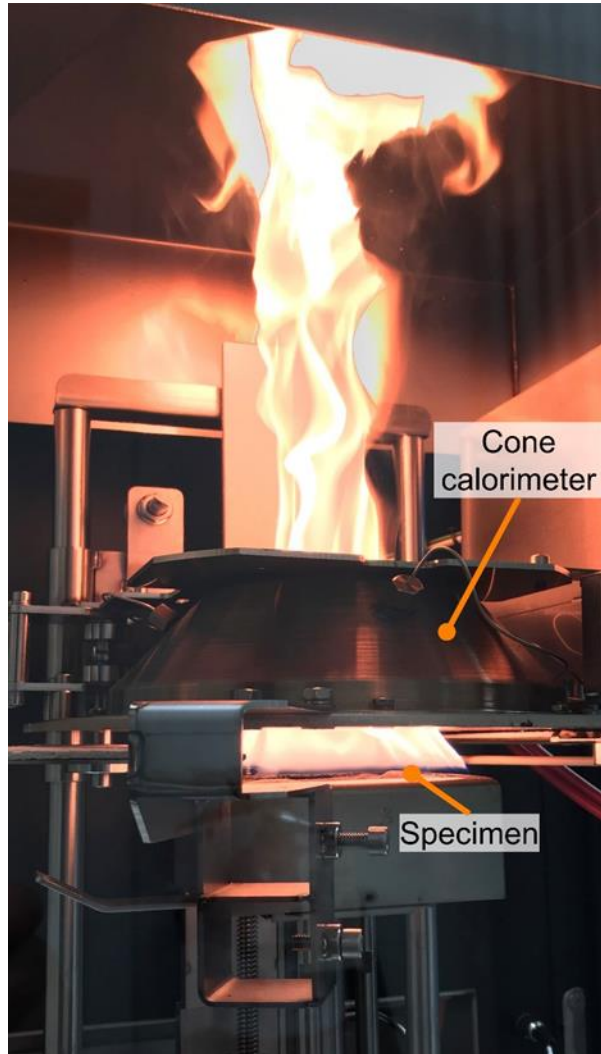


Figure 64. Cone calorimetry testing of 4 x 4 in² 2 32-ply Cytac CAI specimen

During indirect fire testing, the CAI sample also experienced large-scale multi-ply-delamination along all four specimen edges that were most severe along the unloaded edges that intersected the composite failure plane (Figure 65(c)). In addition, large amounts of melt dripping emanated from the edges of the specimen and flowed onto a horizontal metallic shelf located immediately below the cone calorimeter assembly (Figure 66). The melt dripping appeared to be a viscous tar-like substance that solidified after cooling; a melt drip sample was collected for carbon-hydrogen and nitrogen (C-H-N) and other chemical composition analyses. Such substance may also have accumulated on extended graphite fiber ends during vertical burn tests on UNCO specimens

(Figure 41), as well as been the source of interfacial bonding between pairs of mating ¼ SBS specimens subjected to vertical burning (as discussed in section 3.2.1.2). These issues remain to be fully explored.

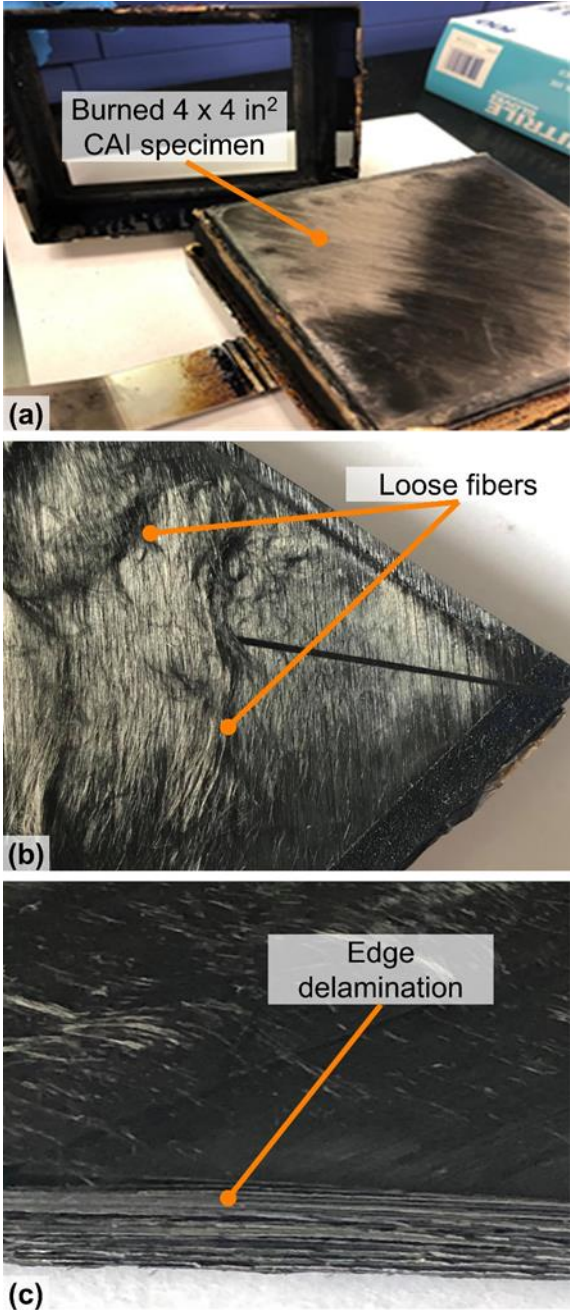


Figure 65. (a) 4 x 4 in² 32-ply CAI specimen after cone calorimeter fire testing with heat flux of 50 kW/ m² (b) loose fibers (c) edge delamination

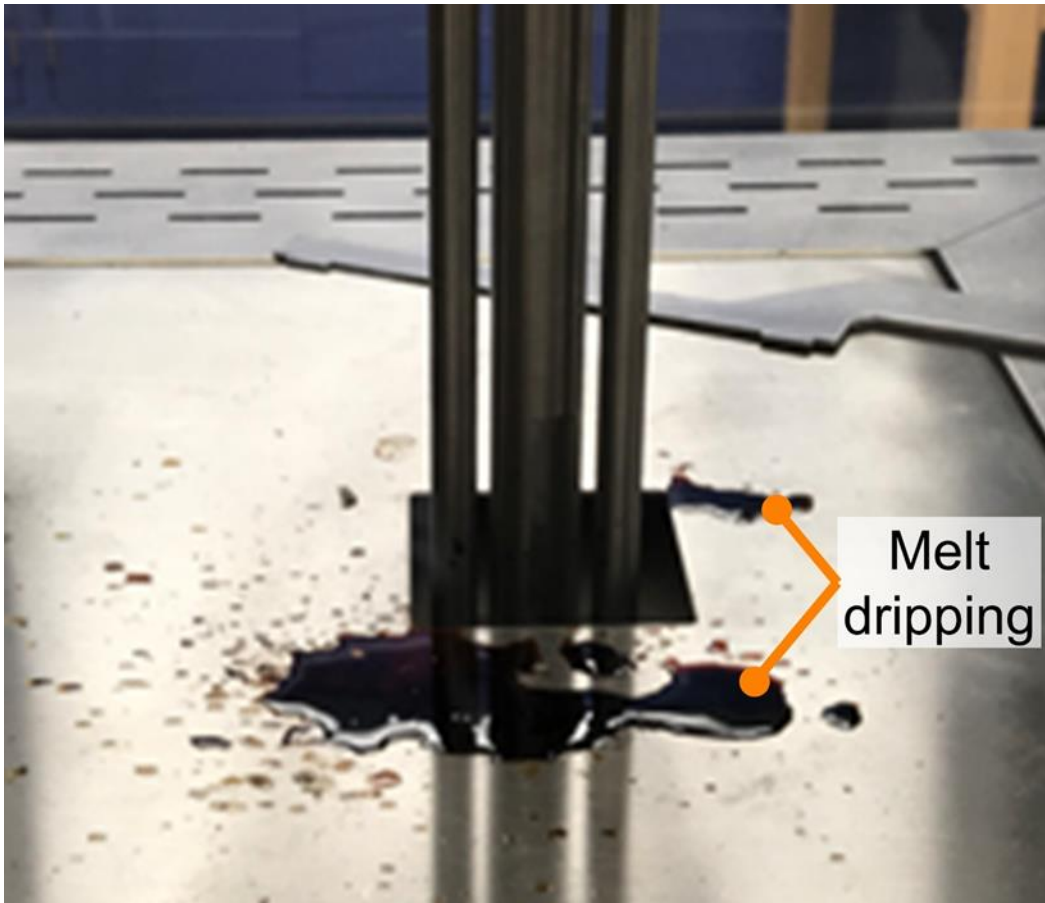


Figure 66. Melt dripping from 4 x 4 in² 32-ply Cytec CAI specimen

During testing, the lower surface of the 32-ply CAI sample rested on a layered structure comprised of a thin aluminum foil, a low-density ceramic wool fiber blanket, and a stainless-steel edge support frame. The lower surface of the specimen loosely adhered to the aluminum foil, likely due to melt dripping. After gently removing the foil, some matrix decomposition was apparent in the bottom 45° ply. Please note that detailed destructive micro-sectioning and ply-by-ply SEM inspection of semi-intact interior regions of the sample were not possible due to COVID-19 restrictions on laboratory access.

In this research, the FAA was primarily interested in the effects of direct fire exposure on thermal damage development in mechanically failed graphite/epoxy composites, as well as the establishment of strategies for char removal from burned aerospace composites. The vertical and horizontal direct fire tests on UNCO, SBS, and IPS specimens demonstrated that varying degrees of fire exposure could result in the deposition of significant amounts of char and other fire by-products that can obscure salient aspects of composite fracture surface morphologies. Such deposits can impede fractographic and forensic assessments aimed at identifying underlying

mechanical failure mechanisms. Although cone calorimetry was not widely employed in this work, it is clear that the application of high heat flux to a graphite/epoxy composite can be used to completely decompose the epoxy matrix, leaving bare fibers with no char. This suggests that char removal from previously burned composite specimens may be possible by subsequently subjecting them to sufficiently high temperatures or flame. If the fiber fracture surfaces are relatively unaffected by the prescribed thermal environment, this would potentially enable post-crash fire forensic analysis of large aerospace principal structural elements. This concept is consistent with those employed in ASTM standard matrix ignition tests (ASTM-D2584-18, 2018) and efforts aimed at recycling carbon fibers from thermoset composites (Fernández, Lopes, González, & López, 2018; Yang, et al., 2012). While outside the scope of this research, one key challenge is to identify the optimal combination of heat source and environment that enables efficient char removal while minimizing thermal degradation to carbon or graphite fibers.

3.3 Effect of specimen geometry, fracture surface morphology, and fire exposure time on fire damage and char formation

Several factors such as the specimen layout, ply orientation relative to the heat source, and the fracture surface morphology affected the thermal damage development in the Cytec composite specimens. For unidirectional continuous graphite fiber-reinforced epoxy plies subjected to fire, thermal damage due to heat conduction, combustion, and thermal deformation is highly dependent on the ply orientation relative to the flame. For unidirectional plies burned perpendicular to the fibers, the highly conductive graphite fibers will conduct heat parallel to the fire-exposed surface (e.g., along the fiber axis). This will promote decomposition and combustion of the epoxy matrix along the primary heat conduction path, parallel to the fibers, with markedly less heat conduction and thermal damage through-the-thickness. In essence, plies with fibers oriented parallel to the heat exposed surface act like a thermal protection layer that can impede heat transfer to the interior of the specimen. This explains, in part, why the horizontal burning of UNCO, SBS, and IPS specimens induced less thermal damage than vertical burning. Similarly, the CAI specimen subjected to cone calorimetry testing sustained far more thermal damage near the heat exposed surface. As an aside, horizontal burning can also result in significant heat transfer due to convection of hot gasses and smoke that can bypass the specimen, which also leads to far less thermal damage than for the case of vertical burning.

In contrast, unidirectional plies burned parallel to the fiber axis will conduct heat perpendicular to the fire-exposed surface. For laminates, 0°-plies aligned with the flame axis will conduct heat into the interior of the composite. This will occur more rapidly than if the fibers were oriented at

90° to the fire-exposed surface. Heat conduction in these 0°-plies may promote the formation of melt dripping, internal pockets of matrix decomposition, and surface char deposition. New matrix cracks and fissures may develop to accommodate explosive outgassing, resulting in a residual thickness increase (Figure 44). Mechanically failed composites, such as the UNCO, SBS, and IPS specimens considered in this study, may contain fractured fiber ends that are either recessed within the specimen or extended beyond the nominal fracture plane. After fire exposure, any melt dripping that occurs may accumulate on the extended filament ends (Figure 41) or coat the entire fracture surface (Figure 61c), depending on the fracture surface orientation relative to the flame.

Depending on the fire exposure time and temperature, any melt dripping or char deposits that form on the extended filament ends can completely obscure salient aspects of fiber fracture surface-morphology. In some cases, however, the fracture surfaces of recessed fibers may be relatively unaffected by fire exposure, which may permit limited post-fire forensic analysis (Figure 38 and Figure 47). Hence, pre-examination of fracture surfaces recovered from post-crash fires should be undertaken before attempting char removal. In contrast, fiber bundles that are excessively extended from the fracture plane are susceptible to extreme thermal degradation during fire exposure (i.e., thinning, oxidation), which renders forensic analysis impossible (Figure 56). This is particularly true for specimens with highly irregular fracture surfaces, such as IPS specimens, that permit enhanced airflow and improved oxygen availability during burning.

Thermal damage development in mechanically failed laminates can be compounded by different ply groupings in a given stack-up. For example, consider vertical burning of a [90/0/90]₇ UNCO specimen where the flame axis was parallel to the 0°-plies. The 90°-plies each acted like a thermal protection barrier that impeded heat flow into the specimen. These plies conducted heat parallel to the fire-exposed fracture surface towards the lateral edges of the specimen, leading to proportionally more char deposition around the specimen perimeter where the airflow and oxygen availability was greater. The 0°-plies conducted heat into the interior of the composite, leading to melt-dripping, matrix decomposition, char deposition, and explosive outgassing, as mentioned previously. Local differences in the coefficients of thermal expansion and thermal conductivities between the 0° and 90° plies resulted in fire-induced ply-delamination (Figure 42), matrix cracking (Figure 43), and intra-ply cracking of 90°-plies (Figure 35); these material discontinuities provided a pathway for matrix outgassing leading to potentially less residual thickness increase relative to unidirectional specimens (i.e., SBS specimens). Similar arguments can be used to explain heat conduction, thermal deformation, and fire damage development in

laminates with different ply groups. The effects of carbon fire orientation on reaction-to-fire properties can have been extensively studied by Eibl & Swanson (2018) (2012)

Another point that is worth consideration is that the balance and symmetry of a given composite laminate may be destroyed by fire exposure. This is particularly true for horizontal burning and cone calorimeter tests, where asymmetry in through-thickness ply properties arises from one-sided burning. The effect of the fire-induced loss of laminate balance and symmetry on thermal damage development was not part of this research and remained to be fully explored.

The composite layup and loading profoundly affect the fracture surface morphology and the free surface area created during mechanical failure. Compression and transverse shear specimens loaded primarily parallel and perpendicular to the ply directions, similar to UNCO and SBS specimens, may display more compact fracture surfaces with a minimum of free surface area creation. During fire exposure, thermal degradation arises from a combination of the burning of the combustible free surface area and heat conduction to the interior of the specimen.

Carbonaceous char deposits forming on the fracture surface may act as a thermal barrier that further impedes oxygen transfer to the interior of the specimen and reduces the rate of thermal degradation until the onset of ply-delamination and matrix cracking. In contrast, angle-ply specimens that are loaded off-axis, similar to IPS specimens, commonly display extremely irregular fracture surfaces, ply-delamination, and proportionally more free surface area creation. In general, specimens with a larger free-surface area will promote better airflow and combustion during fire exposure, which can accelerate matrix decomposition and severe fiber thermal degradation for a given fire duration.

The total number of plies (i.e., stack-up thickness) also affects the degree of damage for given fire exposure. Thicker specimens with higher thermal mass may require greater heat input and longer fire exposure times to induce the same degree of thermal degradation as for thinner specimens. Also, the local oxygen availability and airflow may be affected by the specimen fracture surface geometry. As mentioned previously, these factors may be exacerbated by variations in ply orientation and layup. Such considerations are crucial in the post-crash fire forensic analysis of aerospace composite structures.

Post-crash forensic analysis of composite aircraft structures typically focuses on principal structural elements. Here, a principal structural element can loosely be defined as a structural component (primary axial load carrying members such as critical wing spars flanges, longerons, carry-through structures, etc.) whose failure would result in the catastrophic loss of an aircraft. These thicker structural components will typically be constructed with larger numbers of 0° -plies. Hence, the $[90/0/90]_7$ UNCO and $[0]_{45}$ SBS specimens are more consistent with

principal structural elements than are the $[45/-45]_{4S}$ IPS specimens. The IPS specimens are akin to aerospace laminates designed to carry either torsional or shear loads (wing skins, spar webs, etc.).

In actual composite aircraft structures, principal structural elements are typically designed to carry high axial or bending loads. As a consequence, they are commonly constructed of *thick* composite laminates (40-100+ plies) containing a majority of 0° -plies, somewhat fewer $\pm 45^\circ$ plies, and a minimum of 90° -plies (of course, other ply groupings are possible). Similar to the UNCO, SBS, and IPS specimens considered in this research, discrepancies in principle structural element local ply properties, layup, and loading may influence mechanical damage development during catastrophic failure, as well as thermal degradation due to a post-crash fire.

The mechanisms responsible for composite thermal degradation during an actual aircraft fire will also be comparable to those discussed here. In extreme cases, post-crash fires can effectively destroy all forensic evidence necessary for accident reconstruction. Therefore, the developed char removal technique has to achieve repeatable results in a cost-effective manner; with optimum operating conditions, mainly user time. The char removal technique has been effective across a wide array of aerospace composite material systems. As an initial attempt, the effectiveness of chemical/combined chemical/physical techniques across pristine Hexcel carbon/epoxy and mechanically failed graphite/epoxy specimens are investigated in the following sections.

4 Char removal and forensic analysis of burned continuous fiber-reinforced aerospace composites

4.1 Fundamental principles of surface cleaning and char removal

4.1.1 The nature of char

It is essential to obtain critical knowledge about the nature of the contaminant and its effect on the underlying substrate to design an effective surface treatment protocol (Kohli & Mittal, 2015). In most cases, the complete thermal decomposition of a polymer or a composite part could result in a uniform layer of char (Mouritz & Gibson, 2007). This char layer acts as a barrier for further burning; however, a discontinuous char layer formed during combustion cannot be an effective barrier against further thermal degradation (Ray & Kuruma, 2019).

The polymer matrix undergoes a series of steps in the process of char formation: cross-linking, aromatization, aromatic fusion, turbostratic char formation, and graphitization

(Levchik & Wilkie, 2000; Ray & Kuruma, 2019). The aromatization of cross-linking polymers during burning produces the building blocks for char formation. The aromatic polymers undergo further pyrolytic decomposition, eventually leading to the fusion of the aromatic free radicals and the expulsion of smaller molecules, such as water, CO₂, CO, CH₄. Turbostratic char formation is an incomplete graphitization process wherein the hydrogen and other hetero-elements (O, N, P, S) are partially eliminated from thermally stable aromatic structures at around 700°C (Levchik & Wilkie, 2000). Most polymeric materials, including epoxy-based composite systems, yield turbostratic char during burning (Levchik, Camino, Costa, & Luda, 1996; Brooks & Taylor, 1968).

Consequently, the chemical bonding and adhesion between the char and underlying undamaged regions are particularly strong. The fire-forensic analysis of such burned composite parts would require developing a comprehensive surface cleaning protocol that can be applied to a broad range of aerospace-grade composite material systems and remove char and soot deposits from large-scale principal structural elements.

Most cleaning protocols are multi-stage processes that involve the following steps: cleaning, rinsing, and drying. While solvent selection is an important aspect of effective cleaning, the method of cleaning should supplement the solvent's functionality by compensating for its limitations (Kohli & Mittal, 2015). An effective char-cleaning process should clean the surface by dissolving the char and soot deposits, removing the char from the composite part surface, and separating the char from the solvent. The mechanical effects produced by ultrasonication can be especially beneficial in dissolution, separation, and char removal. A lower intensity repetition of sonication can also provide effective rinsing of the composite part after cleaning (Awad S. B., 1996).

4.1.2 Selection of chemical solvents for surface cleaning experiments

Solvent and detergent selection is essential for the effective cleaning of contaminated surfaces (Kanegsberg & Kanegsberg, 2011). The key considerations in the solvent selection process are; type of substrate, type of soil/contaminant, part complexity, safety considerations, and environmental considerations (McLaughlin & Zisman, 1999). Since very little to no information is present in the existing literature on the available chemical products applicable for dissolving burn-residue from composite surfaces, commercial carbon residue cleaners, as listed in Table 3, commonly used in the treatment of metallic surfaces such as stainless steel, nickel, copper, aluminum, brass, and cast iron were selected for initial char removal experiments.

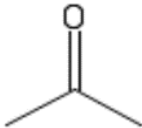
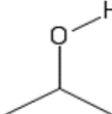
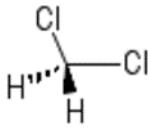
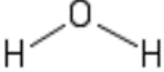
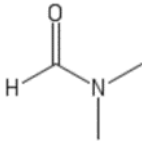
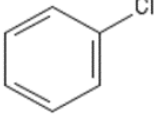
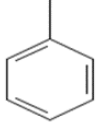
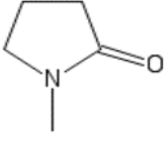
Most commercially available carbon cleaners are complex mixtures consisting of multiple solvents, surfactants, wetting agents, emulsifiers to provide solvency and detergency for metallic surfaces. Their applicability for char and soot removal from burned aircraft composite surfaces was examined through preliminary soaking experiments. Pristine cross-ply 4-ply cross-ply [0/90/90/0] Hexcel carbon/epoxy specimens were burned in a setup consistent with the FAA fire test setup (Appendix B, Figure B - 2). The burned Hexcel specimens were soaked in the cleaning products outlined in Table 3. The cleaning product was first applied on the fire-damaged Hexcel specimen surface and subsequently rinsed with water. This was followed by an extended soaking of the burned specimens in an 80% by-volume aqueous solution of the cleaning products for 24-48 hours.

Table 3. List of commercially available cleaning products for carbon residue removal

Product Name	Applications	Chemical composition
Carbon-Off!® , Quest Specialty Corporation, Brenham, TX	Excellent for removing char from metallic surfaces (brass, stainless steel, nickel steel, used in high-temperature cookware.	Dichloromethane (75-09-2), Ethanol (67-17-5), Methyl Alcohol (67-56-1), Aromatic Hydrocarbon (108-88-3), 2-Butoxyethanol (111-76-2), Ammonia (7664-41-7), Propane/n-Butane (68476-86-8).
Chem-Dip® Carburetor Parts Cleaner, Berryman Products, Inc., Arlington, TX	Highly effective at removing char and fuel combustion by-products (gum, varnish, fuel residue) from carburetor parts in 15-30 minutes without heat, aeration, or agitation. Safe for use with most plastic and metallic parts, including steel, aluminum, and their alloys.	Heterocyclic and Aliphatic Amines (Mixture), 2-Butoxyethanol (11-76-2), 2-(2-Butoxyethoxy) ethanol (112-34-5), and Ethoxylated Alkyl Amines (Mixture)
Carbona® 2-In 1 Oven Rack and Grill cleaner	Effective at removing chars from oven rack and grills.	< 5% anionic surfactants.

The final stage involved the rinsing away of the cleaning product solution with water. Since this process did not significantly change the burned surface, alternate cleaning methods like ultrasonic cleaning were considered. Commonly available organic solvents, as listed in Table 4, were used for these experiments.

Table 4. Chemical solvents used in char removal experiments

Chemical Solvent Name	Molecular Formula	Boiling Point (°C)
Acetone		56.3
Isopropanol		82.3
Dichloromethane (DCM)		39.8
Distilled Water		100.0
Dimethylformamide (DMF)		153.0
Chlorobenzene		131.7
Toluene		110.6
N-methyl-2-pyrrolidone (NMP)		202

4.2 Surface cleaning of pristine burned aerospace composite specimens

4.2.1 Sonication experiments on pristine burned Hexcel carbon/epoxy composites

Sonication technology has been predominantly used as an effective precision cleaning process to remove metallic, organic, film-based, and other particulate contaminants in multiple industrial applications (Ranade, 1987; Cooper, 1986; Menon, 2018). The high-velocity jets clean the surface, chipping away at the contamination, and transporting additional solvent to the contaminated surface (Awad & Nagarajan, 2010). Acoustic streaming is defined as the bulk movement of the solvent due to the transfer of acoustic waves. During this process, the sonication residues are transported away from the clean surfaces to prevent particle redeposition.

Acoustic streaming is a boundary layer phenomenon; it increases with decreasing boundary layer thickness. Higher operating frequencies during ultrasonic cleaning facilitate more acoustic streaming (Blitz, 1971; Shwartzman, Mayer, & Kern, 1985). At lower operating frequencies (20 kHz), acoustic cavitation is more prominent. Cavitation results in the development of extreme local temperatures and pressures (in the order of 10,000°F and 10,000 psi) for a few microseconds (Kanegsberg & Kanegsberg, 2011; Awad S. B., 1996). These conditions can help in the generation of free radicals within the solvents that are highly reactive (Riesz, Berdahl, & Christman, 1985; Prasad, Vithanage, & Kapley, 2019) and could provide pathways for controlled pyrolysis/oxidation required to initiate the chemical breakdown of char and soot deposits from the burned composite surface. The addition of hydrogen peroxide to a solvent may serve as a secondary source for the hydroxyl (OH•) free radical, which is highly oxidative (Das & Varughese, 2016) and thus favorable for char removal.

4.2.2 Initial sonication experiments for solvent selection

The chemical solvents shown in Table 4, along with Chem-Dip® Carburetor Parts Cleaner (Chem-Dip) and Carbona® 2-in-1 Oven Rack and Grill Cleaner (Carbona), were used to perform preliminary ultrasonic cleaning experiments on burned pristine 4-ply cross-ply [0/90/90/0] Hexcel specimens. Thermo Fisher Scientific supplied the chemical solvents used in the experiments. Chem-Dip and Carbona were purchased from locally sourced vendors. A Branson 1510 series ultrasonic cleaner with a 1/2-gallon tank, an operational frequency of 40 kHz, and an input power of 80 W was used to perform the tests. In the initial series of tests, the burned specimens were placed in 50 ml conical tubes and filled with the solvents specified in Table 4. The tank of the sonication chamber was filled to the operational level with distilled water. The filled conical tubes were placed in the tank, and the power was turned on. The sonication energy supplied to the tank can be controlled by controlling the amplitude setting provided on the

control panel. A constant sonication amplitude of 100% was selected for all the initial tests. The specimens were sonicated 15 min under these conditions. After the sonication process is completed, the specimens were extracted from the conical tubes and the sonication residues were visually inspected to observe the extent of soot and char removal. Visual inspection noting change in color of the solvents before and after sonication and surface characterization of the burned specimens before and after sonication using SEM were used to narrow down the list of usable solvents for future sonication tests. Out of all the solvents, acetone showed the most promise, both in terms of visual inspection of sonication residues and SEM imaging. The SEM micrographs in Figure 67 show the surface characteristics of a burned Hexcel specimen before and after 15 min of ultrasonic cleaning. The specimen was vertically burned for 12 s in the fire test setup (Appendix B, Figure B - 2). The micrographs point to a specific region of (in-plane) 90° fibers, where the heat is conducted along the composite's lateral edge. Prolonged fire exposure could inhibit heat conduction to lateral sides of the carbon fiber due to the lack of oxygen or combustible gaseous products resulting in the textured char as shown in the micrographs Figure 67a. The micrograph in Figure 67b shows the difference in the char morphology before and after 15 min of ultrasonic cleaning.

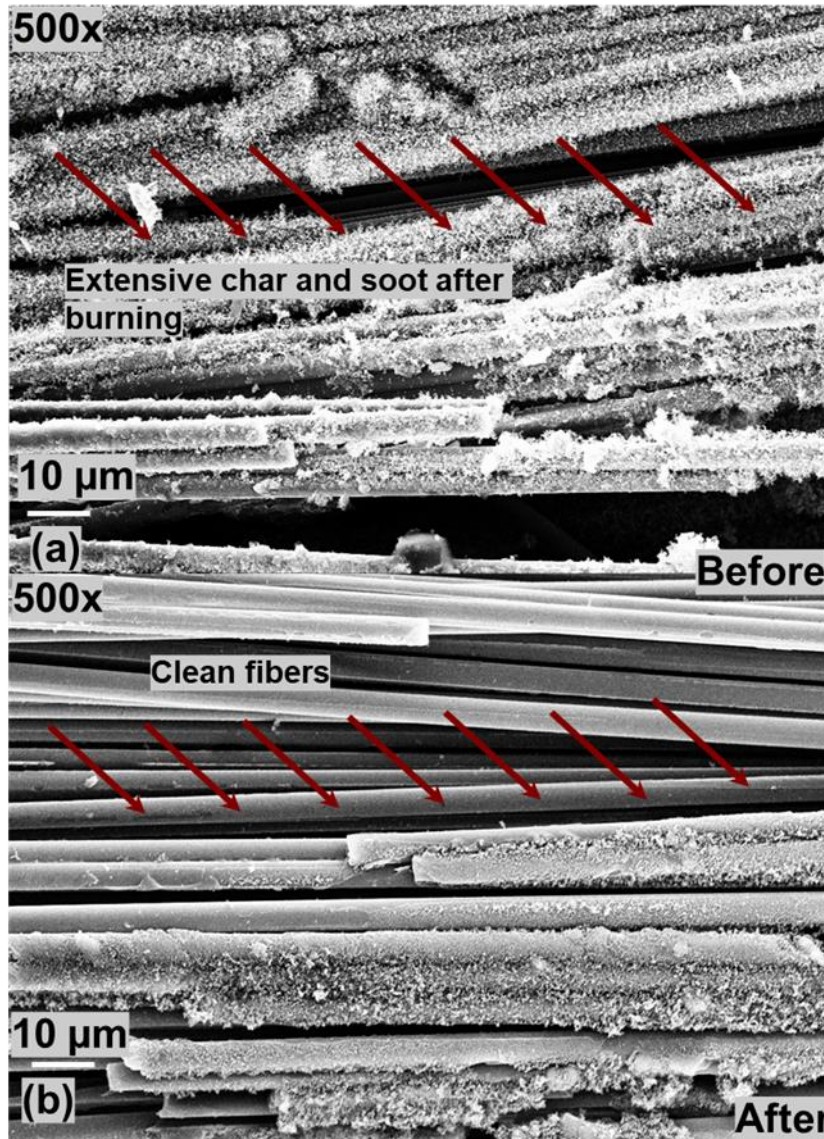


Figure 67. Sonication action along surface of in-plane fibers of burned pristine 4-ply cross-ply Hexcel specimens

There is a significant reduction in char along the lengths of the in-plane fibers in the upper section of Figure 67b. Clean fibers can be observed on the top half of the image, indicating an effective penetration of the cavitation bubbles about the char and fiber surface interface. However, the lower section of the micrograph remained unchanged. This could be attributed to 15 min being insufficient sonication time or inadequate sonication effects such as acoustic streaming, which promotes the transfer of the solvent into those specific regions, or free radical generation, which allows for oxidation/reduction reactions to occur to separate the char from the composite surface chemically. Therefore, additional ultrasonication experiments were performed

with acetone as the solvent with a higher sonication duration to evaluate the effectiveness of acetone as a solvent for ultrasonic cleaning.

A series of ultrasonication experiments were performed on the burned pristine 4-ply cross-ply [0/90/90/0] Hexcel specimens. Two different sonication durations (30 and 60 min) were considered for these experiments. Three replicates were used for each sonication durations. The ideal sonication time was selected based on visually inspecting the sonication residues obtained after the tests were finished.

Representative specimens were selected for each test duration, and their surface characteristics were observed using the scanning electron microscope. The specimens subjected to ultrasonication for 30 min possessed similar surface characteristics to the specimens sonicated for 15 min. the color of the acetone after sonication was also similar. However, the sonication residues were more pronounced in the acetone after the burned Hexcel specimens were sonicated for 60 min, producing a darker shade of discoloration in the solvent after sonication as shown in Figure 68.

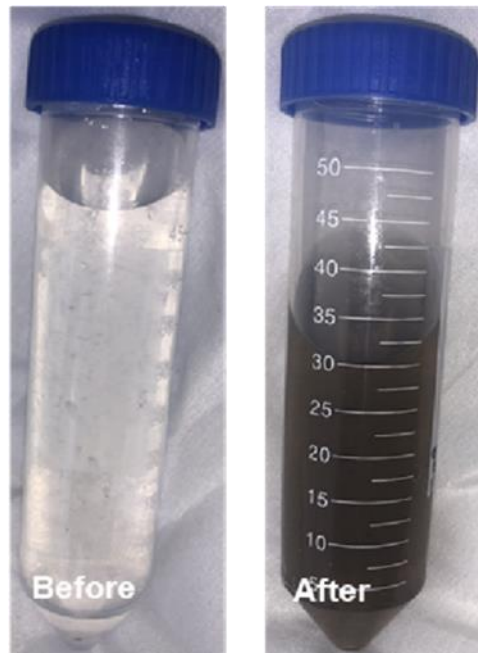


Figure 68. Color change of acetone before and after 60 min of ultrasonication of representative pristine burned Hexcel specimen

4.2.3 Surface characterization of pristine burned Hexcel specimens after ultrasonic cleaning in acetone

Surface cleaning is achieved in multiple ways during ultrasonication. The propagation of ultrasonic waves through the liquid medium causes a continuous erosion of solid surfaces present in the path. The erosion occurs due to acoustic streaming (bulk movement of the solvent) and the bubble-implosion near the solid surface due to cavitation. Sonochemical reactions occur at three possible sites; in the cavity, at the gas-liquid interface, or within the solvent. The presence of the cavitation bubbles adjacent to the solid surface would allow for the oxidation/reduction reaction between the free radicals and the surface (Suslick, 1989).

Therefore, the C-C, C=C, C-N, and C-O bonds at the interface between the undamaged polymer composite surface and the char layers can be broken at high local temperatures and pressures resulting from the simultaneous occurrence of bubble implosion and the oxidation/reduction reactions due to highly oxidative free radicals ($\text{H}_3\text{C}\cdot$, $\text{OH}\cdot$, $\text{HO}_2\cdot$) (Das & Varughese, 2016). For a near-total removal of char, cavitation and free radical generation should occur exclusively at the char and composite surface interface. The combined effect of free radical generation and acoustic cavitation would attack the interface and allow for the effective removal of char.

Therefore, sonication parameters, such as frequency, duration, and power play a major role in improving surface cleaning efficiency.

Fire-damaged Hexcel specimens were first air-dried to remove loosely bonded soot and dirt from the composite surface. A total of three replicates were considered for the ultrasonic cleaning experiments. The specimens were then cleaned using the Branson 1510 series ultrasonic cleaner with acetone as the solvent. After ultrasonication, the sonicated specimens are rinsed in isopropanol, dried off, and stored in small vials. The vials containing the Hexcel specimens are then placed in a vacuum oven for 24 hours for drying. The sonication residue is filtrated and preserved in the conical tubes for further chemical characterization. The fire-damaged surfaces are analyzed using SEM to observe the change in surface char morphology due to ultrasonication.

The surface characteristics of the burned pristine 4-ply cross-ply [0/90/90/0] Hexcel specimens were evaluated using the ZEISS Supra 40 FE-SEM. Scanning electron microscopy was performed before and after ultrasonic cleaning. The region of initial fire exposure was considered the primary area of interest. The burned specimens were mounted on a 45°/90° angle stub with the lateral surfaces secured with carbon tape. An accelerating voltage of 15 kV was used, and the SEM micrographs were taken at a WD of 9 mm.

The fire-exposed ends of the out-of-plane 0° fibers possess highly dense and fuzzy char residue, as shown in the optical micrographs in Figure 69a. Similar structures were successfully identified as char in the preceding sections. In these out-of-plane 0° fibers, heat is conducted through the thickness of the composite. In this case, the interior in-plane plies can cut off the airflow required for heat conduction, resulting in the high-dense char on the fiber ends. Therefore, the surface char generated after burning is significant, with highly dense char on the fiber ends. Figure 69a and Figure 69b show representative SEM micrographs of the 0° fibers before and after ultrasonic cleaning. After 60 min of ultrasonic cleaning in acetone, the reduction in char on the fiber-ends is significant. Effective removal of char indicates that the cavitation bubbles successfully penetrated the char and the fiber surface interface (Figure 69(b)). The mechanical action of the agitation of solvent along areas closer to the charred regions could also contribute to the overall char removal process. The bulk movement of the liquid due to acoustic streaming around the sonicated regions would help transport the solvent into the char-dominated regions and transport the sonication residue away from the regions of interest.

Figure 70(a) and Figure 70(b) show the surface characteristics of the in-plane 90° fibers for a burned pristine 4-ply cross-ply [0/90/90/0] Hexcel specimen before and after ultrasonic cleaning. The in-plane 90° fibers have a uniform distribution of a textured char along the fiber length. In these fibers, the heat is conducted along the lateral sides of the fiber. Prolonged fire exposure could result in the inhibition of heat conduction to lateral sides due to the lack of oxygen or combustible gaseous products resulting in the textured char morphology as seen in Figure 70(a). After 60 min of ultrasonic cleaning in acetone, the amount of char present on the fiber surface is markedly less. The fibers in the inner ply appear to be clean and devoid of surface char. The overall reduction in the surface char can be attributed to the acoustic streaming phenomenon during ultrasonication. The sound waves rapidly transfer fluid to the burned regions of the specimens. During this event, the fluid impinges onto the fiber surface, leading to increased sonication effects like cavitation and free-radical generation. In these conditions, char can be mechanically removed due to the high pressure and temperature conditions of cavitation-bubble implosion or chemically due to the oxidation-reduction pathways provided by the free radicals generated during sonication.

Ultrasonic action was more prevalent on the in-plane 90° fibers than the out-of-plane 0° fibers. As in Figure 69(b) and Figure 70(b), the amount of char deposited was higher on the 90° fibers than the 0° fibers. Although the fiber ends of the 0° fibers appear to be clean due to the prevalence of ultrasonication, material removal (char) was greater in the case of the in-plane plies (Figure 70). While the total available region for acoustic streaming and cavitation is more for the 90° fibers, the difference in sonication effects can be attributed to two issues: the

difference in the char density between these two configurations, and the difference in the char morphology. Further experimentation is required to fully understand the interface-level phenomena occurring during ultrasonication in these two cases.

While char structures chemically consist of 85-98% carbon, they also possess aromatic-aliphatic compounds, often with heteroatoms (O, N, P, S) (Mouritz & Gibson, 2007). Moreover, char is a highly cross-linked and porous material. The crystalline or amorphous nature of char is essentially a function of specific fire conditions, the nature of the burning polymer, and the state of combustion (Levchik & Wilkie, 2000). Therefore, to assess the interfacial bond strength between burned fibers and the charred surface for both cases, the elemental chemical composition and the molecular structure of the char must be evaluated.

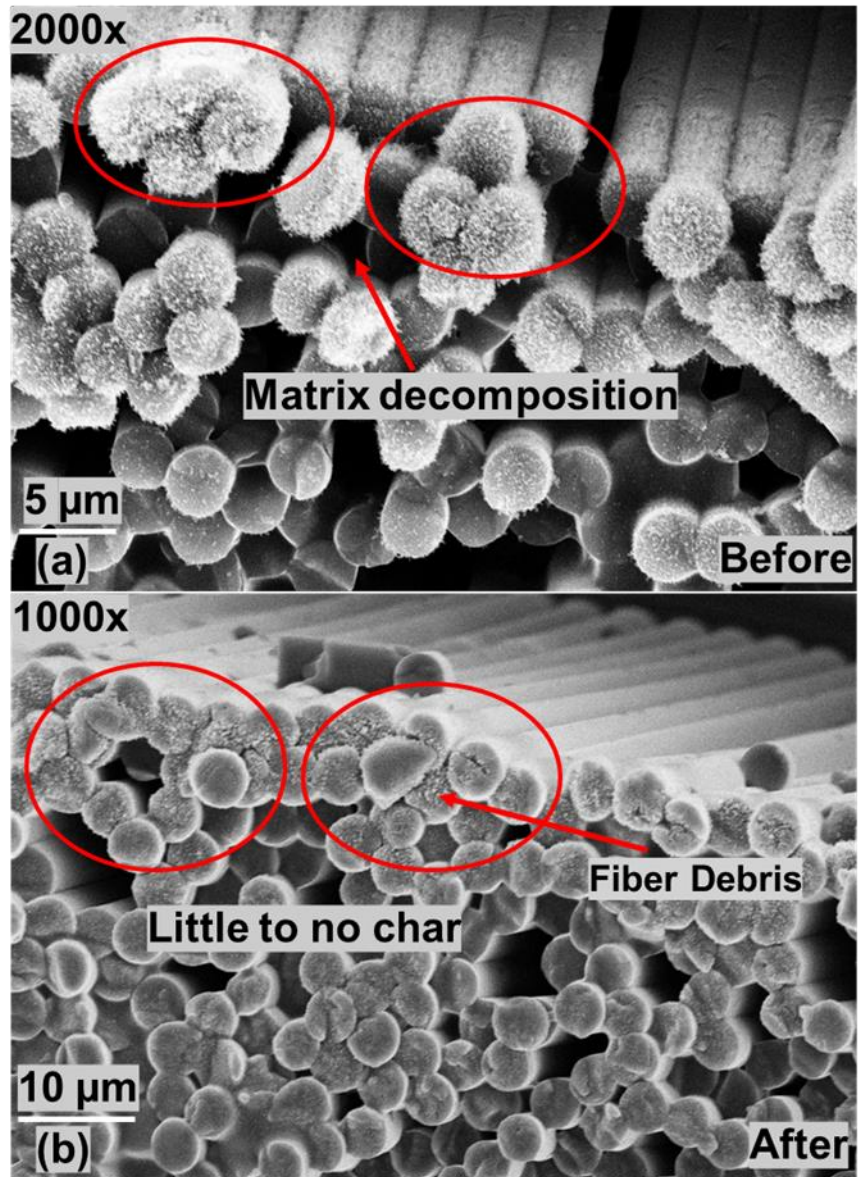


Figure 69. Sonication results (60min, acetone) of 4-ply cross-ply Hexcel woven fabric

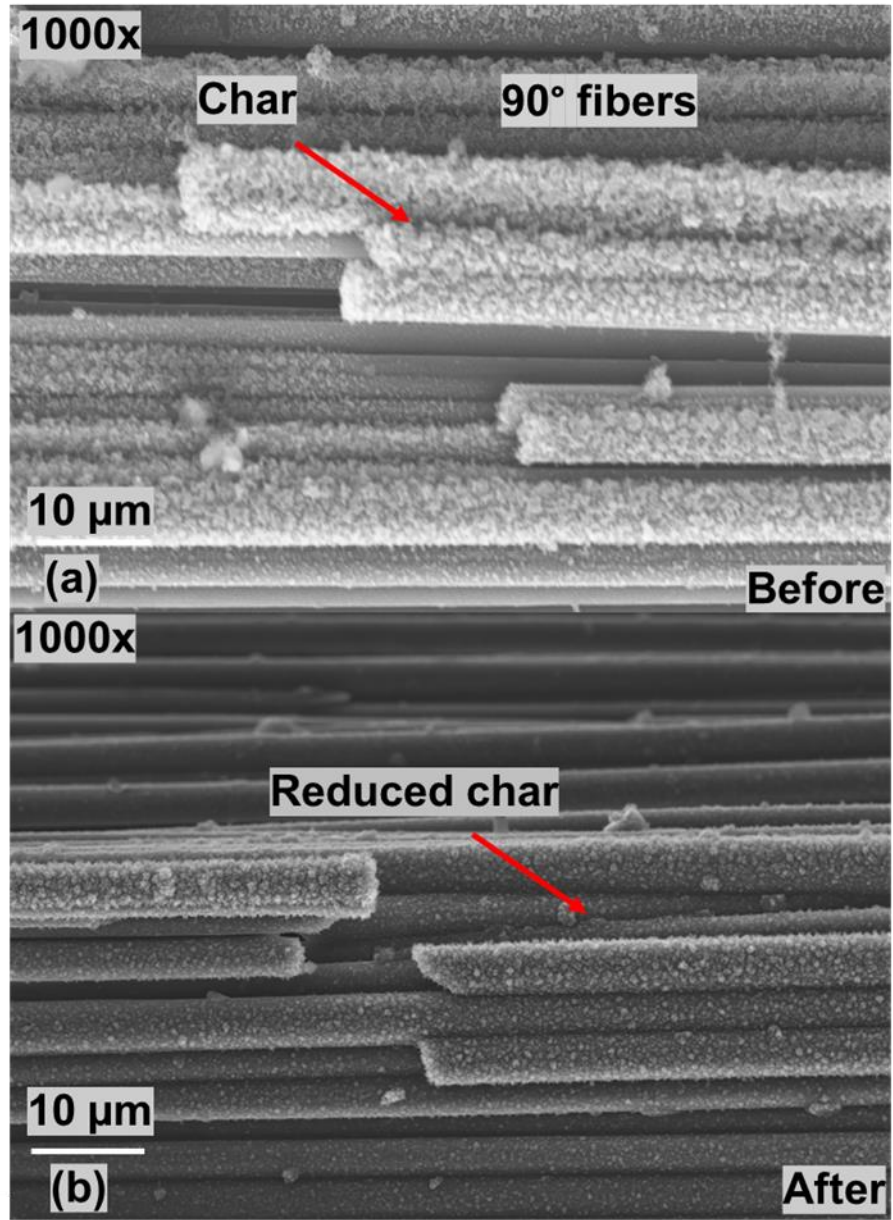


Figure 70. Sonication (60min, acetone) results of 4-ply cross-ply [0/90/90/0] Hexcel woven fabric

The char removal process can be effectively enhanced by exploring additional processes that could aid in material removal. Techniques to weaken the interfacial bonds between the char and polymer composite surfaces (such as thermal-shocking) should be explored to understand the interface-level phenomena and improve overall efficiency.

4.3 Surface cleaning of mechanically failed Cytec T40-800/Cycom[®] 5215 graphite/epoxy composite specimens

The effect of ultrasonic cleaning in removing char from mechanically failed aerospace composite specimens was explored through ultrasonication experiments in acetone. Cytec UNCO specimens mechanically failed using the ASTM standard D6641 for compression testing were used for this evaluation. UNCO half specimens, which are 3×0.5 in², were subjected to direct fire exposure in the MSU fire test setup for 12 s in the vertical orientation (Appendix B, Figure B - 2). The fractured tip of the UNCO half specimens was submerged in the flame at a distance of 0.75 in from the burner tip. A total of 12 specimens were burned in this manner. It was previously established that char and soot deposition was more pronounced in the UNCO specimen's perimeter at a distance from the laminate mid-plane. In these regions, while the airflow is greater, it also served as a path for flame spread. Therefore, the thermal degradation due to combustion is incomplete, resulting in char and soot deposition. Consequently, these regions will be focused during surface characterization before and after the char removal experiments.

4.3.1 Ultrasonic cleaning of mechanically failed Cytec T40-800/Cycom[®] 5215 graphite/epoxy specimens

Three different sonication durations (15 min, 30 min, and 60 min) were considered for these experiments. Three test cases were adopted for testing, and three replicates were used for each case. The first test case involved the ultrasonic treatment of burned Cytec specimens in 5 ml of acetone for 60 min. The second test case employed a pretreatment step: instabilities due to thermal stresses were induced at the char/fiber interface by quenching in liquid nitrogen (N₂). In the third test case, thermal stresses were induced by submerging the burned tip of the now room-temperature specimens in boiling water for 15 min. Since the 15 and 30-min test cases (for ultrasonic cleaning) did not result in a significant change in the char profile, they are not discussed in this report for brevity.

In the pretreatment step with liquid nitrogen, the burned tips of the Cytec specimens initially at 70°F were submerged in a flask of liquid nitrogen (-410°F) for a small duration (5 s). After the specimens were extracted, they were gently air-dried and held at 70 °F for 5 min and

resubmerged in liquid nitrogen. This process was repeated fifteen times. The sudden change in surface temperature during quenching acts as a thermal shock that accelerates the development of compressive thermal loads between the fiber/matrix interface due to the difference in thermal expansion coefficients (Wei, 2019). The pretreatment step with boiling water (212 °F) was performed similarly for a small duration (5 s), with fifteen total immersions spaced out in 5 min intervals. After pretreatment, the specimens were sonicated in acetone for 15 min. This process (thermal shock and sonication) was repeated three times on individual Cytec specimens for an effective sonication duration of 45 min. The specimens were then extracted and prepared for surface char evaluation in SEM. After pretreatment, the specimens were visually inspected for damage features like ply-splitting, delamination, and other features that might arise due to the induction of thermal stresses in the specimen.

The ultrasonication step was carried out in the Branson M5800H ultrasonic cleaner with a 2.5-gallon tank, an operational frequency of 40 kHz, and an input power of 160 W. The burned specimens were initially air-dried and maintained at ambient conditions. After pretreatment (test cases 2 and 3), the Cytec specimens were placed in 50 ml conical tubes and filled with acetone. The tank of the sonication chamber was filled to the operational level with distilled water. The filled conical tubes were placed in the tank, and the power was turned on. The sonication energy supplied to the tank can be controlled by adjusting the amplitude setting provided on the control panel. A constant sonication amplitude of 100% was selected for all the tests. After ultrasonication, the sonicated specimens are rinsed in isopropanol, dried off, and stored in small vials. The vials containing the Cytec specimens are then placed in a vacuum oven for 24 hours for drying. The fire-damaged surfaces are analyzed using SEM to observe the change in surface char morphology after ultrasonication.

4.3.2 Surface characterization of mechanically failed Cytec T40-800/Cycom[®] 5215 graphite/epoxy specimens after ultrasonic cleaning in acetone

Scanning electron microscopy was performed before and after ultrasonic cleaning. The perimeter section of the burned tip away from the laminate mid-plane was considered to be the region of interest. The Cytec specimens were burned vertically for 12 s using the MSU fire test setup (Appendix B, Figure B - 2). The burned specimens were mounted on a 45°/90° angle stub with the lateral surfaces secured with carbon tape. An accelerating voltage of 15 kV was used—and the SEM micrographs were taken at a WD of 9 mm.

4.3.2.1 Sonication of Cytec UNCO specimen in acetone for 60 min

The SEM micrographs shown in Figure 71 demonstrate the surface char morphology on the in-plane fibers (90°) in the perimeter region of the fracture surface. The fibers of the inner plies are

visible in the background, indicating delamination between the two plies. The significant char and soot deposition and the visible space between adjacent fiber surfaces point to a high degree of matrix decomposition. The optical micrographs in Figure 71 belong to a representative vertically oriented Cytec half-specimen burned for 12 s followed by 60 min of ultrasonication in acetone. A pretreatment step was not adopted for this specimen to assess the effectiveness of pretreatment on char removal. Salient fiber-failure features like micro-buckling, chop marks, and recessed fibers can only be observed in the out-of-plane direction (Figure 72). However, excessive char and soot deposition was observed on the cylindrical surfaces, providing adequate regions for sonication action, shown in Figure 71(a).

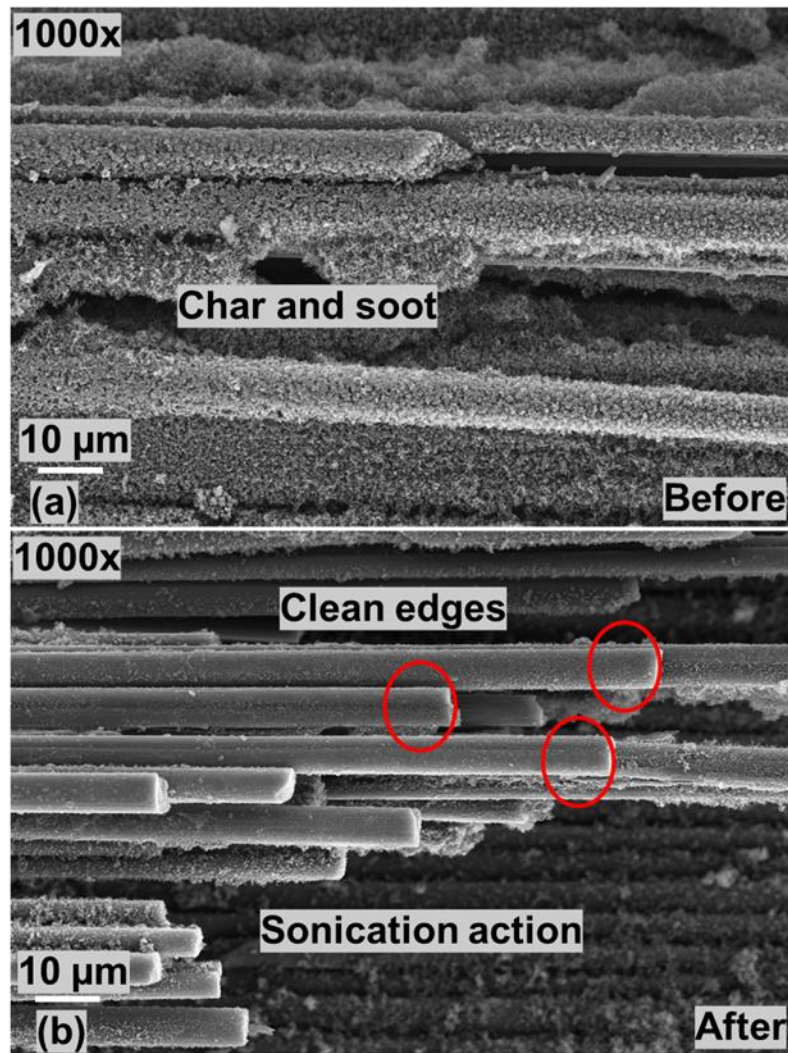


Figure 71. Sonication (60min, acetone) results of Cytec UNCO

After 60 min of ultrasonic cleaning in acetone, the amount of char present on the 90° fibers is significantly less, indicating the prevalence of the sonication action. While the fibers in the inner

ply appear to retain the char and soot deposits, the fibers that appear to be clear are the misaligned in-plane fibers. Constant acoustic streaming continuously erodes the char from the fiber surface. The bulk movement of the liquid during acoustic streaming might be a contributing factor for the fiber misalignment. The area between adjacent fibers and the fibers located in the ply's interior still seem to retain their char layers. The presence of char after sonication could be attributed to improper penetration of solvent in these regions. Since ultrasonic wave propagation, cavitation, and bubble implosion are dynamic phenomena, it can be challenging to accurately predict the sonication power/time needed to irradiate char from the composite surface without the use of computational modeling. It would be interesting to observe the change in the surface char morphology of the test specimens after multiple passes of ultrasonication.

The char formation on the out-of-plane 0° fibers was markedly different from the fuzzy char globules noticed so far on the fiber ends. Char and soot deposition was found to be textured and present on the cylindrical lateral surfaces of the fibers (similar to the in-plane 90° fibers) at the perimeter of the fracture surface. This change in the char morphology could be attributed to incomplete combustion and inadequate air supply during combustion. Airflow could be restricted about the interface between consecutive fibers tightly arranged in tow, leading to the textured char along the fiber length. While micro-buckled fibers are visible in the micrograph, the char and soot deposits at the fiber-ends ostensibly masked the fracture features like chop marks on the fiber ends (Figure 72(a)). As shown in Figure 72(b), the optical micrographs point to a reduction in char on the cylindrical surfaces of the 0° fibers. Salient failure features like the chop marks on the compressive faced of the 0° fibers at the fiber ends are still masked by either char or melt dripping-like substance on these surfaces. This problem could be addressed by multiple ultrasonication passes or controlled pyrolysis of the fiber surfaces to burn off the surface depositions. It would be interesting to observe the effects of an additional pretreatment stage to 60 min of ultrasonic cleaning.

In summation, sonication action was equally prevalent in removing char from both the in-plane and out-of-plane fibers. However, in the presence of other fire by-products like melt dripping covering the fiber surface, alternate surface treatment techniques like controlled pyrolysis or ice-blasting should be explored. It would be interesting to see if thermal shock due to quenching or immersion in boiling water creates the requisite instability at the interface level between the deposits and the fiber to dislodge and separate the char and increase the effectiveness of ultrasonic cleaning.

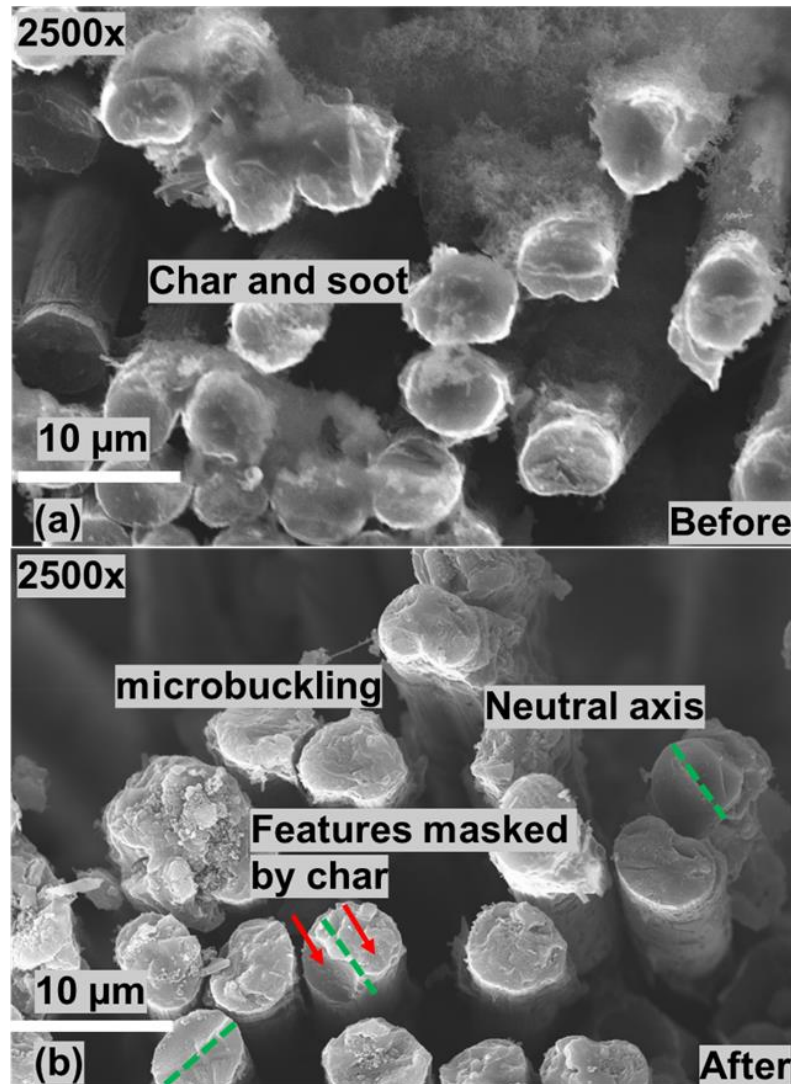


Figure 72. Sonication (60min, acetone) results of 21-ply cross-ply Cytec UNC0

4.3.2.2 Pretreatment with liquid N_2 followed by ultrasonic cleaning

Three vertically oriented mechanically failed 21-ply Cytec [90/0/90]₇ UNC0 specimens previously burned for 12 s using the MSU fire test setup (Appendix B, Figure B - 2) were used to study the effect of thermal shocking on the ultrasonication process and the removal of surface char from the burned surface. The burned UNC0 half-specimens were subjected to thermal shocking by immersing them in liquid nitrogen (N_2) (-410 °F) for 5 s, followed by holding them at ambient conditions for 5 min (70°F). This immersion process was repeated 15 times.

Ultrasonication was then performed for 15 min in acetone. This process (thermal shock and ultrasonication) was repeated three times before the specimens were extracted for SEM imaging. The resulting thermal cycling was posited to weaken the interface bonding between the surface char and the underlying composite part and help in material erosion during ultrasonic cleaning.

After ultrasonication, the sonicated specimens are rinsed in isopropanol, dried off, and stored in small vials. The vials containing the Cytec specimens are then placed in a vacuum oven for 24 hours for drying. The fire-damaged surfaces are analyzed using SEM to observe the change in surface char morphology due to ultrasonication.

The optical micrographs in Figure 73(a) show representative images of a collection of in-plane 90° fibers with a significant amount of surface char and soot deposits on the cylindrical surfaces of the Cytec specimen. The angled orientation in the micrograph results from reorienting the specimen stub within the SEM chamber to get quality images. The presence of gaps between the inner and outer plies indicates a degree of inter-ply matrix decomposition.

Also worth noting is the uneven distribution of char on the surface of the graphite fibers.

After thermal shock and ultrasonication, a significant reduction was observed in the overall amount of char and soot deposits (Figure 73(a)). The fibers in the lower half of the image seem to be completely devoid of any surface char deposits. In contrast, the overall amount of char in the upper half of the micrograph was drastically reduced. Since the ultrasonication time used was 15 min for each cycle, it could be theorized that thermal cycling played a crucial role in weakening the interfacial bonding between the char and the underlying specimen. For a near-total removal of char, the specimen can be subjected to additional rounds of thermal cycling and higher duration of ultrasonication. However, care has to be taken to ensure that the composite surfaces are not damaged. Also, the effect of thermal shock on the fiber ends of the 0° fibers is an important factor to observe since the fiber ends often possess distinctive fracture surface features that help identify the nature of the failure. The effectiveness of thermal shocking assisted ultrasonic cleaning at higher sonication times in removing surface char from the fiber ends of the 0° fibers has to be studied to assess the viability of the cleaning process. Due to a technical difficulty, optical micrographs showing the effect of liquid N₂ induced thermal cycling (with subsequent sonication) on the 0° out-of-plane fiber ends and the accompanying salient fracture characteristics. The experiment will be repeated at a later date, and the SEM micrographs will be obtained.

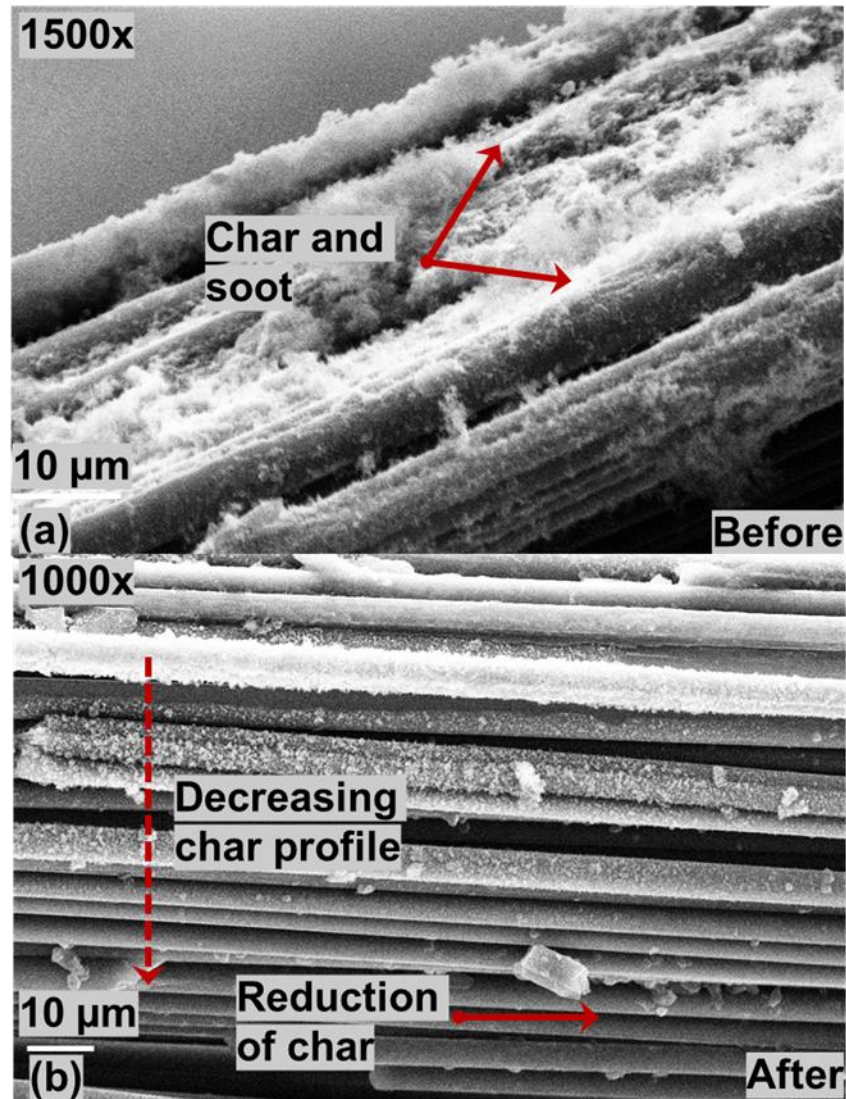


Figure 73. Thermal cycling and sonication results of 21-ply cross-ply Cytec UNCO

4.3.2.3 Pretreatment with boiling water followed by ultrasonic cleaning

Three vertically oriented mechanically failed CytecUNCO specimens were burned for 12 s using the MSU fire test setup (Appendix B, Figure B - 2). These specimens were then used to study the effect of thermal shock on the ultrasonication process and remove surface char from the burned surface. The burned UNCO half-specimens were subjected to thermal shocking by immersing them in boiling water for 15 min. Ultrasonication was then performed for 15 min in acetone. This process (thermal shock and ultrasonication) was repeated three times before the specimens were extracted for SEM imaging. The specimens were visually inspected for surface-warping and ply delamination.

After ultrasonication, the sonicated specimens are rinsed in isopropanol, dried off, and stored in small vials. The vials containing the Cytec specimens are then placed in a vacuum oven for 24 hours for drying. The fire-damaged surfaces are analyzed using SEM to observe the change in surface char morphology due to ultrasonication.

The SEM micrographs shown in Figure 74 represent the (out-of-plane) 0° fibers before and after surface cleaning for a representative Cytec specimen that has undergone thermal cycling due to boiling water and the subsequent ultrasonic cleaning. Before the surface cleaning, extensive char and soot deposits covering the fiber ends and spanning the image can be observed in Figure 74(a). In these (out-of-plane) 0° fibers, heat is conducted through the thickness of the composite. In this case, the interior in-plane plies can cut off the airflow required for heat conduction, resulting in the high-dense char on the fiber ends. Therefore, the surface char generated after burning is significant, with highly dense char on the fiber ends. However, after performing pretreatment in boiling water and ultrasonication, there seems to be a near-total reduction in the char and soot deposits on the fiber ends (Figure 74). Pretreatment with boiling water showed more promise than pretreatment with liquid N_2 . The fiber debris visible in the micrograph could result from mechanical failure, fire exposure, or surface cleaning. Multiple experiments with thermal cycling of the Cytec specimens in boiling water followed by ultrasonication will be conducted to investigate thermal cycling effectiveness.

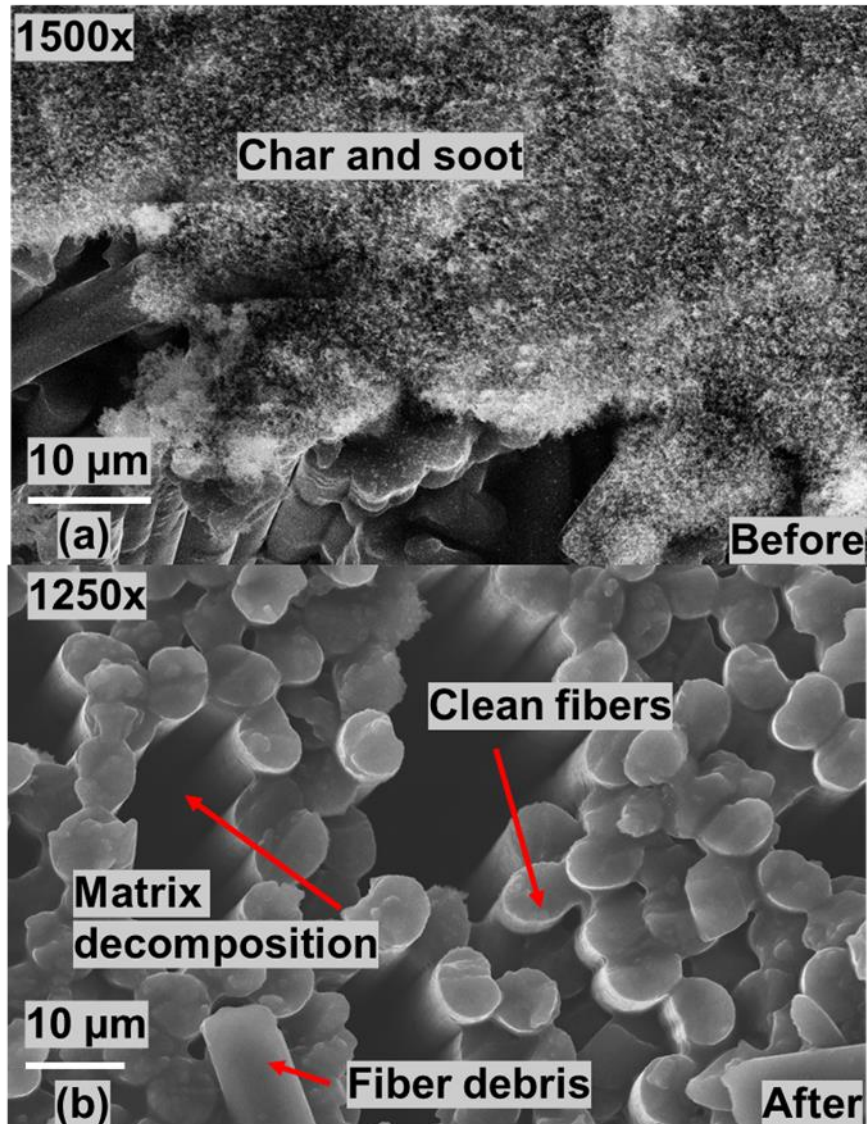


Figure 74. Thermal cycling and sonication results of 21-ply cross-ply Cytec UNCO

Additional experiments are necessary to delineate the individual contributions of ultrasonication and the pretreatment stages, quantify the surface cleaning efficiency, and improve the surface cleaning process. These experiments will be performed in the second phase of research. In the future, the effect of fracture surface morphology on char removal and the overall effectiveness of the ultrasonic cleaning will be determined by repeating the ultrasonication experiments on various types of mechanically failed Cytec specimens.

4.4 Effect of sonication parameters, pretreatment, and char morphology on char removal

This research aims to investigate the effectiveness of ultrasonic cleaning of burned mechanically failed graphite/epoxy composites. In a post-crash fire, thermal damage results in extensive char formation on the burned surfaces, resulting in the masking of salient fracture-surface morphologies. Fractographic analysis of these failed surfaces can aid in the identification of the root cause of failure. Therefore, developing an effective fire-damage assessment methodology and an efficient surface treatment protocol applicable to a wide range of aircraft composite material systems and critical structural components. This section summarizes key observations associated with various surface cleaning experiments on burned pristine carbon/epoxy specimens and mechanically failed graphite/epoxy specimens. The findings from this research can motivate future efforts to develop a comprehensive surface treatment protocol that can aid in the fire-forensic analysis of principal structural components of aircraft in the event of a crash and the resulting post-crash fire.

Fire exposure tests were conducted on pristine 4-ply cross-ply [0/90/90/0] Hexcel specimens, with a test setup consisting of a metal enclosure, metal frame, and a Bunsen burner. A more detailed discussion on the burning of the pristine Hexcel specimens and the resultant fire damage is presented in Appendix B. Both vertical and horizontal orientations were tested for various exposure durations. The Hexcel specimens were positioned at 0.75 in from the burner tip for both orientations. Vertical burning produced the most char, with the lowest exposure time (12 s) producing the most char. This is possibly due to the increased probability of incomplete combustion at the exposed fiber ends. Since the goal of these tests was to generate dummy test specimens for char removal experiments, vertical burning for 12 s was chosen for further burn tests. The woven-fabric carbon/epoxy material system was selected to examine the interlacing effect (7,1) on char formation and removal and ease of availability. After burning, visual inspection and scanning electron microscopy of these specimens suggested that specimen orientation and layup had a significant influence on the extent and nature of fire damage (i.e., matrix decomposition, char, soot, matrix cracking, delamination, melt dripping, and residual thickness increase).

Thermal damage in the woven-fabric (eight-harness satin weave) carbon fiber reinforced epoxy plies was similar to the unidirectional continuous graphite fiber-reinforced epoxy composite plies—except at the regions of overlap where the (7,1) interlacing occurs. Since heat conduction primarily occurs along the fiber length, the plies oriented parallel to the flame conducted heat into the specimens and had cotton-candy-like char deposits on the fiber ends. For plies oriented

perpendicular to the flame, char formation was along the length of the fibers mainly due to the diversion of heat transfer away from the interior of the specimens. This would result in the incomplete combustion of the epoxy matrix leading to incomplete decomposition of the matrix into char. At the (7,1) interlacing regions, the effective heat transfer rate is greater—leading to the near-total combustion of the matrix leading to increased production of gaseous by-products rather than char and soot. Therefore, the (7,1) interlacing regions could contribute to lower char density in the lateral surfaces—above and below the laminate mid-plane. Consequently, SEM micrographs of pristine Hexcel woven-fabric carbon/epoxy specimens only featured regions close to the laminate mid-plane, and the sonication effects were primarily examined in these regions.

Observations from thermal damage assessment of burned pristine Hexcel specimens helped in the development of initial char removal experimental strategies. Initial ultrasonic cleaning experiments were performed using commercially available organic solvents. A sonication time of 15 min was set for these experiments since the impact of higher sonication durations on the specimen geometry was not initially established. Based on visual inspection and SEM imaging, acetone was selected as a viable solvent for sonication. Also, a higher sonication duration (60 min) was adopted for subsequent sonication studies.

After 60 min of ultrasonic treatment in acetone, the specimens were extracted from the sonicator, rinsed in isopropanol, dried off, and stored in small vials. The vials were then placed in a vacuum oven for 24 hours to facilitate drying. There was a significant reduction in the surface char on the plies containing the out-of-plane (0°) fibers and the in-plane (90°) plies. Several factors could be responsible for the effective removal of surface char. Ultrasonication is a dynamic phenomenon with several simultaneously occurring processes. The movement of ultra-high frequency acoustic waves within the liquid results in localized high pressure and temperature conditions. This, in turn, causes cavitation, i.e., the evolution of bubble growth and subsequent implosion.

Moreover, a bulk phenomenon known as acoustic streaming causes mass movement of fluid within the sonication chamber. The generation of highly oxidative free radicals ($\text{H}_3\text{C}\cdot$, $\text{OH}\cdot$, $\text{HO}_2\cdot$) and their subsequent interactions with the charred regions would be beneficial in breaking the C-C, C=C, C-N, and C-O bonds at the interface between the char and the composite surface by providing pathways for complex oxidation/reduction reactions. Effective ultrasonic treatment/char removal would also entail chipping away the char and soot deposits due to the impinging of jets of pressurized liquid (due to bubble implosion) on the stained surface. The char residue also needs to be transported away from clean surfaces (to prevent redeposition), and additional solvent has to be transported to regions of interest (acoustic streaming). If the

comparison of the SEM micrographs before and after sonication produces a difference in the char morphologies, it would be reasonable to hypothesize that the char removal could be attributed to the factors previously discussed.

The effectiveness of sonication was tested on the mechanically failed Cytec UNCO specimens. A total of 12 Cytec specimens were burned in the vertical orientation for 12 s using the MSU fire test setup. Scanning electron microscopy was performed on the burned samples before and after ultrasonication to compare the change in the surface char characteristics. The sonication experiments were extended to include a pretreatment stage in which specimens were subjected to thermal cycling due to exposure to either liquid N₂ or boiling water. The pretreatment stage was adopted to observe the influence of thermal cycling on the burned Cytec specimens. Repeated exposure to extreme temperatures would result in thermal stresses on the burned surface and weaken the interfacial bonding between the surface char and the unburned graphite/epoxy substrate. Out of the 12 Cytec specimens, four specimens were pretreated with liquid N₂. Four specimens were pretreated with boiling water, and the remaining four specimens were not subjected to any pretreatment. The specimens that were not pretreated were sonicated for 60 min, whereas the pretreated specimens were sonicated for an effective duration of 45 min.

SEM micrographs obtained for representative Cytec specimens showed that the pretreatment stage played a significant role in char removal. After pretreatment with boiling water, the sonication action was far more prevalent in removing char from the burned composite surface. The SEM micrographs revealed a near-total removal of char from the fire exposed fiber ends of the out-of-plane (0°) fibers with visible fracture surface features. The specimens pretreated with liquid N₂ had a reduced char density in the upper section of the SEM micrograph and a greater reduction of char in the lower section. However, the sonication effects on the out-of-plane (0°) fibers were not captured for this specimen due to issues with the SEM machine. While the sonication action was prominent on the specimens pretreated with liquid N₂, it was not as intensive as the previous case. In the case of the specimens that were not subjected to a pretreatment stage, the out-of-plane (0°) fibers had markedly different surface features before and after sonication, with a reduction in surface char on the fiber ends. However, the fracture surface features were masked even after sonication due to melt drippings underneath the surface char.

Another important high-level observation made during the surface cleaning experiments was that the charred surfaces of the in-plane (90°) fibers appeared to have a greater reduction in the surface char than the out-of-plane (0°) fibers. This could be attributed to several different factors. The difference in the char (textured vs. fuzzy) physical features between the in-plane and out-of-

plane fibers could be an important factor to consider. The char on the in-plane fibers is layered and amorphous, whereas the char on the out-of-plane fibers appears to be more of a mixed (amorphous/crystalline) phase. This difference in char profile would mean that the interfacial bonding between the char and underlying composite might be different.

Moreover, since sonication is a surface phenomenon, the availability of free surface area could play a role in the cleaning action. In this case, the in-plane fibers possess a significant advantage since char is present on a greater surface area. Higher the surface area, the greater the possibility of bubble implosions adjacent to the charred regions, which would also positively affect the extent of free radical generation and acoustic streaming. Moreover, the exposed fiber ends of the out-of-plane (0°) fibers are of higher importance in fractographical assessment and failure determination. Therefore, additional processes uniquely suited to char removal from exposed ends of out-of-plane (0°) fibers will be investigated in phase II.

While ultrasonication has shown much promise, the repeatability and accuracy of the process need to be further explored. The acetone-based ultrasonication experiments on pristine Hexcel carbon/epoxy and mechanically failed graphite/epoxy composite specimens resulted in char removal. The sonication action caused free-radical generation, bulk movement of dissolved char (solute), extreme pressure and temperature conditions within the solvent, and adjacent char deposits. Prolonged sonication action results in the removal of char due to chemical and mechanical breaking down of char. The dissolved char is then transported away from the composite specimen.

However, sonication parameters, the nature of pretreatment, and the char morphology affected the extent of char removal. Since thermal degradation is different after burning and ultrasonication are dynamic processes, greater care should be taken during future research efforts to adequately replicate the results for thicker principal structural elements with complex multi-mode failures. A design of experiments approach can be adopted for future experimentation efforts to account for the variability of thermal damage characteristics during fire exposure and ultrasonic treatment. On micro-buckling terrace structures, any presence of char on the fiber ends can be machined away. Alternative chemical char removal techniques that provide pathways to the oxidation and removal of char deposits from the burned composite surface should be explored. Acid-peroxide mixtures have been used in conjunction with ultrasonication to promote an enhanced recovery of carbon fiber from CFRP waste (Das & Varughese, 2016). The effect of such solutions on char and the overall effectiveness of acid-based solutions in the ultrasonic treatment of burned aerospace composites. Thermolytic recovery of carbon/graphite fibers from CFRP/GFRP wastes is a prominent fiber-recovery process used in the fiber-recycling industry

(Giorgini, 2014; Jianying Deng, 2020). The effectiveness of the thermolytic process on the char formed due to post-crash fire will be explored in phase II. The applicability of the ultrasonication across additional failure modes (SBS, UNT0, and IPS) and its effects on these fracture morphologies will be further investigated in the next phase of research efforts.

5 Conclusions

This report investigated the effects of small-flame exposure on thermal damage development in mechanically-failed Cytec composite specimens. These included unnotched compression (UNC0), short beam strength (SBS), in-plane shear (IPS), and compression after impact (CAI). Pre-fire fractography of the fractured surfaces revealed various failure features, including chop marks, riverlines, microflows, hackles, matrix cracking, fiber splitting, microbuckling, and delamination. Similar features were seen in the existing *Composite Failure Analysis Handbook* for different resin-fiber epoxy systems (Kar, 1992). These key features were documented and are used to determine the pre-existing loading conditions (e.g., tension, compression, or shear) before a composite structural failure.

In this study, a total of 21 vertical and horizontal fire tests were conducted using a Bunsen burner on mechanically-failed UNC0, SBS, and IPS graphite/epoxy specimens. Visual inspection and scanning electron microscopy of the mechanically failed specimens suggested that the specimen layup, orientation relative to the heat source (i.e., vertical versus horizontal burning), fire exposure duration, and fracture surface morphology all significantly impacted fire damage formation. The damage included melt dripping, matrix decomposition, char, soot, matrix cracking, delamination, and residual thickness increase due to explosive outgassing. In all cases, the surrounding resin matrix decomposition removed fracture surface characteristics typically produced by mechanical failure.

In addition, char deposits forming on the fracture surface may act as a thermal barrier that further impedes oxygen transfer to the specimen's interior and reduces the rate of thermal degradation. The thermal damage development was also influenced by the total available free surface area generated during mechanical failure. Specimens with greater free surface area promote better airflow and oxygen availability for combustion and sustained far more thermal degradation for given fire exposure. For instance, thicker specimens such as SBS required longer fire exposure times to induce the same degree of char as thinner specimens (IPS). In addition, unidirectional fibers oriented parallel to the flame axis conducted heat into the interior of the composite, which resulted in severe matrix decomposition, melt dripping, and surface char deposition. In contrast, unidirectional fibers oriented perpendicular to the flame axis acted like a thermal protection layer

that impeded heat transfer to the specimen's interior. Fire damage can mask the fracture surface morphologies, making identifying the root cause of failure very difficult. For extended burn durations, key failure features in exposed fiber bundles might be susceptible to extreme thermal degradation due to severe oxidation and thinning, which impede the forensic analysis. This is particularly true for specimens with highly irregular fracture surfaces (such as IPS specimens) that permit enhanced airflow and improved oxygen availability during burning.

As part of this research, several char removal techniques were performed on vertically burned pristine cross-ply Hexcel specimens and mechanically failed graphite/epoxy specimens, as described in Appendix B. Ultrasonication experiments were conducted to determine the best char removal approach using burned pristine Hexcel specimens for 60 min in acetone. The sonication action was more effective in char removal for the in-plane (90°) fibers than the exposed fiber ends of the out-of-plane (0°) fibers.

Ultrasonication experiments were also conducted on Cytac UNCO specimens. In the first set of experiments, the specimens were sonicated for 60 min in acetone. Additionally, the effect of thermal cycling on the effectiveness of char removal was investigated. The Cytac specimens were sonicated in acetone in three intervals, each duration of 15 min. Thermal cycling was achieved in the form of a pretreatment step, and two thermal cycling processes were explored: quenching with liquid N_2 and heating in boiling water. The pretreatment step with boiling water showed the most promise, with a near-total removal of char from the fire-exposed fiber ends of the out-of-plane (0°) fibers. While the sonication experiments showed more promise in removing char from the circumferential surfaces of the in-plane (90°) fibers, char removal from the exposed fiber ends of the out-of-plane (0°) fibers was more challenging.

6 Future work

Fuel-fed post-crash fires can be high-intensity, long-duration phenomena distinct from the small-scale fire tests on ASTM standard composite specimens performed in this work. Nonetheless, this research represents an essential first step in developing an effective strategy for post-crash forensic analysis of composite aircraft structures. Actual post-crash fires can burn and then smolder for hours after initial ignition, resulting in the deposition of massive amounts of char and other fire by-products (including those due to paint, hydraulic fluid, and foam cores) on the composite failure surfaces. In addition, floor wax, or an equivalent sealant, is typically added to the burned composite structures to reduce the risk of respirable fibers to first responders. In the future, a combination of char removal techniques, including acid-based oxidation/decomposition of char, elevated temperature exposure (near matrix decomposition temperature) in inert and

oxidative atmospheres, and micro-machining will be explored along with ultrasonication. In addition, future phases include oil-fed burner tests to be performed on thicker principal structural elements. These tests will enable the characterization of thermal degradation in realistic composites and develop viable in-field strategies for char removal from commercial and general aviation aircraft.

7 References

- ASTM-D2584-18. (2018). *Standard test method for ignition loss of cured reinforced resins*. West Conshohocken, PA, USA: ASTM International.
- Atchley, A., & Crum, L. (1985). *Acoustic Cavitation and Bubble Dynamics*. Mississippi University, Physical Acoustics Research Lab.
- Awad, S. B. (1996). *Ultrasonic cavitations and precision cleaning*.
- Awad, S., & Nagarajan, R. (2010). *Ultrasonic cleaning*. Elsevier.
- Babrauskas, V., & Peacock, R. D. (1992). Heat release rate: the single most important variable in fire hazard. *Fire safety journal*, 18(3), 255-272. doi:[https://doi.org/10.1016/0379-7112\(92\)90019-9](https://doi.org/10.1016/0379-7112(92)90019-9)
- Beyler, C., Croce, P., Dubay, C., Johnson, P., & McNamee, M. (2017). Oxygen consumption calorimetry, William Parker: 2016 DiNunno Prize. *Fire Science Reviews*, 6(1), 1-7. doi:<https://doi.org/10.1186/s40038-016-0016-z>
- Blitz, J. (1971). *Ultrasonics: methods and applications*.
- Botelho, E. C., Silva, R. A., Pardini, L. C., & Rezende, M. C. (2006). A review on the development and properties of continuous fiber/epoxy/aluminum hybrid composites for aircraft structures. *Materials Research*, 9(3), 247-256.
- Brooks, J., & Taylor, G. (1968). The formation of some graphitizing carbons. *Chemistry and physics of carbon*, 4, 243-286.
- Calle, C. I., McFall, J. L., Buhler, C. R., Snyder, S. J., Arens, E. E., Chen, A., . . . Trigwell, S. (2008). *Dust particle removal by electrostatic and dielectrophoretic forces with applications to NASA exploration missions*. ESA Minneapolis, MN.
- Camanho, P., Bowron, S., & Matthews, F. (1998). Failure mechanisms in bolted CFRP. *Journal of reinforced plastics and composites*, 17(3), 205-233.
- Chen, Z. M. (2018, June 26). Composite failure analysis after post-crash fire. Presentation. Mississippi State, Mississippi, USA.
- Clarkson, E. (2012). *Cytec Cycom 5215 T40-800 Unitape Gr 145 33% RC Qualification Statistical Analysis Report*.

- Cooper, D. (1986). *Particulate contamination and microelectronics manufacturing: an introduction*.
- Das, M., & Varughese, S. (2016). *A novel sonochemical approach for enhanced recovery of carbon fiber from CFRP waste using mild acid–peroxide mixture*.
- Ebnesajjad, S., & Landrock, A. (2014). *Adhesives technology handbook*. William Andrew. Retrieved from <https://www.epigentek.com/catalog/episonic-multi-functional-bioprocessor-1100-p-2997.html>
- Fernández, A., Lopes, C. S., González, C., & López, F. A. (2018). Characterization of carbon fibers recovered by pyrolysis of cured prepregs and their reuse in new composites. In R. Khanna, & R. Cayumil, *Recent Developments in the Field of Carbon Fibers* (pp. 103-120). London, United Kingdom: IntechOpen.
- Gilchrist, M. D., & Svensson, N. (1995). A fractographic analysis of delamination within multidirectional carbon/epoxy laminates. *Composites Science and Technology*, 195-207.
- Giorgini, L. (2014). Pyrolysis as a way to close a CFRC life cycle: carbon fibers recovery and their use as feedstock for a new composite production. *AIP conference proceedings*. 1599, pp. 354-357. AIP publishing LLC.
- Greenhalgh, E. S. (2009). *Failure analysis and fractography of polymer composites*. Woodhead Publishing.
- Hernandez, D. A., Soufen, C. A., & Orlandi, M. O. (2017). Carbon fiber reinforced polymer and epoxy adhesive tensile test failure analysis using scanning electron microscopy. *Materials Research*, 951-961.
- Horner, A. (2000). *Aircraft materials fire test handbook*. William J. Hughes Technical Center, Fire Safety Section, AAR-422. New Jersey: Federal Aviation Administration.
- Jianying Deng, L. J. (2020, December). Efficient method of recycling carbon fiber from the waste of carbon fiber reinforced polymer composites. *Polymer Degradation and Stability*, 182.
- Kanegsberg, B., & Kanegsberg, E. (2011). *Handbook for critical cleaning: cleaning agents and systems*. CRC press.
- Kar, R.J. (1992). *Composite Failure Analysis Handbook, FAA Technical Report, DOT/FAA/AR-91/23/WL-TI-91-4032, CINDAS/USAF, CRDA HANDBOOKS*, West Lafayette

- Kar, R. J. (1992). *Composite failure analysis handbook Volume II: Technical Handbook Part 2 - Atlas of fractographs*. Hawthorne, CA: FAA.
- Kohli, R., & Mittal, K. (2009). *Developments in surface contamination and cleaning-Vol 2: Particle deposition, control and removal*. William Andrew.
- Kohli, R., & Mittal, K. (2015). *Developments in Surface Contamination and Cleaning, Vol. 1: Fundamentals and Applied Aspects*. William Andrew.
- Kohli, R., & Mittal, K. (2018). *Developments in Surface Contamination and Cleaning: Applications of Cleaning Techniques: Volume 11* (Vol. 11). Elsevier.
- Kumar, M. S., Raghavendra, K., Venkataswamy, M. A., & Ramachandra, H. V. (2012). Fractographic analysis of tensile failures of aerospace grade composites. *Materials Research*, 990-997.
- Kwan, W., MacCleod, J., Ng, Y., & Tomblin, J. (2007). *NCAMP process specification: Fabrication of NMS 323 qualification, equivalency, and acceptance test panels (Cytac Cycom 5215)*. Wichita Aircraft Certification Office.
- Levchik, S. V., & Wilkie, C. A. (2000). Char Formation. In A. F. Grand, & C. A. Wilkie, *Fire Retardancy of Polymeric Materials* (pp. 171-215). Taylor & Francis.
- Levchik, S., Camino, G., Costa, L., & Luda, M. (1996). Mechanistic study of thermal behaviour and combustion performance of carbon fibre-epoxy resin composites fire retarded with a phosphorus-based curing system. *Polymer Degradation and Stability*, 54(2-3), 317-322.
- Liechti, K. M., Masters, J. E., Ulman, D. A., & Lehman, M. W. (1982). *SEM/TEM fractography of composite materials*. Fort Worth: General Dynamics.
- Man, M., Ng, Y., Tomblin, J., & Hooper, E. (2012). *Cytac Cycom 5215 T40-800 unitape Gr 145 33% RC, Qualification material property data report*. Wichita State University. Wichita, KS: National Institute of Aviation Research.
- Mason, T. (1998). *Practical Sonochemistry: User's Guide to Applications in Chemistry and Chemical Engineering*, Ellis Howood Ltd, New York, 1992.
- McLaughlin, M., & Zisman, A. (1999). *Aqueous Cleaning Handbook*.
- Menon, V. (2018). *Particle Adhesion to Surfaces Theory of Cleaning*. Routledge.
- Mouritz, A. P. (2003). Fire resistance of aircraft composite laminates. *Journal of Materials Science Letters*, 22(21), 1507-1509.

- Mouritz, A. P., & Gibson, A. G. (2007). *Fire properties of polymer composite materials* (Vol. 143). Springer Science & Business Media.
- Mouritz, A. P., & Mathys, Z. (2001). Post-fire mechanical properties of glass-reinforced polyester composites. *Composites Science and Technology*, 61(4), 475-490.
- Mouritz, A. P., Feih, S., Kandare, E., Mathys, Z., Gibson, A. G., Des Jardin, P. E., . . . Lattimer, B. Y. (2009). Review of fire structural modelling of polymer composites. *Composites Part A: Applied Science and Manufacturing*, 40(12), 1800-1814.
- Mouritz, A. P., Gardiner, C. P., Mathys, Z., & Townsend, C. R. (2001). Post-fire properties of composites burnt by cone calorimetry and large-scale fire testing. *Proceeding of the ICCM13*. Beijing, China.
- Naito, K. (2018). Stress analysis and fracture toughness of notched polyacrylonitrile (PAN)-based and pitch-based single carbon fibers. *Carbon*, 346-359.
- O'Donnell, M. J. (2009, September 28). *First Responders' responsibility for protecting evidence at the scene of an aircraft accident/incident*. Federal Aviation Administration.
- Opelt, C. V., Cândido, G. M., & Rezende, M. C. (2018). Fractographic study of damage mechanisms in fiber reinforced polymer composites submitted to uniaxial compression. *Engineering Failure Analysis*, 520-527.
- Prasad, M., Vithanage, M., & Kapley, A. (2019). *Pharmaceuticals and Personal Care Products: Waste Management and Treatment Technology: Emerging Contaminants and Micro Pollutants*. Butterworth-Heinemann.
- Purslow, D. (1986). Matrix fractography of fibre-reinforced epoxy composites. *Composites*, 289-303.
- Rakow, J. F., & Pettinger, A. M. (2007). *Failure analysis of composites: A manual for aircraft accident investigators* (First ed.). International Society of Air Safety Investigators.
- Ranade, M. (1987). *Adhesion and removal of fine particles on surfaces*.
- Ray, S. S., & Kuruma, M. (2019). *Halogen-free flame-retardant polymers: next-generation fillers for polymer nanocomposite applications*. Springer Nature.
- Ray, S., & Kuruma, M. (2019). *Halogen-free flame-retardant polymers: next-generation fillers for polymer nanocomposite applications* (Vol. 294). Springer Nature.

- Riesz, P., Berdahl, D., & Christman, C. (1985). *Free radical generation by ultrasound in aqueous and nonaqueous solutions*.
- Rinaldi, A., Frank, B., Su, D. S., Hamid, S. B., & Robert, S. (2011). Facile removal of amorphous carbon from carbon nanotubes by sonication. *Chemistry of Materials*, 23(4), 926-928.
- Santos, H., Lodeiro, C., & Capelo-Martinez, J.-L. (2009). *The power of ultrasound in Ultrasound in chemistry: analytical applications*. Wiley-VCH, Weinheim.
- Shemwell, B., & Levendis, Y. (2000). *Particulates generated from combustion of polymers (plastics)*.
- Shi, J., Bao, L., Kobayashi, R., Kato, J., & Kemmochi, K. (2012). *Reusing recycled fibers in high-value fiber-reinforced polymer composites: Improving bending strength by surface cleaning*.
- Shwartzman, S., Mayer, A., & Kern, W. (1985). *Megasonic particle removal from solid-state wafers*.
- Smith, B., Grove, R., & Munns, T. (1986). *Failure analysis of composite structure materials*. Seattle: Boeing Military Aircraft Company.
- Snogren, R. (1969). *Selection of Surface Preparation Processes - Part 1: Process Selection Guide*.
- Special conditions: Boeing model 787-8 airplane; composite wing and fuel tank structure-fire protection requirements*. (2007, October 11). Retrieved April 8, 2020, from Federal Register: <https://www.federalregister.gov/documents/2007/10/11/E7-20031/special-conditions-boeing>
- (2009). *Standard Test Method for Determining Material Ignition and Flame Spread Properties*. ASTM.
- (2010). *Standard Test Method for Heat and Visible Smoke Release Rates for Materials and Products Using an Oxygen Consumption Calorimeter*. ASTM.
- Suslick, K. (1989). The Chemical Effects of Ultrasound. *Scientific American*, 260(2), 80-87.
- Sussholz, B. (1980). *Evaluation of micron size carbon fibers released from burning graphite composites*. TRW Defense and Space Systems Group. Redondo Beach, CA: National Aeronautics and Space Administration.

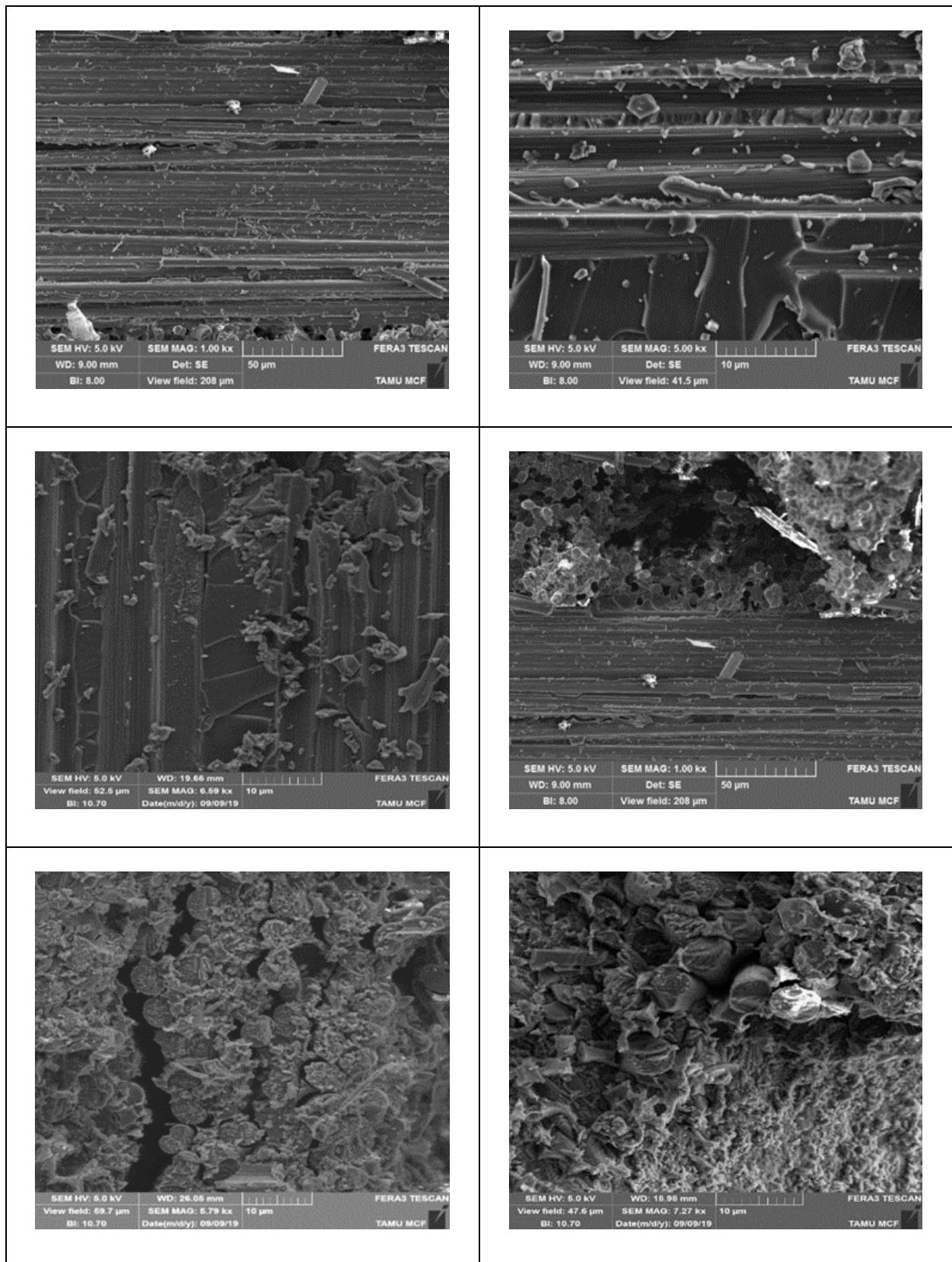
- Tagawa, Y., & Gotoh, K. (2010). Removal of carbon black particles from polymer substrates in water/ethanol mixtures. *Journal of oleo science*, 59(2), 109-112.
- Thill, C. E. (2010). Composite corrugated structures for morphing wing skin applications. *Smart Materials and Structures*, 12(19), 124009.
- Tuziuti, T. (2016). *Influence of sonication conditions on the efficiency of ultrasonic cleaning with flowing micrometer-sized air bubbles*.
- Wang, H., Singh, R., & Lowden, R. (1997). *Thermal shock behaviour of unidirectional, 0/90, and 2-D woven fibre-reinforced CVI SiC matrix composites*.
- Wei, W. S. (2019). Investigation of Impacts of Thermal Shock on Carbon Composite Materials. *Materials*, 12(3), 435.
- Wood, R. H., & Sweginnis, R. W. (1995). *Aircraft accident investigation*. Endeavor Books LLC.
- Xiao, Y., & Ishikawa, T. (2005). Bearing strength and failure behavior of bolted composite joints (part I: Experimental investigation). *Composites Science and Technology*, 65(7-8), 1022-1031.
- Yang, Y., Boom, R., Irion, B., van Heerden, D.-J., Kuiper, P., & de Wit, H. (2012). Recycling of composite materials. *Chemical Engineering and Processing: Process Intensification*, 51, 53-68.
- Zhang, Z. (2010, 06 29). *Thermo-mechanical behavior of polymer composites exposed to fire*. Dissertation, Virginia Tech.

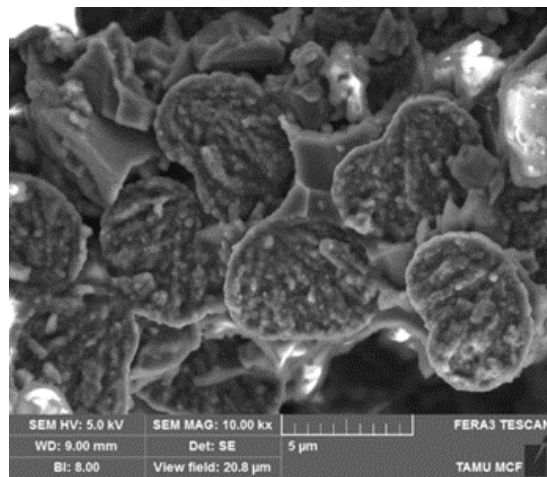
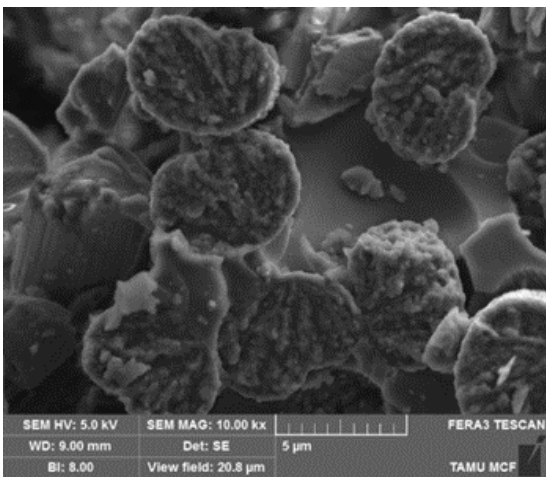
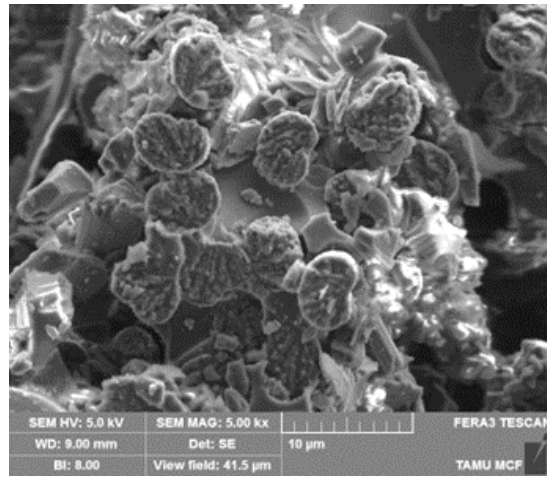
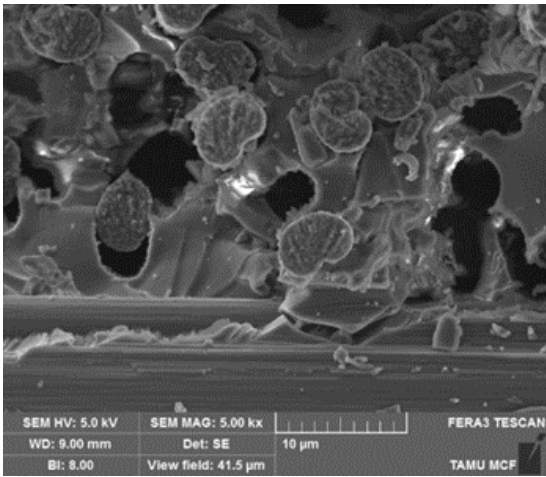
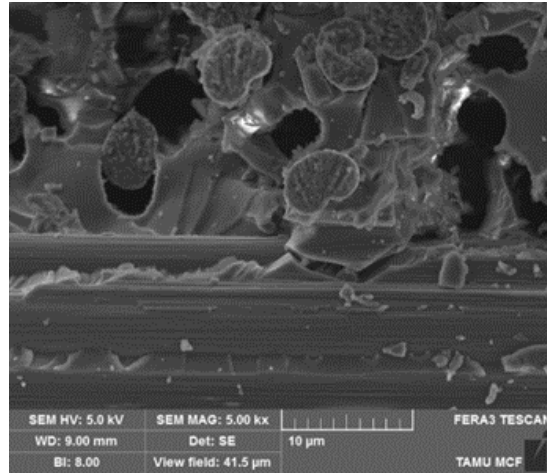
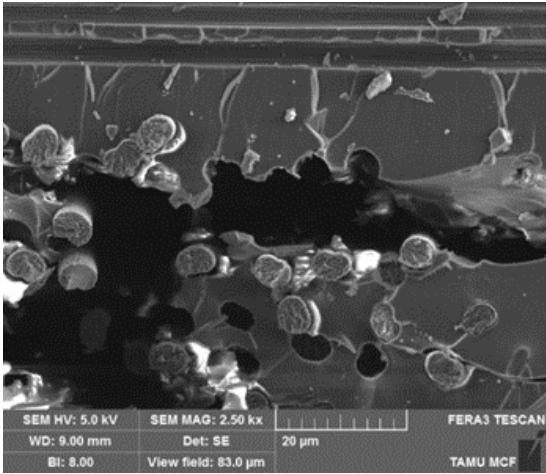
A SEM micrographs of Cytec T40-800/Cycom® 5215 specimens that failed under mechanical loading conditions

This appendix includes reference images of SEM micrographs of Cytec T40-800/Cycom® 5215 graphite/epoxy specimens that failed under various mechanical loading conditions (i.e., tension, compression, and shear). These images are presented in four tables, grouped into specimen categories.

Table A- 1: SEM micrographs of ASTM D3039 unnotched tensile (UNT0) specimens	A-2
Table A- 2. SEM micrographs of ASTM D6641 unnotched compression (UNC0) specimens.	A-5
Table A- 3. SEM micrographs of ASTM D2344 short beam strength (SBS) specimens	A-9
Table A- 4. SEM micrographs of ASTM D3518 in-plane shear (IPS) specimens	A-12

Table A- 1: SEM micrographs of ASTM D3039 unnotched tensile (UNT0) specimens





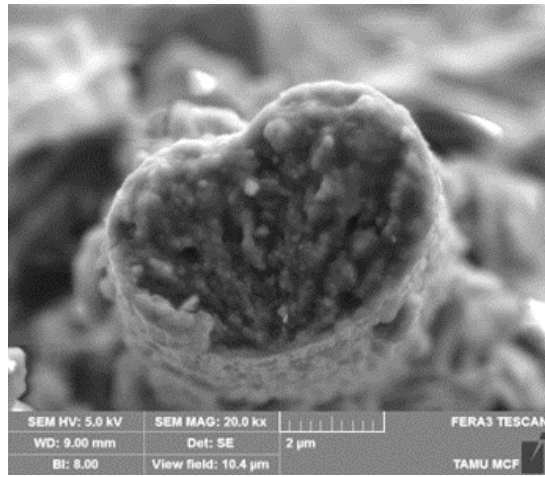
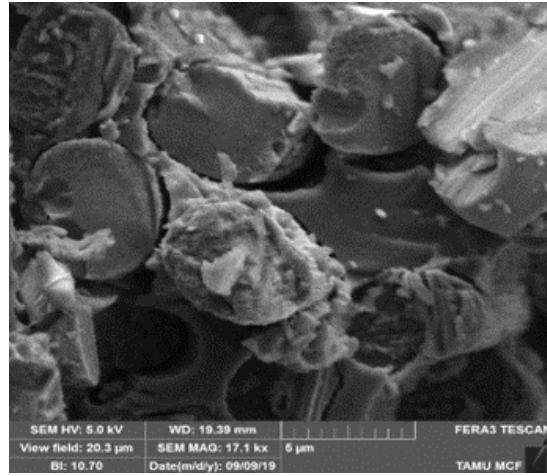
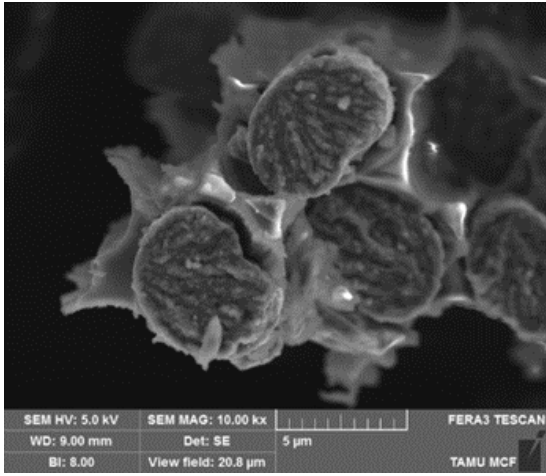
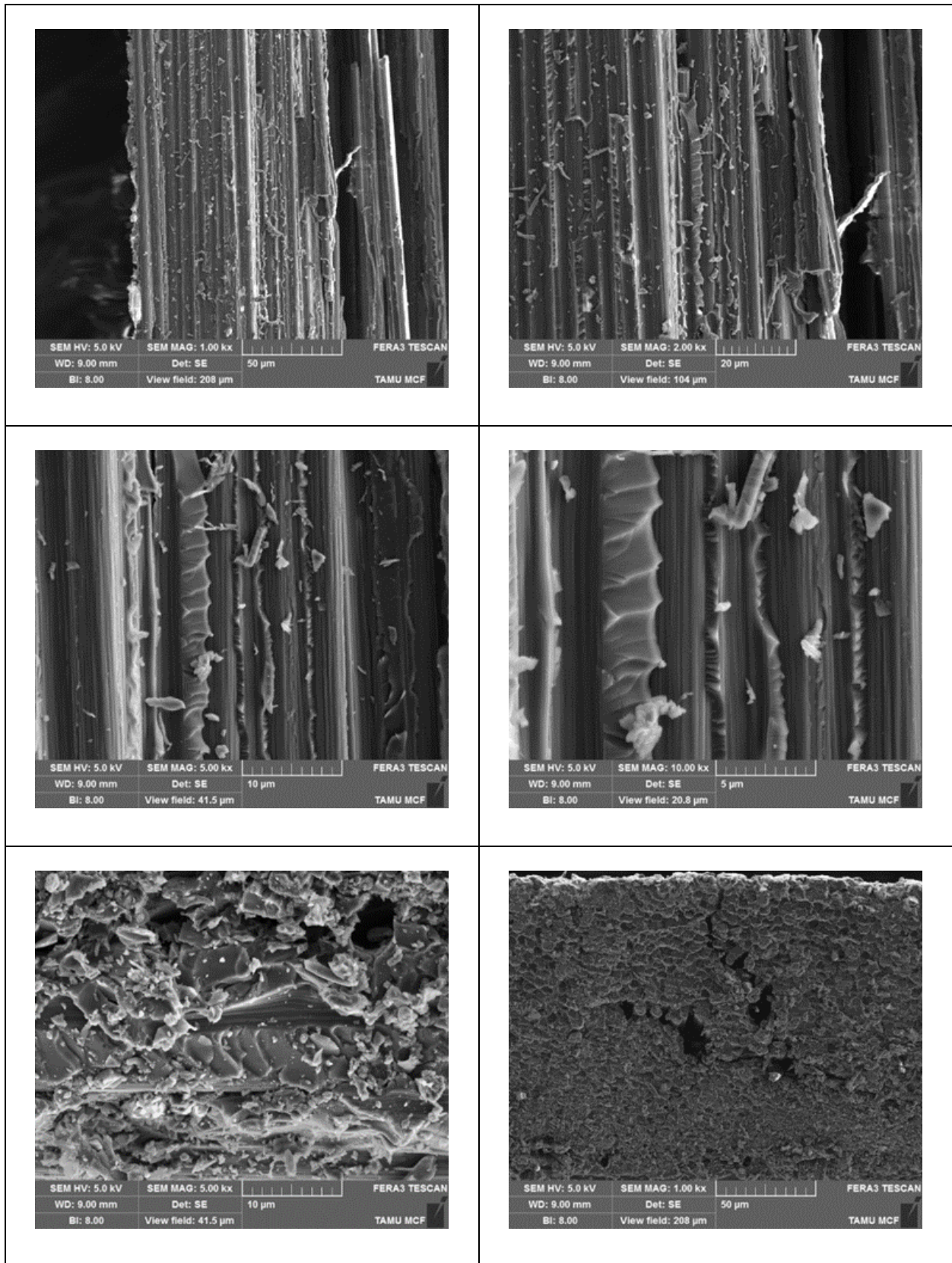
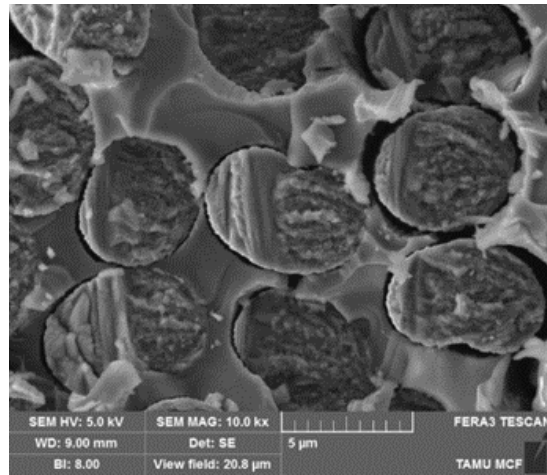
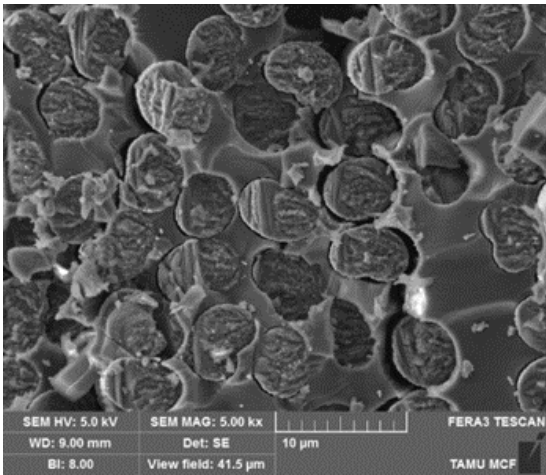
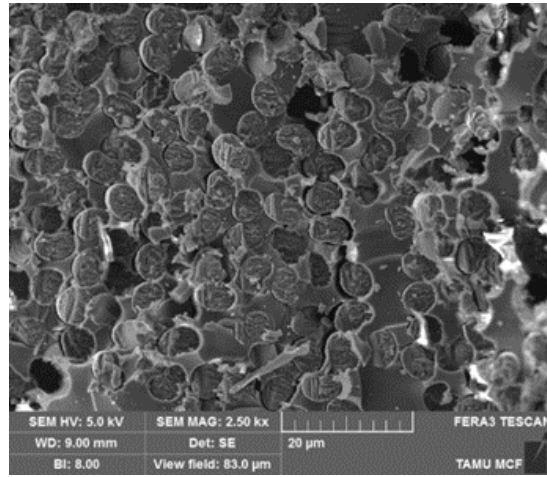
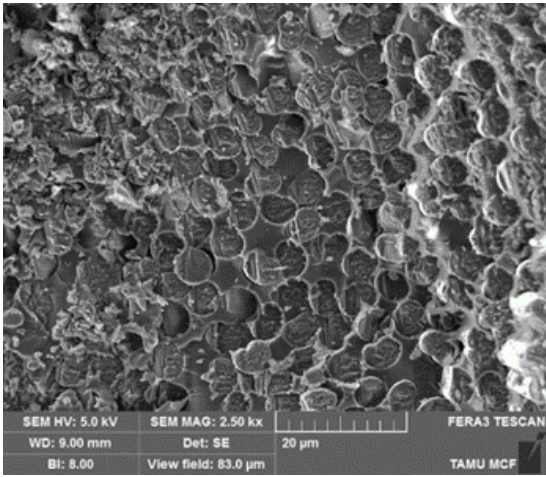
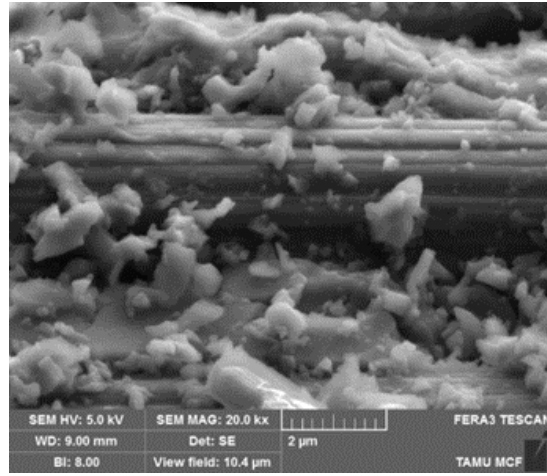
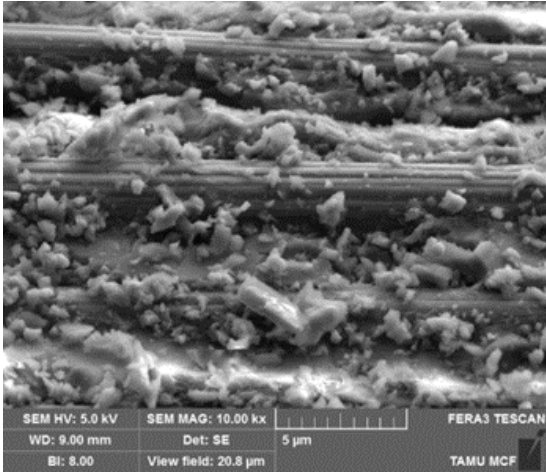
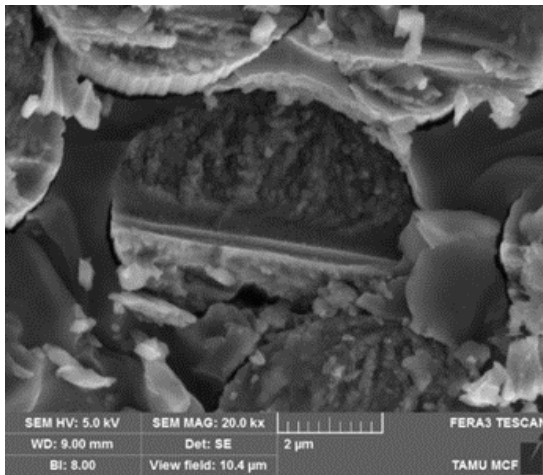
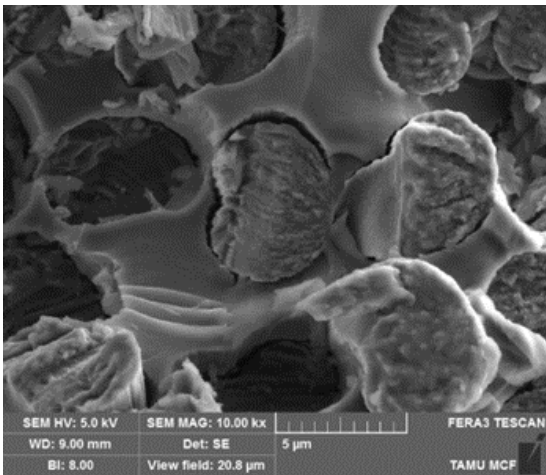
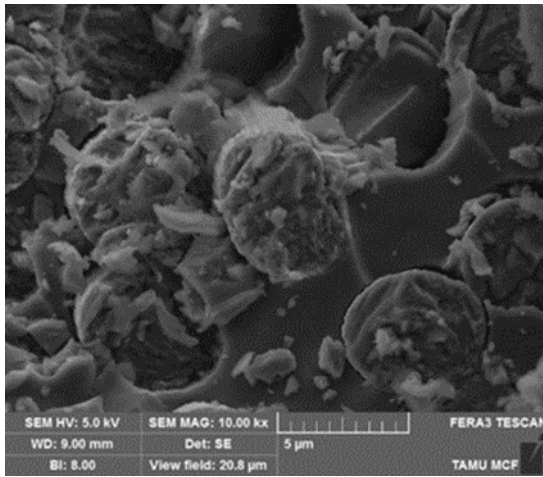
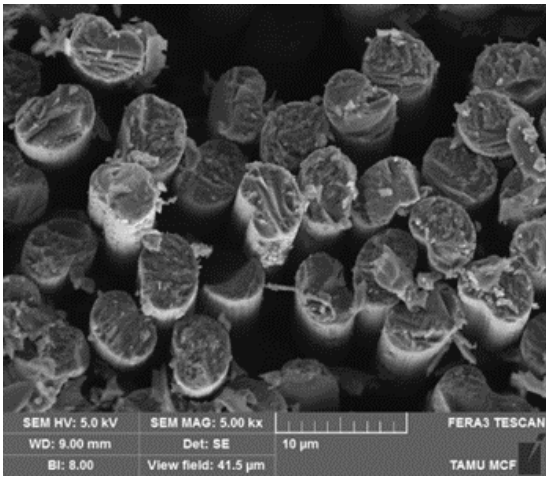
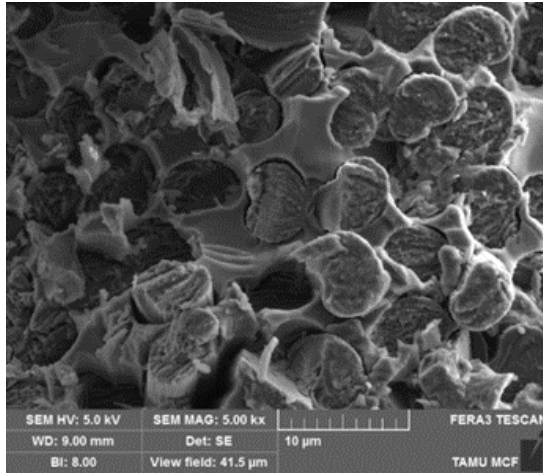
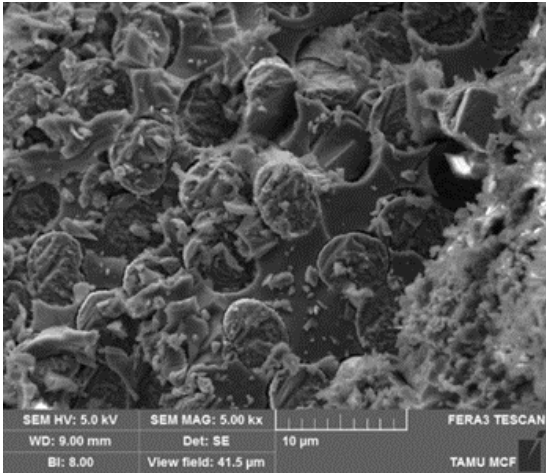


Table A- 2. SEM micrographs of ASTM D6641 unnotched compression (UNC0) specimens







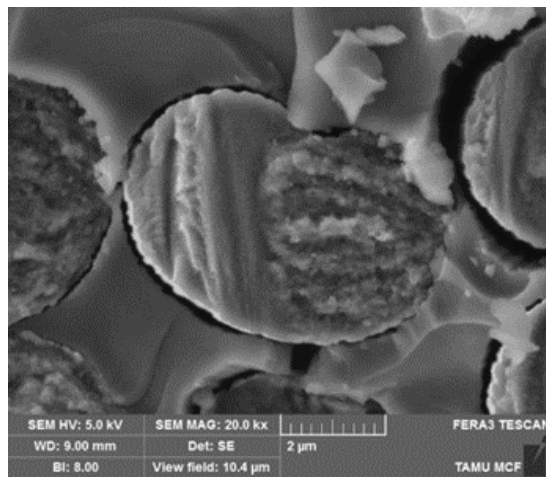
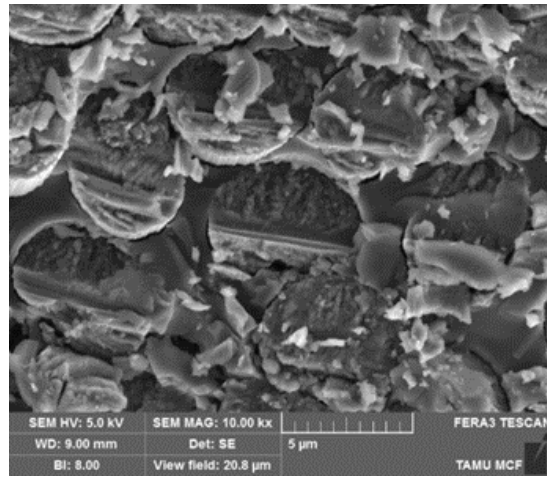
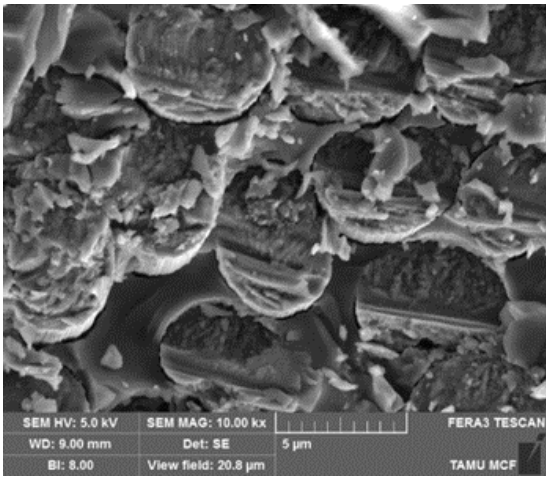
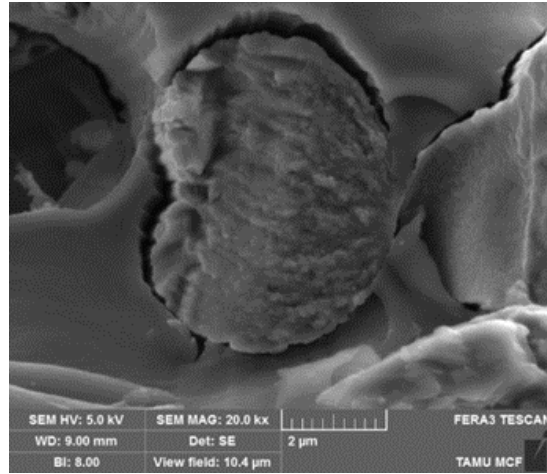
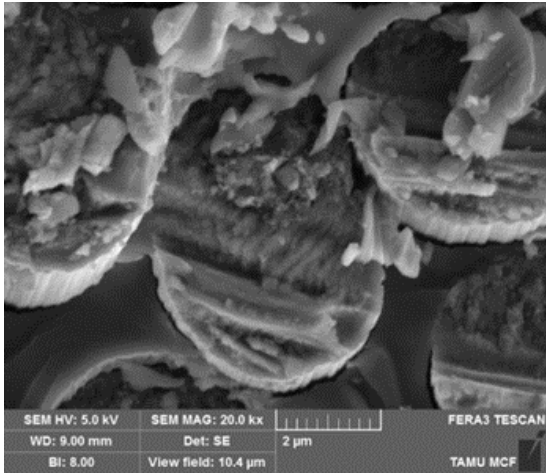
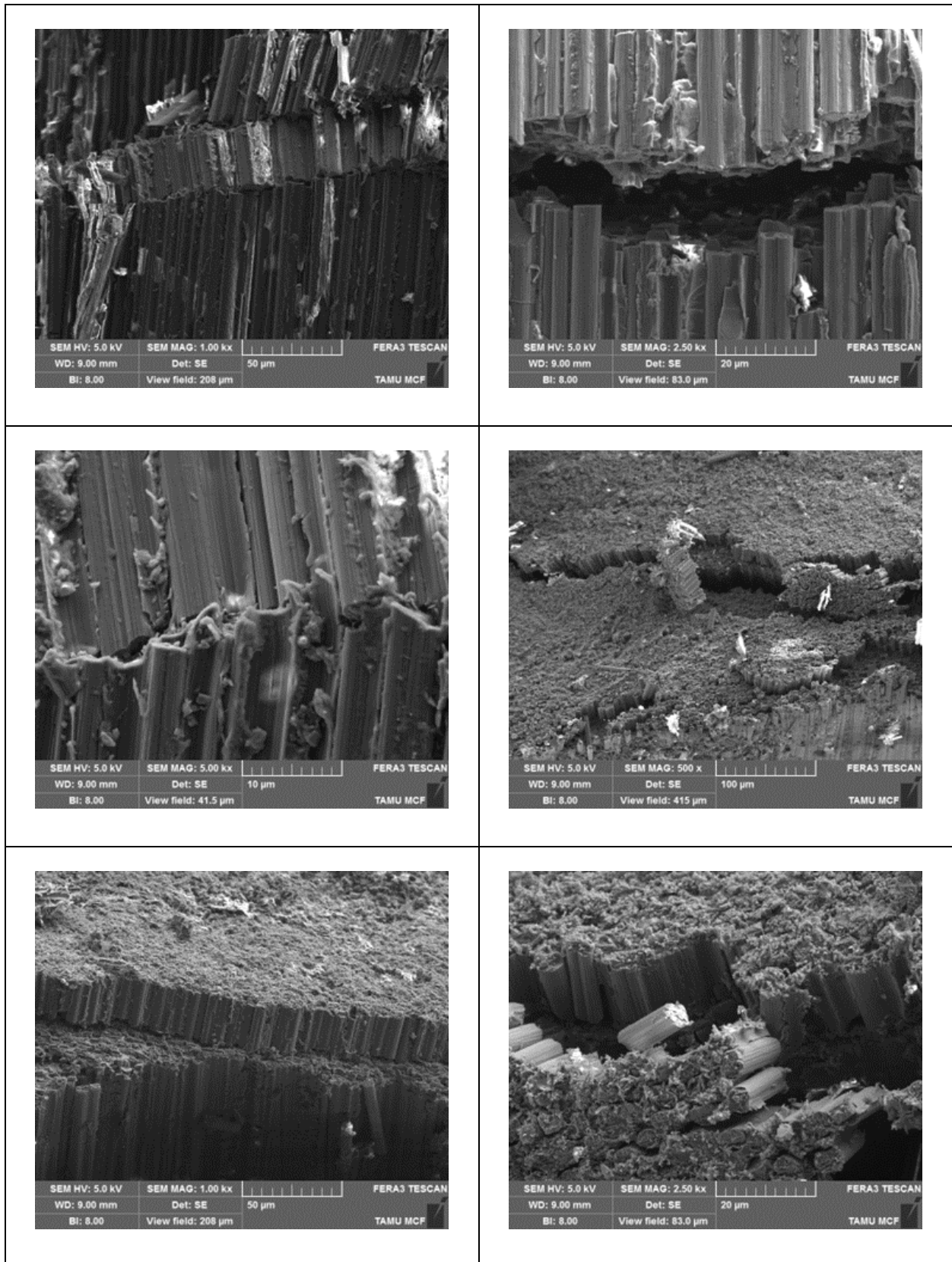
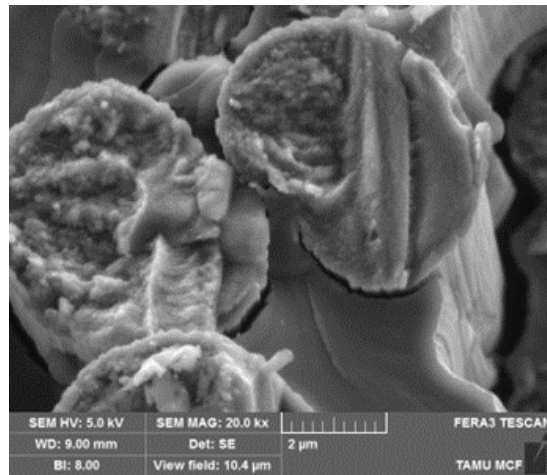
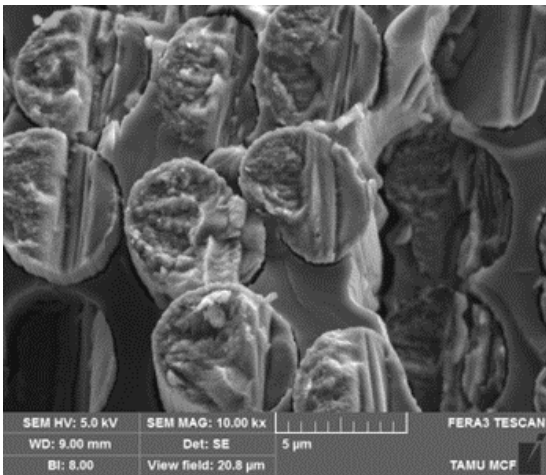
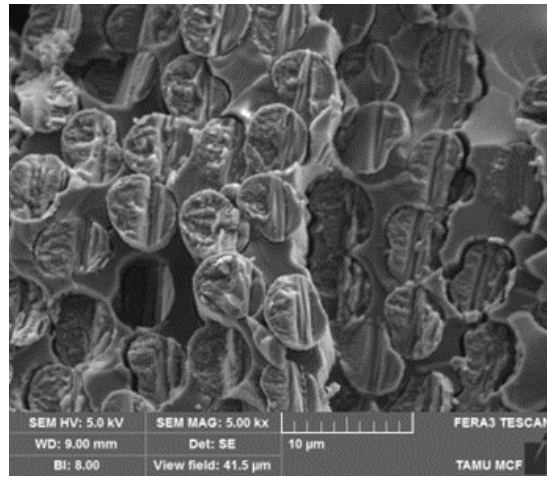
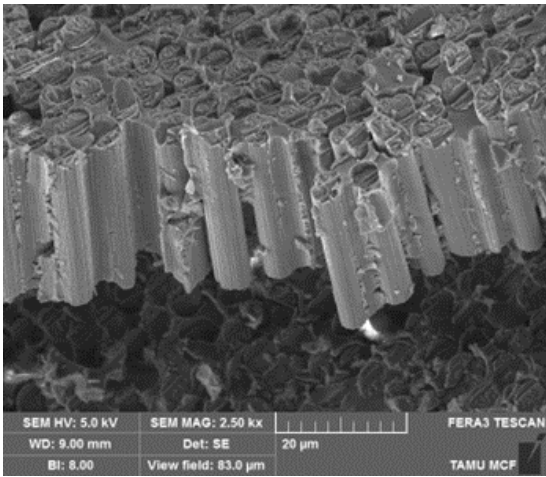
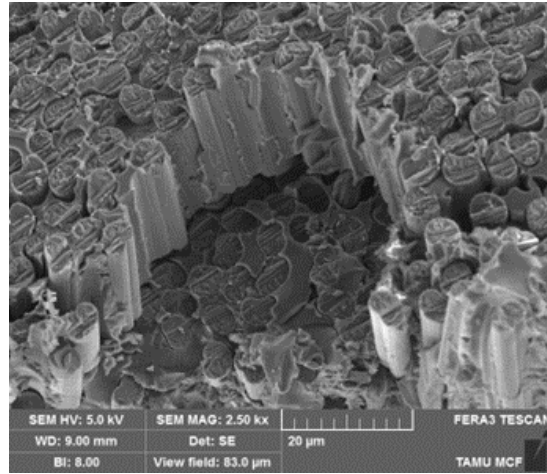
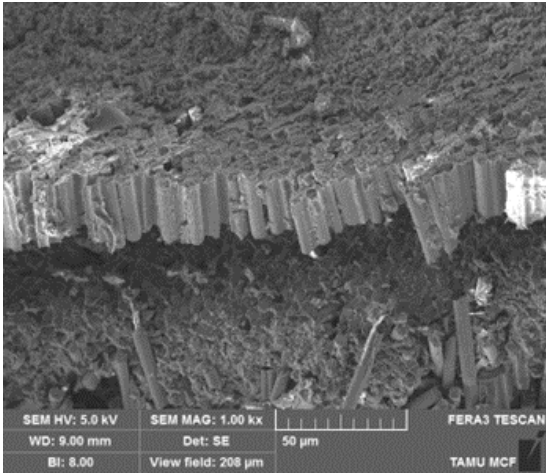


Table A- 3. SEM micrographs of ASTM D2344 short beam strength (SBS) specimens





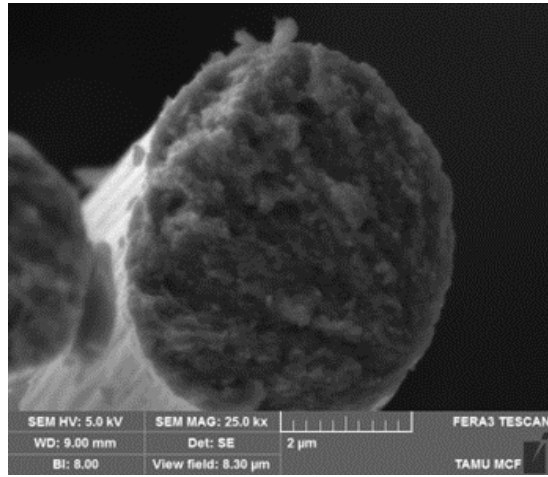
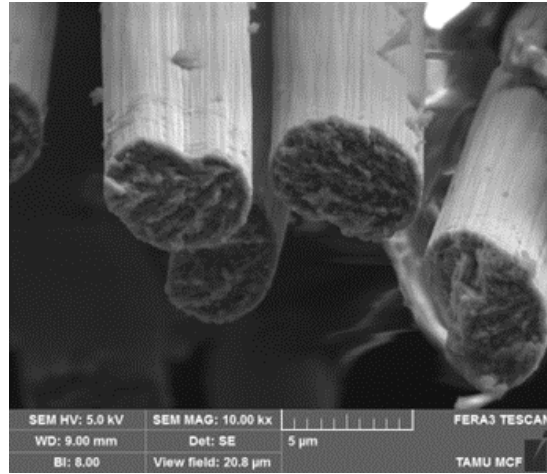
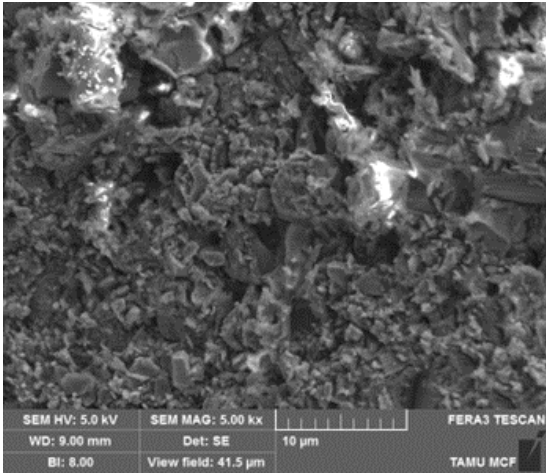
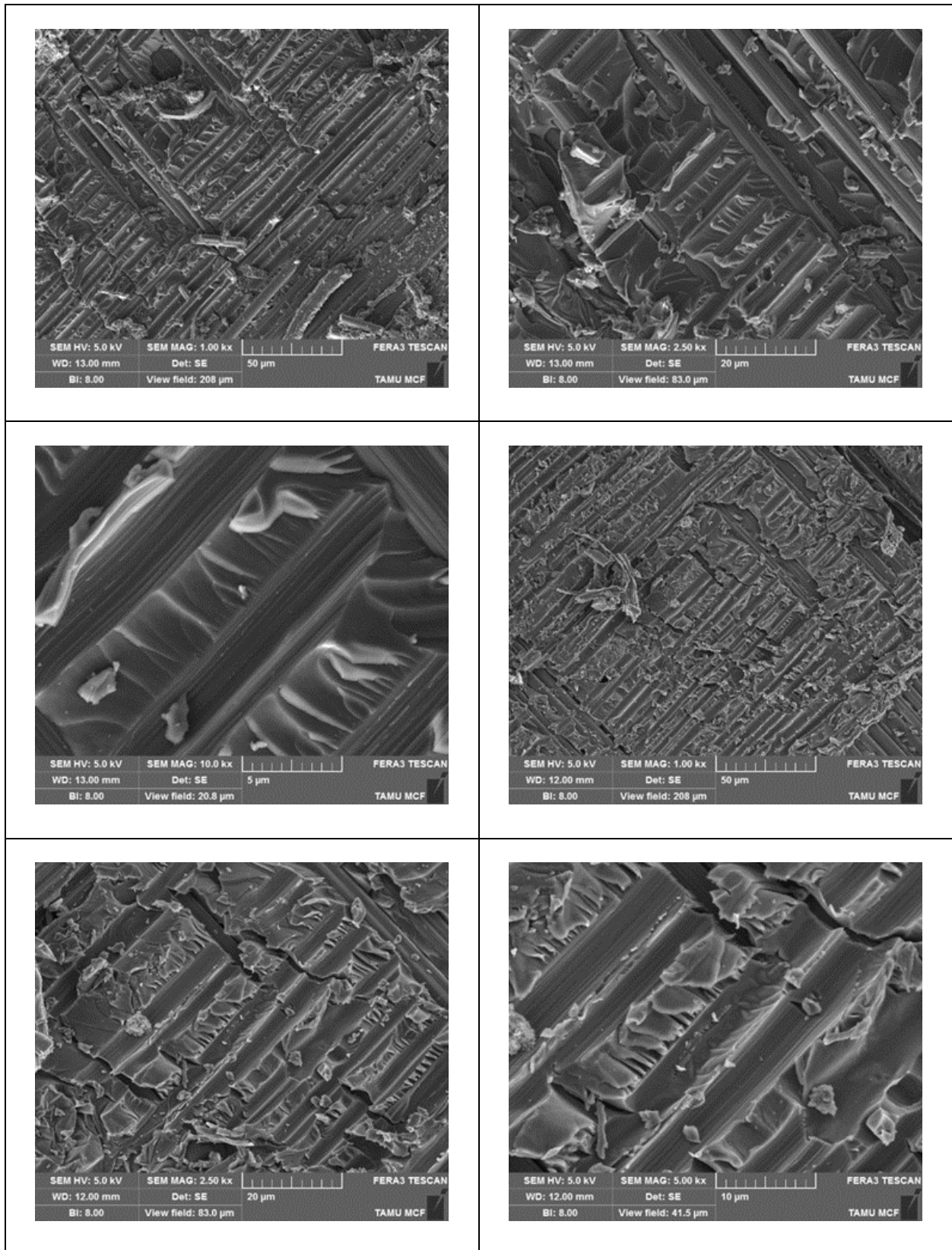
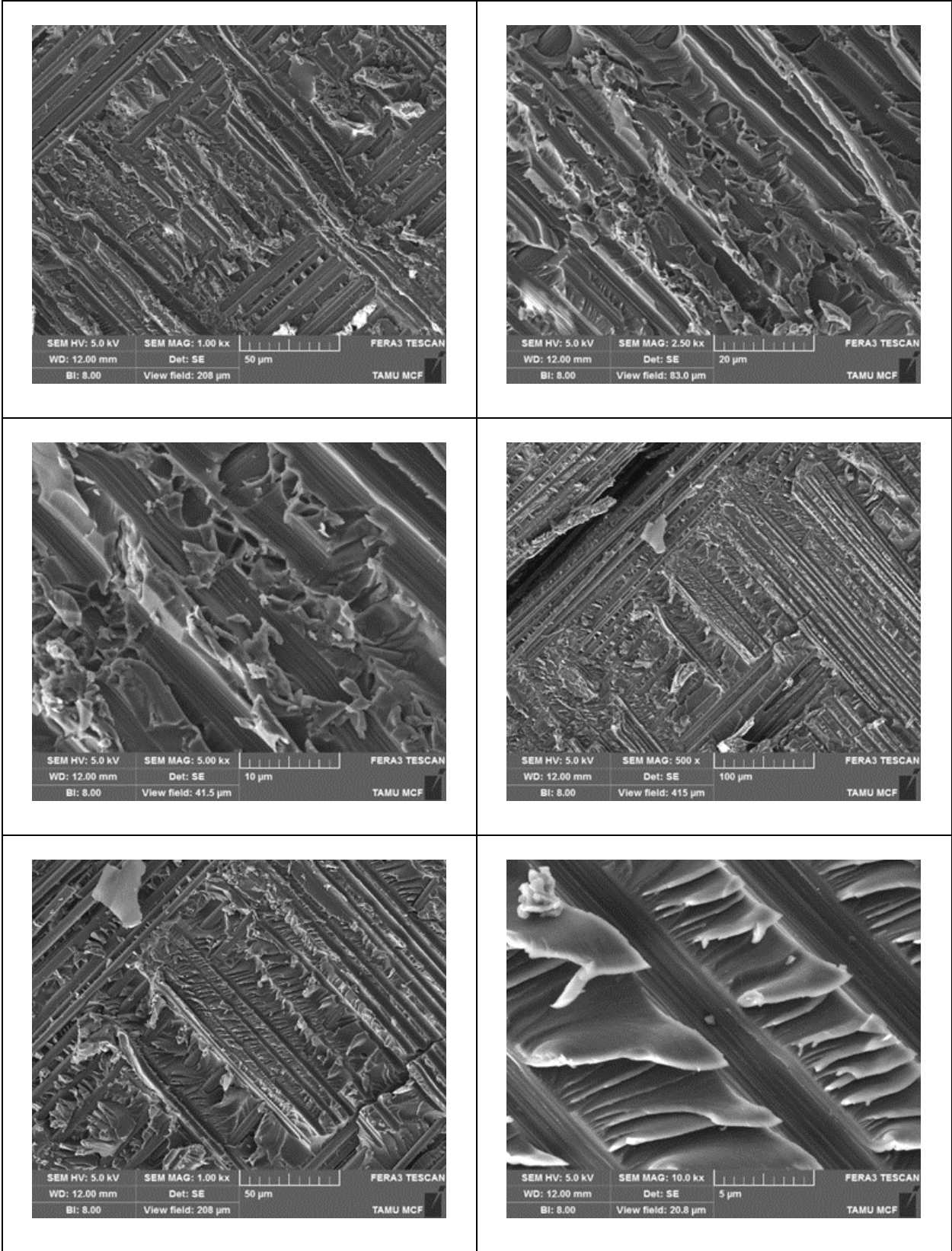
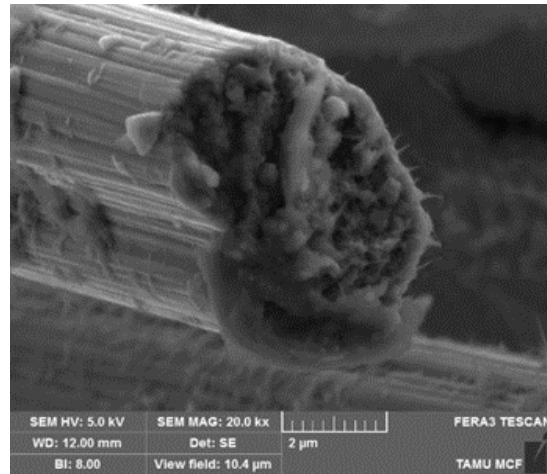
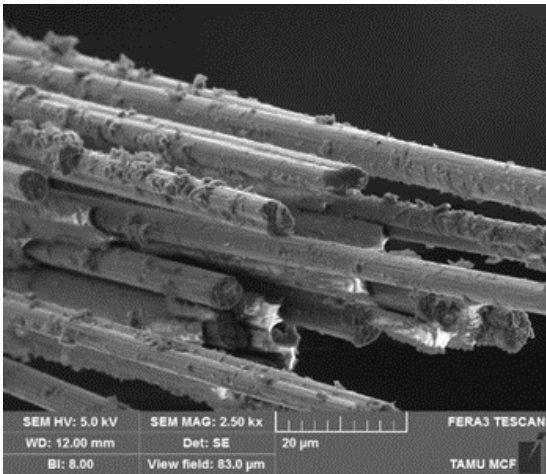
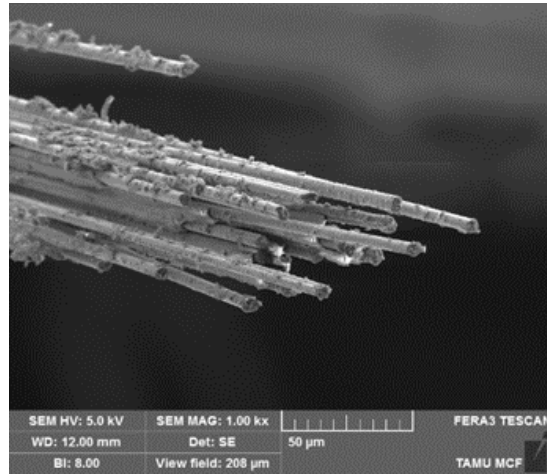
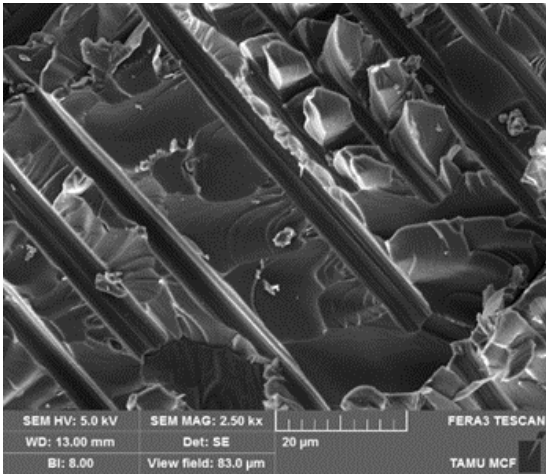
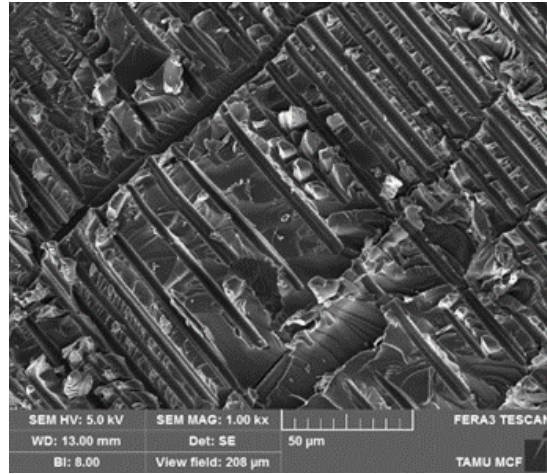
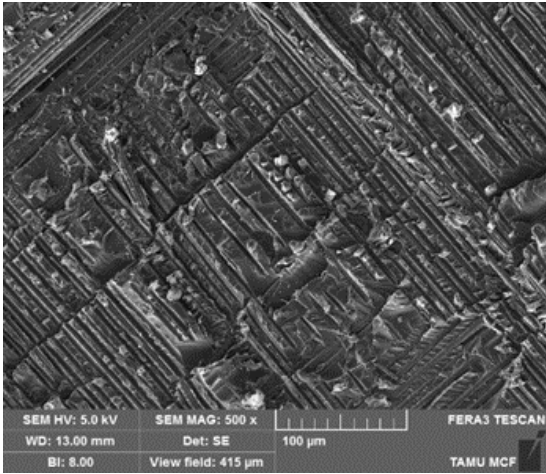


Table A- 4. SEM micrographs of ASTM D3518 in-plane shear (IPS) specimens







B Effect of fire exposure on pristine Hexcel® SGP370-8H/8552 woven-fabric carbon/epoxy composites

List of Figures

Figure B - 1. Eight-harness satin weave configuration with the [7,1] interlacing.....	B-2
Figure B - 2. SU fire test setup	B-3
Figure B - 3. Vertical and horizontal specimen orientations	B-4
Figure B - 4. Vertical fire test setup of a Hexcel composite specimen	B-5
Figure B - 5. Sample preparation: pristine 4-ply cross-ply [0/90/90/0] Hexcel specimens before SEM imaging	B-6
Figure B - 6. Flame evolution during 12 s vertical burn test of Hexcel specimens.....	B-7
Figure B - 7. Initial fire exposed regions of 4-ply cross-ply [0/90/90/0] Hexcel specimens	B-8
Figure B - 8. Lateral surfaces of 4-ply cross-ply [0/90/90/0] Hexcel specimens	B-9
Figure B - 9. In-plane (0°) and out-of-plane (90°) fibers of burned 4-ply cross-ply [0/90/90/0] Hexcel specimens burned vertically for 12 s.....	B-10
Figure B - 10. Fire damage on 12 s vertically burned 4-ply cross-ply [0/90/90/0] Hexcel specimens	B-11

B.1 Pristine woven-fabric aerospace composites

The Hexcel® SGP370-8H/8552 woven-fabric carbon/epoxy composite specimen (Hexcel specimen), is used in aerospace applications in primary and secondary aircraft structures (Hexcel, 2016). Most commonly, woven fabrics are used to fabricate aircraft skin structures (Thill, 2010; Botelho, Silva, Pardini, & Rezende, 2006). Pristine cross-ply [0/90/90/0] Hexcel specimens were used for fire testing and char removal experiments. The thermal degradation behavior of the eight-harness carbon/epoxy specimens is unique due to the (7,1) interlacing of the warp and fill fibers. The overlapping of the two orientations at these junctions would affect the propagation of heat flux, the rate of heat transfer into the composite during burning, and char formation.

Table B - 1 shows the thermal properties of the Hexcel carbon/epoxy material system. It is worth noting that the thermal conductivity of the IM7 carbon-fiber is non-isotropic, with the thermal conductivity value in the axial direction being 5-10 times greater than the transverse fiber thermal conductivity and more than 30 times greater than the thermal conductivity of the matrix (Hind & Robitaille, 2010). Therefore, heat conduction will predominantly occur along the length

of the fiber in all burn scenarios. On a part level, the (7,1) interlacing of the eight-harness satin weave configuration, as shown in Figure B - 1 would influence the nature of heat conduction at those regions of overlap. Consequently, it would be worthwhile to study the thermal degradation behavior of woven-fabric skin structures.

Table B - 1. Thermal properties of Hexcel woven-fabric carbon/epoxy composites

HexTow® IM7 Fiber Yarn/Tow Properties	SI Units
Specific Heat	0.21 cal/g-°C
Coefficient of Thermal Expansion	-0.64 ppm/°C
Thermal Conductivity (Axial)	5.40 W/m-°C
Thermal Conductivity (Transverse)	n/a (but estimated to be 5-10 times lower than axial)
HexPly® 8552 Matrix Properties	
Glass-transition Temperature (T _g -dry) (neat resin)	200 °C
Thermal Conductivity	0.148 W/m-°C

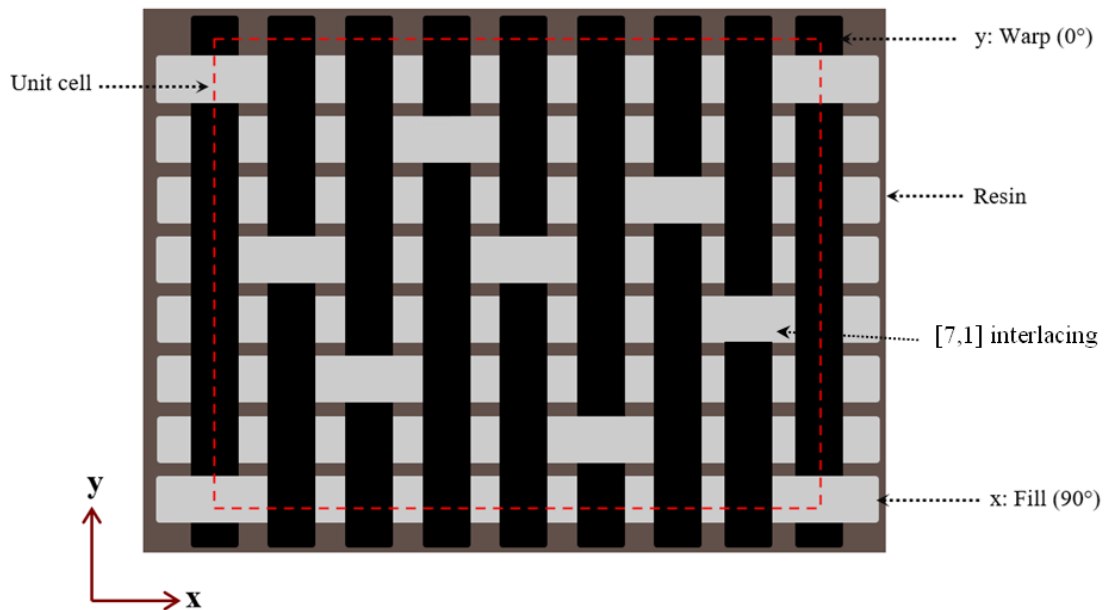


Figure B - 1. Eight-harness satin weave configuration with the [7,1] interlacing

Additional fire exposure tests were conducted on pristine 4-ply cross-ply [0/90/90/0] Hexcel specimens in a test setup consisting of a three-sided sheet metal enclosure, a metal stand with a clamp to hold the specimen, and a Bunsen burner. The fire tests were conducted to produce test

specimens for initial char removal exercises. LPG (liquid propane + butane mix) was used as fuel for the Bunsen burner. The burn test setup was placed inside a fume hood. Airflow within the enclosure was minimized by placing the burner 10 in from the hood's opening to reduce flame movement during testing. A timer was placed outside the hood to track the test durations. Figure B - 2 shows a picture of the MSU fire test setup with the three-sided sheet metal enclosure in a glass fume hood. The Hexcel specimens were used to generate trial specimens for char removal experiments for the initial round of tests.

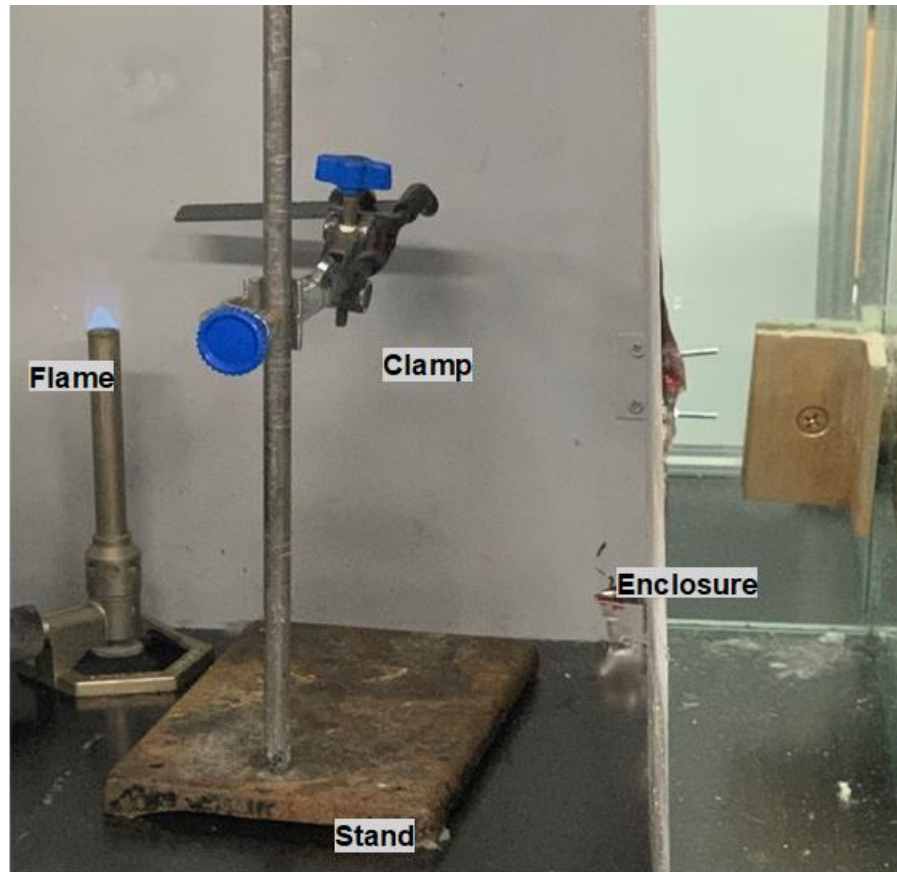


Figure B - 2. SU fire test setup

At the start of the fire tests, flame height and specimen position from the flame are manually adjusted with a measuring tape. The flame profile for the LPG flame consisted of a flame of 1.5 in height. The tip of the inner cone was 0.375 in from the burner. Before fire application, the specimen was positioned at a standoff distance of 3/4 in from the Bunsen burner tip. A schematic showing the flame profile and position of the specimen in the sheet metal enclosure relative to the flame is shown in Figure B - 3.

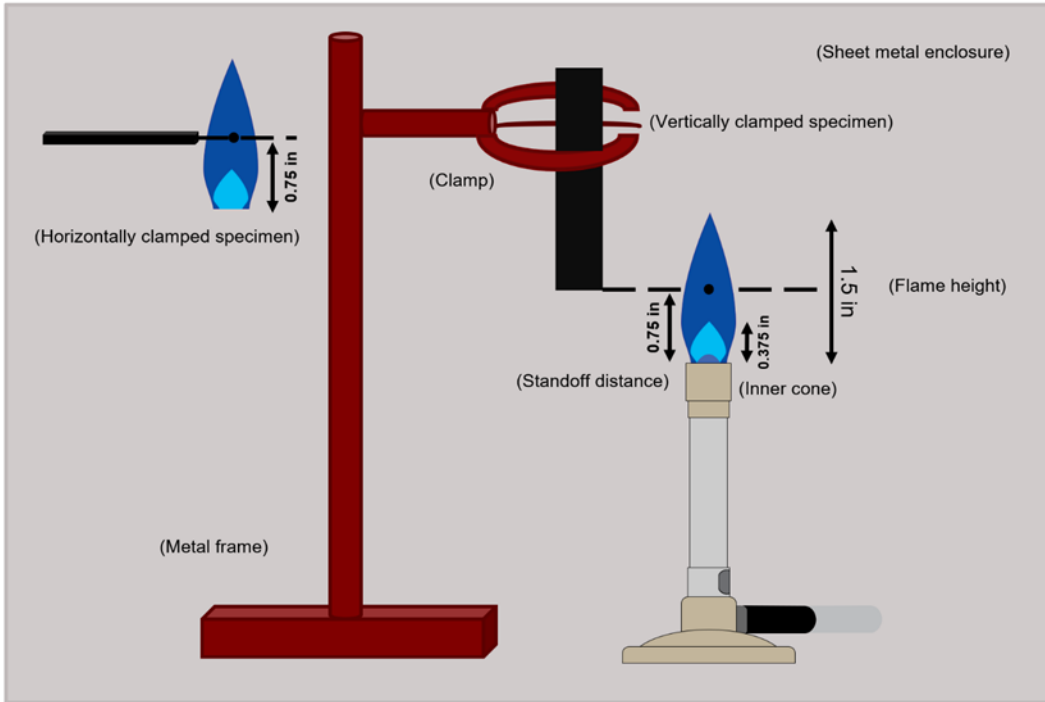


Figure B - 3. Vertical and horizontal specimen orientations

The exposure durations selected for the vertical burning of pristine carbon/epoxy cross-ply specimens are 12, 36, and 60 s. Three replicates were used for each fire test duration to ensure the reproducibility of the results. Figure B - 4 shows a 4-ply cross-ply [0/90/90/0] Hexcel specimen during a vertical Bunsen burner test.



Figure B - 4. Vertical fire test setup of a Hexcel composite specimen

B.2 Analysis of pristine aerospace composites subjected to fire

Vertical and horizontal fire tests were conducted on pristine cross-ply [0/90/90/0] Hexcel specimens. The goal of the fire tests was to generate charred specimens for preliminary investigative char removal experiments. However, the fire damage induced during the horizontal fire tests was significantly lower than the vertical fire tests for comparable exposure durations. Therefore, only the vertical fire-exposure tests will be discussed in this section. The tests were performed using a Bunsen burner enclosed in a three-sided sheet metal enclosure within a fume hood. The fire damage on the pristine composite surface was observed using the ZEISS Supra 40 FE-SEM. The region of initial fire exposure was considered as the primary area of interest. The burned specimens were mounted on a 45°/90° angle stub and subjected to a nominal gold-palladium sputter coating of 5 nm. The lateral surfaces of the specimens were secured with

conductive carbon tape (Figure B - 5) to reduce specimen charging. The SEM micrographs of the fire-exposed regions were obtained at an accelerating voltage of 15 kV, at a WD of 9 mm (unless otherwise stated).



Figure B - 5. Sample preparation: pristine 4-ply cross-ply [0/90/90/0] Hexcel specimens before SEM imaging

Vertical fire tests were performed on 4-ply cross-ply [0/90/90/0] Hexcel specimens for 12 s, 36 s, and 60 s. A k-type thermocouple and a four-channel temperature logger were used to monitor temperature fluctuations near the fire-exposed regions. Three repeat tests were performed for each exposure duration. The specimens for the repeat tests had comparable dimensions and were also cured in the same batch to reproduce results.

At the onset of the fire tests, the Hexcel specimens are vertically oriented, such that their longitudinal axis is perpendicular to the Bunsen burner flame. As the flame begins to spread along the specimen surface, matrix decomposition occurs, resulting in the outgassing of volatiles at high local temperatures (Mouritz & Gibson, 2007). As the volatile gases move into the combustion zone, the heat release rate increases, causing the flame to spread rapidly across the specimen surface. The flame front travels upwards along the length of the specimen till the fire engulfed the whole specimen. At this point, severe thermal damage occurs in the specimen resulting in the rapid consumption of the matrix constituents. The flame intensity is visibly higher on the lateral sides of the specimen than the central regions since the flame-spread is far higher from the lateral edges of the fire-exposed region than the laminate mid-plane.

With the Bunsen burner turned off, the flame intensity reduced within seconds, and the remaining flame proceeds from the lateral edges of the fire-exposed region to the interior regions. However, due to the rapid depletion of the combustion material (matrix and volatile gases) and the formation of fire by-products that inhibit flame-spread (non-combustible gases, char), the flame begins to self-extinguish (Mouritz & Gibson, 2007). The flame traversing from the laminate mid-plane into the interior of the burning specimens self-extinguishes faster than that from the lateral edges of the initial fire exposure region.

The series of images in Figure B - 6 shows the flame evolution before and after initial fire exposure for a vertically oriented cross-ply [0/90/90/0] Hexcel specimen burned for 12 s. The flame spread is initiated first in the lateral edges till the entire specimen is engulfed in the fire. After the burner is turned off, the specimen continued to burn for 20 s, and the specimen broke free from the clamp with a loud bang. The expulsion of the specimen from the clamp could be attributed to the pressurized release of non-combustible gaseous products. Once on the ground, the specimen smoldered for about 15 s.

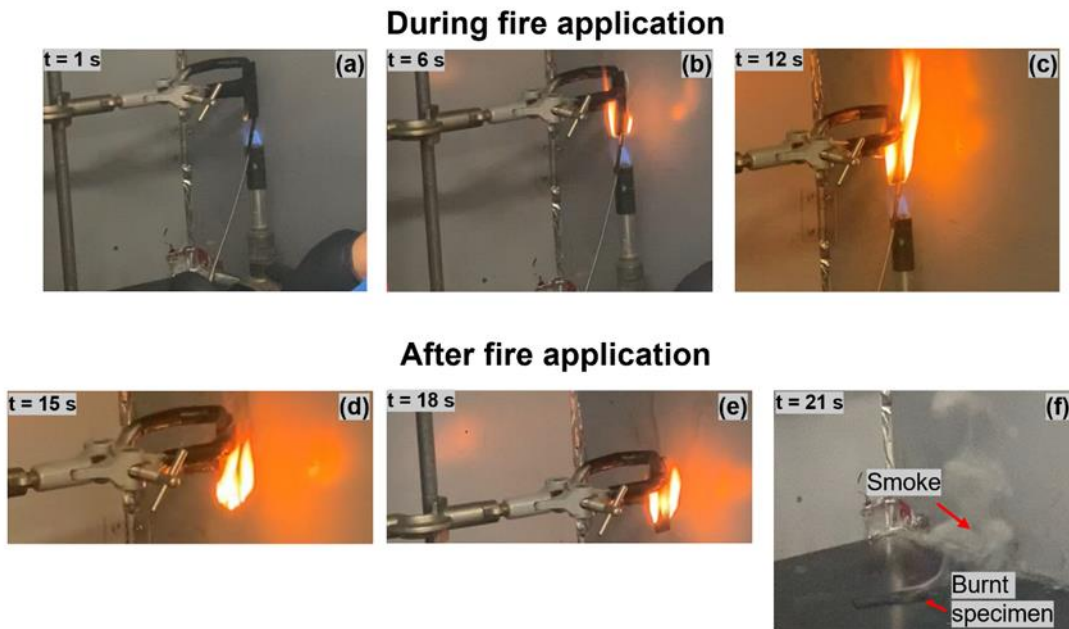


Figure B - 6. Flame evolution during 12 s vertical burn test of Hexcel specimens

Fire damage in the form of matrix decomposition, ply delamination, and residual thickness increase was more severe on specimens burned for 36 s and 60 s durations than for the 12 s fire exposure. In the case of the 60 s exposure duration, the 4-ply cross-ply [0/90/90/0] Hexcel specimens showed more significant through-thickness damage than the other exposure times, with excessive matrix decomposition. The lateral plies sustained a greater magnitude of delamination than the internal plies in all three cases, with the 60 s test yielding the highest

degree of ply-delamination. However, char formation was minimal on the fire-exposed region after burning for 60 s, possibly due to the excessive matrix decomposition since the specimen was exposed to the fire for a longer time. Char formation was more significant for the 12 s and 36 s exposure durations on both the fire-exposed region and the lateral surfaces of the specimens. The increase in the residual thickness was highest for the 60 s exposure duration, possibly due to a higher level of volatile outgassing and matrix decomposition. A similar trend was observed for the Cytec T40-800/Cycom[®] 5215 graphite/epoxy UNCO specimens. The fire damage on the lateral surfaces and the region of initial fire exposure is shown in Figure B - 7 and Figure B - 8. From the figures, that the ply-delamination was least for the vertically oriented specimen burned for 12 s. There is some fiber-tow separation, from the top plies on the lateral edges of the specimens, possibly due to pockets of matrix decomposition at those locations. Overall, char formation on the fire-exposed region was higher for the 36 s test specimen, followed by the 12 s test specimen.

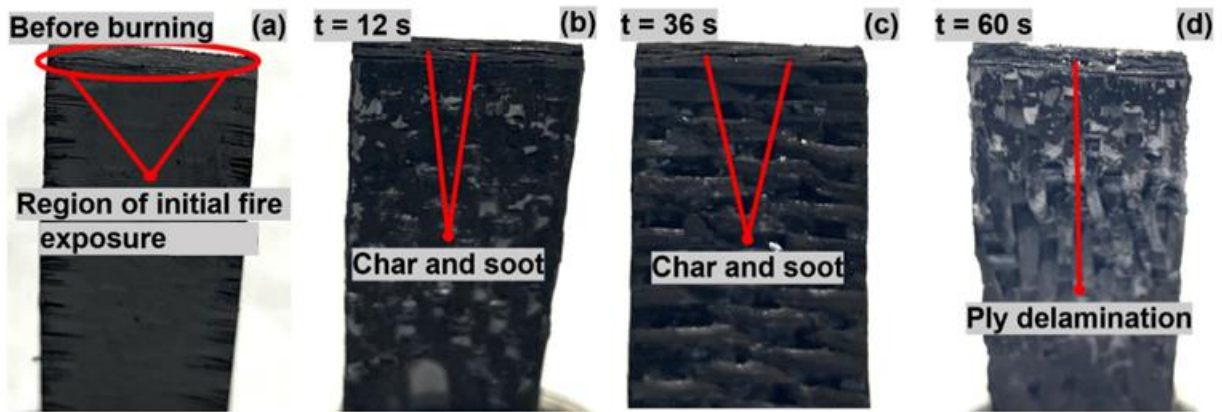


Figure B - 7. Initial fire exposed regions of 4-ply cross-ply [0/90/90/0] Hexcel specimens

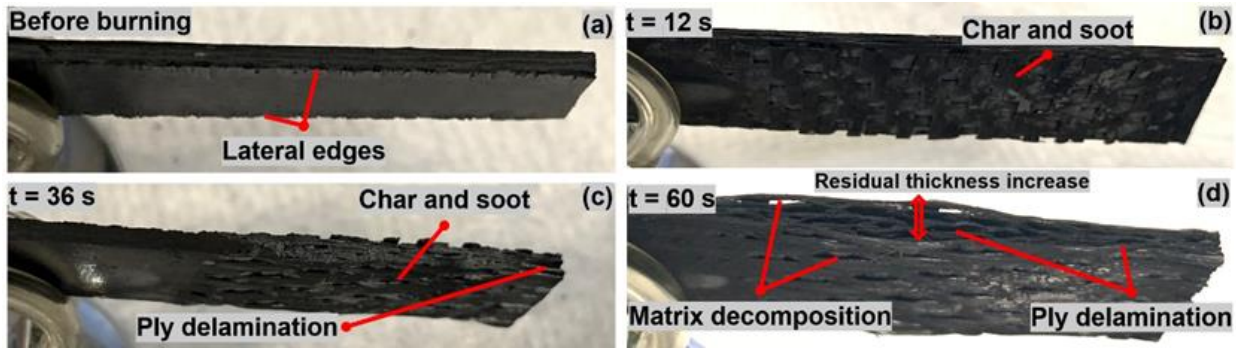


Figure B - 8. Lateral surfaces of 4-ply cross-ply [0/90/90/0] Hexcel specimens

Char morphology for all three exposure durations was studied using scanning electron microscopy. Fiber orientation, exposure duration, and position relative to the flame all impacted char formation. The initial fire exposure region, the planar surface adjacent and perpendicular to the burner, was the region of importance. For both 12 s and 36 s exposure times, char formation was excessive at the mid-plane region of the fire-exposed region. The 90° fibers oriented perpendicular to the flame conducted heat away from the mid-plane towards the lateral sides of the fire-exposed region. Therefore, these fibers possessed a substantial amount of char along the lateral sides of the carbon fibers in the form of amorphous (‘velvet’) textured deposits. The 0° fibers oriented parallel to the flame conducted heat into the specimen's interior, with a more globular and mixed-phase (amorphous and crystalline) ‘fuzzy’ char on the exposed fiber ends. Figure B - 8 shows the char and soot profile described for a Hexcel specimen burned vertically for 12 s. While plies close to the mid-plane contained char throughout the plies, the char density was higher in the middle regions of the plies for both 12 s and 36 s exposure times. The char density is noticeably high in the 90° fibers in Figure B - 8b, with char occupying the whole of the lateral cylindrical surface. For all cases, char was markedly less on the lateral sides of the top and bottom plies, with more prominence in the middle portions of the plies. This could be attributed to flame-concentration along the lateral edges, causing near-total matrix combustion. Overall, char formation on the lateral sides is a function of exposure duration, with the 60 s test yielding the least amount of char due to the high heat convection away from the specimen and the combustion of matrix constituents.

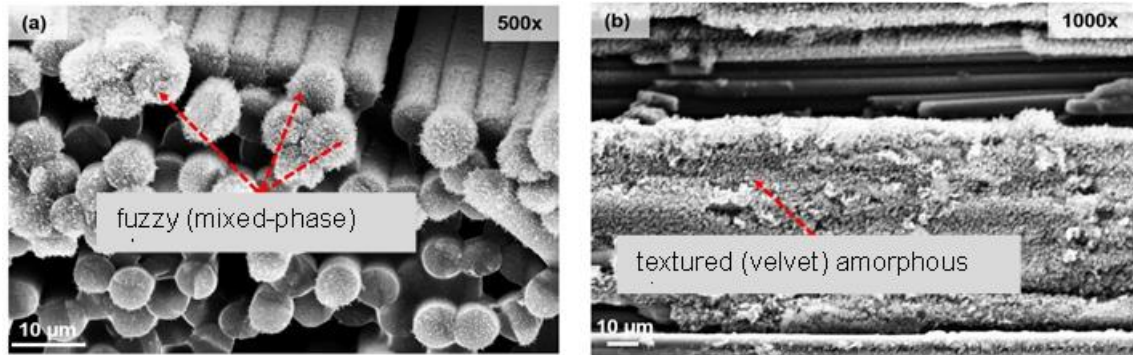


Figure B - 9. In-plane (0°) and out-of-plane (90°) fibers of burned 4-ply cross-ply [0/90/90/0] Hexcel specimens burned vertically for 12 s

The SEM micrograph in Figure B - 9 shows the fire damage on the fire-exposed region of a vertically oriented Hexcel specimen burned for 12 s. The fire-exposed region is marked with thermal damage, including matrix cracking, ply-delamination, char and soot deposition, matrix decomposition, and melt-dripping. The top ply [0/90/90/0] has a varied fire damage morphology. The lateral sides of the 0° fibers show strand-like fibers with near-complete matrix combustion and the middle portions undergoing incomplete burning with regions where the matrix was relatively untouched. The extreme decomposition at the lateral sides can be explained by the distribution of the flame, which tends to diffuse into the lateral sides of the specimen. The top ply also has pockets of matrix combustion with relatively low char on the fibers. The 90° fibers in the top ply showed signs of melt dripping across their surface in the middle regions of the ply.

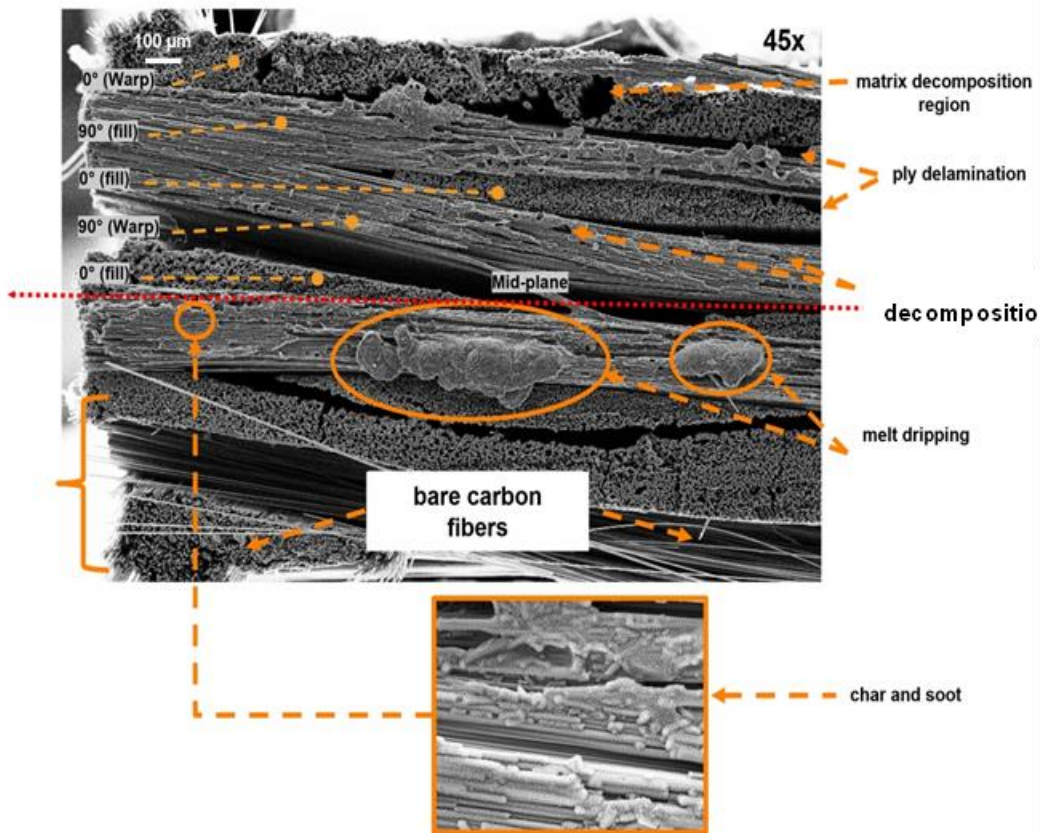


Figure B - 10. Fire damage on 12 s vertically burned 4-ply cross-ply [0/90/90/0] Hexcel specimens

Ply delamination was significant in the interfaces between plies where the fiber orientations were opposite—such as the 90° and the 0° fibers in Figure B - 10; which happens to be the interface between the first 90° ply and the second 90° ply in the cross-ply [0/90/90/0] configuration. The excessive delamination can be attributed to the coefficient of thermal expansion-mismatch between the two perpendicular orientations leads to a greater degree of distortion in between the plies (Mouritz & Gibson, 2007). Thermal degradation behavior at the (7,1) interlacing sites (for the flame propagation coincident with the 0° plies) resulted in the near-total combustion of the epoxy matrix (cf., Figure B - 10, “bare fibers”) surrounding the 0° plies at those regions. This caused a change in the direction of heat conduction away from the interior of the specimen. Therefore, the lateral surfaces of the composite specimen would be subjected to a greater effective heat transfer rate in these regions, leading to the near-total combustion of the matrix leading to increased production of gaseous by-products rather than char and soot. Therefore, the (7, 1) interlacing could contribute to lower char density in the lateral surfaces above and below the laminate mid-plane.

Char formation is extensive on the sides, and the middle regions on the 0 and 90° plies closer to the laminate mid-plane. The middle regions of the second ply show signs of incomplete combustion, with excessive melt dripping and matrix cracking. The incomplete combustion can be attributed to the low exposure duration and the fact that most of the heat is conducted away from the middle regions to the lateral sides of the fire-exposed region. Melt-dripping is an intermediate step in the matrix decomposition process where a phase change from solid to liquid occurs at temperatures higher than the glass transition temperatures of the resin and lower than the decomposition temperature. While melt-dripping is a product of a solid-viscous phase change, decomposition occurs due to bond breakage (Ray & Kuruma, 2019; Shi, Bao, Kobayashi, Kato, & Kemmochi, 2012). The damage characteristics are more severe in the plies below the laminate mid-plane. In regions closer to the mid-plane, there is excessive char and soot deposition, particularly on the lateral sides of the specimen. This is likely due to the persistence of the flame in these regions after removing the Bunsen burner. The bottom ply showed excessive matrix combustion, with the in-plane 90° fibers showing signs of transverse deflection (having the appearance of bent-fibers, as shown in Figure B - 10. This behavior could be attributed to the high pressure in these regions to the high rate of outgassing of volatiles and non-combustible by-products during burning (Mouritz, et al., 2009).